Final Report on

NASA Grant 05-020-019

to

PERFORM A GYRO TEST OF GENERAL
RELATIVITY IN A SATELLITE
AND DEVELOP ASSOCIATED
CONTROL TECHNOLOGY

NOV 1977

RECEIVED
NASA STI FACILITY

High-Energy Physics Laboratory

W. W. Hansen Laboratories of Physics

STANFORD UNIVERSITY
STANFORD, CALIFORNIA

Δθ = 7 sec   GYRO 2

T = 1 YEAR

t = 0

Δθ = 0.05 sec

t = 1 YEAR

t = 0

GYRO 1
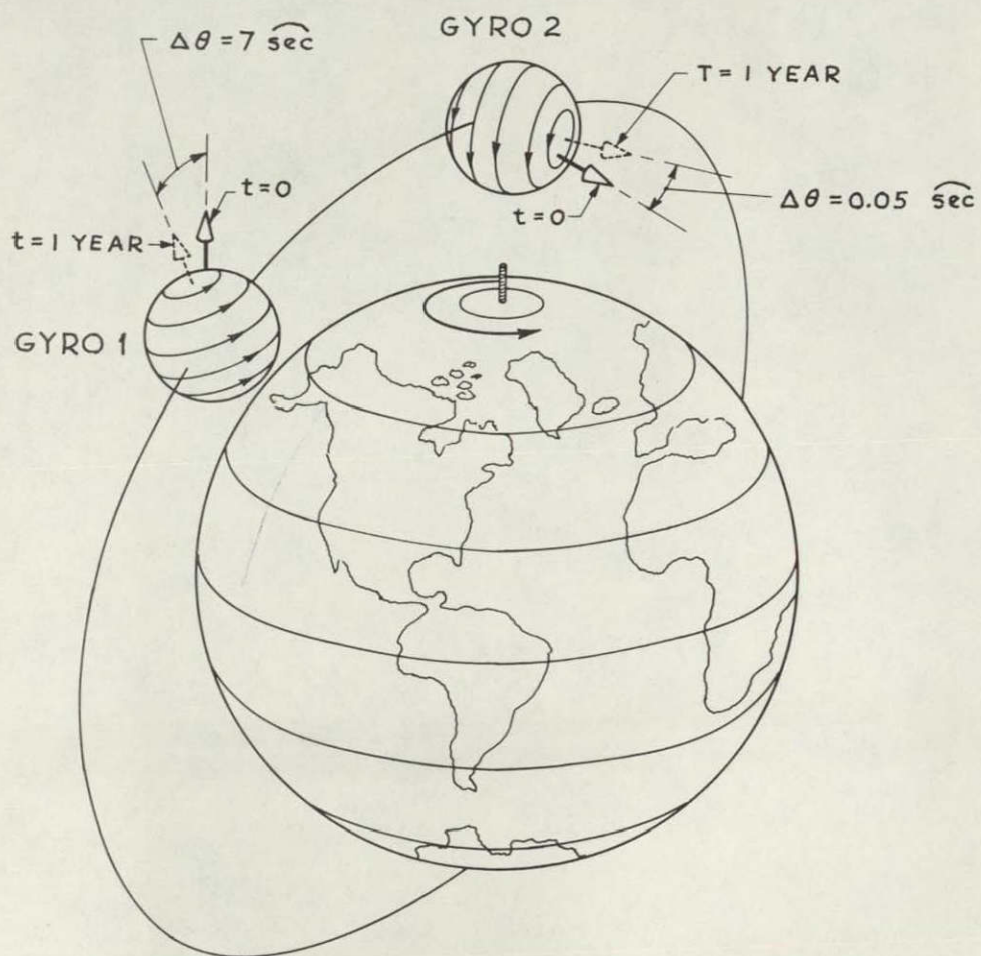
LEONARD SCHIFF AND THE RELATIVITY GYROSCOPE EFFECTS

Final Report on

NASA Grant 05-020-019

to

PERFORM A GYRO TEST OF GENERAL
RELATIVITY IN A SATELLITE
AND DEVELOP ASSOCIATED
CONTROL TECHNOLOGY

Co-Principal Investigators:

W. M. Fairbank, C. W. F. Everitt, D. B. DeBra

Report coordinated by:

C. W. F. Everitt

.

Contributors:

J. T. Anderson, B. Cabrera, R. R. Clappier,
D. B. DeBra, J. A. Lipa, G. J. Siddall,
F. J. van Kann, R. A. Van Patten

W. W. Hansen Laboratories of Physics
and the
Department of Aeronautics and Astronautics
Stanford University
Stanford, California 94305

July 1977

PREFATORY NOTE

This report describes research on the Stanford Gyro Relativity program from 1963 until January 1977 when NASA Grant 05-020-019 was terminated and replaced by Contract NAS8-32355.

The history of the Gyro Relativity program has been unusual in a number of ways both as a physics experiment and as a NASA program. From the beginning we have had to meet the challenges and pitfalls that await everyone who enters the difficult but exciting field of experimental gravitation. James Clerk Maxwell in one conversation recorded by Joseph Larmor said that part of his purpose in writing his <u>Treatise on Electricity of Magnetism</u> after fifteen years' research in that field was to "educate himself by presenting a view of the stage he had reached." In so far as we may compare the activities of a research team with that of an individual of genius we may say that our purpose also in writing this long report has been in part self-education, and for this reason we have not hesitated to set down candidly our failures and mistakes as well as our successes. We hope it may be as useful to others as it has been to us.

Typing of the manuscript is due to Deborah A. Legge.

TABLE OF CONTENTS

LIST OF FIGURES

Frontispiece: Leonard Schiff and the Relativity Gyroscope Effects

LIST OF TABLES

A. INTRODUCTION

The idea that a gyroscope in orbit around a massive body would undergo a relativistic precession due to its orbital motion was first discussed by A. D. Fokker in 1921[1] following earlier calculations by W. de Sitter and J. A. Schouten. Fokker showed that the Earth's axis has a precession, additional to that deducible from Newton's theory, amounting to 0.019 arc-sec/year, due to the curvature of space produced by the sun's gravitational field. The motion of a spinning particle in General Relativity was afterwards investigated more completely by A. Papapetrou and others, and in 1960 L. I. Schiff[2] showed that a gyroscope in orbit around the Earth would undergo a precession

$$\Omega = \frac{3GM}{2c^2R^3} \; (\underline{R} \wedge \underline{v}) \; + \; \frac{GI}{c^2R^3} \left[\frac{3\underline{R}}{R^2} \; (\underline{\omega} \cdot \underline{R}) \; - \; \underline{\omega} \right] \qquad (1)$$

where $\underline{R}$ and $\underline{v}$ are the coordinate and velocity of the gyroscope and M, I and $\underline{\omega}$ are the mass, moment of inertia and angular velocity of the central body. The first term represents the spin-orbit coupling between the gyro and the Earth, commonly known as the geodetic precession. In a 400 nautical mile orbit it amounts to a drift-rate of the gyroscope of 6.9 arc-sec/year, measured with respect to the framework of the fixed stars. The second term represents the spin-spin coupling between the gyroscope and the Earth's rotation. It has sometimes incorrectly been called the Lense-Thirring effect. A better term would be the "Schiff motional effect."* In a satellite following an ideal 400 nautical mile polar orbit the motional effect on an appropriately oriented gyroscope is +0.05 arc-sec/year. In an equatorial orbit the effect is -0.1 arc-sec/year. The + and − signs denote whether the rotation is in the same or opposite sense as the Earth's rotation. Calculations similar to Schiff's but less complete were made at about the same time by G. E. Pugh.[3]

ᴨ

---

*S. Weinberg, Gravitation and Cosmology (New York 1972), p. 237, calls it the hyperfine term.

In 1961 Professors L. I. Schiff and W. M. Fairbank
of Stanford Physics Department submitted to NASA a short
non-funding proposal for an experiment to measure the
relativistic precession of an orbiting gyroscope.[4] The
proposal followed discussion with Professor R. H. Cannon
of the Stanford Department of Aeronautics and Astronautics.
A NASA-sponsored conference on tests of General Relativity
was held at Stanford in August 1961. In 1961 Mr. (later
Professor) B. O. Lange of the Aero-Astro Department proposed
a technique for compensating external non-gravitational
disturbances on a spacecraft by means of thrusters controlled
by signals derived from measurements of the location of an
internal shielded proofmass. The "drag-free satellite"
concept was put forward by others also, including G. E. Pugh
at the meeting just referred to, but the first systematic
analysis of drag-free satellite design was given in Professor
Lange's 1964 Stanford University Ph.D. thesis.

From the beginning Professor Fairbank had emphasized the
advantages of applying cryogenic techniques to the Gyro Rela-
tivity experiment. The first idea was a gyroscope based on a
magnetically supported superconducting sphere, similar to the
superconducting gyroscope then under development at G. E.
Schenectady by G. Buchholz and at JPL by J. Harding, but
employing a novel kind of readout based on the Mössbauer
effect. Some work on the Mössbauer readout was undertaken in
1962 by M. Bol, who also performed an experiment on the
"London moment" in a spinning superconductor as an outgrowth
of interest in magnetic torques on the superconducting gyro-
scope. The London moment, predicted in 1953 by F. London
following an earlier calculation by Becker, Sauter and Heller
in 1935, is a magnetic moment in a rotating superconductor
corresponding to a field magnitude

$$H_L = \frac{2mc}{e} \omega_s = 10^{-7} \omega_s \text{ gauss}$$

where e and m are the charge and mass of the electron and ω_s
the angular spin rate. Independent observations of the London

moment were reported by A. F. Hildebrandt in 1964 and by Bol and Fairbank and by King, Hendricks and Rohrschach in 1965.[5] Bol's experiments were the most complete since they included observation not only of the magnetic moment generated when a superconductor is spun up below its transition temperature, but also the spontaneous appearance of the same moment in a solid type I superconductor cooled through its transition temperature while spinning.

In October 1962 C. W. F. Everitt joined the Stanford Physics Department as a full-time Research Associate on the Gyro Relativity experiment under Air Force support. Shortly after arriving at Stanford he pointed out that the London moment itself might provide a basis for a gyro readout if a sufficiently sensitive magnetometer were available to measure the direction of the magnetic moment. He tentatively suggested using the Blackett astatic magnetometer. A more convenient approach was suggested by Professor Fairbank who proposed applying the vibrating plane magnetometer just then being conceived by Bol, Deaver and Fairbank.[6] Everitt and Fairbank then recognized that a gyroscope with a magnetic readout would be better served with an electric suspension of the type invented by A. Nordsieck in 1953 and marketed by Honeywell Incorporated rather than the superconducting magnetic support. With this the Gyro Relativity experiment took on essentially the conceptual shape it has today. One very critical development was to find an appropriate method of spinning up the gyro rotor. Eventually after many possibilities had been conceived and rejected, the gas spin up system now in use was worked out by T. D. Bracken and C. W. F. Everitt in 1967.[7] Further developments of the gyroscope are described in Sections C and D.

In March 1964 the National Aeronautics and Space Administration awarded Stanford University Grant NSG-582 in the amount of $180,000 retroactive from November 1, 1963 through October 31, 1964: "To Develop a Zero-G Drag Free Satellite and Perform a

Gyro Test of General Relativity in a Satellite." The research was to be performed jointly by the Department of Aeronautics and Astronautics and the Department of Physics. The Principal Investigators were Professors R. H. Cannon, Jr. (Aero-Astro) and W. M. Fairbank (Physics). Professor L. I. Schiff served as Project Advisor. The original research team included Dr. Everitt and Professor Lange; in September 1964, following the award of the NASA Grant the team was strengthened by the addition of Dr. D. B. DeBra and Messrs. J. C. Mathiesen and R. A. Van Patten to the staff of the Department of Aeronautics and Astronautics.

Concurrently with Grant NSG-582 the U. S. Air Force awarded $90K in support of the program. In the first year the Air Force funding was given to NASA for transmittal to Stanford as a supplement to NSG-582. Subsequently it was made part of Air Force Contract F33615-67-C-1245 in support of a broad based program in guidance and control at Stanford. The Air Force support continued at the $90K level for a number of years but was then reduced progressively over three years to $20K until it terminated in 1968.

The NASA identification NSG-582 was changed in 1968 to NGR-050-020-019. Initially, as the proposal title indicated, the program covered two distinct (though related) areas of research: development of a drag-free satellite and development of the Gyro Relativity experiment, the intention then and now being to perform the Gyro Relativity experiment in a drag-free satellite. The principal research on drag-free satellites per se performed under the combined NASA and Air Force funding comprised analytical studies, the design and construction of the GEM (Ground Effect Machine) two-axis air-bearing simulator of a drag free satellite, and the preparation of a proposal for a zero-g aeronomy satellite to be developed jointly between Stanford and UCLA. From 1967 the Electronics Research Laboratories Cambridge provided a contract to study geodesy research

with drag-free satellites. Support of this work was afterwards taken up by NASA Goddard Space Flight Center. In December 1969 Stanford submitted a proposal to Johns Hopkins Applied Physics Laboratory for a subcontract to "Develop and Build a Disturbance Compensation System (DISCOS) for the TRIAD II and III Satellites" (Principal Investigator: D. B. DeBra). The U. S. Navy's TRIAD II transit navigation satellite with DISCOS was launched in July 1972 and operated for nearly three years, attaining drag-free performance at the 5×10^{-12} g level. The TRIAD II is the only drag-free satellite operated to date.

With the transfer of support for drag-free satellite research to other programs the title of NGR-05-020-019 was changed in 1968 to a program "To Peform a Gyro Test of General Relativity in a Satellite and Develop Associated Control Technology."

The Gyro Relativity program has been supported throughout by SRT Funding from NASA-OSS, Astronomy Division under Dr. Nancy Roman. From 1964 through January 1970 Mr. E. J. Ott was Program Monitor. He was succeeded by Mr. C. Dixon Ashworth who remained associated with the program until his retirement from NASA in December 1973. In August 1970 NASA issued Contract No. NASW-2284 to Ball Brothers Research Corporation to perform a "Mission Definition Study of the Stanford Relativity Satellite." The study was completed in January 1971 (BBRC Report F71-07). Two further studies were performed by Ball Brothers in 1973 and 1975.

In 1967 Mr. Ott initiated a cooperation between Stanford and NASA George C. Marshall Space Flight Center, Huntsville, Alabama. The Marshall Center lead was provided by Dr. Rudolf Decher, then of the MSFC Astrionics Laboratory, later of the MSFC Space Sciences Laboratory. Practical cooperation began with the fabrication of gyro rotors at Marshall Center in the Manufacturing Engineering Laboratory (now the Engineering Physics Laboratory) under Mr. Wilhelm Angele. In 1969 NASA Marshall Center issued Contract No. NAS8-26312 "To Design Fabricate, Perform Tests, and Deliver Ceramic Envelopes in Support of

Electrostatic Gyro Development" to Honeywell Incorporated to
fabricate a ceramic gyro housing, following the earlier Stanford
subcontracts discussed in Section D (1) (a). In 1970 NASA
Marshall Center issued Contract No. NAS8-25705 to Stanford to
"Build and Test a Precision Star Tracking Telescope," with
fabrication subcontracted to Davidson Optronics Corporation.
In 1970 NASA Marshall Center issued Contract No. NAS8-27333 to
Stanford for "Fabrication of an Electronic Suspension Subsystem
(ESS) for a Cryogenic Electrostatically Suspended Gyroscope for
the Relativity Experiment." In 1971 administration of NGR 05-
020-019 was transferred from NASA Headquarters to NASA Marshall
Center with Mr. R. A. Potter as Program Monitor.

Research on the Gyro Relativity program falls roughly into
three periods. The principles of the experiment were worked
out conceptually between 1963 and 1967, during which period
a preliminary error analysis was completed showing the experiment
was capable of reaching 0.001 arc-sec/year accuracy. The years
1968 through 1974 were spent fabricating prototype hardware:
gyroscopes, gyro readout magnetometer, gyro suspension systems,
the star-tracking telescope and North Star simulator, ultra-low
magnetic field technology, a long hold time non-magnetic helium
dewar embodying many of the design features of the flight dewar,
a porous plug device for controlling the flow of liquid helium
in space, proportional helium thrusters for attitude control
and translational control, a fixed base simulator, and other
items. Demonstration of the London moment in a live gyroscope
supported on Earth in the ceramic housing was achieved in March
1975. From April 1975 through the termination of Grant NGR 05-
020-019 in January 1977 we have concentrated on developing an
ultra-low magnetic field facility for precision gyro readout
work, along with laboratory demonstration of integrating a
readout signal to the equivalent of 0.0024 arc-sec angular
resolution in 140 hours of observation time. Improved quartz
gyro housings have also been designed and are being fabricated

by the Speedring Corporation under contract from NASA Marshall Center. In cooperation with NASA Marshall Center and Rank Taylor Hobson of Leicester, England we have mounted a concerted attack on the problem of measuring and fabricating gyro rotors and housings to improved limits on sphericity and concentricity. ·

The following are the contributors to the Gyro Relativity program since 1964, excluding Principal Investigators:

Research Staff

J. T. Anderson
(Hansen Laboratories 1970-present: magnetometry)

B. Cabrera
(Hansen Laboratories 1975-present: ultra-low field technology)

R. R. Clappier*
(Aero-Astro 1968-present: electronics)

R. Hacker*
(Aero-Astro 1970-1976: mechanical design)

J. A. Lipa
(Hansen Laboratories 1969-present: gyro operations, cryogenic technology, experiment planning)

J. Mathiesen†*
(Aero-Astro 1964-1969: mechanical design)

J. R. Nikirk†
(Aero-Astro 1970-1975: electronics, gyro operations)

J. E. Opfer§
(Physics 1965-1969: magnetometry)

F. Rehsteiner
(Aero-Astro 1967-1970: attitude control thrusters)

D. Rose*
(Physics 1971: sputtering research)

F. J. van Kann
(Hansen Laboratories 1973-1976: precision gyro experiment)

R. A. Van Patten*
(Aero-Astro 1964-present: electronics and control design)

Visiting Research Staff and Faculty

D. P. Chandler*
(Aero-Astro 1967: control theory)

Joseph Eccher**
(Electrical Suspension System)

W. L. Pondrom, Jr.*
(Aero-Astro 1968-1970: control theory, telescope design)

J. M. Reynolds||*
(Physics 1968: cryogenics)

G. J. Siddall‡
(Hansen Laboratories 1976-present: roundness measurement,
 telescope testing)

Graduate Students

J. N. Aubrun
(Aero-Astro 1969: helium thrusters)

M. Bol
(Physics 1960-1966: London moment measurements, Mössbauer
 readout)

R. Bourke
(Aero-Astro 1961-1964: magnetic support of spinning
 superconductor)

T. D. Bracken
(Physics 1965-1968: gas spin up system)

J. S. Bull
(Aero-Astro 1968-1973: attitude control and thruster design)

B. Cabrera§
(Physics 1968-1975: ultra-low field technology)

D. DiPietro
(Aero-Astro 1969: magnetometer amplifiers)

Z. Hadass§
(Aero-Astro 1974: parameter sensitivity of control)

A. F. Hebard
(Physics 1964-1966: low magnetic field research)

D. Klinger
(Aero-Astro 1970-1973: fixed base simulation)

B. Nesbit
(Aero-Astro 1975-1976: sputtering)

B. Neuhauser
(Physics 1969-1970: magnetometry)

P. M. Selzer
(Physics 1967-1970: superfluid plug for space)

D. C. Wilkins§
(Physics 1968-1972: relativistic effects in perturbed orbits)

E. Wilson
(Physics 1966-1968: superconducting shielding)

J. Witsmeer
(Aero-Astro 1966-1967: attitude control)

P. W. Worden, Jr.
(Physics 1969-1970: inside-out dewar for magnetometer
amplifiers)

Undergraduate Students

J. Boca (Aero-Astro 1972)
D. Brown (Physics 1974-1975)
T. Edeli (Physics 1966-1967)
A. Katz (Physics 1976)
J. Napoleon (Physics 1965)
S. Ride (Physics 1972)

Technicians

H. Frosch*
(Aero-Astro 1972-1976: mechanical)

J. J. Gilderoy, Jr.
(Hansen Laboratories 1970-present: mechanical cryogenics)

F. Hill*
(Physics 1965-1971: electronics)

W. Holding, Jr.*
(Physics: 1970-present: electronics)

G. Jones*
(Aero-Astro 1967-present: electronics)

G. Sander*
(Physics 1968-1969: mechanical)

C. Smith
(Physics 1970-1974: sputtering)

J. Wassermann
(Physics 1968-1970: sputtering)

H. Wisniewski
(Aero-Astro 1970-1972: electronics)

Secretary/Administrative Assistant (half-time)

G. Clark (1968-1973)
I. C. Pereira (1973-1976)
D. A. Legge (1976-present)

* part-time

† deceased

§ working on the Gyro Relativity program but supported from
non-NASA sources

|| on sabbatical leave from Louisiana State University

‡ Lindemann Fellow

** on loan from Ball Brothers Research Corporation

B. DESCRIPTION OF THE EXPERIMENT

According to an error analysis by C. W. F. Everitt[8] present day technology offers the capability of making a gyroscope with a residual drift-rate under suitable orbital conditions of 10^{-16} rad/sec (6×10^{-4} arc-sec/year). Such performance, if achieved and if matched by the accuracies in other parts of the experiment, would lead to a measurement of the geodetic precession Ω^G to 1 part in 10,000 and of the Schiff motional precession Ω^M in polar orbit to 1 part in 70.

The gyroscope precessions are measured in the framework of the fixed stars. An experiment to measure them requires one or more gyros and a reference telescope pointed at an appropriate star. In addition to the principal terms there are three smaller relativistic effects measurable by a gyro with 6×10^{-4} arc-sec/year drift rate: (1) the geodetic precession due to the Earth's motion about the Sun (0.021 arc-sec/year), (2) the higher order geodetic term calculated by Barker and O'Connell[9] and by Wilkins[10] from the Earth's quadrupole mass-moment (0.010 arc-sec/year in a 400 nautical mile polar orbit), (3) deflection by the Sun of the starlight signal for the reference telescope. During the time of year when the line of sight approaches the Sun the starlight deflection superimposes on the gyro drifts an apparent motion away from the sun which reaches a maximum at closest approach. It can be extracted from the data by in effect turning the experiment around and using the gyros as reference for the telescope. For Rigel, which is 30° from the ecliptic plane, the maximum deflection is 0.016 arc-sec.

The data from the experiment also contain large periodic signals due to the annual and orbital aberrations of starlight. The annual aberration is $\pm$ 20.116 arc-sec in the plane of the ecliptic; the orbital aberration is approximately $\pm$ 5 arc-sec in the plane of the satellite orbit. These

signals which seem at first a nuisance turn out to be extremely useful in providing a built in reference signal of known amplitude for scaling the relativity signals. A further point of interest is that the experiment should yield a singularly precise measurement of the parallax of the reference star. It therefore has the potential of considerably improving our knowledge of the distance scale in the nearer region of the universe.

Various possibilities exist for the choice of orbit and the configurations of the gyroscopes. The simplest is an ideal polar orbit with two gyro pairs, one parallel and antiparallel to the Earth's axis and sensitive only to Ω^G, the other parallel and antiparallel to the orbit-normal and sensitive only to Ω^M. The telescope is then pointed at a bright star on the celestial equator orthogonal to both gyro axes. In reality no star is in the right place and no orbit is exactly polar. The Newtonian regression of the orbit-plane from the Earth's quadrupole mass-moment causes a mixing of terms, as a result of which some people have argued that the experiment cannot distinguish Ω^G and Ω^M unless the orbit is within a few arc-minutes of the poles. This opinion is mistaken; the nodal regression actually makes inclined orbits richer in relativity information than polar orbits. The information that can be extracted from different orbits depends on practical considerations briefly summarized below.

A better configuration is a spacecraft that rolls slowly around the line of sight to the star, containing two gyroscopes with axes parallel to the boresight of the telescope and two at right angles to the telescope and approximately parallel and perpendicular to the Earth's axis. As before one of the perpendicular gyros primarily sees Ω^G and the other Ω^M; both serve also as accurate roll references. With a star lying on the celestial equator and an ideal polar orbit the

two gyros parallel to the boresight see a signal periodic in the rollrate of amplitude $t \sqrt{_\Omega G^2 + _\Omega M^2}$ and phase $\tan^{-1} \Omega^M/\Omega^G$. The method of carrying through the separation of terms in inclined orbits with real stars is discussed below. The advantage of the configuration is that torque on the gyros and drift in the gyro and telescope readouts are strongly averaged by roll. The roll period may be about 10 minutes.

Figure 1 is a general view of the experiment. The experimental package comprises a telescope, four gyroscopes and a proof mass for a drag-free control system. For mechanical stability all these parts are made from fused quartz, optically contacted together and maintained at liquid helium temperatures to eliminate thermal distortion. The apparatus is mounted in an evacuated chamber inside a superinsulated dewar vessel, containing about 800 liters of liquid helium, designed to maintain cryogenic temperatures for about two years. Boil-off of liquid helium is controlled by a porous plug device invented by Selzer, Fairbank and Everitt.[11] The gyroscopes are quartz spheres, coated with superconductor and suspended electrically in a quartz housing attached to the telescope. Each gyro is surrounded by a spherical superconducting magnetic shield. The telescope is a folded Schmidt-Cassegrainian system of 5.5 inch aperture and 150 inch focal length, also made entirely of fused quartz.

Pointing control of the spacecraft is based on signals from the telescope, switched automatically to the gyroscopes during the portion of each orbit when the star is occulted. Thrust is obtained from the helium boil-off from the dewar, which is copious enough to mechanize in a very smooth proportional control system. Drag-free control is mechanized through the same thrusters referenced to the internal proofmass. Making the satellite drag-free helps in two ways: it improves averaging of residual accelerations on the gyroscopes and it reduces errors in the orbit determinations needed in analysing relativity data.

INSTRUMENTATION

GYRO

ZERO-G PROOF MASS

FILL LINE

CRYOGENIC ACTUATORS

TELESCOPE

He

He

GOLD COATED WINDOWS

DEWAR WITHIN DEWAR

HEAT EXCHANGERS

ATTITUDE CONTROL JET (1 OF 12)

SUPERINSULATION

SUPERFLUID PLUG

0   12
INCHES
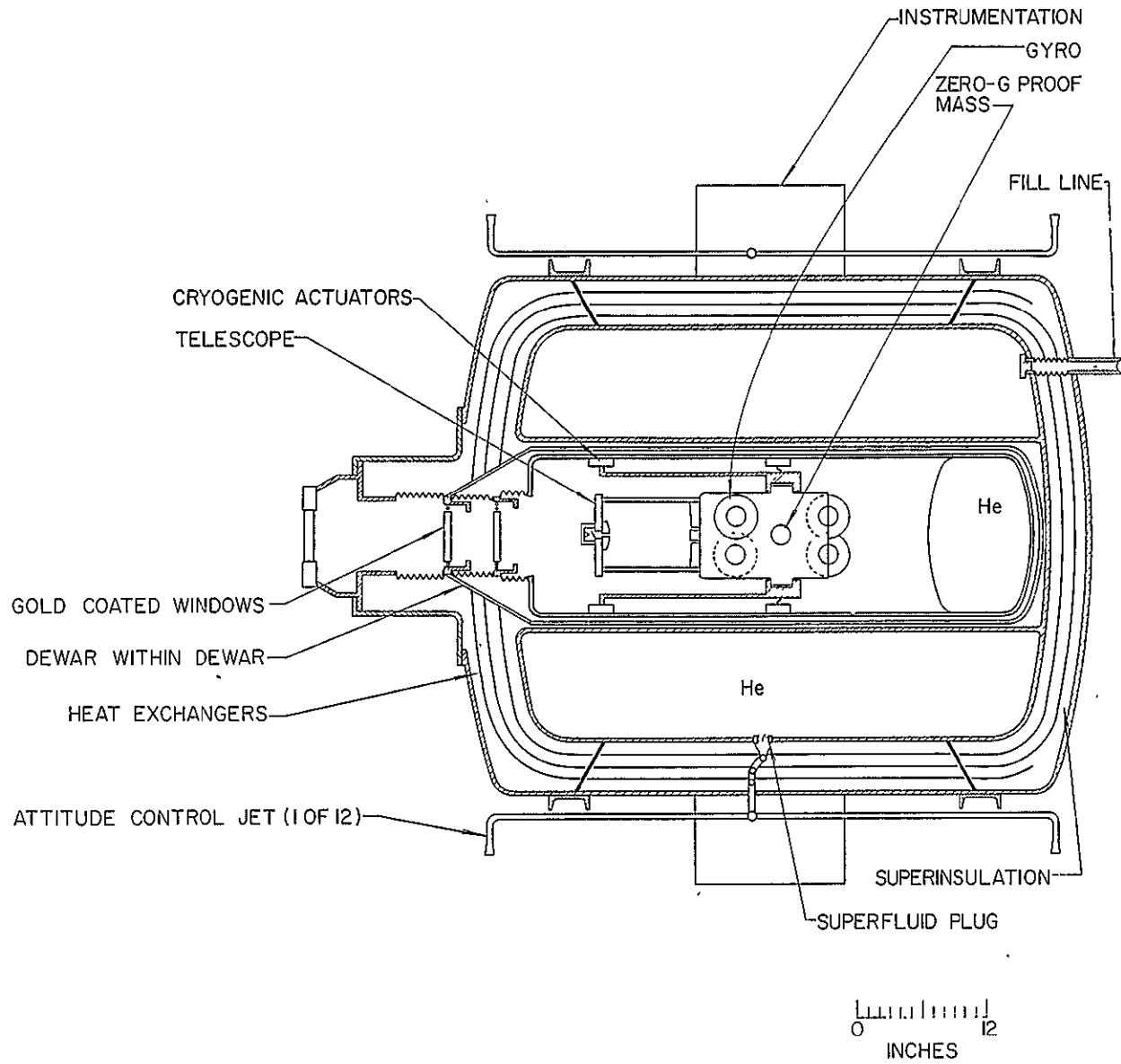
Figure 1: Gyro Relativity Satellite: Cross-Section

Figure 2 illustrates the solar panels and electronics boxes mounted on a girth-ring around the outside of the dewar, together with the sunshield to prevent stray light entering the telescope when the line of sight passes near the sun. The sunshield is designed for operation with Rigel as the guide star. The configuration of the solar array, due to R. E. Woolley of Ball Brothers Research Corporation, was chosen to yield maximum average power through the year, again with Rigel as guide star. A fixed array is greatly to be preferred to a steerable one, despite the reduction in power for a given area, in view of the critical importance of avoiding disturbance to the spacecraft. The paddles are arranged in two oppositely canted pairs to prevent the spacecraft from turning into a radiation pressure mill. For details on spacecraft design see the Ball Brothers Research Corporation 1971 Mission Definition Study.[12]

The spacecraft is launched into the chosen orbit by a Delta or Shuttle vehicle. After launch the reference star is located and acquired by one of two standard procedures discussed in the Study; the gyros are then suspended and spun up. Spin-up takes about half an hour. During this time the satellite is rolled about the line of sight to the star at a fairly rapid rate (roll period 30 to 60 sec) to help align the spin axes with the line of sight to the star. Spin-up is done with gas pressures between 10 and 20 torr after which the gas is pumped out and the gyro is allowed to coast freely in a 10^{-9} torr vacuum. The roll is then stabilized at its normal period which is probably about ten minutes. Procedures exist for refining the gyro pointing if the high speed roll has not achieved the few arc-second alignment required for the experiment.

The heart of the experiment is the gyro-telescope package. Gyro development is reviewed in Sections C, D and E; telescope development in Section G. Given gyro and telescope designs of adequate drift performance and readout sensitivity to reach the goal of 1 milliarc-sec/year, much remains to be done before

ELECTRONICS BOX

THRUSTERS

FAN BEAM SOLAR SENSOR

STAR SENSOR

ANTENNA

DEWAR

SUN SHADE

ATTACH FITTING

TO STAR

HELIUM TANK SUPPORTS

SOLAR ARRAY PADDLE

15
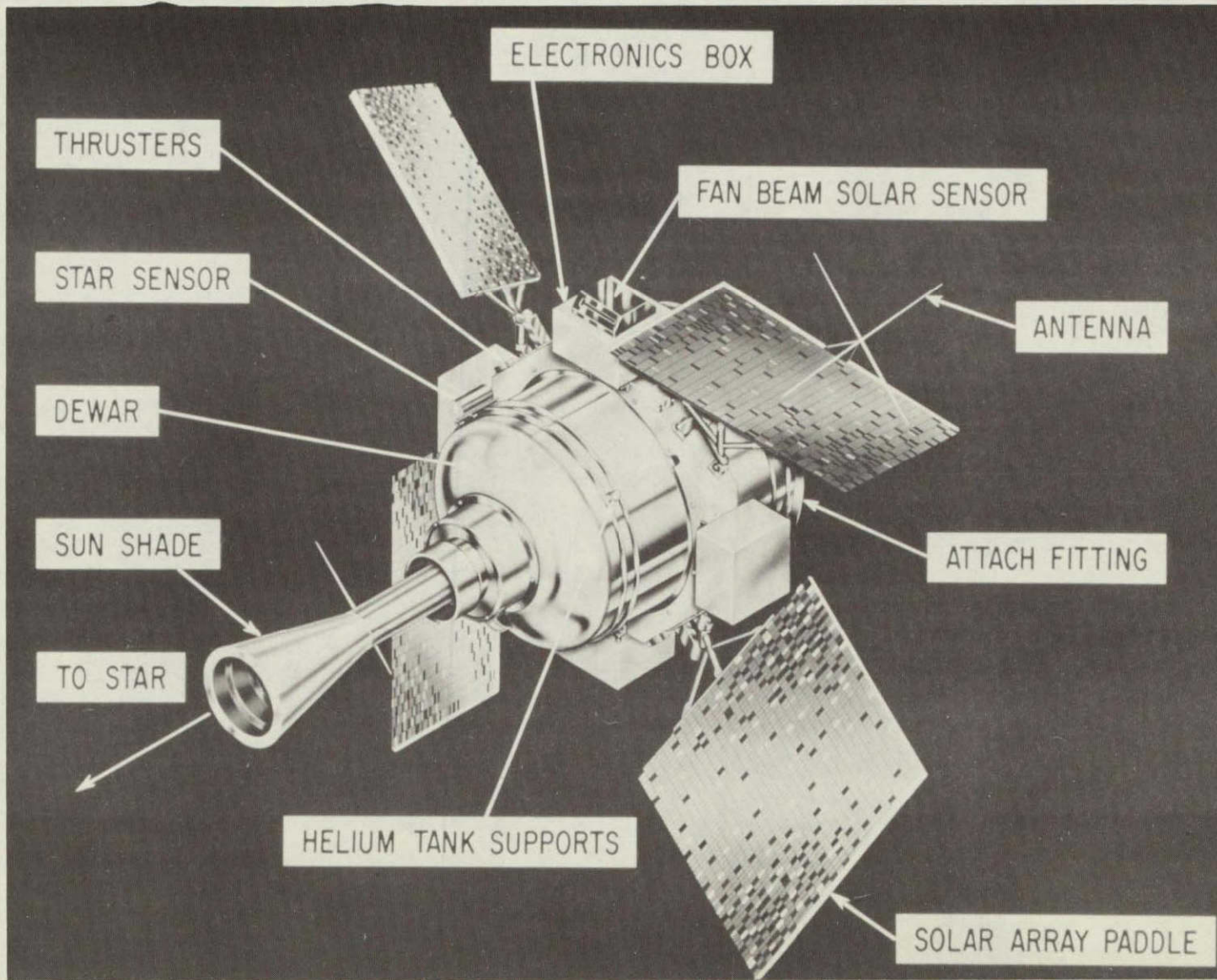
Figure 2: Gyro Relativity Satellite: General View

obtaining satisfactory relativity data. The chief problems are:

(i) devising a data instrumentation system to ensure
proper scaling and subtraction of the gyroscope and telescope
signals

(ii) establishing criteria for drag-free control and attitude
control, designing control systems which meet the criteria and
incorporate safeguards to preserve gyro suspension and prevent
accumulation of false data if the spacecraft is struck by micro-
meteorites or the telescope chases off after a flare caused by
sunlight falling on a speck of dust in the line of sight

(iii) establishing tracking requirements and an algorithm
for calculating the expected relativity signals in the actual
satellite orbit.

The requirements on pointing control and instrumentation
are determined by the form of the gyro and telescope readouts.
The gyro readout, being based on measuring the current generated
in a superconducting loop by a change of orientation of the
London moment can be made extremely linear so long as the spin
axis lies near the plane of the loop. The limit is ultimately
the limit on linearity of the electronics systems, which in
practice may be 16 or 17 bit. With 17 bit accuracy a readout
capable of resolving 0.5×10^{-3} arc-sec has an effective linear
range of $\pm$ 32 arc-sec. The possibility does exist, and is dis-
cussed in Section C (3) (ℓ) of applying flux counting techniques
in SQUID magnetometers to improve the resolution to 24 or 25
bits,[13] but this is not required, and is probably best avoided,
in the present experiment.

The telescope, unlike the gyroscopes, has very limited
linear range. The particular design chosen depends on locating
the centers of two focused diffraction limited star images,
which for the 5.5 inch aperture used have an effective angular
diameter of 0.9 arc-sec and give signals linear to 0.5×10^{-3}

arc-sec over the central 0.05 arc-sec range. Although the
linear range may in principle be increased either by defocusing
the image or by having encoded tipping plates in the converging
beam, in practice neither idea is a good one: it is best to
accept the limitation on the telescope and work around it. The
plan is therefore to point the telescope always within ± 0.05
arc-sec of the apparent position of the star, and take up all
the remaining displacements between the gyro and star, including
the aberration of starlight, in the gyro readout. With a ± 32
arc-sec linear range for the gyro, this procedure is just feasible
provided the null planes of the gyro and telescope readouts are
aligned to within a few arc-seconds.

A preliminary analysis of the spacecraft attitude control
system by D. B. DeBra in 1966 indicated that with the compliances
in the spacecraft structure then expected the control system
would be hard put to maintain pointing to better than 1 arc-sec,
a factor of 20 less precise than is needed. Consideration of
this problem led C. W. F. Everitt to suggest in 1967 the addition
of an inner fine pointing servo loop acting directly on the
gyro-telescope package, using cryogenic magnetic forcers as
illustrated in Figure 1. A possible mechanization for such
a two loop system was suggested and analysed by R. A. Van Patten
and reviewed by D. P. Chandler,[14] after which a detailed analysis
and laboratory simulation of the loop system was performed using
modern control theory by J. S. Bull and D. B. DeBra,[15] who
established pointing accuracies well within the required ± 0.05
arc-sec range in the presence of telescope noise and normal
satellite disturbances. Sensitivity to parameter changes was
investigated and model helium thrusters were built and tested
on line with an analogue simulation of the control system and
plant.

In 1967 satellite pointing to better than 1 arc-sec
seemed unbelievable. The two loop system, by transferring the
burden from the satellite attitude control system to the inner

fine pointing servo, had the dual merit of being technically
sound and also having a certain sales appeal to persons familiar
with attitude control systems. As time has gone on, attitude
control systems have tended to improve, making the sales pitch
easier, while the design for the relativity satellite has also
advanced, allowing us to take less conservative numbers for
the compliance between the helium well and the outer shell of
the dewar vessel. Eventually one asks whether $\pm$ 0.05 arc-sec
pointing might not become feasible without the inner servo,
simplifying the design of the pointing controllers and saving
development costs for cryogenic actuators. Reviews performed
in parallel at Stanford and Ball Brothers Research Corporation
between 1970 and 1972 suggested that we might indeed be able
to get away without the inner loop. A final decision has to
be based on analysis of the final satellite layout.

Given pointing within the linear range of the telescope
the next problem is the data instrumentation system to subtract
the gyro and telescope signals. Figure 3 illustrates the prin-
ciples of the system conceived by R. A. Van Patten.[16] The
heavy lines represent an integrating data loop which supplies
continually updated relativity information in digital form,
after subtracting and summing the gyro and telescope signals
with the final signal in the precision summing amplifier Σ_1.
The output of Σ_1 consists of an amplitude-modulated suppressed-
carrier alternating current signal. This signal is processed
in a sampling demodulator and filter to obtain a direct current
output with extremely low zero offset, and then integrated by
means of a 17 bit up-down binary counter, which contains the
readout signal for storage and telemetry. The integrating loop
is closed via a 17 bit digital to analog converter summed into
Σ_1. Its operation may be understood as follows. Call the gyro
output G, the telescope output T and the signal in the up-down
counter R. The summing amplifier provides the function (T-G+R)
which is maintained at null, making the final signal R equal to
(G - T), the quantity of interest in the experiment.
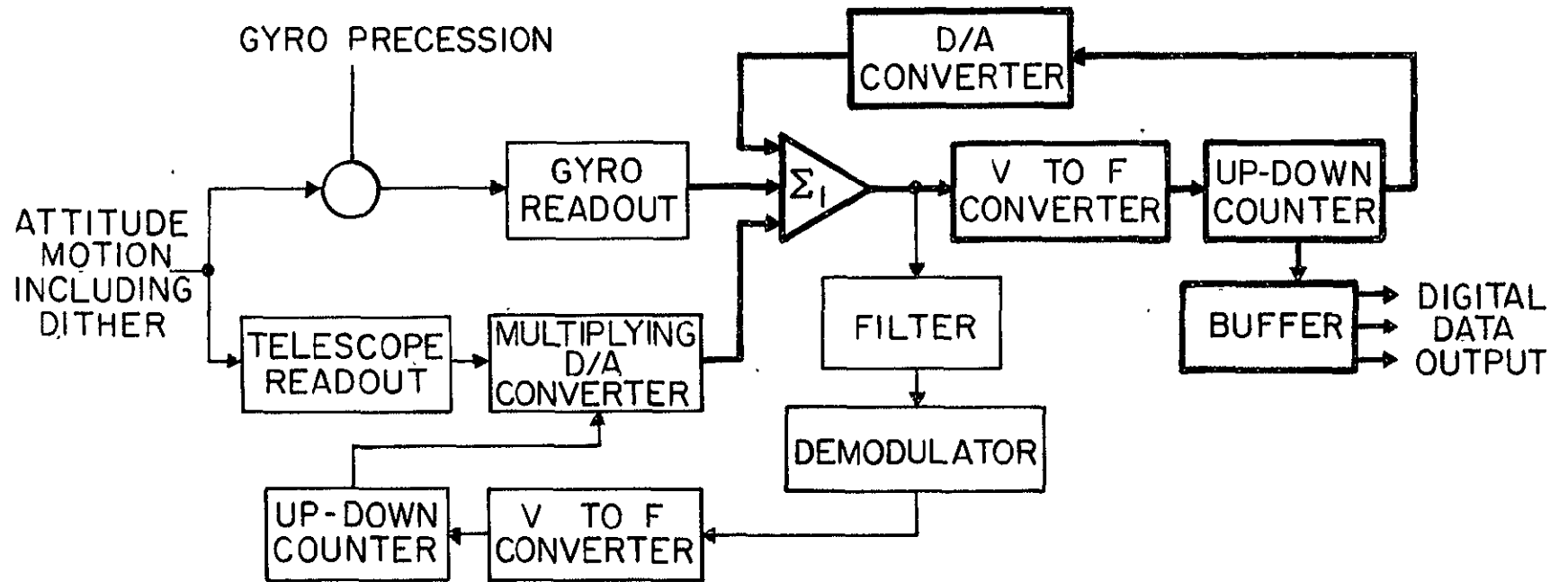
Figure 3: Principle of Relativity Data Instrumentation
System

To avoid error, the scale factors of the gyro and telescope readouts have to be carefully matched; for differences in scale factor will lead in the presence of a pointing error Δ' to a null shift identical in form with the relativity signal. If the nominal scale factor of each readout is k, but there is a difference Δk between them, the upper limit on $\Delta k/k$ is θ_o/Δ' where θ_o is the maximum allowed angular error. Hence if the pointing servo has an offset of 0.03 arc-sec the maximum scaling difference to keep the error below 5×10^{-4} arc-sec is 1.5%.

Various techniques have been studied for forcing the scale factors of the gyro and telescope readouts to a common value.[17] The cleanest method, suggested by R. A. Van Patten, depends on introducing a low frequency dithering motion into the pointing servo (see Figure 3) to make the entire gyro-telescope packing swing back and forth across the line of sight to the star with an amplitude of about 0.03 arc-sec at 0.1 Hz. If the scale factors of the two readouts are not equal an 0.1 Hz signal appears at the output of the summing amplifier Σ_1 where it is synchronously detected, and integrated by means of a voltage to frequency converter and up-down counter to provide a digital signal driving a multiplying digital to analog converter which scales the telescope readout in the manner shown in Figure 3. An analysis due to the late J. R. Nikirk[18] shows that the system may be designed to maintain 1% scaling accuracy with reasonable settling time in the presence of gyro noise.

Signals are taken from the telescope output for use in attitude control electronics. Since the telescope bore sight lies in the orbit plane the star is occulted during half of each orbit. During this and other interruptions such as the occasional visual flare or meteorite impact, control logic is activated to inhibit the telescope output T and refer the controller to the equivalent function (G - R) which is available from the instrumentation system. Thus the telescope remains

pointing in the correct line of sight by reference to the gyroscope. Reacquisition and resumption of measurement occurs automatically when the telescope is turned on again. The only loss is the immediate loss of data for the final statistical analysis.

In the actual rolling satellite, encoders and resolvers are added to the data instrumentation system to unroll and process the signals for both parallel and perpendicular gyroscopes. Figure 4 shows the instrumentation system as mechanized for two gyroscopes with spin axes parallel to the telescope axis. It provides four 17 bit digital readouts, two for each gyro. By combining the data with 19 bit roll angle information obtained from the two perpendicular gyro-scopes, measurements of both geodetic and motional relativity effects are obtained from each gyro. Drift errors in either the gyro or telescope readout are rejected in ground proces-sing by identification with the satellite roll period. Figure 5 shows the instrumentation system for the perpendicular gyro-scopes. It provides two 17 bit readouts one for each gyro, of which one yields geodetic data and the other motional data. The gyro readout signals in the two channels stay essentially fixed in inertial space but the telescope signals, being referred to the body coordinates of the rolling spacecraft, must be resolved into inertial coordinates before processing. Conversely the control signals for calibrating the telescope scale factor against the gyro have to be converted back to body-fixed coordinates before closing the gain control loop. For the perpendicular gyroscopes drifts in the gyro readout cannot be simply distinguished from relativity data but drift of the telescope readout can be identified with the roll period and rejected in data processing.

All portions of the data instrumentation system may be made with solid state integrated circuiting for maximum reliability. The choice of time constant for the integrating
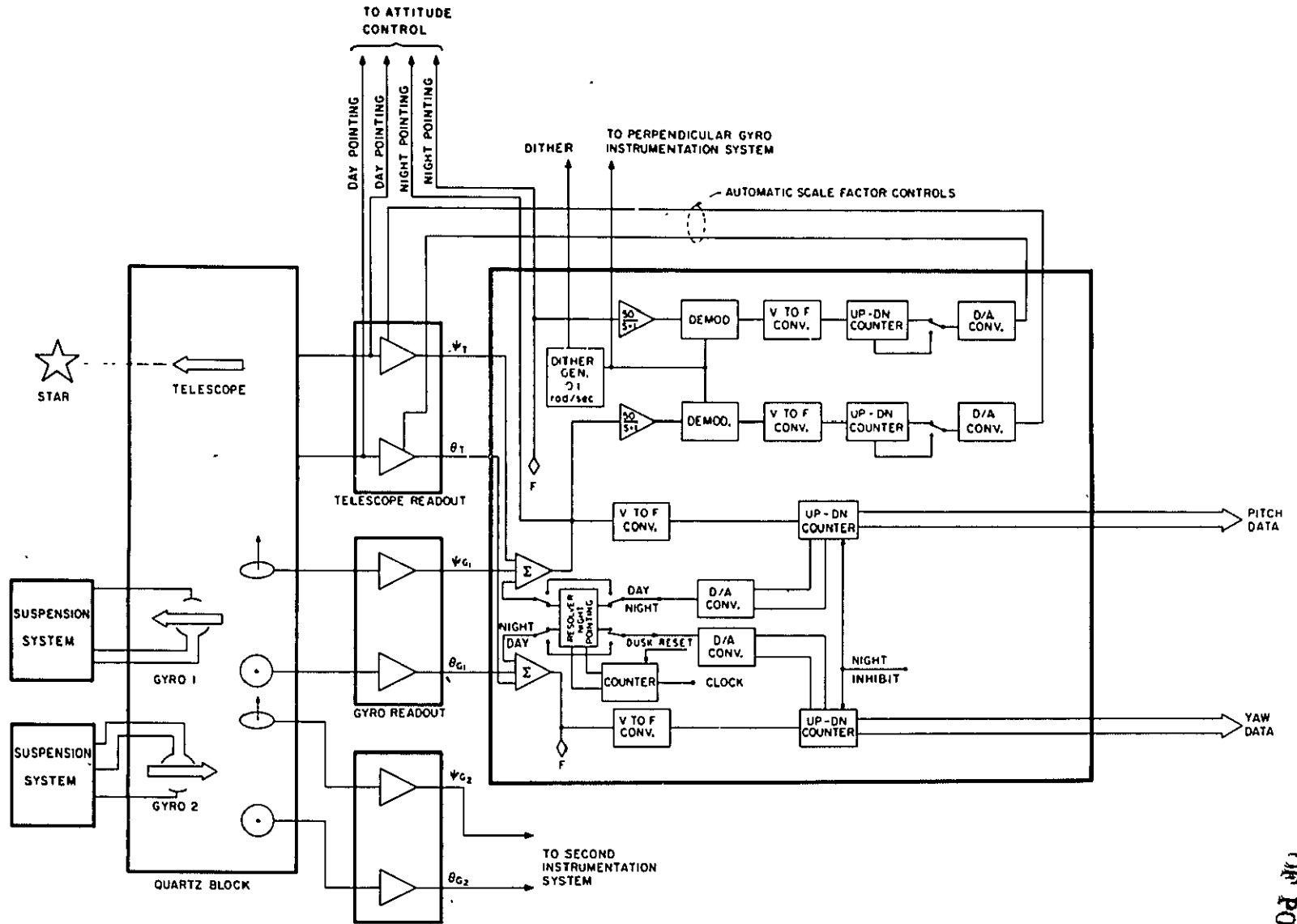
Figure 4: Parallel Gyro Instrumentation System
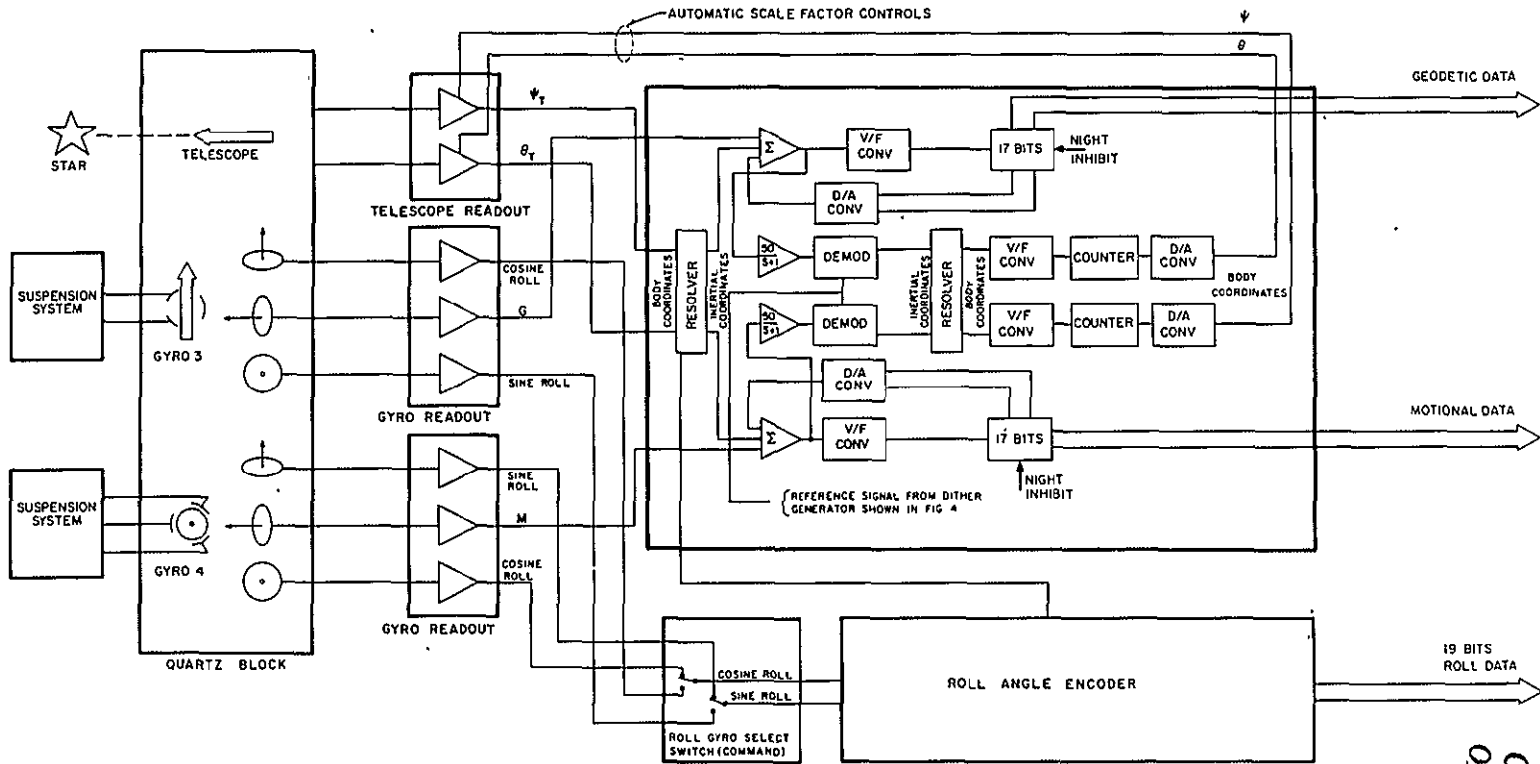
Figure 5: Perpendicular Gyro Instrumentation System and Roll Angle Encoder

23

loop depends on several factors. The optimum appears to be about 20 seconds. This is long enough to give substantial noise filtering while allowing recovery from interruptions within one or two minutes. The output is sampled every few seconds and stored in a core memory containing 10^4 words of 17 bits, from which it is transmitted once per orbit for further processing on the ground.

With a time constant of 20 seconds the output of the data loops consists of

(1)   the geodetic and motional relativity signals higher order terms

(2)   annual aberration of 20.116 arc-sec amplitude in ecliptic plane

(3)   99.98% of the orbit aberration in the orbit plane

(4)   residual gyro and telescope readout noise.

A beautiful feature of the experiment is that the aberration signals, being known with great precision, calibrate the data. Thus the telescope scale factor (which may be expected to change through effects such as aging of the photomultiplier and tarnishing of the mirrors) is driven automatically to the same value as the gyroscope by the dithering technique, while the gyroscope scale factor (which should remain constant) is automatically checked and calibrated in space by the aberration signals. The importance of exploiting the aberration data becomes clear if one reflects on the difficulties of calibrating any angular measurement system in the laboratory to 0.001 arc-sec absolute accuracy.

The algorithm for calculating the relativity signals in the actual satellite orbit is described in a Stanford University memorandum by D. C. Wilkins.[19]   Related calculations have been published by B. M. Barker and R. F. O'Connell.[20]   Applying Geyling's method Wilkins has shown that the relativity equations can be legitimately integrated over a single orbit, but that the

approximations break down after a few orbits, so that it is necessary to proceed by piecewise fitting of data from each orbit applying tracking information obtained every few passes. The tracking requirements for an 0.001 arc-sec/year experiment are as follows: (1) maximum allowed error in measure of orbit radius r_c ∿ 1/2 mile, (2) in track velocity error ∿ 1/2 mile/ hour, (3) error in right ascension of ascending node ∿ 30 arc-sec, all of·which are comfortably within the performance of existing tracking networks.

In off-polar orbits, the motional and geodetic terms become mixed through the Newtonian regression of the orbit plane due to the Earth's oblateness. Separation of Ω^M and Ω^G is further complicated by the action of the Earth's gravitational gradient on the quadrupole mass moment of the gyro rotor, which·causes a torque in the plane formed by the gyro spin axis and the orbit normal with a resultant secular drift rate in a circular orbit of radius R

$$\dot{\Omega}^g = \frac{3}{4} J_2 \frac{GM}{\omega_s R^3} \sin 2\beta \tag{2}$$

where J_2 is the quadrupole coefficient of the gyro rotor and β the angle between the spin axis and orbit normal. Equation (2) is identical with Laplace's formula for the precession of the equinoxes. For the quartz gyro rotor used in the experiment J_2 has components of order 10^{-7} from the inhomogeneities and polishing errors of the ball, which are not well known, and a component magnitude about 3×10^{-6} due to centrifugal distortion of the ball at its 200 Hz spin speed. The magnitude of the centrifugal J_2 is known to about 1%. In a polar orbit with the gyro spin axis lying in the orbit plane Ω^g vanishes, but in a 45° orbit the centrifugal J_2 causes a drift rate corresponding in the worst case to about 30×10^{-3} arc-sec/year.

The presence of Ω^g and the mixing of Ω^G and Ω^M through nodal regression have persuaded some people that the experiment can only be done in a polar orbit and quite severe constraints

on inclination angle have been written down in various papers. Several of the published statements are fallacious. A fairly complete discussion of the problem has been given by Everitt in an unpublished document,[21] to which reference should be made for further information. The separation of terms has to be handled differently in near-polar and steeply inclined orbits, depending whether the regression period is longer or shorter than a year. Both cases will be summarized. To sharpen the discussion we consider the effects in near polar, 37° and 28.5° minimum energy orbits from Wallops Island and Cape Canaveral, giving numerical values for each.

The launch accuracy obtainable with a Thor-Delta vehicle yields (according to 1971 figures quoted in Table 7.5 of Reference (12)) an inclination error of 0.04° and an error of right ascension of the ascending node of 0.5°; both with 3σ accuracy. These figures were predictions before the DIGS guidance system was put into use in mid 1972. Recent information from the NASA Delta Office at Goddard Space Flight Center confirms the figure 0.04° for the inclination error, but puts the error in ascending node (which is determined by the launch window and the burn characteristics of the rocket) as somewhat less than the quoted figure, perhaps 0.2°. Since the predictions are to 3σ accuracy the probability of doing better is high: about 300 to 1. From the standard equation for nodal regression about the oblate Earth, a 400 nautical mile orbit inclined 0.04° from the pole regresses or advances 1.7° in a year. The total deviation between gyro spin axis and orbit plane for a polar orbiting experiment may, in unfavorable circumstances, amount to 1.9° at the end of a year. The gravity gradient drift Ω^{g} from the elliptical distortion of the ball is then 2.5×10^{-16} rad/sec or 1.5 milliarc-sec/year and should be corrected for.

We now identify the contributions of Ω^{G}, Ω^{M} and Ω^{g} to the precessions of parallel and perpendicular gyroscopes in a near-polar orbit.

Define a reference plane POS, through the pole P and center O of the Earth, and the true position S of the star, along with a second plane NOS, also intersecting the line OS but orthogonal to POS. Complete the system of coordinates by a line OP' lying in POS and orthogonal to NOS. The angle POP' is ζ the elevation of the reference star above the celestial equator.

The telescope points nearly along OS, but not quite because of attitude control errors ($\pm$ 0.05 arc-sec), the relativistic correction for bending of starlight by the Sun (a maximum of 0.016 arc-sec for Rigel), orbital aberration ($\pm$ 5 arc-sec) and annual aberration ($\pm$ 20 arc-sec). The gyroscopes remain nearly parallel or perpendicular to the mean direction of the telescope at gyro spin-up, but not quite because of initial misalignment (about 1 arc-sec) and relativistic drift (about 6.9 arc-sec). Depending then on initial conditions chiefly on the magnitude of the component of annual aberration existing at spin-up, the different gyro axes are inclined at angles γ, γ', γ'' to the lines ON, OP', OS, having maximum values somewhere between 10 arc-sec (0.0028^O) and 30 arc-sec (0.0083^O). These deviations of the gyro axes from the coordinate axes should be noted, though they will prove negligible in the remaining calculations on the effects in near polar orbit.

The orbit-plane is initially misaligned with the plane POS in both right ascension ϕ_0 and inclination i. It is convenient to use the co-inclination $i' = \frac{\pi}{2} - i$ since it is a small angle for a near polar orbit. During the year i' remains constant with respect to the Earth's polar axis OP, but the nodal line advances or regresses through an angle $\phi = \omega_n t$, where ω_n is given by the nodal regression formula. Consider any orbit near enough to polar for the sines of i' and ($\phi_0 + \omega_n t$) to be approximated by the angles. Observe that for Rigel $\sin\zeta$ is 0.142 and $\cos\zeta$ is 0.99. Observe also that ϕ after one year amounts to 40 i in a 400 mile orbit and that the probable value of ϕ_0 is about five times the probable value of i. We

have then the following:

(i)   For the parallel gyros (the ones nearly aligned with OS) the angle β between the gyro axes and the orbit-plane is $\sqrt{(\phi_0 + \omega_n t)^2 \cos^2\zeta + i'^2 \sin^2\zeta}$, which reduces to $(\phi_0 + \omega_n t)$ to within 1%, the error from neglecting the deviation γ between OS and the gyro axes being between 0.2% and 0.5% if $(\phi_0 + \omega_n t)$ is 1.9°.

(ii)   For the perpendicular gyro aligned with ON the angle $(\frac{\pi}{2} - \beta)$ is also very nearly $(\phi_0 + \omega_n t)$.

(iii)   For the perpendicular gyro aligned nearly with OP' the angle β is $\sqrt{(\phi_0 + \omega_n t)^2 \sin^2\zeta + i'^2 \cos^2\zeta}$, where the two terms within the square root are now comparable but the total value of β is much less than for the other two gyros: about 0.06° rather than 1.9°.

(iv)   The gravity gradient precessions $\Omega^{g'}$ in the different gyroscopes are found by substituting the β's into Equation (2). The admixture of Ω^G to the precessions of the gyroscopes in the plane NOS is found by resolving the orbit-vector into components along ON, OP', OS. Since the Earth's rotation axis lies in the plane POS, there is no admixture of Ω^M to the components of precession in that plane: there are in principle corrections due to the gyro misalignments γ, γ', γ'' and the telescope motions, but they are utterly negligible.

Collecting results we find the precession angles for parallel and perpendicular gyroscopes in near polar orbit are to a sufficient approximation given by the four terms in Table 1. The results are all referred to the system of planes PSNO defined by the Earth's polar axis OP, the line of sight OS to the star and the normal ON to the plane POS.

Table 1:   Precession Angles of Gyroscopes in Near Polar
Orbit Around Oblate Earth

Parallel Gyros

Motion in plane POS
through Earth's axis
and line of sight to
star (nearly coincident
with orbit plane)

$$\theta^S_{POS} = (\Omega^G \pm A^g \phi_0)t \pm A^g \omega_n t^2$$

Motion in plane NOS
through line of sight
to star and orthogonal
to POS

$$\theta^S_{NOS} = (\Omega^M \cos\zeta \pm \Omega^G i')t$$

Perpendicular Gyros

Gyro nearly aligned
with Earth's axis.
Drift in plane POS
(the "near-orbit"
plane

$$\theta^{P'}_{POS} = \Omega^G t \pm A^g t \sqrt{(\phi_0 + \omega_n t)^2 \sin^2\zeta + i'^2}$$

Gyro nearly aligned
with orbit normal.
Drift in plane NOS.

$$\theta^N_{NOS} = (\Omega^M \cos\zeta + \Omega^G i')t$$

Ω^G, Ω^M – geodetic and motional drift rates

A^g – gravity gradient coefficient $3/2\ J_2\ GM/\omega_s R^3$ (i.e. twice
the term multiplying $\sin 2\beta$ in Equation (2). The $\pm$ sign
indicates that the term is in opposite senses in gyros
with opposite angular momenta

ϕ_0 – initial error in ascending node, i – initial error in
coinclination, ζ – elevation of star above celestial
equator

ω_n – nodal regression rate

In θ^S_{POS} the term in $A^g \phi_0$ amounts to 2×10^{-4} arc-sec/year if ϕ_0
is 0.2^o; in $\theta^{P'}_{POS}$ the complicated term in A^g has a maximum of
$8. \times 10^{-5}$ arc-sec/year if i' is 0.04^o, ϕ_0 0.2^o and $\omega_n t$ 1.7^o.
Both terms therefore are negligible in a 1 milliarc-sec/year
experiment. The contributions of A^g to θ^S_{NOS} and θ^N_{NOS} are too
minute to be worth writing out formally: their magnitudes
are about 8×10^{-7} arc-sec/year. Thus the only significant
gravity gradient effect in a polar-orbiting experiment is the

term involving $A^g\omega_n$ in θ^S_{POS}. Unlike the two relativistic
terms it is quadratic rather than linear with time.

It may seem odd that the term in θ^N_{NOS} involving A^g is negli-
gible since the gyro axis is noticeabley misaligned with the
orbit plane. For this gyroscope the gravity gradient drift lies
predominantly in the plane NOP' not NOS; it affects the roll-
reference of the satellite (negligibly) but has no influence
on the relativistic measurement. In fact for the Gyro Relativity
experiment in its original forms with perpendicular gyros only,
the gravity gradient drifts would not interfere with the rela-
tivity measurement in either gyro.

To summarize, the only possibly significant gravity-gradient
term is the one quadratic in time which appears in the plane
POS for the parallel gyros. Assuming that an exact polar orbit
is attempted the probability of an orbit error enough to make
the effect perceptible is 0.3%. If such an error occurs it
will be known from tracking observations, and -- "thrice to
slay the slain" -- the effect can be eliminated in three ways:

(i) by direct calculation to 2% accuracy from the known
magnitude of the centrifugal J_2

(ii) by observation of its occurrence in opposite senses
in the two gyros, the magnitudes of the two terms being equal
to about 2%

(iii) by data processing to identify and remove any term in
the gyro readout that is quadratic with time.

Substitution of numerical values in Table 1 shows that
the geodetic contribution $\Omega^G i'$ to the gyro precessions in the
plane NOS is about 10% of the motional term $\Omega^M \cos\zeta$ if i' is
0.04^O. From the measurement in the plane POS Ω^G is known to
1 part in 7000. The standard NASA minitrack system determines
right ascension and inclination to 10 arc-sec per orbit. The
co-inclination i' is therefore known easily to 7%, and the

error in Ω^M due to the admixture of Ω^G is less than 0.7%, which is small compared with the design goal of 2% accuracy for the measurement. Observations over many orbits with a drag-free satellite should pull down the error much further.

A near-polar orbit has obvious merits for the Gyro Relativity experiment, because of the neat separation of terms. In the space business, however, one cannot always get what one wants when one wants it, so it is useful, as well as intellectually stimulating, to examine other orbits, in particular the 37° and 28.5^O minimum energy orbits from Wallops Island and Cape Canaveral.

Before examining the real problems of an experiment in an inclined orbit it is as well to dispose of some of the more superficial objections. It has been argued that the straight-forward separation of the terms Ω^G and Ω^M is lost in a non-polar orbit. True, but that does not imply that experiments in other orbits give no information about Ω^G and Ω^M. Consider the simplest alternative to the polar-orbiting experiment: a spacecraft moving in a pure equatorial orbit with the gyro spin axes lying in the orbit-plane. The gyroscopes would measure the sum or difference $(\Omega^M \pm \Omega^G)$ of the two terms, depending on the sense of the orbit, and the agreement or otherwise of the result with Einstein's theory would be a significant event. Agreement would confirm the theory nearly as convincingly as the polar-orbiting experiment. Disagreement would surely lead to another flight, presumably in a polar orbit; and then the existence of data from different orbits would be an advantage not a disadvantage. Indeed a merit of the equatorial orbit is that the motional effect there is roughly twice what it is in a polar orbit. From that one might argue that if NASA were committed in advance to flying two experiments, the best choice, or if not the best at any rate a very good choice, would be to fly them in opposite equatorial orbits, and compute Ω^G and Ω^M from the sum and difference of the two results.

In an inclined orbit Ω^G and Ω^M are even more mixed up, and the situation is complicated by the regression of the orbit-plane. There is however a chance of twisting around the apparent disadvantages into an advantage by exploiting the nodal regression to separate the terms.[8] Practical barriers have to be surmounted to achieve this happy end; they will be discussed below; for the moment they can be ignored to concentrate on principles.

Consider a typical inclined orbit, say a 400 nautical mile 37° orbit. The nodal regression period $2\pi/\omega_n$, calculated from the standard formula, is 62 days. The outputs of Ω^G and Ω^M become a mixture of linear and sinusoidal terms whose forms are explained below. The period of the sinusoidal terms is 62 days; the predicted amplitude of the largest, a component of the geodetic precession in the vertical plane, is 0.224 arc-sec. Small though this is it can in principle be measured accurately enough to use in combination with the linear terms to separate Ω^G and Ω^M.

Define a system of unit vectors $\underline{n}_e$, $\underline{n}_o$, $\underline{n}_s$ parallel to the Earth's axis, the orbit normal and the gyro spin axis. The gyro drift rate $\underline{\dot{n}}_s$ from the geodetic, motional and gravity-gradient effects $\underline{\Omega}^G$, $\underline{\Omega}^M$ and Ω^g is found by integrating each term around the orbit and forming the product $\underline{\Omega} \wedge \underline{n}_s$ for each. In an inclined orbit around the oblate Earth $\underline{n}_e$ and $\underline{n}_s$ remain nearly fixed in space but $\underline{n}_o$ cones about the Earth's axis. Neglecting the correction to the relativistic terms from the Earth's oblateness, the gyro drift-rates in circular orbit around the Earth assume the vector form given in Table 2. For elliptic orbits with corrections for oblateness the integrations are effected by Wilkins' method already referred to.[19]

Table 2: Gyro Drift Terms Averaged Over a Single Orbit

geodetic $\qquad \dot{\underline{n}}_s^G = A^G \, (\underline{n}_o \wedge \underline{n}_s)$

motional $\qquad \dot{\underline{n}}_s^M = A^M \, [\underline{n}_e \wedge \underline{n}_s - 3(\underline{n}_o \cdot \underline{n}_e)(\underline{n}_o \wedge \underline{n}_s)]$

gravity
gradient $\qquad \dot{\underline{n}}_s^g = \pm \, 3A^g \, (\underline{n}_o \cdot \underline{n}_s)(\underline{n}_o \wedge \underline{n}_s)$

where $A^G = \dfrac{3}{2} \dfrac{GM}{c^2 R} \bar{\omega}_o \qquad\qquad \underline{n}_e$ – unit vector parallel to Earth's axis

$\qquad\quad A^M = \dfrac{1}{2} \dfrac{GI}{c^2 R^3} \omega_e \qquad\qquad \underline{n}_o$ – unit vector parallel to orbit normal

$\qquad\quad A^g = \dfrac{1}{2} \dfrac{GM}{R^3} \dfrac{\Delta I}{I} \dfrac{1}{\omega_s} \qquad\quad \underline{n}_s$ – unit vector parallel to gyro spin
$\qquad\qquad\qquad\qquad\qquad\qquad\qquad\qquad$ axis

$\bar{\omega}_o$ – mean motion, ω_e – Earth's rotation rate, ω_s – gyro spin rate

Then forming a second system of unit vectors $\underline{n}_N$, $\underline{n}_{p'}$, $\underline{n}_S$ parallel to the three directions ON, OP', OS; defining time zero as the time when the three vectors $\underline{n}_e$, $\underline{n}_o$, $\underline{n}_s$ are all in the same quadrant of the plane POS, we can express $\underline{n}_e$, $\underline{n}_o$, $\underline{n}_s$ in terms of $\underline{n}_N$, $\underline{n}_{p'}$, $\underline{n}_s$ and i the orbit inclination, ζ the elevation of the star above the celestial equator and ω_n the nodal regression rate. The expressions for drift rate of the parallel gyros in planes POS and NOS then assume the form given in Table 3. Numerical values of the predicted gyro motions the two planes for 37° and 28.5^O inclined orbits when the reference star is elevated at $8^O 15'$ above the celestial equator (corresponding to Rigel) are given in Table 4.

The following points are worth noting about the results of Tables 3 and 4.

(i) The gravity gradient torques are the only ones producing gyro drift components periodic in $2 \omega_n$. In principle therefore it is possible to identify them unambiguously from data analysis; however in practice these components are too small to be useful: in a 37° orbit the largest one has a peak-to-peak amplitude of only 0.27 milliarc-seconds perpendicular to the readout plane NOS.

Table 3: Components of Drift in the Two Readout Planes for Gyroscopes with Spin Axes Parallel or Anti-parallel to the Line of Sight to Star at Elevation ζ above the Celestial Equator

	ANGULAR RATE PERPENDICULAR TO READOUT PLANE POS THROUGH EARTH'S AXIS AND LINE OF SIGHT TO STAR	ANGULAR RATE PERPENDICULAR TO READOUT PLANE NOS THROUGH LINE OF SIGHT TO STAR AND PERPENDICULAR TO POS
Geodetic	$A_G [\cos\zeta \cos i - \sin\zeta \sin i \cos \omega_n t]$	$A_G \sin i \sin \omega_n t$
Motional	$-\frac{1}{2}A_M [\cos\zeta (1 + 3 \cos 2i - 3 \sin\zeta \sin 2i \cos \omega_n t]$	$\frac{3}{2} A_M \sin 2i \sin \omega_n t$
Gravity Gradient	$+\frac{3}{8}A_g [\sin 2\zeta (1 + 3 \cos 2i) + 4 \cos 2\zeta \sin 2i \cos \omega_n t - 2 \sin 2\zeta \sin^2 i \cos 2 \omega_n t]$	$+\frac{3}{2}A_g [\sin\zeta \sin 2i \sin \omega_n t + \cos\zeta \sin^2 i \sin 2 \omega_n t]$

Table 4: Numerical Values of Predicted Gyro Motions in the Two Readout Planes for 37° and 28.5° Inclined Orbits

		linear drift (milliarc-sec/year)	$\cos \omega_n t$ (milliarc-sec peak to peak)	$\cos 2\omega_n t$ (milliarc-sec peak to peak)	$\cos \omega_n t$ (milliarc-sec peak to peak)	$\cos 2\omega_n t$ (milliarc-sec peak to peak)
37° Orbit	Geodetic $\dot{n}_G$	4.74×10^3	33.1	--	224	
	Motional $\dot{n}_M$	32.8	0.54	--	3.65	--
	Gravity Gradient $\dot{n}_g$	±3.7	±1.41	$\pm.040$	±0.22	±0.27
28.5° Orbit	Geodetic $\dot{n}_G$	5.23×10^3	24.0	--	160	--
	Motional $\dot{n}_M$	52.0	0.43	--	2.9	--
	Gravity Gradient $\dot{n}_M$	±5.0	±1.14	$\pm.022$	±0.17	±0.16

(ii) If the reference star lies exactly on the celestial equator the terms in $\sin \zeta$ and $\sin 2\zeta$ disappear and the results undergo considerable simplification. The linear component of Ω^g disappears from the motions perpendicular to the readout plane POS, and so do the sinusoidal components of Ω^G and Ω^M in the same plane. The separation of terms then becomes much simpler. Extending the argument, one may, if one wishes, set an upper limit on ζ to keep the linear component of Ω^g below 0.001 arc-sec/year, the design goal of the experiment. For a 37° orbit the star must lie within $\pm$ 2.2^O, and for a 28.5^O orbit within $\pm$ 1.6^O of the celestial equator.

(iii) When the inclination is 54° 16', the quantity (1 + 3 cos 2i) is zero and the linear component of Ω^g vanishes for all values of the elevation ζ of the reference star. However this result is more curious than useful, because at that inclination the linear component of the relativistic term Ω^M also vanishes.

(iv) Although the terms Ω^G, Ω^M and Ω^g are intermingled, the ratios of their different components can be adequately measured, therefore, a separation can be effected by forming products and ratios of the various components. In addition, the gravity-gradient terms can be calculated out with high confidence and the result can be checked from the differences between the terms in the parallel and anti-parallel gyros.

We now comment briefly on the practical question of separating the different linear and sinusoidal terms presented in Tables 3 and 4. First a general observation. Although the amplitudes of the sinusoidal terms are much less than the values of the linearly measuring signals at the end of a year, that in itself does not mean that measurements of them are inherently less accurate. The peak <u>rates</u> of the gyro motion are comparable for the two sets of terms, so with phase information the limits in resolving signals from noise in the two cases are nearly identical. The question

whether the separation can be made depends on (i) drifts
of the gyro spin axes due to extraneous torques and four prop-
erties of the gyro readout, to wit: (ii) noise performance,
(iii) null stability, (iv) accuracy and stability of the scale
factor and (v) fineness of resolution.

Answers to these points depend on technical details covered
in later sections of this report. The issues are reviewed in
Section 3.6 of Reference (21) where it is shown that the
decisive limitation on separating sinusoidal and linear gyro
drift terms are the scale factor calibration (iv) and fineness
of resolution (v). Inclined orbits present special problems,
but the general conclusion seems to be that useful relativity
data can be obtained in them. In one sense the inclined orbit
offers an advantage: the modulation of terms through the
regression of the orbit plane makes the data richer. Thus the
term $3A^M$ $(\underline{n}_o \cdot \underline{n}_e)(\underline{n}_o \wedge \underline{n}_s)$ vanishes in a polar orbit, but
in an inclined orbit this term and the term A^M $(\underline{n}_e \wedge \underline{n}_s)$
each differently affect the components of motional precession
in the two readout planes, and both are measurable. If the
accuracies could be met, the test of Einstein's theory would
be more complete.

There is some interest also in off-polar orbits in the
regime where $(1 + 3 \cos 2i)$ becomes negative, that is for
inclinations between 54° and 90°. The sense of the motional
effect then reverses, coinciding with that of the Earth's
rotation. An advantage is that the regression period of
the orbit becomes larger in this regime, so that the sinusoidal
components of Ω^G, Ω^M and Ω^g have larger amplitude. Thus the
regression period in an orbit 15° away from the pole is about
220 days and the sinusoidal component of Ω^M perpendicular
to the readout plane NOS has an amplitude of about 7 milliarc-
seconds.

C. THE GYROSCOPE

(1) General Principles

A gyroscope may be a spinning body, a nucleus, a superconducting current or a circulating light beam. Present laser gyros are orders of magnitude from the performance needed. Nuclei and currents have the shortcoming of being highly susceptible to magnetic torques; their gyromagnetic ratios are up to 10^{14} times those of ordinary bodies; a free precession He^3 gyroscope would have to be in a field below 10^{-20} gauss to do the experiment.[22] The only horse in the race is a supported spinning body, and no elaborate thought is needed to see that the most torque-free body is a very round, very homogeneous sphere. The problems come down to four: the size of the sphere, and how it is to be supported, spun up and read out.

Size turns out not to be critical. The drift-rate $\dot{\underline{n}}_s^r$ of the gyro spin vector $\underline{n}_s$ due to some extraneous non-relativistic torque $\underline{\Gamma}^r$ is $\underline{\Gamma}^r \wedge \underline{n}_s / I\omega_s$ where I is the moment of inertia and ω_s the spin angular velocity. Substituting $(8\pi/15)\, \rho r^s$ for I and replacing ω_s by v_s/r, where v_s is the peripheral velocity, we have

$$\dot{\underline{n}}_s^r = \left(\frac{15}{8\pi}\right) \frac{\underline{\Gamma}^r \wedge \underline{n}_s}{\rho r^4 v_s} \tag{3}$$

with a limit on v_s from elastic distortion under centrifugal forces given by

$$(v_s)_{max} = 1.88 \left(\frac{\Delta r}{r}\right)_{max} \left[\left(\frac{E}{\rho}\right)^{1/2} (1 - 11\sigma/28)\right] \tag{4}$$

where E is the Young's modulus and σ the Poisson's ratio for the ball, and $(\Delta r/r)_{max}$ the maximum allowed difference between the polar and equatorial radii.

With a few exceptions, the torques may be divided into two categories: those related to the surface area of the ball and those related to its volume. Each surface dependent torque Γ^σ is proportional to (area) x (radius) x $\sigma(r)$, where $\sigma(r)$ is a function which in some instances is constant and in others depends on deviations of the ball from perfect sphericity. Each volume dependent torque is proportional to (density) x (volume) x (radius) x $\phi(r)$, where $\phi(r)$ is a function measuring deviations from perfect homogeneity. Over a fair range of radii $\sigma(r)$ may be taken proportional to r^S and $\phi(r)$ proportional to r^V where s and v each lie between 0 and 1. Thus Γ^σ varies as $r^{(3 + s)}$ and Γ^ϕ as $r^{(4 + v)}$ and from (4) the drift rates $\dot{n}_s^\sigma$ and $\dot{n}_s^\phi$ from all torques in these categories vary as $r^{(s - 1)}$ and r^V. Thus some errors increase and some decrease with increasing rotor size; in neither case is there much advantage to a change of diameter.

The actual rotor is a ball 4 cm in diameter made from optically selected fused quartz homogeneous in density to 1 part in 10^6 and spherical to a few parts in 10^7. Figure 6 is a general view of the gyroscope. The ball is electrically suspended within a spherical quartz housing by voltages applied to mutually perpendicular sets of condenser plates. It is spun up initially to a speed of about 200 Hz by a gas jet system designed by Bracken and Everitt,[6] after which the gas is pumped out and the ball is allowed to run freely in the vacuum. The entire device is surrounded by a spherical superconducting shield in which the trapped field level is maintained below 10^{-7} gauss. Readout is by SQUID magnetometers attached to super-conducting rings surrounding the rotor. Details of the spin up and readout systems are given in Sections C (2) and C (3). The electrodes are 2 cm diameter circular pads 4×10^{-3} cm from the ball. The suspension system used in most of the work was designed
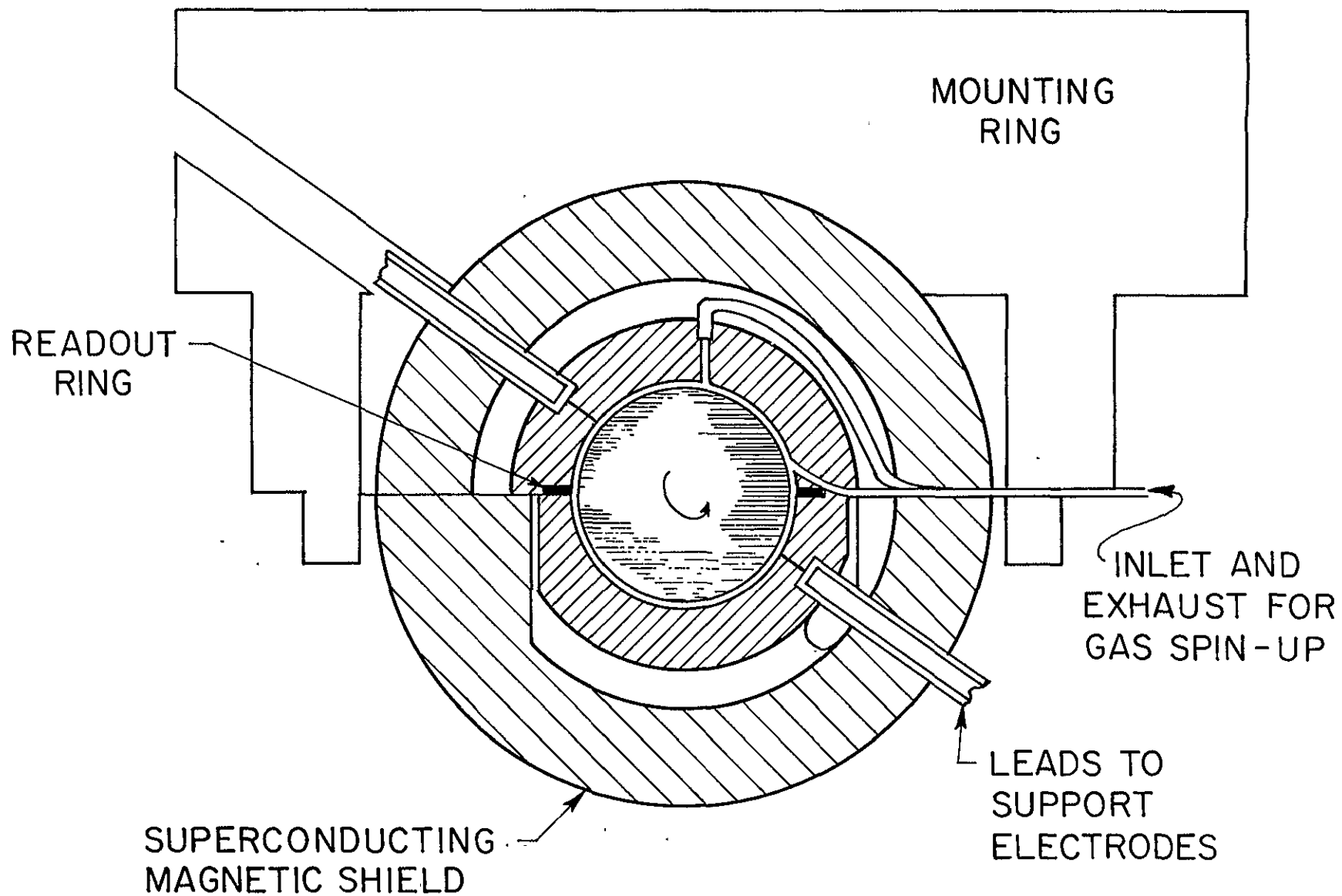
Figure 6: The Gyroscope

by the late J. R. Nikirk. It holds the ball against accelerations
up to 5 g by 20 kHz signals of amplitude between 2 and 3 kV rms.
The ball position is sensed by a 1 MHz 2 V signal. The suspen-
sion servo has a bandwidth of 600 Hz and long term centering
stability good to 10^{-5} cm. In space the support voltage is
about 0.5 V. For further details of the suspension system
see Section D (2) and Reference (23). An earlier suspension
system with different characteristics was purchased from
Honeywell in 1967.

The choice of magnetic readout, electrical suspension and
gas spin up neatly separates problems in the three areas. The
separation is less complete on Earth than in space because the
large 20 kHz suspension signals generate pickup in the readout.
In fact suspension interference was an awkward problem in the
first stages of the laboratory experiment, as described in
Section D (4)(d).

Assuming a London moment readout one might ask if other
alternatives are worth considering for suspension and spin up.
The best claim another suspension might have would be that it
exerts a smaller torque on the ball, particularly if the
torque were low enough to do a relativity experiment on Earth,
originally as suggested by W. M. Fairbank (note (7) to Reference
(2), second paper). Various support schemes have been proposed for
spherical gyro rotors -- gas bearings, superconducting magnets, flo-
tation in superfluid helium, and so on -- and amazing claims are
sometimes heard about torque levels. No universal judgement
can be offered; the following argument shows where the heart
of the problem lies.

Any scheme for supporting a massive body against gravity
depends on creating pressure differences across the surface.

If the body is nearly but not quite spherical a change in
orientation results in work being done against these pres-
sures; conversely the pressures exert a torque that drives
the body towards an energy minimum. The torque evidently
vanishes for a true sphere; it depends on the size and shape
of deviations from perfect sphericity. Discounting extraneous
effects, such as the interaction of a magnetic suspension with
the London moment or turbine torques in a gas bearing, we may
expect different suspensions to exert similar torques on bodies
of the same form, for the pressure that has to be applied over
a given area to balance a given acceleration is always the same.
More accurately we may think of two extreme suspension mechani-
zations between which all others fall. One which may be called
the plain man's suspension generates pressure simply to counter-
act gravity. To fix ideas think of a light sphere floating on
mercury. If the total deviation from sphericity is Δr the
difference between maximum and minimum energies is $Mf\Delta r$ where
f is the residual acceleration. Upper bounds on the torques
are found by expanding the shape of the spinning body in
Legendre polynomials and identifying Δr with each polynomial
in turn. The drift-rates are

$$\dot{\underline{n}}_r^m = \frac{5m\chi}{2v_s} \left(\frac{\Delta r}{r}\right) \underline{f} \wedge \underline{n}_s \tag{5}$$

where m is the order of the polynomial and χ is a quantity
between 0 and 1 depending on m and the size of the support
pads. If the diameter of the pad is d then $m\chi \to 0$ as $m \gg \pi r/d$,
and satisfactory limits are got by considering the first few
even and odd harmonics. Taking $\Delta r/r$ as 3×10^{-7} and f in space
as 10^{-9} g the expected drift rate with a plain man's suspension
and $\underline{f}$ perpendicular to $\underline{n}_s$ is around 10^{-15} rad/sec, a factor of
ten higher than the design goal for the experiment. Further
improvements depend on the extent to which f averages through
the orbit or the plain man's suspension can be improved on.

To do better the energy put in at one point must be taken out elsewhere. The simple picture is not a sphere on mercury but a neutral density body immersed in an incompressible fluid. The pressure extends over the whole surface and the torque vanishes. Remembering Archimedes we may call this the eureka suspension. An electrical suspension can be arranged to mimic a eureka suspension by applying voltages to all six electrodes at once. It is then said to be <u>preloaded</u>. In the most common mechanization the voltages V_2, V_4 on opposite electrodes are adjusted to keep $(V_2 + V_4)$ constant and the preload acceleration h is the acceleration along a support axis required to send the voltage on one plate to zero. The most critical shape is the oblate spheroid, since it determines the gyro drift due to centrifugal distortion of the ball, and for a ball spinning at 200 Hz the centrifugal $\Delta r'/r$ is 3×10^{-6}, a factor of ten larger than the polishing errors. Defining a preload compensation factor $\zeta = (h_x - h_y)/h_z$ etc., the torque on an oblate spheroid inclined to the electrode axes turns out to be proportional not to f as in the plain man's suspension but to $\left[\frac{f}{h} + \zeta\frac{h}{f}\right]$ f. There is therefore an optimum preload h = $f/\sqrt{\zeta}$; and if the preloads are matched to 1%, as is reasonable, this torque is an order of magnitude less than with the plain man's suspension (actually nearer a factor of 40 less since the numerical coefficient is smaller).

Two other, more elaborate, mechanizations deserve mention. One known as "sum of the energies" control has voltages continually adjusted to hold $\Sigma C_i V_i^2$ constant where C_i and V_i are the capacitance and voltage of the $i\underline{\text{th}}$ electrode. The energy is independent of orientation; this is a true eureka suspension. The second is "sum of the squares" control, for which the voltages on the three axes fulfil the condition $V_2{}^2 + V_4{}^2 = V_1{}^2 + V_6{}^2 = V_3{}^2 + V_5{}^2$. This leaves the higher order terms but makes the torque on an ellipsoid vanish. Defining a sum

of squares control factor ξ analogous to the preload compensation factor, the ellipsoid torque is proportional to $\left[\frac{h}{f} + \zeta\frac{f}{h}\right] f\xi$, still further down from the plain man's suspension.

Other suspension techniques such as a superconducting bearing might also outperform the plain man's suspension. The trouble always is that eventually the analytic arguments break down through secondary effects like polishing errors in the housing. The eureka suspension is a will o' the wisp. In fact in Honeywell's studies of electrical suspensions sum-of-the-squares control really helps, sum-of-the-energies does not. One may conjecture that with comparable work all suspension techniques will beat the plain man's suspension in about the same degree.

Consider now an attempt to do a Gyro Relativity experiment on Earth, say in an observatory near the equator. The combined relativistic precession ($\dot{n}_{-s}^{G} + \dot{n}_{-s}^{M}$) is 0.4 arc-sec/year. Suspension errors may be reduced either by approximating a eureka suspension or by averaging. If the spin axis n_{-s} lies in the equatorial plane the quantity $\underline{f} \wedge \underline{n}_{-s}$ in Equation (5) averages to $g\bar{\lambda}$, where $\bar{\lambda}$ is the average uncertainty in $\underline{f} \wedge \underline{n}_{-s}$ from fluctuations in the local vertical, say 10^{-5} rad. Then with $\Delta r/r$ for a spinning ball equal to 3×10^{-6}, the uncertainty in gyro drift with a plain man's suspension is about 100 arc-sec/year. Better things might be hoped from a preloaded suspension. Alas not! The residual torques, instead of being parallel to the local vertical are in an unknown direction in the housing: experience at Honeywell with live gyros suggests a limiting drift-rate nearer 1000 arc-sec/year -- worse than straight averaging with the plain man's suspension.

Consider another torque: mass-unbalance from inhomogeneities in the rotor. If u is the distance from center of mass to center of geometry the torque is Mfu and the drift rate

$$\dot{n}_{-s}^{u} = \frac{5}{2} \left(\frac{u}{r}\right) \frac{\underline{f} \wedge \underline{n}_{-s}}{v_{s}} \tag{6}$$

which with $(u/r) \sim 10^{-6}$ and $\overline{\underline{f} \wedge \underline{n}_s} \sim 10^{-5}g$ averages to 60 arc-sec/year, comparable to the suspension torques. In space with $f \sim 10^{-9}$ g, the drift-rate is below 0.001 arc-sec/year. The mass-balance might be improved by evaporating material on the surface of the ball and checking its pendulum period before spin up. If Ω_0 is the design goal and ω_s the gyro spin-rate the pendulum period T must exceed $2a \sqrt{\sin\lambda \, \Omega_0 \, \omega_s}$, and with $\lambda \sim 10^{-5}$ the period for an 0.1 arc-sec experiment is four hours -- perhaps a factor of 20 beyond the limits of feasibility. An Earth based experiment is hopeless.

An analysis of the torques on the orbiting gyroscope has been presented in papers by C. W. F. Everitt,[8][24] to which reference should be made. The torques may be divided into two classes: those like the suspension and mass unbalance terms which scale with the residual acceleration on the spacecraft, and those like the effects of residual magnetic fields, residual gas in the cavity, residual electric charge on the rotor, and the gravity gradient form discussed above, which are essentially the same on Earth and in space. The result of the analysis is a set of design restrictions, on the rotor, housing suspension system, spin up system, and environment, needed to attain gyro drift performance of 10^{-16} radians/sec (0.6 x 10^{-4} arc-sec/year). Table 1 summarizes the results both for a rolling and non rolling satellite, assuming a 500 mile near polar orbit, with a 4 cm diameter gyro rotor spinning at 200 Hz. Some of the numbers quoted are restrictions, others, such as the Earth's gradient acceleration are know fixed values. The various restrictions are not indepen-dent: an improvement in performance in one area would allow relaxation of restrictions elsewhere. The immense challenge that exists in achieving all the requirements at once needs no emphasis; each does seem within the bounds of possibility. The three areas where most work remains to be done are: (1) mechanizing the suspension electronics for space, (2) reaching satisfactory operating pressures, (3) maintaining low residual charge on the ball.

Table 5 represents the state of understanding of experimental limitations reached in 1973. Some of the estimates used in evaluating the support-dependent drifts were unnecessarily conservative because they failed to take into account in a proper mathematical way the averaging of quantities $\underline{f} \wedge \underline{n}_s$ and higher order drift terms in a rolling drag-free satellite. A satisfactory procedure for handling these terms was formulated by C. W. F. Everitt in 1975[25] and utilized by T. M. Spencer of Ball Brothers Research Corporation in the analysis of a non drag-free spacecraft presented in BBRC report: Mission Definition for a Relativity Explorer for the Stanford Relativity Experiment. Mr. Spencer showed that an averaging of as much as a factor of 40 better than earlier estimates was to be expected in a non drag-free spacecraft in near-circular inclined orbit. The gain in a rolling drag-free spacecraft is less; it has yet to be properly worked out, but may be between a factor of 5 and 10 better than the figures used in deriving Table 5. There is therefore good reason to expect support-dependent drifts to go below 10^{-4} arc-sec/year in the final experiment.

Table 6 provides a comparison of the magnitude of the leading support dependent gyro drift terms in the laboratory and space (the final flight mission), together with the formulae on which they were based. Most of the suspension torque equations from which the formulae are derived were obtained by Mr. G. Matchett, formerly of Honeywell Incorporated, in an important U.S. Navy Report to which reference should be made.[26] The analysis, being based on electrostatics, should be considered rather trustworthy in principle, and the results have been verified in practice in the laboratory at Honeywell Incorporated. Terms up to the seventh harmonic in rotor shape have been satisfactorily identified in observations on drift performance of live gyros. Very considerable confidence can therefore be attached to the analysis of support dependent torques.

Table 5: Design Requirements for a Relativity Gyroscope with Limiting Accuracy 10^{-16} rad/sec

			Fixed Space Craft	Rolling Space Craft
Gyro Rotor	Homogeneity	$\frac{\Delta\rho}{\rho}$	$\sim\ 3\times 10^{-7}$	$\sim 3\times 10^{-7}$
	Sphericity at rest	$\frac{\Delta r'}{r}$	$\sim\ 5\times 10^{-7}$	$\sim 5\times 10^{-7}$
Gyro Suspension	Sphericity of cavity	$\frac{\Delta r''}{r}\ \sim$	10^{-5}	$\sim 10^{-5}$
	Centering accuracy $\begin{cases} t/d \\ t \end{cases}$	$\sim$	10^{-2}	$\sim 10^{-2}$
		$\sim$	4×10^{-5} cm	$\sim 4\times 10^{-5}$ cm
	Preload $\begin{cases} \text{acceleration} \\ \text{voltage} \end{cases}$	h $\sim$	10^{-6} g	$\sim 3\times 10^{-6}$ g
		V $\sim$	0.7 volts	~ 2.1 volts
	Preload compensation factor	$\zeta\ \sim$	3×10^{-3}	$\sim 10^{-2}$
	Symmetry	$\theta_o \big\} \sim$	5×10^{-3}	$\sim 10^{-4}$
	or sum of squares control factor	$\xi\ \big\}$		
	Distance of gyros from drag-free proof mass	$\ell\ <$	20 cm	< 20 cm
Environment	Acceleration due to self-gravitation	f $\sim$	10^{-9} g	$\sim 10^{-9}$ g
	Acceleration due to earth's gradient	$f_o\ \sim$	2×10^{-8} g	$\sim 2\times 10^{-8}$ g
	Residual magnetic fields $\begin{cases} \text{best} \\ \text{using symmetry} \end{cases}$	H $<$	10^{-7} gauss	$< 10^{-7}$ gauss
		H $<$	4×10^{-6} gauss	$< 4\times 10^{-6}$ gauss
	Residual electrification on ball $\begin{cases} \text{charge} \\ \text{voltage} \end{cases}$	Q $<$	10^8 electrons	$< 7\times 10^9$ electrons
		V $<$	0.03 volts	< 2.1 volts
	Residual gas pressure $\begin{cases} \text{magnitude} \\ \text{gradients} \end{cases}$	p $\sim$	10^{-9} torr	$\sim 10^{-9}$ torr
		$\Delta p/p\ \sim$	5×10^{-2}	~ 0.5
Spin up system	Torque switching ratio	$\Gamma_r/\Gamma_s\ \sim$	2×10^{-13}	$\sim 2\times 10^{-13}$

47

Table 6: Principal Support-Dependent Gyro Drift Terms on Earth and In Space

Source and Sensitivity to Residual Acceleration f or Preload h	Main Mission milliarc-sec/year	Lab arc-sec/day
MASS UNBALANCE		
$\Omega_u < \left(\dfrac{C_u}{2}\right)\left(\dfrac{\Delta\rho}{\rho}\right)\left(\dfrac{1}{v_s}\right) f < \left(2 \cdot 10^{-11}\right) f \dfrac{rad\text{-}sec}{cm}$	0.13	300
MISALIGNED ELLIPSOID		
$_1\Omega_e < 1.35 \left(\dfrac{\Delta r}{r}\right)\left(\dfrac{\theta_0}{v_s}\right)\left[\zeta h + \dfrac{f^2}{h}\right]$		
$_1\Omega_e^0 = \left(1.6 \cdot 10^{-11}\right)\zeta h$	0.5	2.4
$_1\Omega_e^{bias} < \left(1.6 \cdot 10^{-11}\right)\left[\dfrac{f^{bias}}{h}\right]$	negligible	200
$_1\Omega_e^{sine} < \left(1.6 \cdot 10^{-11}\right)\left[\dfrac{f^{sine}}{2h}\right]^2$	0.1	100
MIS-CENTERED ELLIPSOID		
$_2\Omega_e < 3.28 \left(\dfrac{\Delta r}{r}\right)\left(\dfrac{t}{d}\right)\left(\dfrac{1}{v_s}\right) f < \left(4.8 \cdot 10^{-11}\right) f$	0.01	400
MISALIGNED PEAR		
$_3\Omega_e^\theta < 2.58 \left(\dfrac{\Delta r}{r}\right)\left(\dfrac{1.5\theta_0}{v_s}\right) f < \left(1.9 \cdot 10^{-12}\right) f$	0.01	32
MIS-CENTERED PEAR		
$_3\Omega_e^t < 0.9 \left(\dfrac{\Delta r}{r}\right)\left(\dfrac{t}{d}\right)\left(\dfrac{1}{v_s}\right)\left[h + f^2/h\right] < 4.3 \cdot 10^{-13}\left[h + f^2/h\right]$	0.05	8
BASIC PEAR		
$_3\Omega_e^0 < 1.4 \left(\dfrac{\Delta r}{r}\right)\left(\dfrac{1}{v_s}\right) f < \left[1.1 \cdot 10^{-10}\right] f$	0.3	1000

In operating precision gyroscopes on Earth it is customary to observe gyro drifts under test and apply the observations to model future gyro performance. The gyro can then be used in navigation to higher accuracy than its observed residual drift rate. The Honeywell electrically suspended gyroscopes, for example, have typical uncorrected drift rates of the order of 3×10^5 arc-sec/year, but their performance can be modelled to reduce the navigational uncertainty after a year to about 3000 arc-sec. The residual uncertainty is due to random walk disturbances; the navigational uncertainty after one day is of order $3000/\sqrt{365}$ or 150 arc-sec.

One may ask whether torque modelling can be attempted in the Gyro Relativity experiment. Our original answer was No, because the procedure used for navigational gyros of following the drift performance and calculating out linear terms is clearly inapplicable since there is no simple way to distinguish these terms from the linear relativistic drifts. Moreover some of the numerical coefficients that enter into any torque calculation cannot be determined in advance. Take, for example, the "mass unbalance" drift rate given by Equation (6), p. 44. The radius r and peripheral velocity v_s of the ball are known, as is the direction $\underline{n}_s$ of its spin axis, and the residual acceleration $\underline{f}$ on the gyro can be measured, but the magnitude of u, the distance between the center of geometry and the average position of the mass center along the spin axis depends on two quantities that are very difficult to determine: the distance d between the mass center and the center of geometry and the mean angle γ between $\underline{d}$ and the spin vector $\underline{n}_s$. The value of γ depends on initial spin conditions. If $\underline{d}$ were aligned at right angles to $\underline{n}_s$ there would be no axial mass unbalance. Thus it is relatively easy to estimate an upper limit on $\underline{n}_s^u$, from the known upper limit on $\underline{d}$, but difficult to determine its actual value.

Difficult does not necessarily mean impossible, however. We have one other parameter to play with: the residual acceleration $\underline{f}$ on the spacecraft. Suppose that at the beginning or

end of the experiment, or at other suitable times, one were to briefly apply accelerations 10^2, 10^3, 10^4 etc. larger than the normal 10^{-9} g, then the support-dependent drifts would dramatically increase and one might be in a position to determine u and other parameters for gyro modelling. Our present view is that tests of this kind are a good idea in checking magnitudes of the support dependent torques, but since these torques are unlikely to be the dominant limitation, extensive modelling is probably not needed. It is nice however to have this card up our sleeves.

The one gyro drift term that can be modelled exactly is the gravity gradient torque on the quadrupole mass moment of the gyroscope. See Section B (Tables 1 to 4).

The gyro spin speed of 200 Hz is chosen to optimize effects of torques from different sources. See Reference (24).

(2) Gyro Spin Up

The development of a suitable gyro spin system proved an exceptional challenge, in meeting which much credit must go to the acumen and determination of T. D. Bracken, then (between 1966 and 1968) a beginning Physics graduate student at Stanford. Important help was given in the conceptual stages by D. Baganoff of Stanford Aeronautics Department. Dr. Bracken's work is described in two papers completed in 1968,[7] one published and one unpublished. In 1971 J. A. Lipa made simulation fixtures to check pressure ratios in the system and discovered a factor of three correction to one calculation, which led to a slight redesign of the differential pumping ports. A further small correction has been pointed out[27] by G. Karr of the University of Alabama, Huntsville, who has also analysed the design from a new point of view. The first gyro spin up at room temperature was done by J. A. Lipa and J. R. Nikirk in January 1973; the first low temperature spin up was in June 1973. See Section D (4) (c).

Figure 7 is a cross-section of the gyro housing showing details of the spin system. It consists of two 2 cm x 0.5 cm

EXHAUST — SUPPORT ELECTRODE

SPIN-UP CHANNEL

INLET FOR GAS SPIN-UP

1.5" QUARTZ BALL

QUARTZ GYRO HOUSING

INLET

FEED-THRU'S FOR SUPPORT ELECTRODES

EXHAUST FOR GAS SPIN-UP

AUXILIARY PUMPING LINE

SPIN-UP CHANNEL

QUARTZ GYROSCOPE HOUSING

a
w   b
δ
Δ

1.5" DIAMETER BALL
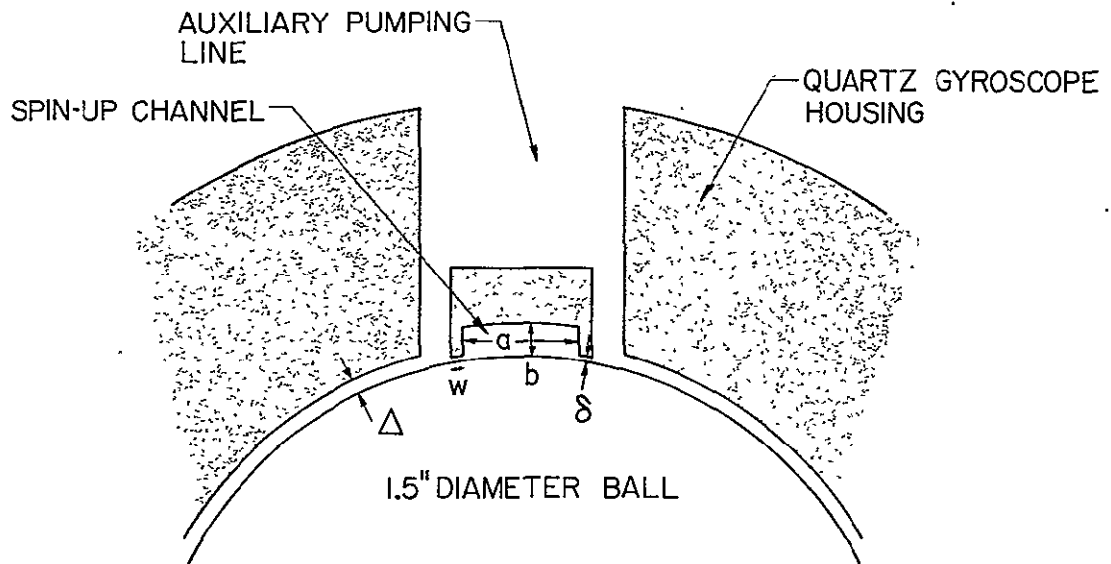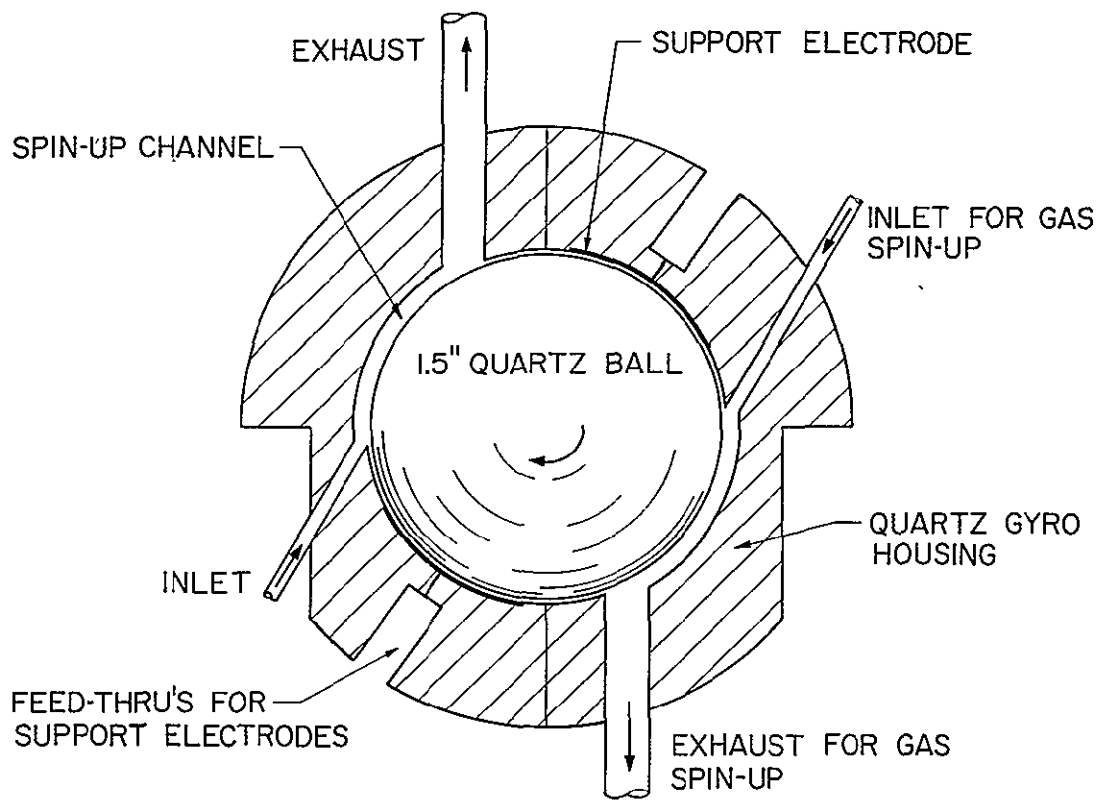
DESIGN PARAMETERS

a	0.5	cm
b	0.05	
w	0.05	
δ	0.00075	
Δ	0.0038	
L = 2.0 cm		

Figure 7: Design of Gyro Spin System

equatorial channels through which turbulent helium gas is passed under choked flow conditions at a mean pressure of about 16 torr. Since on Earth the suspension electrodes would undergo electrical breakdown at about 0.02 torr, the gas pressure in the electrode area must be kept below that value. This is achieved by a differential pumping system. The spin up channel is surrounded by raised lands with a clearance of about 5×10^{-4} cm from the rotor. About 96% of the gas entering the channel leaves through the outlet port at the end; the remaining 4% seeps over the raised lands and is exhausted at low pressure through a guard ring of pumping slots surrounding the channel. Details of the design optimization are given in the papers of Bracken and Everitt already cited; at maximum operating pressure the constraint on pressure from electrical breakdown is met with a safety factor of two. On Earth differential pumping is provided by a high speed diffusion pump; in orbit the system is exhausted to the vacuum of space. The maximum spin speed is determined by the competition of the spin up gas torque with the viscous drag torque between the rotor and the raised lands plus the drag from the low pressure gas in the main portion of the housing. The maximum rotor speed attainable at 2K with our geometry is close to the optimum 200 Hz, with a characteristic spin up time constant of 15 min.

One might imagine that in space, where the support voltages are low, electrical breakdown would cease to be a problem and the elaborate differential pumping system of Figure 7 could be avoided. J. A. Lipa has pointed out that this is not so. Although a spin system can be devised which works at higher pressures and avoids differential pumping, the pressure required to generate enough torque to overcome the additional drag in the cavity is about 0.6 atmosphere. Now the area of each channel is about 1 cm^2. Applying 0.6 atmosphere pressure over 1 cm^2 causes an acceleration of 10 g on the ball, and although this is balanced by the corresponding force from the other channel, the difference will be enough to cause appreciable accelerations

of the ball. The natural procedure for overcoming such accel-
erations would be to raise the suspension voltage. Calculations
based on the well-known pressure/breakdown curve for helium gas,
confirmed experimentally by T. Edeli at Stanford, show that the
minimum breakdown for the present electrodes at a temperature
of 4K occurs at a pressure of about 5×10^{-2} torr. The breakdown
voltage is 230 V (peak value). With a 230 V suspension the maxi-
mum support acceleration is about 3×10^{-3} g. Thus without
differential pumping the gas pressures in the two spin up channels
would have to be balanced to something like 1 part in 10^{4} to
avoid the ball hitting the wall.

After spin up the gas is pumped out and the ball allowed
to coast in the vacuum. Residual gas in the cavity gradually
slows the ball. Assuming diffuse reflection the exponential
spin down time is given by

$$\tau = \frac{1}{5} \sqrt{\frac{2\pi k}{m}} \frac{\rho r T^{1/2}}{p} \tag{7}$$

where m is the mass of the helium atom, k Boltzmann's constant,
ρ and r the density and radius of the ball, T the absolute temp-
erature and p the pressure in the cavity. For helium at 2K and
10^{-9} torr the time τ is about 300 years. Gas damping is by far
the most dominant process in slowing the ball. Intuitively
therefore one might expect serious gyro drifts due to departures
from sphericity or centering of the rotor in the gyro housing.
Actually such terms vanish so long as the pressure is uniform.
This rather surprising result comes about because the momentum
transfer between two moving surfaces is proportional to
(number of molecules) x (frequency of collision per molecule).
The first factor is proportional to the spacing d between the
ball and the housing; the second factor is proportional to 1/d.
Thus τ is independent of d as Equation (7) shows. However
pressure gradients in the cavity may cause gyro drifts, as
investigated in Section 3.7 of Reference (8). In a rolling

satellite with an operating pressure below 10^{-9} torr they should be of order 10^{-4} arc-sec/year or less.

The difficulty with gas torques might lead one to suppose that another method of spin up would have smaller residual torques. On the contrary, some quite general considerations show that the difficulties of gas spin up, bad as they are, are less forbidding than those of any other system that can be devised.

To spin a gyro rotor suitably at rest, a torque Γ^S of some kind must be applied for a time t_s, after which Γ^S must be reduced to a level where the residual component perpendicular to the spin axis does not cause significant drift errors. Neglecting drag torques $\Gamma^S = I\dot{\omega} = I\omega_s/t_s$. Now the drift rate Ω^r due to Γ^r is $\Omega^r = \Gamma^r/I\omega_s$. Replacing Ω^r by Ω_0 the gyro drift rate chosen as the design goal for the experiment and expressing the result as a limit on Γ^r we have

$$\frac{\Gamma^r}{\Gamma^S} < \Omega_0 t_s \tag{8}$$

Since it is operationally convenient to spin up in times less than the half-period of the satellite orbit, t_s has to be less than 2000 seconds and with $\Omega_0 \sim 10^{-16}$ radians/sec, the ratio Γ^r/Γ^S has to be less than 2×10^{-13}. Gas forces are among the very few for which such a torque switching is possible. Almost the only conceivable alternative is a mechanical clutch and drive motor.

But there is another consideration of great cogency. To obtain the full London moment the gyro has to be spun up below its superconducting transition temperature. Now any spin system will dissipate some heat. At cryogenic temperatures the only way of getting rid of the heat is by having gas in the cavity. Let η be the mechanical efficiency, so that $(1 - \eta)$ represents the proportion of energy dissipated in heat; and let T_c be the temperature of the cavity, T_r the maximum temperature rise

allowed, and α the reduced mutual accommodation coefficient for the true surface. Then the minimum acceptable operating pressure during spin up by gas with specific heat ratio γ is

$$p > \frac{2}{15} \sqrt{\frac{2m}{k}} \left(\frac{\gamma - 1}{\gamma + 1}\right) \left(\frac{1 - \eta}{\alpha}\right) \sqrt{\frac{T_c + T_r}{T_c - T_r}} \frac{p r v_s^2}{t_s} \quad . \tag{9}$$

For helium gas the numerical factor reduces to 1×10^{-5} egs units. Taking α as 0.5, T_c as 2K, T_r as 6K, the minimum value for p is 2×10^{-4} $(1 - \eta)$ torr. To allow the gyro to be spun up at the final operating pressure of 10^{-9} torr the efficiency would need to be 99.9995%. Actually that figure can be relaxed slightly by taking advantage of the specific heat of the fused quartz, allowing the ball to warm up and then cool down slowly afterwards; but the efficiency still has to exceed 99.993%. There seems no escape, whatever the spin system, from having some gas present at higher than normal pressure during spin up. Since the difficulty in reaching low pressure is nearly all in covering the last orders of magnitude from 10^{-7} to 10^{-9} torr, no alternative method is likely to be easier than gas spin up.

The problem of obtaining 10^{-9} torr pressures in the gyro housing has been investigated by J. A. Lipa. Since spin up must be done below the superconducting transition temperature, conventional cryopumping techniques, which depend on cooling from high temperatures, are of little direct use. The initial venting to space at an altitude of about 400 nautical miles, coupled if necessary with a second stage of internal cryosorption pumping, should readily give pressures below 10^{-7} torr. The remaining pressure reduction can probably be achieved by "baking" the gyro housing and its surroundings at a temperature four or five times their normal 1.6K operating temperature. The procedure has a rough similarity to the removal of water from a room temperature ultra-high vacuum system by bake out at 700°C

(a bake out temperature much higher than is conventional).
The bake out does not appreciably heat up the ball, and
therefore does not appreciably alter the vapor pressure of
the adsorbed helium on it. As this gas is gradually desorbed
it impinges on surfaces that are relatively helium free.
Since the vapor pressure of adsorbed helium is a strong
function of surface coverage, gas atoms impinging on the
housing will not return to the ball at a significant rate
even when 60% of the gas has been transferred. The one way
gas transfer does not exert any drift torque on the ball and
the effective pressure in the housing ultimately becomes that
due to the gas from the ball readsorbed on the housing wall,
which leads at the end of a year to a maximum vapor pressure
of 1 or 2 x 10^{-9} torr.

(3) Gyro Readout

(a) Background

Conventional optical readouts for electrically suspended
gyroscopes depend on having a gyro rotor with unequal moments
of inertia so that it spins about a preferred axis. Patterns
are applied to the surface of the ball from which light is
reflected to photodetectors to determine the position of the
spin axis. The Honeywell gyro has a hollow beryllium rotor,
welded from two half shells with a heavy internal belt around
the equator. Two detectors are used to find the polar coordinates
θ and ϕ of the spin axis with respect to the housing, by obser-
vations of a D shaped pattern at the pole to determine θ and a
sawtooth pattern at the equator to determine ϕ. The principle
of the D pattern readout is identical with that of the color-
mixing readout applied by Maxwell between 1857 and 1861 to
his "Dynamical Top" and magnetic momentum experiment.[28]

The Honeywell readout has limited angular range. To
obtain wide-angle information and minimize gyro torques

the gyro is operated in a gimballed mode: the housing tracks
the ball and signals are taken from the gimbal output. An
electrically suspended gyroscope with direct wide angle readout
has been developed by Rockwell International (Autonetics Division).
The rotor is given radial mass unbalance and read out electrically
from the periodic signal in the centering servo.

No existing readout comes near the performance needed in
the Gyro Relativity experiment. Honeywell's optical pickoff
has four shortcomings in our application:

(i) the light flux causes an excessive heat input into the
cryogenic rotor which could only be removed by raising the oper-
ating pressure to an unacceptable level. Since cryogenic opera-
tion is called for other reasons besides readout, this objection
alone is decisive.

(ii) the inequality in principal moments of the ball,
required to make the readout work, gives the ball a quadrupole
mass moment of about 3×10^{-2}, which causes a drift rate Ω^g in
the Earth's gravity gradient of $150 \sin 2\beta$ arc-sec/year: too
large to be conveniently separated from the relativity terms
Ω^G and Ω^M by the methods described in Section B.

(iii) readout noise is excessive. Latest performance
figures reported by Honeywell give a resolution of 15 arc-sec
in 100 radian bandwidth. The time required to obtain a single
1 milliarc-sec data point would be six months under the most
favorable assumption. Not only is this far too long in any
case, but, even worse, centering errors prevent meaningful
integration of data over such long periods.

(iv) centering errors. The optical pickoff locates the
poles of the spinning rotor with respect to a point on the
surface of the housing. A displacement t of the center of
the ball with respect to the center of the housing causes
an error in readout angle of order t/r. The long term centering

stability of the electrical suspension system is 5 to 10
microinches, so t/r for a 1.5 inch diameter ball is about 10^{-5}
radians or 2 arc-sec. Drifts in gyro readout of this order
may occur in days or weeks.

The relatively poor angular resolution of the Honeywell
pickoff may seem surprising in view of the extraordinary
resolutions attained with classical optical levers. The Jones-
Richards optical lever, for example,[29] resolves 10^{-5} arc-sec
in a 10 Hz bandwidth. The difficulty with the gyro is diffraction
and scattering of light reflected from the D pattern: the
effective aperture is no more than thousandths of an inch,
making the angular diameter of the diffraction image several
hundred arc-seconds. A method of overcoming the difficulty
in principle was conceived under the present Grant by C. W. F.
Everitt. A rotor is made of two glass hemispheres, fused
together with a mirror sputtered on the interface, and given
a preferred axis so that it spins about the normal to the
mirror. The rotor is coated with a few hundred angströms
of normal or superconducting metal, thick enough to conduct
electricity and allow the suspension system to operate, but
thin enough to transmit light. The curved surface of the ball
serves as a lens element in a precision optical lever. A readout
of this kind should give excellent angular resolution and be
independent of centering errors of the ball. An easy way of
mechanizing two axis information would be to have optical
levers for the X and Y axes looking in from opposite ends of
the axis at the front and back surfaces of the mirror. The
extremely thin coating on the ball would preclude use of
such a readout in a ground-based gyroscope because of the
electrical arcing problems described in section D, unless
the thin coating were restricted to very small areas near the
poles which were never allowed into the region of high electric
field. In space, however, it might be feasible.

The Autonetics electrical suspension readout in its most sensitive mode has comparable limitations in angular resolution to the Honeywell optical pickoff.

(b) Principle of the London Moment Readout

According to the London equations of superconductivity there is in a rotating superconductor a magnetic moment aligned with the instantaneous spin axis which reduces in spherical geometry to a dipole of magnitude

$$M_L = \frac{mc}{2e} r^3 \omega_s = 5 \times 10^{-8} r^3 \omega_s \text{ gauss} \tag{10}$$

Figure 8 illustrates the principle of the London moment readout of the gyroscope. The ball is surrounded by a superconducting loop connected to a sensitive SQUID (Superconducting QUantum Interference Device) magnetometer. A change in orientation of M_L changes the flux through the loop and can therefore be measured by the magnetometer. Three mutually perpendicular loops give a three axis readout.

Work at Stanford since 1971 on applying the SQUID magnetometer to the London moment readout has been principally the responsibility of J. T. Anderson and R. R. Clappier. Earlier research on the vibrating plane magnetometer conceived by Bol, Deaver and Fairbank was carried on principally by W. O. Hamilton, J. E. Opfer and J. M. Pierce.[30]

SQUID magnetometers provide a very sensitive measure of d.c. magnetic fields by determining quantum interference in a super-conducting circuit containing a weak link. In such a circuit there is a critical current I_0 (the Josephson current) above which the weak link reverts from the superconducting to the normal state. If the current is below I_0 it automatically adjusts to cancel any changes in the applied field and conserves the magnetic flux in the ring, but if it ever exceeds the critical value a flux quantum will pass into or out of the ring
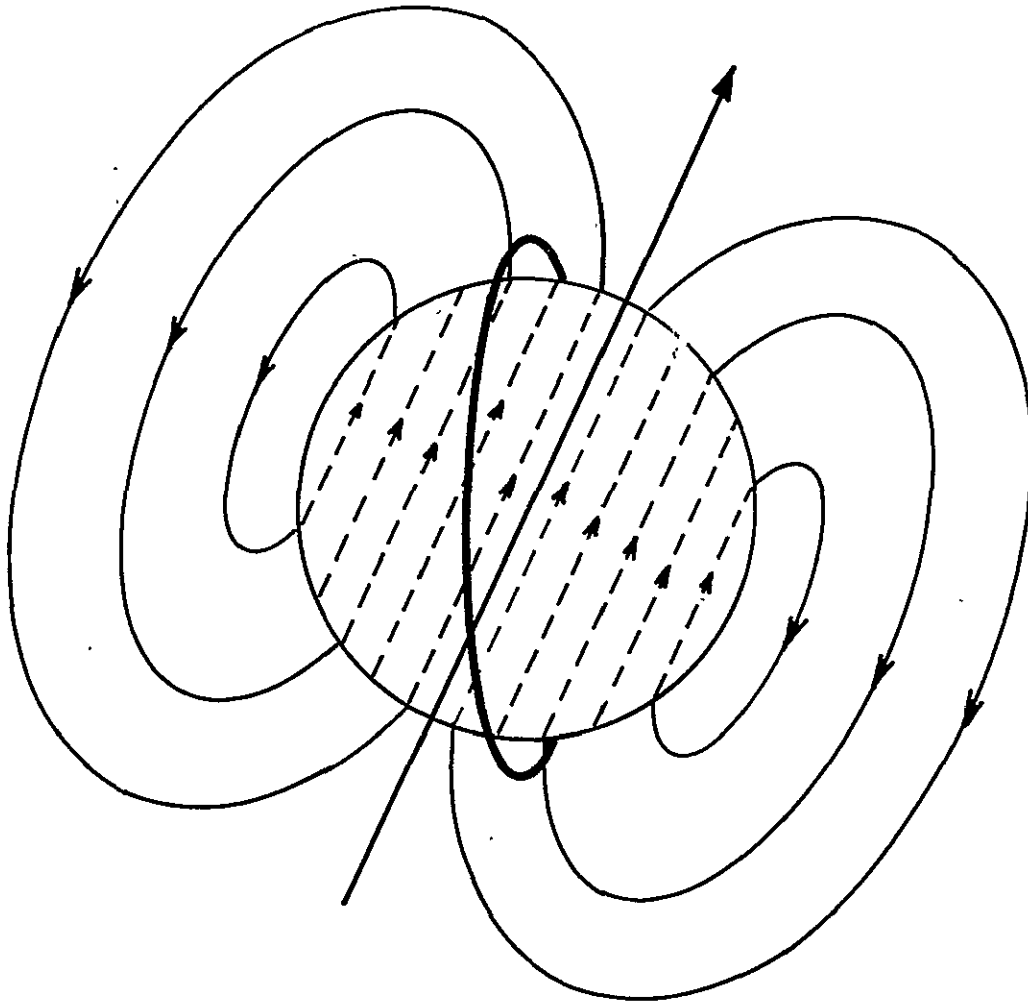
LONDON – MOMENT FIELD $H = 10^{-7}\omega$ GAUSS

Figure 8: Principle of London Moment Readout

to drop the current below I_o. During such a transition the ring is a magnetic dipole radiator. A SQUID detector works by superimposing an rf field greater than the critical value on the d.c. field H_s to be measured. In our existing systems 20 MHz or 30 MHz drive frequencies are used. Pulses of radiation are generated each time the weak link goes normal; the resultant power coupled to an adjacent tuned circuit turns out to be periodic in H_s. With appropriate audio modulation and phase sensitive detection techniques, a servo system may be designed which locks the magnetometer to a given maximum in the curve of rf tank voltage versus magnetic field by feeding back a magnetic field to the weak link circuit. The feedback current is directly proportional to the field being measured.

The difficulty in applying SQUID magnetometry to gyro readout lies in handling extraneous a.c. magnetic fields from the gyro suspension system and from residual trapped magnetic flux in the rotor. These signals average to zero, but if the rate of change of field is too rapid the feedback system cannot keep the magnetometer locked on the quantized flux step, and if the amplitude is too great there will be rectification errors due to nonlinearities in the system. Investigations described elsewhere[31] show that the trapped field levels are best kept below 10^{-7} gauss. Pickup from the electrical suspension system consists of 20 kHz signals from the suspension voltages (2kV on Earth; 0.3V in space). Two different approaches have been followed in reducing suspension pickup. One is "bucking": that is injecting drive signals of appropriate frequency, amplitude and phase into the magnetometer to reduce the disturbance to an acceptable level. The other is filtering either by means of a resistor across the SQUID input or a "damping cylinder" between the two coils of the transformer coupling the readout coil to the SQUID. The damping cylinder also serves as an electrostatic shield. The use of a resistive filter increases the readout noise, so the method should not be pushed too far.

Figure 9 shows the general layout for a single axis of the readout system now in use. It comprises a SQUID coupled to the gyro through a transformer with a damping cylinder of 300 Hz bandwidth, and connected on the output side to an rf tank circuit, oscillator, detector, 100 kHz demodulator, integrator and feedback loop. The damping cylinder kills off the 1 MHz signal and most of the 20 kHz signal; some 20 kHz bucking is available to help reduce pickup at that frequency. The noise introduced by a 300 Hz damping cylinder is about a factor of 5 higher than the readout noise from the SQUID. The noise at 10kHz bandwidth would be negligible. Since 20 kHz interference is three orders of magnitude lower in space than on Earth, the filter bandwidth can be opened up in space to a value for which the noise should become negligible. The best configuration is still under study.

Particular advantages and problems of the London moment readout are discussed in the next eight subsections. The comparison of angular resolution with the resolution of conventional gyro readouts is given in Section C(3)(e).

(c) Mechanical and Electrical Stability of the Readout Ring

An angle of 1 milliarc-sec is 5×10^{-9} radians. Subtended over a readout ring 4 cm in diameter, this corresponds to a requirement of mechanical stability to within 2 Å during the lifetime of the experiment. The distribution of current in the ring corresponding to a particular orientation of the gyro spin axis should also remain constant to the same level. The requirements can be eased somewhat by taking into account the averaging effect from rolling the spacecraft, but the need for extremes of mechanical and electrical stability in the readout ring is clear. Mechanical stability is achieved by having the ring sputtered on the housing. Electrical stability depends on the geometry of the ring as discussed in the next subsection.
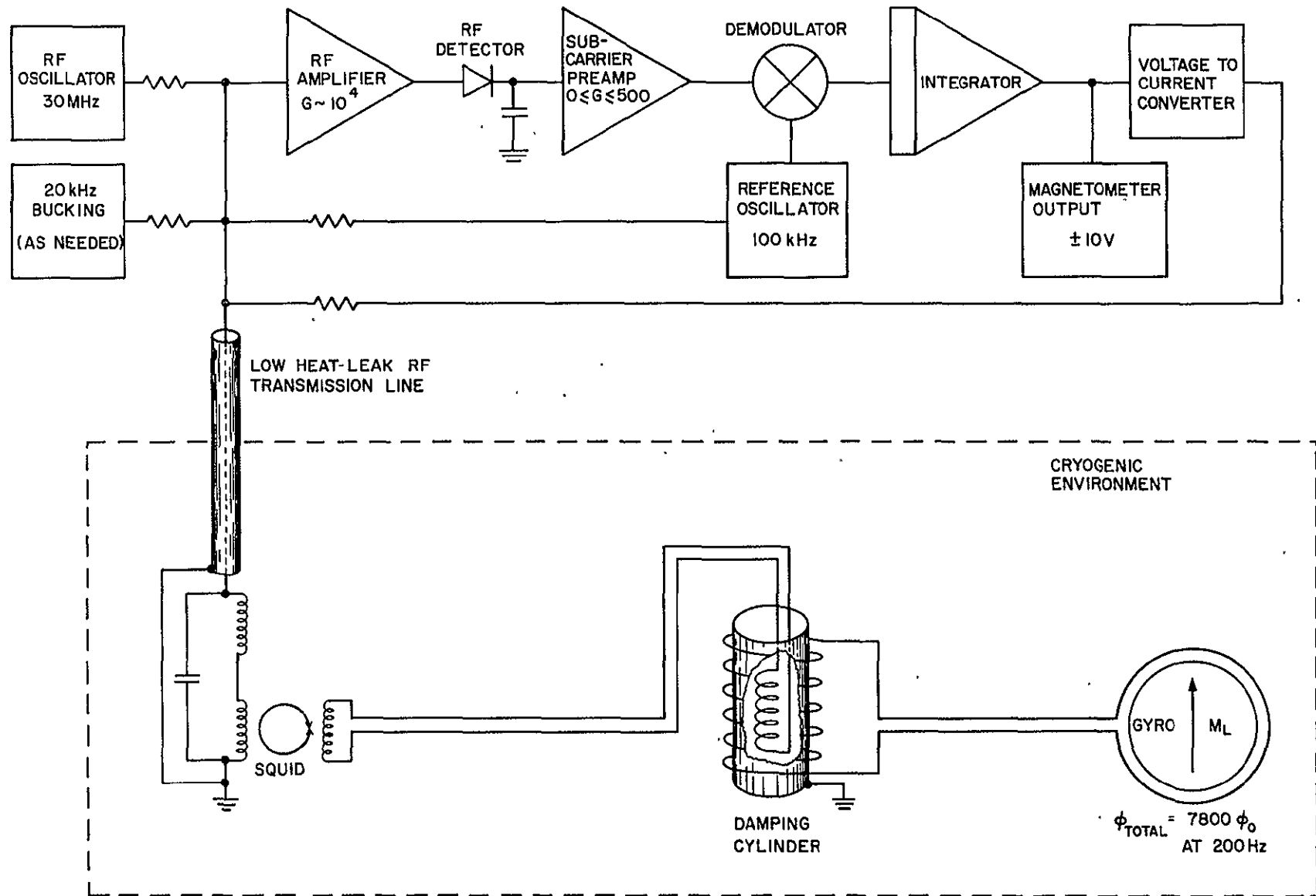
Figure 9: London Moment Readout System

(d)   Optimization of Readout Loop Performance: Saturn's
      Ring versus Wedding-Band Readouts

One configuration for the primary readout loop is a ring
sputtered on to the parting plane between the two halves of
the gyro housing (see Figure 11, p. 82). A typical geometry
would be a loop a few mils wide and 1000 Å thick located
about 30 mils from the surface of the ball, with lines running
to a convenient place at the edge of the housing to attach the
leads of the matching transformer. A second loop can be sputtered
on to an auxiliary ring sliding over the outside of the housing
(Figure 11). This particular arrangement may be called the
Saturn's ring readout. The current nearly all flows in the two
edges of the sputtered loop; one has in effect two wires 1000 Å
in diameter separated by a few mils. The inductance is about
$0.3\mu H$.

The sensitivity of the London moment readout increases with
decreasing readout loop inductance, L_r, as will be discussed
below. A method of reducing L_r is to exploit the superconductivity
of the gyro rotor by having a readout ring in the form of a broad
flat band inside the gyro housing close to the surface of the
ball. The inductance of a superconducting strip of width w and
length ℓ situated at a distance d from a superconducting plane is
proportional to $\ell d/w$. With an extended strip 20 mils wide at a dis-
tance of 0.2 mils from the surface of the ball the inductance can
be made a factor of 200 less than that of the Saturn's ring, i.e.
about 1.5 nH.   This second configuration may be called the
wedding-band readout. The current is spread more or less uniformly
over the band.
At this point we must examine more closely the problem of
optimizing readout loop performance and the significance of flux
transferred to the SQUID. Because the SQUID output is periodic
in the flux quantum ϕ_0, the tendency is to discuss the SQUID
sensitivity, and hence gyro readout sensitivity, in terms of
the magnetic flux. It is correct and often convenient to do so,
but it is often more illuminating to work with energies rather
than flux.

The best approach to understanding the relationship between SQUID sensitivity, readout circuit characteristics, and readout sensitivity is from an analogy with the usual signal transfer theory in electrical engineering. In a.c. circuitry theory an ordinary signal source can be characterized by its impedance and signal power, and the receiver by its input impedance and internal noise power per unit bandwidth; signal and noise voltages and currents are used where appropriate. In d.c. superconducting circuits, by contrast, there is no voltage, no steady-state power flow, and no resistance. Thus whereas in a non-superconducting circuit a voltage drives a current through an impedance, in a superconducting circuit a flux drives a current through an inductance, and power flow into an impedance is replaced by energy stored in an inductance. The analogous quantities are given in Table 7.

Table 7:   Analogous Quantities in Normal and
           Superconducting Circuits

Normal	Superconducting
power P	energy W
voltages V	flux ϕ
impedance Z	inductance L
current I	current I

In ordinary circuits, the maximum available signal power is transferred to the receiver when the source and receiver impedances are equal. Considering the readout ring of the gyroscope as the signal source and the SQUID as the receiver, the analogous objective is to transfer the maximum energy from the readout ring to the SQUID, and this will occur when the readout ring and SQUID have equal inductances.

If the source and receiver have different impedances, then the maximum available signal power can still be transferred from the source to the receiver if a transformer is inserted in the circuit between them. The transformer makes an arbitrary impedance change between its input and output; it can be designed to "match"

a source to a receiver having a different impedance. When an impedance matching transformer is used in an ordinary a.c. circuit, the voltage at the receiver can be hundreds of times larger or smaller than the voltage at the source, to obtain maximum power flow, depending on their relative impedances. In superconducting circuits, the transformer plays an equivalent role, but it matches inductances rather than impedances, and allows the flux at the receiver to be significantly different from that at the source.

Typical SQUIDs have intrinsic inductances between 0.1 nH and 1 nH. Higher inductances are unsatisfactory for two reasons. First, if the kT noise in the SQUID exceeds $\phi_0^2/2L_s$, the SQUID will cease to operate properly; at a temperature of 4K, this sets an upper limit on L_s of about 10 nH. Second, the signal power P_s out of the SQUID becomes difficult to observe if it is less than the amplifier noise in the rf box, and P_s is proportional to $1/L_s$. However, the upper limit on L_s set by this constraint is several orders of magnitude larger than that set by kT noise.

With a Saturn's ring readout, then, having an inductance of 0.3μH, a transformer is required for inductance matching. In the work done so far on the Gyro Relativity experiment, the matching has been provided by means of both a transformer built into the SQUID and the damping cylinder transformer referred to in Section C (3) (b). The fraction of available energy transferred from the readout ring to the SQUID is in the range 2% to 20% depending on the design and efficiency of the transformer, and the effects of stray inductances. The corresponding amounts of gyroscope _flux_ appearing at the SQUID range from 0.2% to 0.7%. Practical implications of these results for precision gyro readout are discussed in Section E (4).

Return to the ordinary electrical engineering situation. Given two signal sources having the same voltage output V_s,

the source having the lower output impedance will be able to deliver more power, since the maximum power obtainable from the source is $v_s^2/4R_s$. The corresponding expression for the maximum energy transferred from a superconducting circuit is $\phi_s^2/8L_s$ (the factor of 8 rather than 4 in the denominator arises because it is convenient in this case to use peak rather than rms signals). Translated to the gyro readout we then have that the maximum energy transferrable to the SQUID for a given angular change α is $\alpha^2\phi_L^2/8L_r$, where ϕ_L is the London moment flux and L_r the inductance of the readout ring. Since the wedding band readout has an inductance 200 times less than that of the Saturn's ring readout, it provides a signal energy 200 times greater. The practical advantage of the wedding band readout is that its high sensitivity, relative to the Saturn's ring readout, reduces the signal integration time to resolve 1 milliarc-sec from tens of hours to tens of minutes.

The reduced inductance of the wedding-band configuration allows another possible modification to the London moment readout, pointed out by Dr. J. B. Hendricks of the University of Alabama, Huntsville, namely to incorporate the weak link directly into the readout loop.[32] This arrangement leads, in principle, to a further improvement in sensitivity by eliminating coupling losses inherent in the circuity and transformer that would otherwise be necessary to connect the readout loop to the SQUID. However the direct coupled SQUID is harder to shield against pickup.

With either form of wedding band readout there are practical difficulties in fitting the ring on center in the housing. For reasons explained below an off-center ring will contribute readout null drifts due to drifts in centering of the gyro rotor. The centering criterion is described in Section C (3) (2).

A readout stability of 1 milliarc-sec means, as stated in the previous subsection, that the readout ring and the current

flowing in it have to be stable to 2 $\overset{o}{A}$ across the diameter of
the ring. The stability of the current distribution in the
Saturn's ring configuration will evidently be much better than
the 1000 $\overset{o}{A}$ thickness of the loop, but a change in temperature
of the loop might cause a redistribution of current that would
alter the null plane by a few $\overset{o}{A}$. With a wedding band 20 mils
(5 x 10^{-2} cm) wide, the null plane of the current has to remain
constant to 4 parts in 10^7 if errors in excess of 1 milliarc-
sec are to be avoided. Small changes in temperature might well
cause changes of this magnitude. Other potential sources of
trouble are the changes in inductance from polhoding of the
out of round ball, and long term drifts in the center of support.
With a gap of 200 micro-inches and a ball out of round by 0.5
microinches the periodic inductance change is 0.25%. The drifts
in center of support are about 5 microinches. Both affect the
current distribution in the wedding band and may therefore change
the null plane of the readout. With the Saturn's ring readout
loop the inductance is nearly independent of the presence of
the ball so that the effects of an out of round ball and centering
drifts are negligible.

In summary there are three possible readout configurations:
(i) transformer coupled Saturn's ring, (ii) transformer coupled
wedding band, (iii) direct coupled wedding band. The choice
depends on sensitivity on the one hand and ease of manufacture
and stability of the readout null on the other. The answers may
differ depending on the use to which the gyro is put.

(e) Readout Resolution

With realistic coupling of a Saturn's ring readout loop to
commercially available shake-tested SQUIDs, the resolution in a
100 radian bandwidth is 1 arc-sec, or 0.001 arc-sec after three
hours integration, provided integration can be carried out for
that length of time at the level of noise under discussion.
The resolution of 1 arc-sec in 100 radian bandwidth must be
compared with the 15 arc-sec in 100 radian bandwidth discussed
above for the Honeywell optical pickoff. Details of a laboratory

demonstration of the equivalent of 2 milliarc-sec resolution
with a 20 MHz SQUID magnetometer are given in Section F.
Further improvements are to be expected with more advanced
magnetometers already in existence.

Thus the Saturn's ring readout has the sensitivity to do
the job.

(f) Application to Homogeneous Gyro Rotors

In contrast to the Honeywell and Autonetics readouts, and
to most other gyro readouts so far proposed, the London moment
readout depends on observing a quantity aligned with the
instantaneous spin axis of the ball, rather than its body axes,
and does not require a rotor with unequal moments of inertia.
Of course any actual rotor, however homogeneous, does have some
residual differences in inertia ΔI_{12}, ΔI_{13} about different axes.
For small ΔI the spin axis cones about the angular momentum axis
at a rate ω_p ($\omega_p \simeq \omega_s \pm \omega_s \Delta I/I$) and with an amplitude θ_s moving
slowly between limits of order $\theta_A \Delta I_{13}/I$ and $\theta_B \Delta I_{12}/I$ where θ_A and
θ_B are maximum and minimum angles of the body cone, and the ΔIs
are the intrinsic differences of inertia, not the extrinsic dif-
ference induced by centrifugal distortion of the ball. Exact repre-
sentations of the motion are given by the standard constructions
of Poinsot and MacCullagh; further details on application of the
classical dynamic formulae to the Gyro Relativity experiment are
given in Reference (21). With $\Delta I/I$ of order 3×10^{-7} the coning
of the spin axis never exceeds 0.1 arc-sec and averages to much
less in each second of time: the London moment readout gives
a true measure of the angular momentum axis regardless of polhoding.

An intuitive understanding of the alignment of the London
moment with the spin axis may be reached in the following way.
Consider the superconductor as a lattice of positively charged
ions containing a resistanceless negatively charged fluid.
When the lattice is rotated the motion of the positive charges
generates a magnetic field aligned with the spin axis. The
charged fluid is subject to electromagnetic forces which make it
too rotate about the spin axis at a rate somewhat less than the

lattice rotation. The London moment is the residue left
over from the differential rotation of the two systems of charge.

(g)   Possible Alternative Gyro Readouts for Use With a Homogeneous Rotor

Two other gyro readouts have been investigated which track
the spin axis of the ball. One studied at Honeywell in the late
1950's was based on observing light scattered from random
scratches on the surface of the ball. The other studied between
1968 and 1970 by Massey[33] and Siegman of Stanford Electrical
Engineering Department applied a laser to measure the Fresnel
drag in a rotating transparent ball. In neither case was the
resolution as good as that of the conventional gyro readouts
described above, let alone good enough for the Gyro Relativity
experiment.

. . A variant on the London moment readout that would measure
the instantaneous spin axis and give better resolution than the
London moment would be to observe the Barnett effect in a rotating
ferromagnetic or superparamagnetic ball. The Barnett effect is
a magnetic moment aligned with the spin axis, with a magnitude M_B
in a spinning sphere

$$M_B = \mu \ \frac{mc}{e} \ \omega_s \tag{11}$$

where μ is the permeability of the medium. It is therefore just
μ times the London moment. With a Mu-metal ball the permeability
may be of order 100; the readout sensitivity would accordingly
be a factor of 100 higher than with the London moment. Just as
the London moment readout has to cope with the problem of residual
trapped flux in the superconducting rotor, so a Barnett moment
readout would have to cope with residual permanent magnetism,
affecting both the linearity of the readout and the reaction
torques discussed in the next subsection. Although the Barnett
moment occurs at room temperature, an application to the Gyro
Relativity experiment would almost certainly require cryogenic

techniques, for even though room temperature magnetometers like Blackett's may have adequate sensitivity, the stability of the readout calls for the kind of stable background fields available only with superconducting shields. Since the troubles with residual permanent magnetism in the ball get worse at low temperatures a Barnett moment readout is unlikely to supplant one based on the London moment. See Sections C (3)(h) and C (3)(j).

(h) Readout Reaction Torques

The first magnetic reaction torque to be considered is the action on the London moment (or Barnett moment) of any residual trapped magnetic flux in the superconducting shield surrounding the gyroscope. The resulting drift rate of the London moment gyro is

$$_1\Omega_m = 2 \times 10^{-8} \frac{H_s}{\rho r^2} \tag{12}$$

where ρ is the density and r the radius of the ball, and H_s is the component of trapped flux perpendicular to the spin axis. It is independent of spin speed. If the gyro shield is held in a fixed orientation Equation (12) sets a limit on H_s for the London moment of 10^{-7} gauss. For a Barnett moment with a μ of 100 the limit on H_s is 10^{-9} gauss. In a rolling spacecraft with the gyros aligned nearly parallel to the roll axis the effect averages except for the residual misalignment (up to 30 arc-sec) which sets a limit of 6×10^{-4} gauss for the London moment and 6×10^{-6} gauss for the Barnett moment. The latter figure is one reason, but by no means the only one, why a Barnett moment readout would need a superconducting shield.

Another effect is the reaction of the gyro readout current on the magnetic moment in the ball. For the London moment the resultant drift-rate with the Saturn's ring configuration is

$$_2\Omega_m = 2 \times 10^{-15} \frac{\sin 2\beta}{K\rho r^2} \tag{13}$$

where K is the gain of the feedback servo to the readout circuit

and β is the readout angle. For the Barnett moment the expression on the right hand side of (13) must be multiplied by μ^2. For the London moment the error is completely negligible even for larger readout angles. For the Barnett moment it can be made negligible provided the feedback gain satisfies the condition $K > 2\mu^2 \sin 2\beta$.

More important than either of the foregoing terms is the effect of rotating trapped flux in the ball. If the readout circuit has any dissipation, the component of spin in the plane of the loop will be slowed down, but the transverse component remains unaffected. This is an example of an important class of gyro drift terms which may be called differential damping torques. It has the form

$$_3\Omega_m = \frac{15}{8} \frac{R_L H_b^2}{\rho r L \omega_s} \sin 2\beta \tag{14}$$

where H_b is the field trapped in the superconducting ball (or for the Barnett moment readout, the component of permanent magnetism in the ball), L is the inductance of the readout circuit and R_L the resistive term describing the losses in the readout. With the SQUID readout the dissipation is principally from losses in the damping cylinder or other resistive filter. With a 2 kHz damping cylinder and a Saturn's ring readout, the typical upper limit on H_b for a gyro with readout range $\pm$ 30 arc-sec is 10^{-6} gauss, which is fairly straightforward in a superconducting ball but exceedingly difficult in a ferromagnetic one. Thus differential damping would be an awkward problem for the Barnett moment readout.

The differential damping from trapped flux, being inversely proportional to the inductance of the loop, is substantially greater in the wedding band readout. Taking the inductance of the wedding band as 10^{-9} henry, the upper limit on H_b assuming the same losses as before is 6×10^{-8} gauss, which is just about the limit of what is feasible with the existing ultra-low magnetic field shields.

(j) Linearity, Stability of the Field and Limits on Trapped
     Flux from the Readout

The need to limit trapped flux in the gyro rotor in order to
prevent the SQUID from losing lock has been discussed in Subsection
C (3) (b). Also mentioned there was 'the danger that the trapped
flux signals might drive the readout into the non-linear regime.
The latter problem falls into two parts: nonlinearity in the
SQUID magnetometer per se and nonlinearities in the feedback
and data instrumentation loops. Laboratory experience at
Stanford and elsewhere has established that the SQUID itself has
analog linearity to 1 part in 10^6 or better in the region of
interest. The digitized feedback and instrumentation loops, on
the other hand, cover only 17 bit ranges, or about 1 part in 65,000.
Now the London moment in a gyro spinning at 200 Hz corresponds to
a field of 1.2 x 10^{-4} gauss; 1 milliarc-sec resolution implies
resolving 6 x 10^{-13} gauss. Suppose there is a trapped field of
10^{-7} gauss in the gyro rotor. This will appear in the readout
as an a.c. field five orders of magnitude bigger than the required
signal resolution; no trouble to the magnetometer, but significant
trouble if it is allowed to reach the feedback or instrumentation
systems. A filter must therefore be designed to attenuate the
trapped flux signal immediately after the SQUID, and this filter
must itself be highly linear.

The foregoing suggests that the trapped field should not
appreciably exceed 10^{-7} gauss with a London moment readout. The
corresponding limit on permanent magnetism with the Barnett moment
is 10^{-5} gauss.

Questions of mechanical and electrical drifts of the readout
have been discussed in Subsections C(3)(c) and C(3)(d). Null drifts
may also occur through changes in the external magnetic field
threading the readout loop. The presence in the loop of the
superconducting ball reduces such effects by reducing the
effective cross-section from πr^2 to $2\pi rd$ where d is the distance

between ball and loop. Discounting any averaging from rolling the spacecraft the requirement on field stability is

$$\Delta H < 2H_L \theta_o \ d/r \tag{15}$$

where θ_o is the minimum angle to be resolved (say 1 milliarc-sec). Inserting numerical values one finds that the maximum allowed change in ambient field for a gyro with a Saturn's ring readout 30 mils from the ball is 10^{-11} gauss. This stability is achievable with a superconducting shield provided care is taken in guarding penetrations into the shield.

The stability requirement with a wedding band readout 0.2 mil from the ball is 10^{-9} gauss. The requirement for the Saturn's ring readout might also be relaxed if desired by exploiting the principle of the counterwound coil. The loop is connected in series with an external coil, not linking the London moment, wound in the opposite sense, and having an area equal to the annular area between it and the ball. Figure 10 illustrates a configuration that is insensitive both to the changes in uniform and first order gradient fields. Probably the cancellation can be made good to a factor of 100, reducing the stability requirements for the Saturn's ring readout also to 10^{-9} gauss.

With the Barnett moment there is no such exclusion of the field; instead the high permeability of the ball concentrates the field in the readout loop. The stability requirement is therefore not 10^{-11} gauss but (assuming a μ of 100) nearer 10^{-13} gauss. Such an extreme of isolation should be reachable with a superconducting shield, but certainly not with any system of conventional mu-metal shields. We are thus forced to the important conclusion that a Barnett moment gyroscope must have superconducting shielding, and must therefore be operated at cryogenic temperatures.
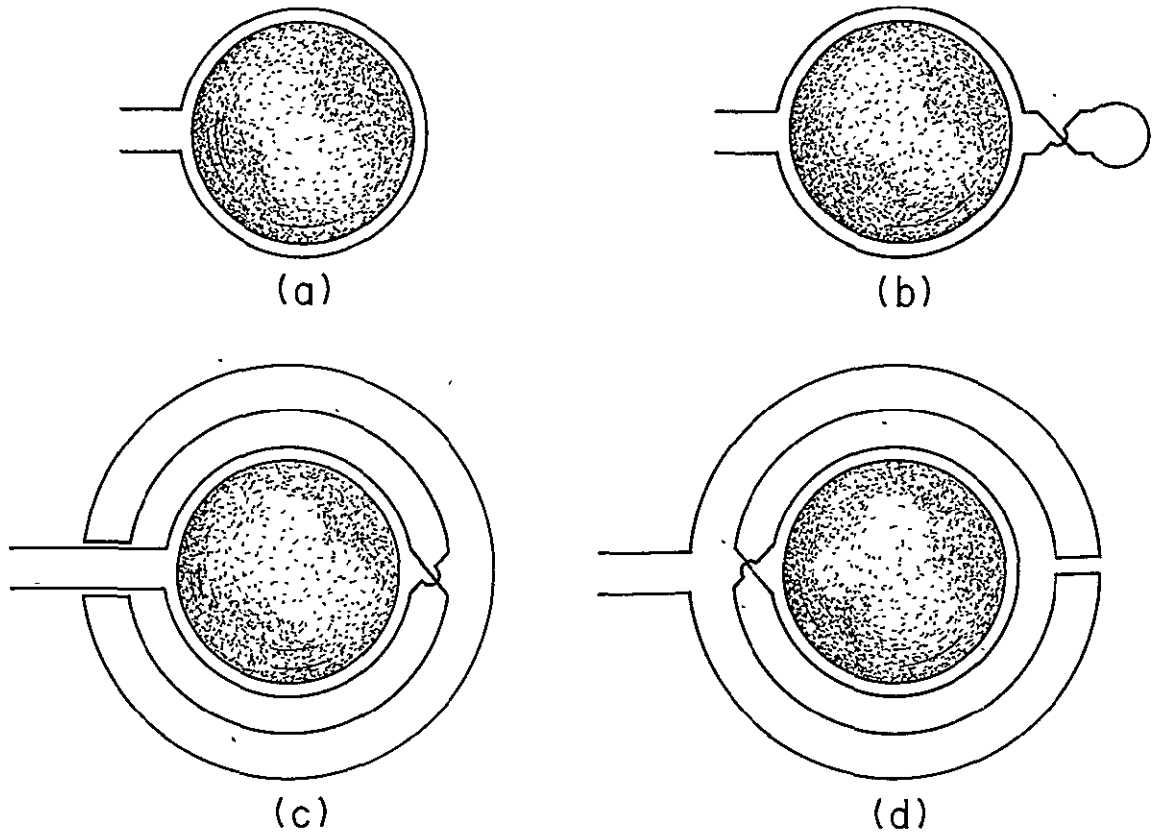
Figure 10: Counterwound Readout Ring

(a) Simple pickup loop (b) Auxiliary coil
added with phase reversed (c) Wrap-around
auxiliary coil (d) Final coil with connections
arranged for winding convenience

(k) Centering Stability

A source of readout error of a different kind, important to design of the gyroscope, is the displacement of the ball from the center of the readout loop. Define axes with x parallel to the spin axis of the ball and z normal to the plane of the loop. An analysis similar to one applied by Maxwell[34] in 1863 during his interesting investigation of the errors in the British Association experiment to determine the ohm in absolute units, yields an error angle θ_d

$$\theta_d = \frac{\pi}{2} \frac{xz}{r^2} + \frac{\pi}{6} \frac{yz}{r^2} \tag{16}$$

Thus in contrast to the error of the Honeywell optical pickoff, discussed in C (3) (a), which are first order in the displacement of the ball from the center of the housing, the centering errors with the London moment readout are second order in the displacement: a most important advantage.

In earlier publications on the subject[7][24] Equation (16) was rightly given (although incompletely so since the second term on the right hand side was left out) but wrongly interpreted. A correct interpretation means evaluating the change $\delta\theta_d$ due to long term drift of the ball with respect to the loop, recognizing that manufacturing errors in the housing will put the ball off center to begin with. Differentiating (16) we have

$$\delta\theta_d = \frac{\pi}{6r^2} \left[(2x + y) \, \delta z + z \, (2\delta x + \delta y) \right] \tag{17}$$

where x, y, z now represent the initial position of the ball determined by manufacturing errors and initial suspension conditions, and δx, δy, δz are displacements of the ball due to drifts in the suspension electronics. The suspension performance is such that δx, δy, δz are of order 10^{-5} cm. Setting a limit on $\delta\theta_d$ of 3×10^{-9} radian (0.6 milliarc-sec), we find limits on x, y, z of order 10^{-3} cm or 0.4 mils. Thus a manufacturing tolerance on the gyro housing is to center the readout loop in all three axes to 0.4 mils: a difficult but feasible task.

The foregoing requirement poses some difficulty with the wedding band readout, since in a housing parted down the middle the easy thing would be to put the wedding band off-center.

(ℓ)   Mechanization as an All Angle Readout

The London moment readout, as so far described, is restricted to operation over a linear range of ± 32 arc-sec. The restriction can be avoided by the use of flux-counting techniques. A SQUID magnetometer has a sawtooth response quantized in fixed steps of hc/2e, each of which can be resolved with great precision. If instead of a conventional digital feedback one combines the feedback loop with a flux-counting system, an all angle readout may be developed having an angular resolution up to 24 bits per quadrant, corresponding to somewhere between 0.1 and 0.01 arc-sec resolution throughout the range. Details are given elsewhere. [35] The best conventional angle encoders have resolutions of 17 bits per quadrant. The all angle readout is not needed in the Gyro Relativity experiment, but would be in applying the gyroscope in inertial references for an astronomical telescope.

D. GYROSCOPE AND GYRO READOUT DEVELOPMENT

(1) Rotors and Gyro Housings

(a) Background

In February 1964 Stanford began discussions with Minneapolis-Honeywell (later Honeywell Incorporated) to design and build piece parts for gyro housings and rotors and an electrical suspension system for a laboratory version of the relativity gyroscope. In July 1964 discussions were also started with D. E. Davidson of Davidson Optronics Incorporated on the design of a star-tracking telescope and mounting ring for attachment to the gyro housing. After negotiations with the two companies we concluded that the best interface between the gyro and telescope package would be for Davidson Optronics to build the quartz mounting ring and gyro

shield assembly (Figure 6, p. 40), with Honeywell building the quartz housing and rotor. Subcontract PR0392: "To Design and Build a Solid Quartz Gyro Rotor, Quartz Gyro Housing and ESG Suspension Electronics," was issued from Stanford to Honeywell in January 1965 to furnish one quartz gyro housing, one or if possible two niobium-coated quartz rotors, one electrical suspension system, dummy loads for the suspension system, and sundry test pieces for electrical breakdown tests, feedthrough tests, etc. Subcontract PR0692: "To Develop and Build a Gyro Shield Assembly and Star-Tracking Telescope," was issued from Stanford to Davidson Optronics Incorporated in September 1965.

Honeywell work on gyro piece parts is described in Sections D (1) (b) and D (1) (f); the work on the electrical suspension system is described in D (2). Davidson Optronics work on the Gyro Shield Assembly is described in D (1) (c); the telescope development is described in Section G. Other work on gyro parts at Stanford, NASA Marshall Center and elsewhere is described in Sections D (1) (d), D (1) (e) and D (1) (f). For reasons that will become-clear as we proceed there will be some overlap between the account of gyro manufacture and the account of gyro testing in Section D (4). In the interests of clarity it seems best to accept some repetition.

(b)   <u>Fabrication of Gyro Piece Parts at Honeywell 1965 - 1971</u>

The first tasks undertaken at Honeywell were the fabrication of gyro rotors and fabrication of the electrical suspension system (see D (2)). Fabrication of the gyro rotors went fairly smoothly. The first niobium coated quartz rotor was delivered to Stanford in August 1967 and tested for superconductivity by partial levitation in a magnetic field. The first rotor had a measured sphericity of about 4 microinches. An attempt to improve on this figure by long-term lapping experiments at Honeywell failed; in fact the experiments were terminated in 1968 when the rotor sphericity

began getting worse with time. Thereafter work on gyro rotors
was transferred from Honeywell to NASA Marshall Center. See
Sections D (1) (d) and D (1) (g).

Development of the gyro housings was to prove a major
problem. Two difficult requirements were that the housings be
made of fused quartz to match the expansion coefficients of the
telescope structure and gyro rotors, and that they have non
magnetic electrodes and feedthroughs. All Honeywell's previous
experiences with electrically suspended gyroscopes had been with
ceramic housings which had (magnetic) electroless nickel electrodes.
Honeywell had begun to gain experience in quartz work, however,
through research on the laser gyro. The first two years of
housing development involved working out details of the interface
with the Davidson gyroshield assembly, making test pieces to
evaluate breakdown characteristics of sputtered titanium electrodes,
and most important T. Dan Bracken's investigation at Stanford of
the spin up problem. Design of the gas spin up system was com-
pleted in August 1967. One critical problem was how to make the
raised lands around the gas channel (Figure 7), whose clearance
from the rotor has to be 0.2 to 0.3 mil, whereas the rotor-
electrode gap is 1.5 mil. The first idea was to electroplate
copper in the appropriate area of the housing, but experiments
at Honeywell in 1968 demonstrated that copper goes down in a
stressed condition and at a thickness greater than 0.5 mil it
tears away the quartz. Honeywell devised a plating procedure
to control the stress, but differential contraction on cooling
to cryogenic temperatures proved (contrary to the evidence of
earlier experiments with sputtered aluminum) stressful enough to
tear the bond. After abortive experiments with sputtered quartz
we decided to follow a new approach suggested by Honeywell: epoxy-
ing into the housing inserts containing separately fabricated
spin channels.

We will refrain from telling the whole melancholy history
of the Honeywell quartz housings, which is detailed in the
Honeywell Customer Engineering Letters of 1968 and 1969 and in
the Stanford Annual Reports and Status Letters for 1971 through
1975. Suffice it that one quartz housing with inserts was com-
pleted and delivered to Stanford in December 1969. This had a
chip on one of the lands and was sent back for rework. In the
first rework at Minneapolis it was damaged through a mistake in
set-up; later after the Honeywell team had been transferred to
St. Petersburg, Florida, it was accidentally destroyed. The
difficulties of insert fabrication led us to try a compromise
housing design in which the rotor-electrode gap was made
nominally the same as the gap from rotor to spin up lands.
This, though less desirable from the torque standpoint, was a
lot easier to make. In April 1970 Stanford issued a new sub-
contract to Honeywell, PR0927: "To Build a Quartz Envelope
Assembly and Deliver As-Fired Ceramic Parts." In July 1972
after some vicissitudes Quartz Gyro Housing No. 2 (as it became
known) with the reduced rotor-electrode spacing was delivered
to Stanford. Its later history is described in D (1) (e)
below.

By 1969 everyone connected with the Gyro Relativity program
could see that housings were a critical problem. Discussions
between Stanford and NASA Marshall Center led to two developments:
the starting up at MSFC of some in-house work on quartz housings
and quartz fabricating techniques, and a decision to obtain from
Honeywell a back up housing of ceramic material. Ceramic with
2 mil copper plating was known to withstand temperature cycling;
we could revert to the plating technique to make the raised spin
up lands. A ceramic housing could only be a stopgap, of course,
in view of its residual ferromagnetism and difference in expansion
coefficient from the quartz rotor and quartz shield assembly,
but the situation was critical. The purchase of three sets of
as-fixed ceramic parts under Stanford Subcontract 0927 prepared

the way, and in July 1970 NASA Marshall Center issued to Honey-
well a Contract NA8-26312: "To Design, Fabricate, Perform Tests
and Deliver Ceramic Envelopes in Support of Electrostatic
Gyro Development." The completed parts were shipped to NASA
Marshall Center in January 1971; after measurements there they
were carried to Stanford on March 12. On March 23 they were
assembled at Honeywell, Minneapolis plant, by L. C. Mellum of
Honeywell and J. A. Lipa and handcarried by Dr. Lipa to Stanford.
As it turned out all the gyro operations at Stanford from 1971
to 1975 were done with the ceramic housing as described in
Section D (4). Figure 11 shows the completed piece parts of the
ceramic housing.

Since the foregoing is inevitably in some degree critical
of Honeywell's contribution to gyro development, we think it
fair to pay special tribute to Mr. D. F. Elwell, who led the
Honeywell group, for his strong effort to push the Stanford
program forward under personally difficult circumstances. Other
Honeywell personnel who contributed to the work were R. E. Johnson,
L. C. Mellum, T. Ritter and J. Seemans. For further reflections
on the difficulties of gyro development see Section D (1) (h).

(c) The Davidson Gyro Shield Assembly

Design of the gyro shield assembly was worked out by D. E.
Davidson and C. W. F. Everitt in 1967. Besides the interface
with the gyro housing, the shield assembly had to be mated to
the telescope mounting ring and incorporate a plenum chamber
and pumping outlets of appropriate dimensions for exhausting the
differential pumping ports of the gyro gas spin up system. After
several design iterations which were checked out on an aluminum
model of the Davidson and Honeywell parts the plans were frozen
in May 1968 and the quartz parts were fabricated and delivered
to Stanford in February 1970. Figure 12 illustrates the gyro
shield assembly.
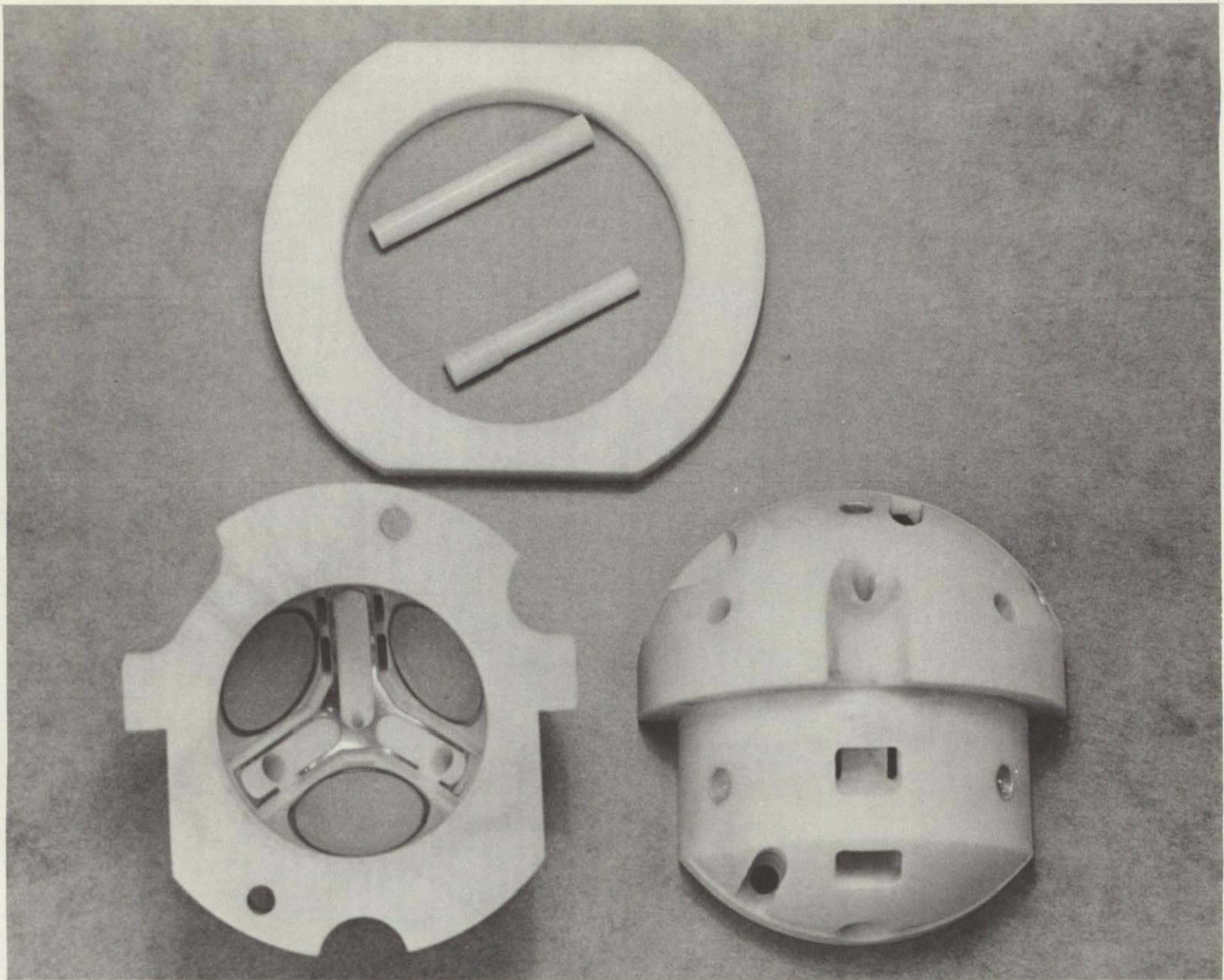
Figure 11:   Ceramic Gyro Housing
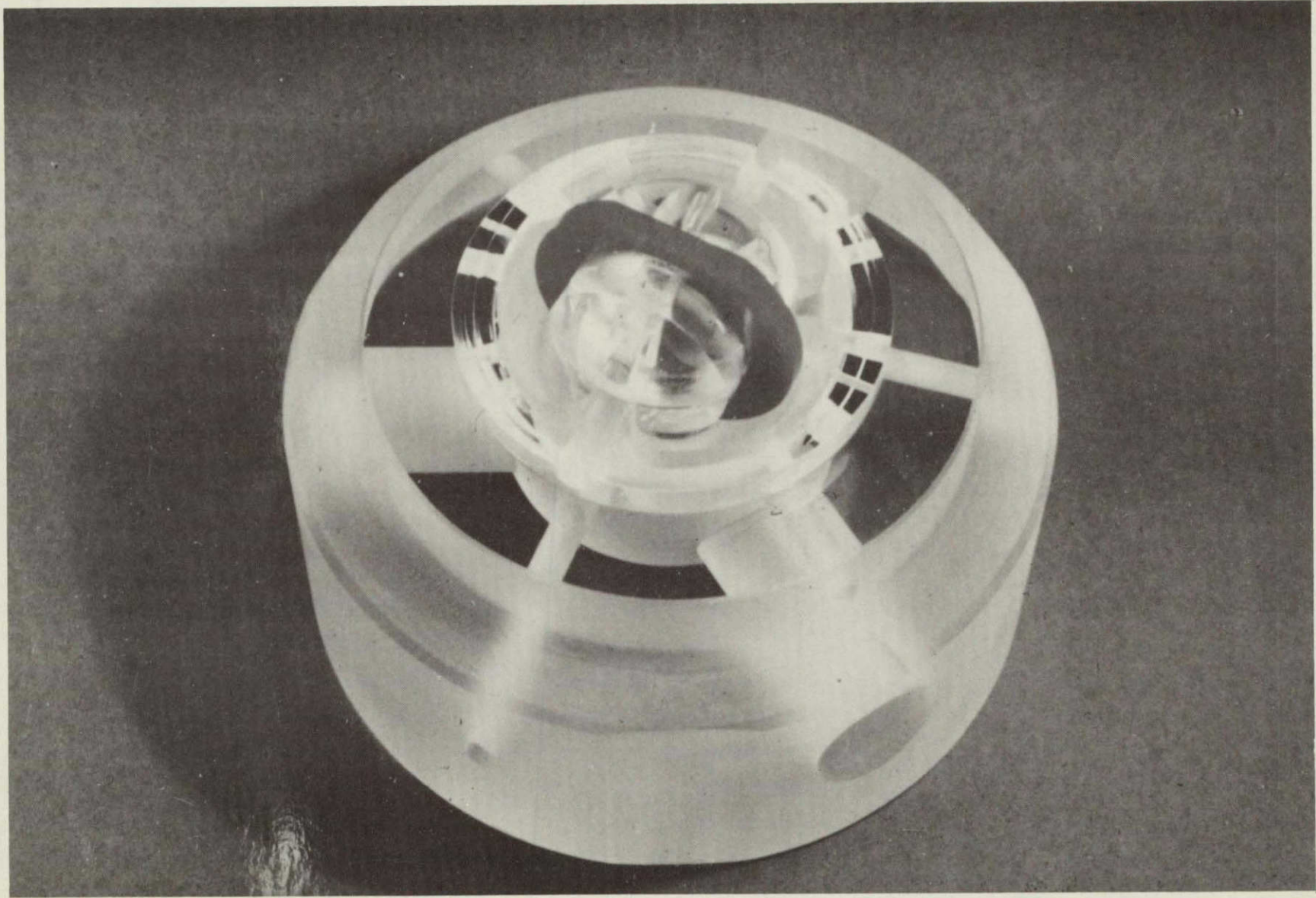
Figure 12: Gyro Shield Assembly

(d) Development of Quartz Gyro Fabrication Techniques at
     NASA Marshall Center 1969 - 1976

Work at NASA Marshall Center on gyro housings and gyro
rotors was directed by Mr. Wilhelm Angele of the Manufacturing
Engineering Laboratory (later the Engineering Physics Laboratory)
between 1969 and 1974. Associated with the work were J. Rasquin,
J. Hill and J. Reid of MSFC and T. Barber and V. Clune, external
contractors, from Hayes International. An important advance was
the fabrication of quartz rotors with sphericity approaching
1 microinch as compared with the 4 microinch sphericity reached
by Honeywell. The 1 microinch sphericity represented the limit
of the measuring equipment. Credit for the careful handwork
needed goes to J. Hill.

In 1969 Mr. Angele conceived a new design for a quartz gyro
housing, different in configuration to the Stanford-Honeywell
design. Gyro housings were built and tried at Marshall Center
from 1970 to 1973 but proved very difficult to assemble and
align. The difficulties proved such that in 1973 Mr. Angele
abandoned his idea and proposed yet another approach to gyro
fabrication, namely to recess the electrodes below the primary
reference surface rather than build up raised lands around the
spin channels. Recessing had been tried earlier at Honeywell
but the jig borer available in the Honeywell plant could not
meet the tolerances. Mr. Angele devised a new machine (a
variant in effect of the Draper optical lapping machine) which
promised well. After reviewing the procedure at NASA Marshall
Center in December 1973 we requested NASA to apply the recessing
technique to Honeywell Quartz Gyro Housing No. 2. The electrodes
had already been applied at Stanford and the parts were undergoing
measurement at Marshall Center. The coating having been not
entirely successful there seemed a good opportunity to do the
recessing before their return to Stanford.

Pressure and delay at MSFC made the recessing take much
longer than hoped. The parts were finally completed and shipped

back to Stanford in October 1975. Work at Stanford to complete
the housing is described in D (1) (e). Meanwhile work at
Marshall Center on the second MSFC designed housing continued.
A shortcoming pointed out by C. W. F. Everitt and J. A. Lipa
in December 1973 at the same meeting in which we decided to
apply the measuring technique to the Stanford-Honeywell
housing, was the absence of proper differential pumping slots.
It was clear to us that this severely limited spin speed at
cryogenic temperatures, but later calculations by G. Karr of
the University of Alabama, Huntsville indicated a limiting speed
much higher than we expected, in the range 40 to 80 Hz. For
reasons of expediency the Marshall Center group decided to pro-
ceed with the design as it stood. The MSFC housing thus became
to some extent a test jig for the electrode recessing technique
rather than a practical configuration for the final housing.

The recessing technique worked fairly well, though not as
well as had been hoped. Alignment accuracies of the electrodes
proved to be 50 to 100 microinches rather than the 20 microinch
tolerance called out in Table 5. A possible alternative reces-
sing procedure, based on quartz etching techniques, has recently
been suggested by Mr. Angele and tried out with some success on
test samples of flat geometry. Meanwhile the second Marshall-
designed gyro was spun up in 1976 at room temperature and cryogenic
temperatures in an apparatus designed by Dr. J. B. Hendricks of
the University of Alabama, Huntsville. The spin speed at low
temperatures was found indeed to be restricted to about 4 Hz.

(e)   Completion of Quartz Gyro Housing No. 2 (1975 - 1976)

This section, though placed here for logical convenience
depends on ideas gained during the ceramic gyro operations des-
cribed in Section D (4) (c) to which reference should be made.

After the completion of the electrode recessing procedure
at NASA Marshall Center in October 1975 we turned our attention
to the remaining tasks required in completing the gyro housing

86

and rotor. These were:

(i)   deposition of monometallic superconducting electrodes
       capable of withstanding electrical breakdown

(ii)   fabrication of superconducting feedthrough pins for
       the electrodes

(iii) development of quartz inlet/outlet plumbing for the
       spin up channels

(iv)   coating of the gyro rotor with a monometallic super-
       conducting film capable of withstanding breakdown.

The main innovation in these tasks was to develop procedures for
applying films of superconducting niobium 100 microinches or more
thick to the quartz parts. These were required for two reasons.
In the work with the ceramic housing described in D (4) the
ball-coating was 10 microinches of niobium overcoated with about
400 microinches of copper for protection against electrical break-
down, and the electrodes were coated with 5 microinches of titanium
for bonding plus about 400 microinches of copper. Since the
electrodes and the outer coating of the ball were not supercon-
ducting the large suspension currents needed to suspend the ball
on Earth dissipated considerable heat, which could only be removed
at low temperatures by operating at a relatively high gas pressure
(10^{-4} or 10^{-5} torr rather than the 10^{-9} torr called out in Table 5).
The presence of gas made the exponential spin down time of the
ball less than a day instead of the 300 years required for the
final experiment, making long term gyro operations in the laboratory
difficult or impossible. Furthermore other investigations des-
cribed in D ·(4)(e) had shown that the process of reducing trapped
magnetic flux in the gyro rotor is severely hampered by thermo-
electric currents, either from bimetallic coatings such as those
on the existing rotors and electrodes or from temperature gradients
across a strained normal metal. We decided on a program to increase
the maximum thickness of the niobium films to the point where
they could withstand suspension arcs.

The first step was to determine the thickness of niobium needed to withstand breakdown without degradation of the film. Using a flat quartz electrode test piece and a specially designed breakdown test rig we found that 100 microinches of niobium were able to withstand "burn in." The electric field at its surface could be increased until arcing began, after which it could be slowly increased initially with heavy arcing, but ultimately stabilizing at a higher level. Less than 10% of the arcing pits penetrated the film, and very few of those that did showed signs of multiple arcing.

Armed with this information we modified the sputtering fixtures to allow deposition of niobium electrodes in the gyro housings and did trial runs on a dummy quartz hemisphere. To test for superconductivity we built a non contacting inductive device which measures the change in coupling between two circuits in the presence of a superconducting ground plane.

After establishing the procedure for making the films we turned our attention to fabricating superconducting feedthroughs to connect the suspension cables to the electrodes. A spring-loaded niobium pin system was developed, mechanically similar to a feedthrough arrangement developed in-house at NASA Marshall Center for the MSFC gyro housings. In the ceramic housing the feedthroughs had been platinum wires fired into the ceramic before lapping. Even with very light spring loading we found the new feedthroughs giving adequate contact and there was no damage to the film.

During June and July 1976 we fabricated the pins for the housing, sputtered the electrodes and assembled the gyro for levitation tests. The first tests were with a lightweight beryllium rotor, levitation of which proved extremely difficult, probably because of the exceptionally large rotor-electrode gap. The arcing did not cause appreciable damage to the electrodes.

Rather than continue with the lightweight ball we set up
to run deposition tests for the quartz rotor. In October 1976
we completed the fabrication of a ball rolling jig which allows
rotation about two orthogonal axes. An old rotor was stripped
and coated. To begin with it was difficult to obtain adhesion
with the required thickness of niobium but after adjusting the
deposition parameters good films were formed. The rotor was
then checked for superconductivity using the non-contacting
inductive device mentioned above. The new rotor was delivered
to Stanford from Marshall Center in November 1976. We coated it
with the four position tetrahedral angle sequence that we had
so far found most useful.

Levitation and spin up tests of the new rotor in Quartz
Gyro Housing No. 2 were performed in November and December 1976
and January 1977. Levitations in the room temperature test chamber
during November were very satisfactory. The first spin tests
in the new gyro test facility (see E (3)) failed because of a bad
joint in one suspension cable, but spin tests in the room tem-
perature test chamber, which had been modified to include spin
up plumbing went very well. In January we did a low temperature
run, with successful spin up at nitrogen temperatures but some
difficulties at helium temperatures which seem to have come from
peeling of the niobium on the ball. No appreciable damage had
occurred on the electrodes. The ball is being recoated.

During the levitation tests we discovered that the gyro
rotor had been made about 0.6 mil undersize as the result of a
longstanding incongruity between the records at Stanford and
Marshall Center. The error was corrected and a new ball ordered,
to be coated in house at NASA Marshall Center by Dr. Palmer Peters
of the Space Sciences Laboratory. Delivery is expected in March
1977. The smaller ball does not cause any difficulty in the
present phase of operations.

Figure 13 illustrates Quartz Gyro Housing No. 2 assembled.
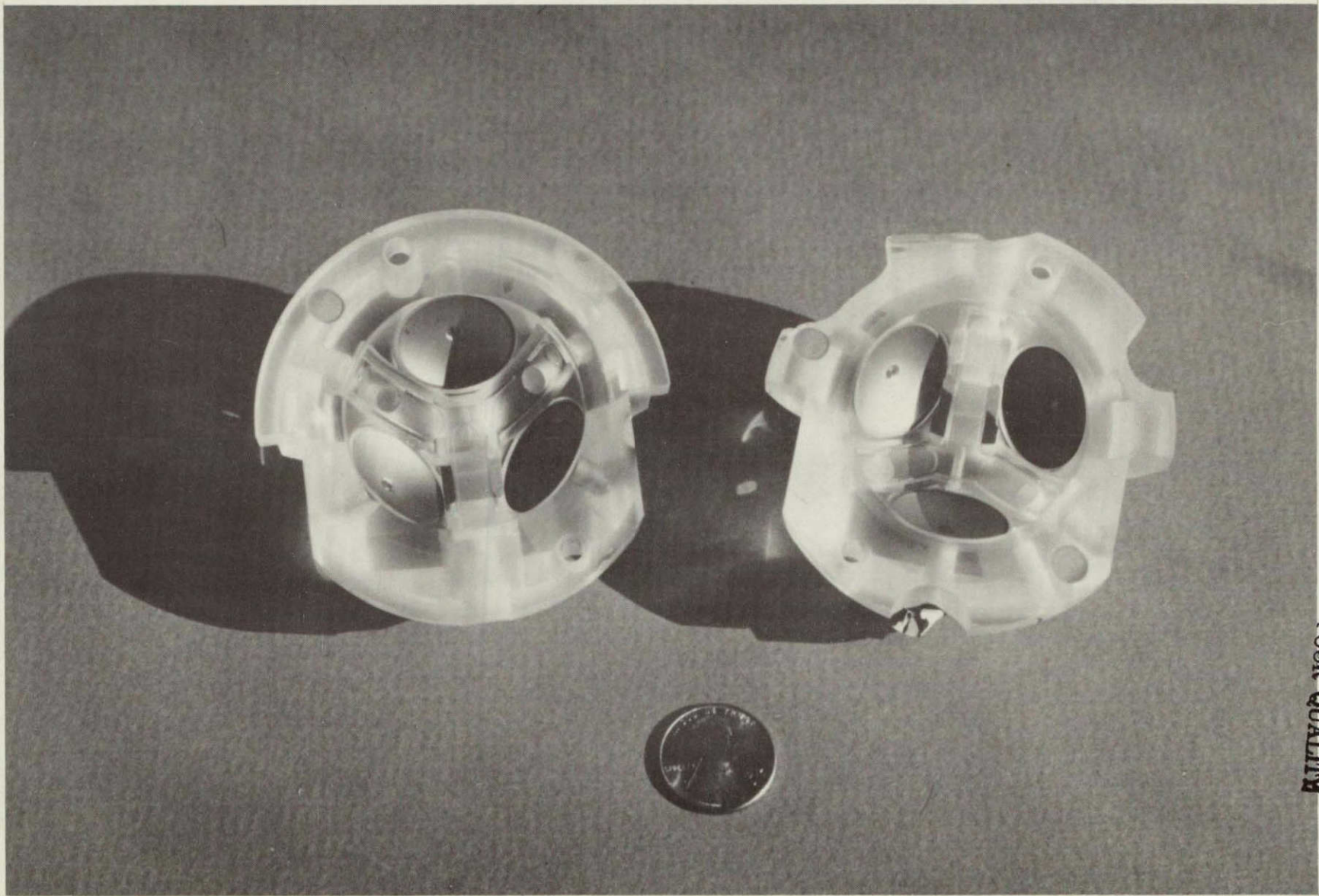
Figure 13: Quartz Gyro Housing No. 2

(f) Termination of Work at Honeywell and Design of a
     Simplified Quartz Gyro Housing

After 1972 further development of the Stanford-Honeywell
housing design turned on a negotiation in which Honeywell
agreed to replace the shattered Quartz Gyro Housing No. 1 at
company expense. The first work on the new housing was completed
by Honeywell in 1973 but unavoidable delays at Stanford pre-
vented further work for about two years, by which time Honeywell
had lost two men and the company found itself unable to finish
the task. A settlement was reached in November 1976 in which
Honeywell wrote off two bills to Stanford in the amount of $13,473
and paid Stanford the sum of $4,158 in lieu of completing the
housing.

Meanwhile, following the successful operations with the
ceramic housing, described in D (4), and the recessing of the
electrodes in Quartz Gyro Housing No. 2 by NASA Marshall Center,
we felt able once more to bring our minds to bear on the funda-
mental problems of housing manufacture. In June 1976 J. A. Lipa
conceived a simplified gyro housing in which the spin channel
assembly would be fabricated as a single unit to be inserted
into the housing from outside. A similar suggestion had been
aired by D. F. Elwell of Honeywell in 1969 but we had never
followed it up. Details of the new design were worked out by
J. A. Lipa and D. E. Davidson in July and August 1976 and reviewed
with NASA Marshall Center personnel in August and November 1976.
An important new aspect of the gyroscope scene has been the
close working relationship developed over the past two years
between NASA Marshall Center and the Speedring Corporation,
Culman Division, Culman, Alabama. Speedring had done preliminary
fabrication of quartz parts for the MSFC housings. The opportunity
therefore existed to identify a new vendor, with experience
in quartz housing work, whose operations could be super-
vised by Marshall Center personnel. During the design stages
Mr. Davidson visited the Speedring plant for consultations which
enabled him to work out a manufacturing process compatible with
the Speedring equipment.

Before working on the details of the new gyro design we reviewed the hard-won experiences of the past nine years, both at Honeywell and NASA Marshall Center, and brought the following points into focus:

(i)   the sphericity of the electrode surfaces is more critical to gyro performance than the sphericity of the surface of the raised spin up lands, and since the tolerances given in Table 5 challenge the state of the art it is essential to put our best manufacturing effort here.

(ii)   the electrodes must be located as far from the rotor as possible to reduce effects of manufacturing imperfections on gyro performance. On the other hand limitations of the suspension system prevent the use of a gap greater than about 3 mils.

(iii) the raised ridge spin channel geometry is the only configuration that can allow spin up to the required 200 Hz. The clearance between the ridges and rotor must not exceed 0.3 mil. In addition high flow rate auxiliary pumping channels are essential to reaching full speed.

At this stage of the program no gyro design can be considered unless it fully addresses these three points. Take point (i). By far the best technique for making a spherical surface within a housing formed from two hemispherical shells is the "tumble-lapping" procedure developed by Honeywell for their gyros. For this the two roughed out hemispheres are pinned together in their final configuration with a weighted lap and grinding compound in the cavity, and then shaken about two or more axes on a special table. Sphericities of 5 microinches are attained--well within the 20 microinch tolerance called out in Table 5.

Points (ii) and (iii), taken together with (i), force us in the direction of making the raised ridges after tumble lapping the electrode surfaces. Only two approaches seem possible: (a) sputter deposition of metal or quartz on the ridges, (b) inserts. Sputtered metal ridges are pretty well ruled out by the experience at Honeywell in 1968 and 1969. Sputtered quartz at that time

also gave poor results, and although progress has been made
since, experiments on quartz sputtering made at Stanford in
late 1975 showed that considerable development was still needed
before the method could be usefully applied to gyro housings.
Our thoughts turned once more to inserts.

In the original insert design four small pieces had to be
fitted and glued into each hemisphere and the final elevation
depended on a correct determination of the depths of the recess,
the height of the insert and the thickness of the glue. Fabri-
cation and positioning were exceedingly difficult. In the new
design the whole spin-up channel is made on a single insert
figured independently of the rest of the housing and glued
laterally to the walls of a slot cut through the housing, its
location being set by a special tooling ball. Figure 14 shows
the housing and inserts.

The most critical problem is gluing the pieces together in
such a way that they are aligned to the right tolerances and
will withstand temperature cycling to 4K. Two test pieces were
built to investigate this. The first comprised two parts from
an optical flat. We found it a simple matter to perform the
alignment and gluing to an accuracy of 3 microinches along the
length of the insert, a factor of ten or more better than is
required. The part was temperature cycled to liquid nitrogen
and liquid helium temperatures with no noticeable change in align-
ment as determined by interferometry. The parallelism was con-
firmed by measurements on the Talyrond 73 instrument described
in Section D (1) (g). In the actual housing the shape of the
parts precludes the use of interferometry for alignment; we shall
be depending on sputtered electrical contact pads. The second
test piece simulates in flat geometry the slot, insert and
gluing wedges for the housing; it will allow simultaneous
electrical and interferometric measurements to determine the
accuracy with which the alignment can be done electrically.
The breakdown voltage for a 5 microinch air gap is about 1 mV.

ELECTRODE HEMISPHERE

SPIN-UP INSERT

GAS INLET

INSERT SLOT

ELECTRODE AREAS (3)

ELECTRODE FEED-THROUGHS (3)

GAS EXHAUST

ALIGNMENT PIN HOLES (2)

CLAMPING HOLES (3)

GAS EXHAUST

GAS INLET

GAS FLOW CHANNEL

SPACERS (2)

0   1   2

SCALE: INCHES

93
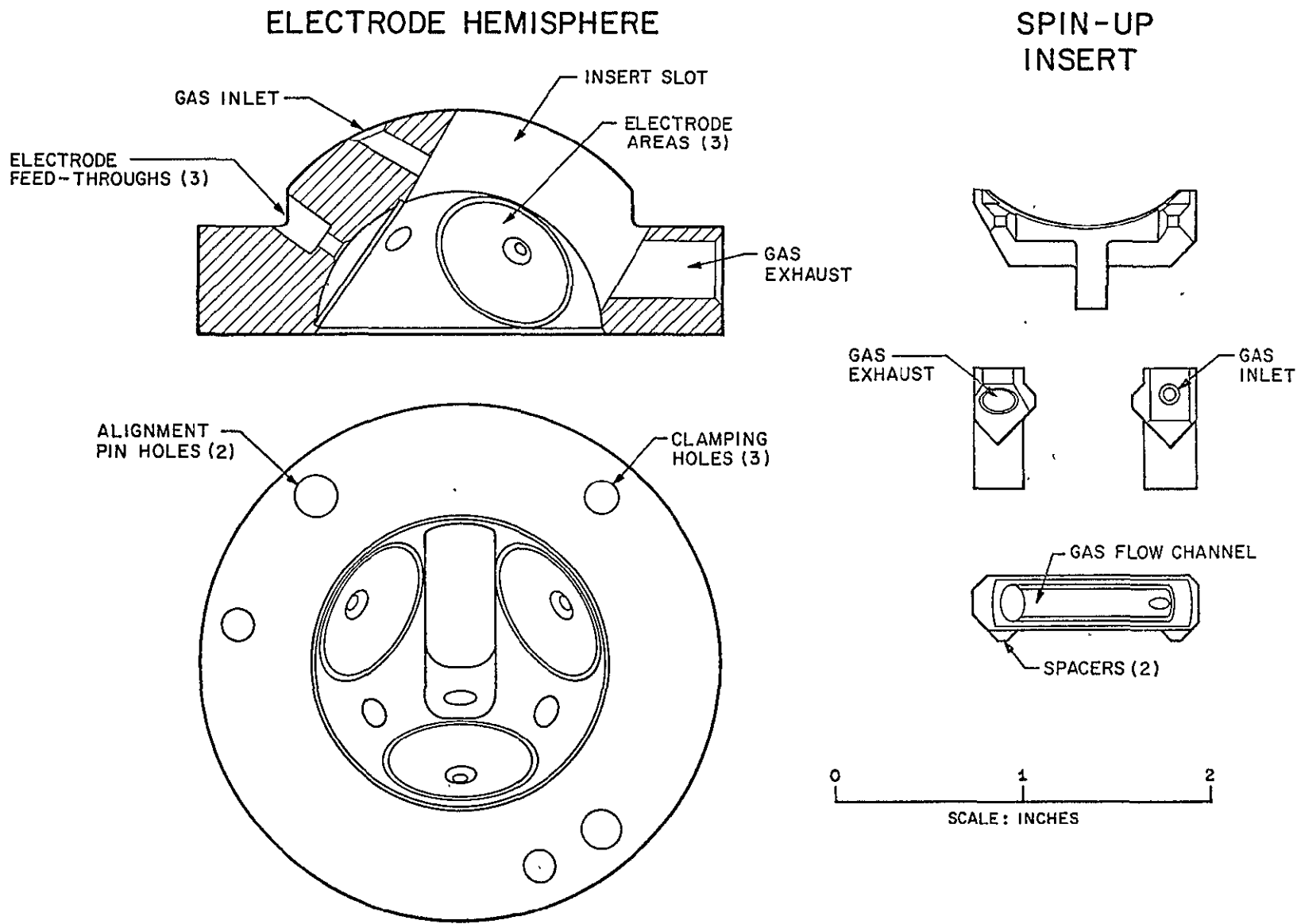
Figure 14:   Design of Simplified Quartz Gyro Housing

One important observation already made on the second test piece is that any dimensional changes through stress relief after cutting the slot are minimal--a few microinches at most. This lays to rest one of the fears about the new gyro design that has been voiced by some people.

With the success of the first test piece we commissioned D. E. Davidson to review the design, establish details of the fabrication procedure, to complete a set of process drawings for the housing and inserts, and supply additional test pieces. The major steps in fabrication are as follows:

(i) Make cylindrical quartz blanks, lap one end flat and grind outer diameter to size

(ii) Bore three axial clamping holes, curve generate the inner and outer hemispherical surfaces and make alignment pins

(iii) Assemble the housing, bore the alignment holes and lap the pins to fit

(iv) Tumble lap the cavity and check sphericity

(v) Determine the cavity size and make a tooling ball with the curvature required to lap the inserts to correct dimensions

(vi) Cut the inserts from curve generated lens blanks which have been fitted to the ball

(vii) Make gluing wedges

(viii) Do all the interior boring and grinding for the cavity and the cuts for the outer readout rings

(ix) Assemble the housing with the insert ball centered on the electrodes by spacers and glue in the inserts and support posts

(x) Finish the tapered ground glass joints for the spin up plumbing

(xi) Sputter the electrodes and readout loops

(xii) Fabricate and sputter the rotor.

The plans for the housing were completed in October 1976 and quotations were obtained from Speedring. Following the visit of D. E. Davidson, C. W. F. Everitt and J. A. Lipa to

NASA Marshall Center on November 22 and 23, 1976, at which time
the final design details were reviewed with MSFC personnel,
NASA issued Contract NAS8-32306 in the amount of $12,400 to
Speedring to fabricate tooling features and three sets of
quartz parts two of which would be brought to completion for
delivery to Stanford in May 1977. Negotiations were also begun
with Mr. Davidson for design, fabrication and delivery of a
tumble lap machine for use in finishing the gyro cavity. The
fixed price quotation for the tumble-lapper was $5,500. A
contract from Marshall Center to Optical Instrument Design
Company to fabricate and test it is in preparation.

Work at Speedring on the new gyro housings began in
January 1977. Experiments at Stanford on the second test jig
were also begun in January.

(g) Precision Measurements on Gyro Rotors and Housings

The limits on the gyro rotor called out in Table 5 are a
density homogeneity of 3 parts in 10^7 and a sphericity of $\pm$ 0.2
microinches. The superconducting coating on the rotor has to be
uniform to about 0.1 microinch. Special instrumentation is
needed to meet these extreme tolerances. The limits on the
gyro housing are less severe (20 microinch sphericity) but the
complicated shape means that it too presents a difficult metrology
problem.

The question of rotor homogeneity was addressed by D. E.
Davidson in 1965. Quartz of Schlieren quality was purchased
from two manufacturers (Corning and Amersil) and cut and
polished into 2 inch cubes with faces parallel to 0.5 arc-sec.
The parts were set up in a Twyman-Green interferometer to
measure the variations in refractive index of the material,
and interference photographs were taken through each of the
three axes for both sets of cubes. The Amersil quartz had
good uniformity in all three axes. With the Corning material
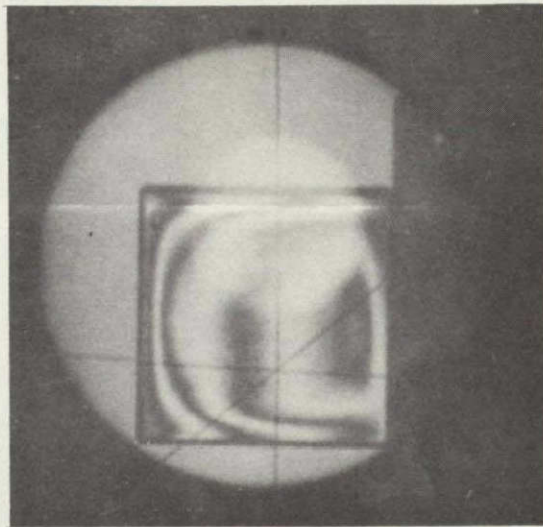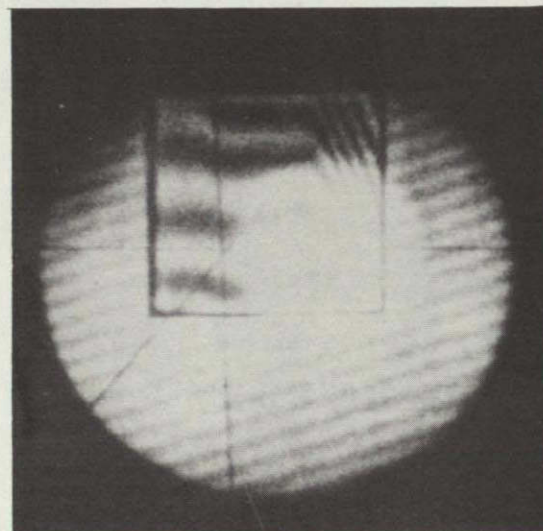
Figure 15: Interferometric Measurements in Uniformity of
Fused Quartz

(a) Homogeneous Cube with Slightly Rounded
Edges

(b) Non Uniform Cube

the interference photograph through the axis commonly chosen as the normal to a Schlieren window showed excellent uniformity, but perpendicular to that axis the material was striated. Figure 15 reproduces interference photographs (a) from an Amersil cube and (b) from one of the bad axes in a Corning cube. The Amersil material was uniform to about a fringe except for a slight shading at the corners attributable to rounding off of the material during polishing. Uniformity of the Corning material was fair across most of the face, but within half an inch of one edge there was a change of several fringesindicating a change in refractive index of about 5×10^{-5}. The different characters of the two materials were accounted for by different manufacturing processes. The Amersil quartz came from boules drawn from a melt; the Corning quartz was vapor deposited downwards in a vacuum furnace and tended to come down in layers as the deposition rate varied.

Refractive index is related to density through the Lorentz-Lorenz formula. Rather than trust formulae which may be hard to apply Mr. Davidson plotted refractive index versus density for a large number of glasses and found the curve reproduced in Figure 16. The conclusion is that a sphere cut from the center of the best Amersil cube examined in 1965 would be homogeneous to 1 part in 10^6 with the density variations fairly symmetrically disposed.

Considerable scepticism has been expressed by some metrologists about our ability to make gyro rotors of the desired sphericity since the target accuracy is at least five times better than the measurement limits of the best available roundness measuring instruments. The doubts are laid to rest by the results of new computer-aided measuring techniques developed by Rank Taylor Hobson of Leicester, England, which have reduced the errors of the roundness measurement to one-tenth of that of the already precise Talyrond instrument at NASA Marshall Center.
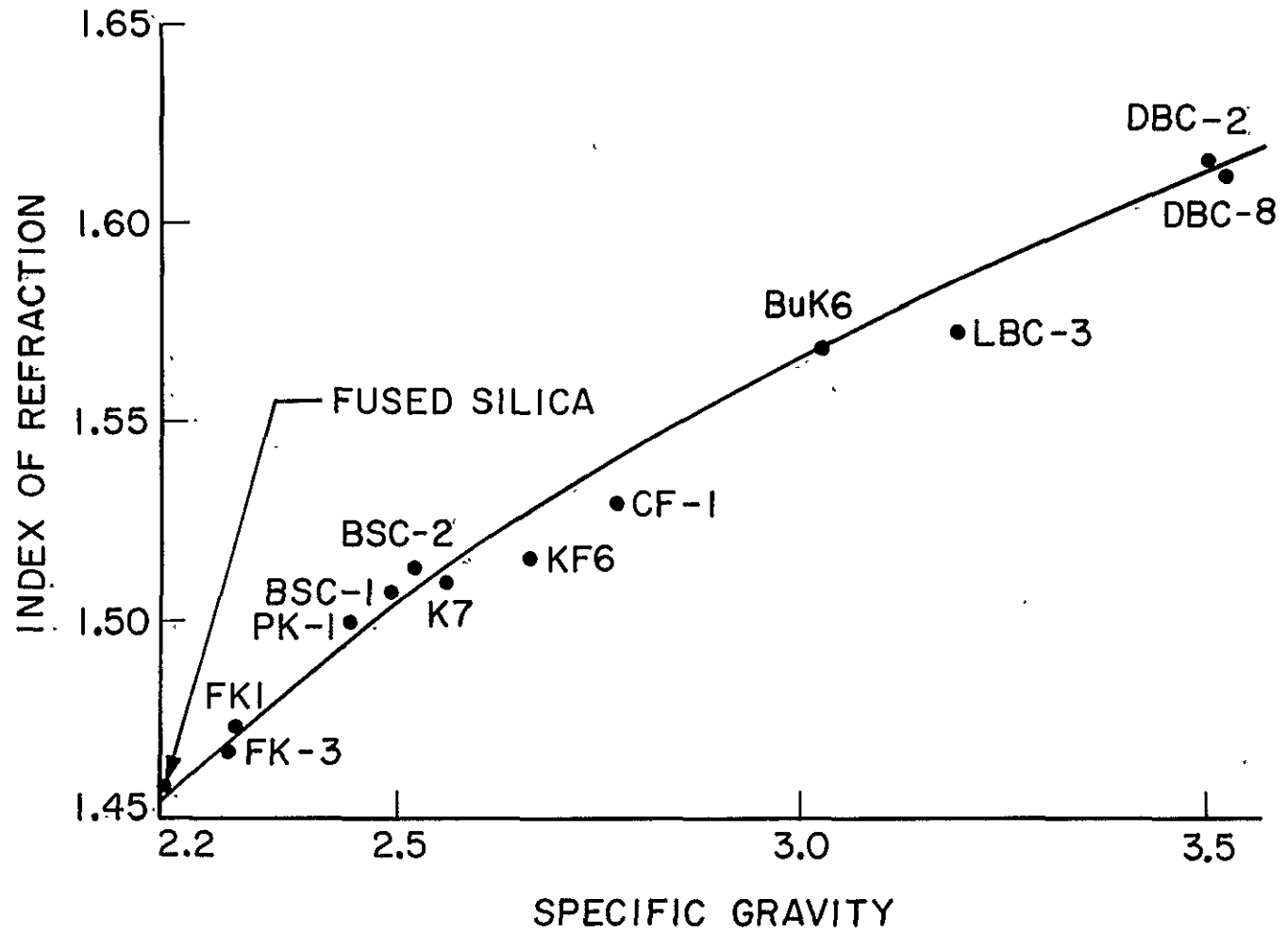
Figure 16: Refractive Index versus Specific Gravity for Various Glasses

We are fortunate to have had one of the key members of the
Rank Taylor Hobson research team, Dr. Graham Siddall, join the
Stanford group in August 1976 under support from a Lindemann
Trust Fellowship.

With modern roundness measuring instruments the principal
limitation on accuracy is the instrument spindle which provides
a reference axis from which the deviations in roundness are
measured, usually with a stylus transducer in contact with the
workpiece. To reduce spindle errors below 1 microinch would be
a prohibitively difficult and expensive task, comparable in
difficulty to the task of producing an 0.2 microinch gyro rotor.
However if the systematic errors of the spindle can be determined
the need for very low absolute errors can be replaced by the
much simpler (though still challenging) requirement of very
low errors in repeatability. Techniques for identifying and
removing spindle errors have been implemented with great success
using digital computers applied to Talyrond roundness measuring
instruments.

An off-line error separation system has been in use at the
British Calibration Laboratory of Rank Taylor Hobson for several
years.[36] It is based on the "multistep" technique which
entails taking a series of roundness profiles in each of which
the component is stepped through equal angles relative to the
spindle. Component errors rotate with the component; spindle
errors remain stationary; analysis of the traces by digital
computer using the Fourier coefficients of the profiles effectively
separates the errors. The BCS multistep system has been used for
checking the accuracy of Talyrond spindles. Figure 17 illustrates
the stability of the instrument error (that is the combined error
of the spindle, hydrodynamic bearing and stylus transducer as
measured at the workpiece) observed over an eight-month period.
The repeatability is impressive. The maximum radial spread
over the total eight months is 0.2 microinches. Variations over
the few minutes required for measuring a single workpiece were

Inside the figure:

Least | squares
circle | centre

ONE DIVISION
REPRESENTS
0·0025 μm
0·1 μin
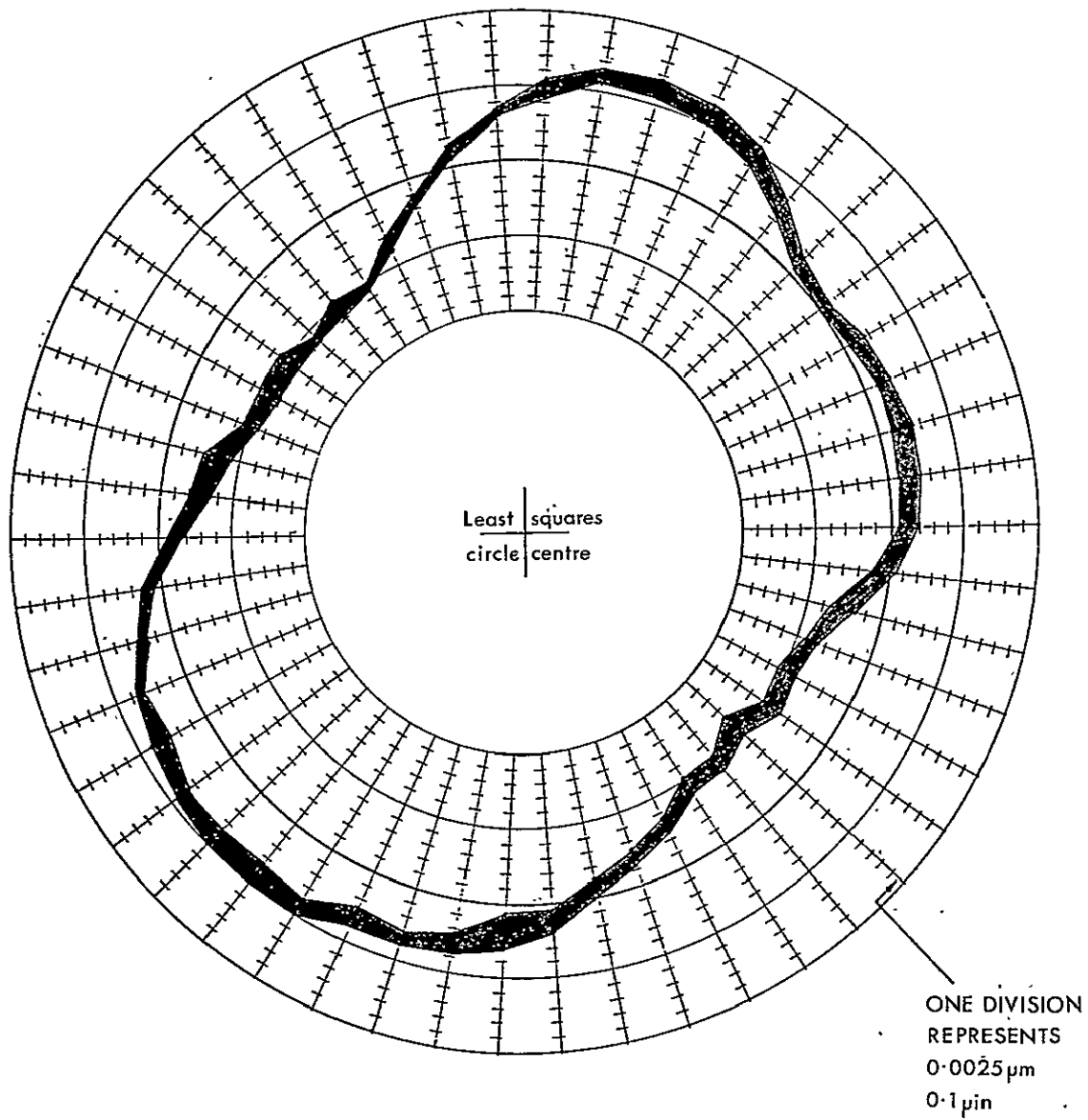
Figure 17: Spindle Error Repeatability of Talyrond 73
Roundness Measuring Instrument over 8 month
Period

substantially less than this. Such repeatibility of the instrument error is an essential condition for successful application of error separation techniques.

Although the BCS system had been shown to give excellent repeatability, its absolute accuracy had never been independently checked. In December 1975, in response to a request from R. Decher of NASA Marshall Center, G. J. Siddall and D. G. Chetwynd[37] of Rank Taylor Hobson carried out further research into error separation techniques, involving comparisons between the BCS multistep method and an on-line system based on a different error separation method first suggested by R. R. Donaldson and L. Bowen[38] of U. C. Berkeley. This method, termed the "reversal technique" requires two traces to be taken, in the second of which the orientation of both the component and transducer is reversed with respect to the spindle. The relative position of stylus and component is unchanged in the two traces, while the effect of the spindle error on the stylus in any position is equal and opposite. The component error is simply the mean of the two traces; the difference gives the spindle error.

Figure 18 gives a comparison of the results obtained using the reversal and multistep techniques to measure the same component: (a) compares the computer plotted polar graph of the component from the reversal technique with data from the computer printout of the multistep technique at a radial magnifcation of 10^6; (b) shows the deviations of fifty equiangularly spaced points on each profile from the mean values obtained by the two techniques. A standard deviation of 0.04 microinches (10 $\overset{o}{A}$) is indicated for each profile. The agreement is the more impressive in that the instruments, operators and environments were all different in the two measurements.

To date, in the absence of computer-aided measurement systems at either NASA Marshall Center or Stanford, manufacture of quartz rotors has been limited by the resolution of the

(a)

ONE DIVISION
REPRESENTS 0 0025 μm
0.1 μin

REVERSAL

MULTI-STEP.

(b)
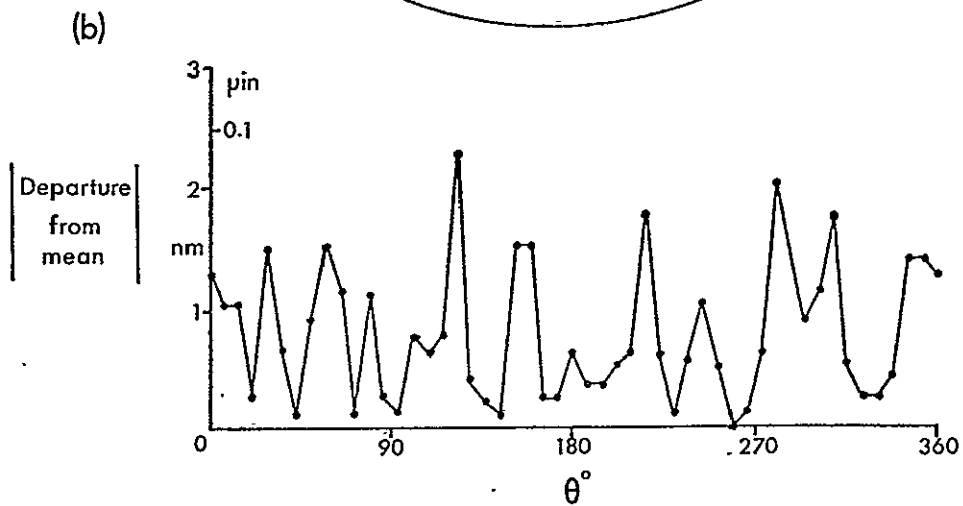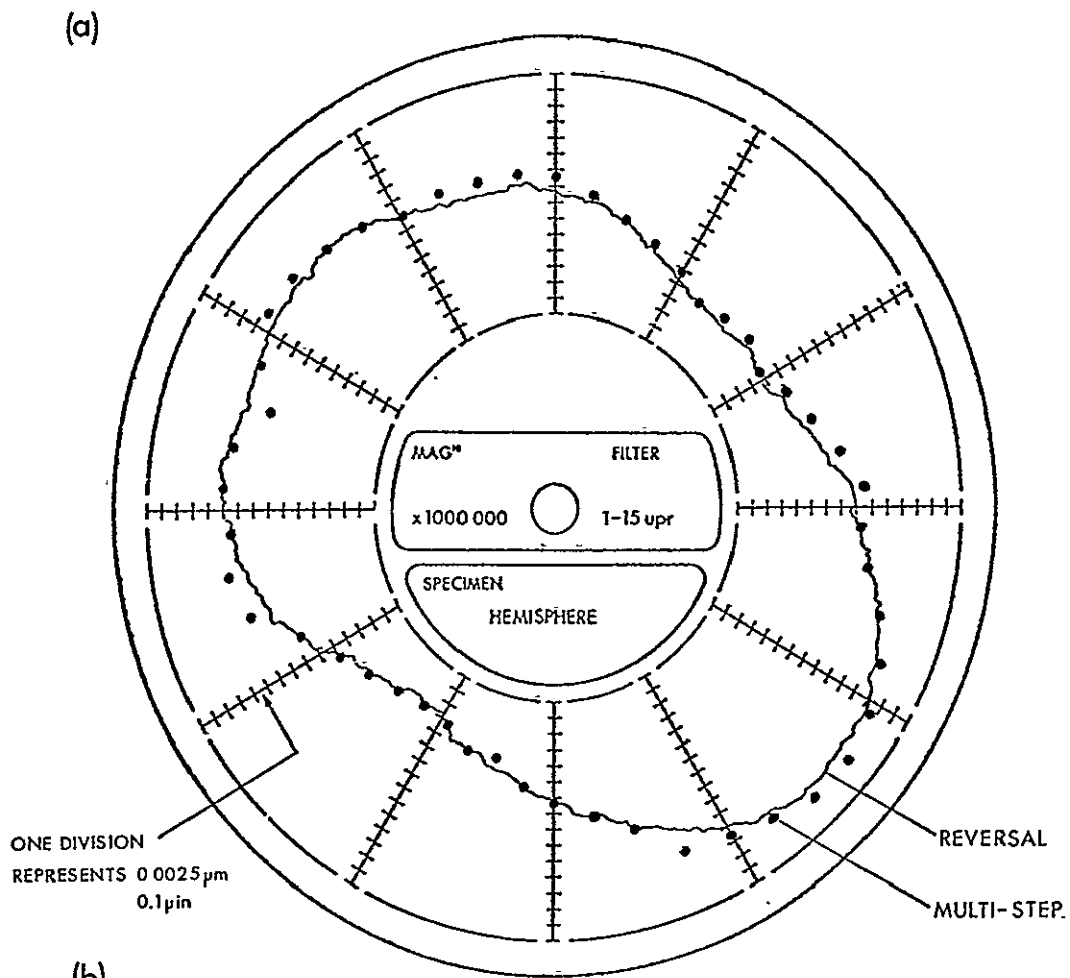
Figure 18: Comparison of Reversal and Multistep Techniques
for Removing Spindle Error from Roundness
Measurements

Talyrond 50 instrument at Marshall Center. In December 1976
we submitted a proposal to the National Science Foundation for
an equipment grant to purchase a Surface Metrology Research
System for use by the Hansen Laboratories and the Department of
Mechanical Engineering and Aeronautics and Astronautics at
Stanford. Figure 19 is a schematic diagram of the proposed
system, comprising a Talyrond 73, a Talysurf 4 surface texture
instrument and an on-line Talynova computer. If funded by the
NSF this system would serve the needs of the Gyro Relativity
experiment and also provide a basis for long-term progress of
research in tribology and adaptive control work at Stanford.

As a stopgap a Talyrond 73 complete with analog reference
computer was obtained on loan for nine months from Rank Precision
Industries, Chicago. This instrument is a later version of the
Talyrond 50 available at NASA Marshall Center, with much improved
electronics. We have used the Talyrond 73 for a series of
measurements on gyro housings, gyro rotors and the levitation
cradles of the equivalence principle accelerometer. One of the
quartz rotors supplied by NASA Marshall Center (rotor No. 8) was
found to have negligible errors on the top magnification (x 20,000)
of the Talyrond 73. In December 1976 the rotor was handcarried
to Rank Taylor Hobson by C. W. F. Everitt, who was in Britain
for another purpose, and measured on the BCS Talyrond system.
Figure 20 reproduces results of measurement in three orthogonal
planes. The maximum deviation of the ball from a perfect sphere
is about 1 part in 10^6, not far from the design goal of the
experiment. It is encouraging that NASA Marshall Center can
do so well without the benefit of adequate measuring equipment,
but the computer-aided measuring equipment will be essential
to making the refinements in ball lapping technique needed to
reach the 0.2 microinch design goal for rotor sphericity.

We have performed measurements on gyro housings also with
the Talyrond 73, and have shown that it can be used to determine
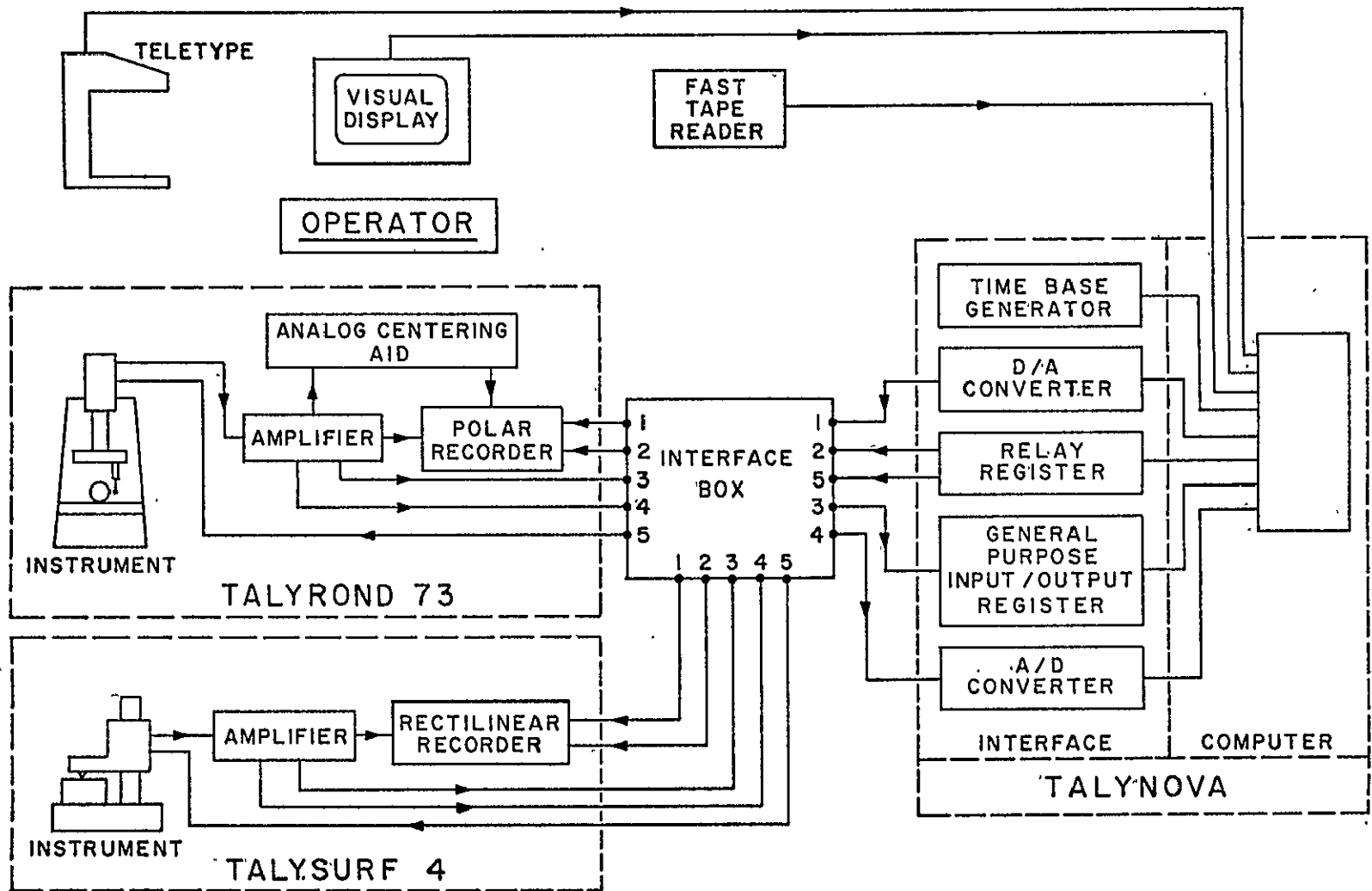
Figure 19:   Proposed High Precision Surface Metrology System

104
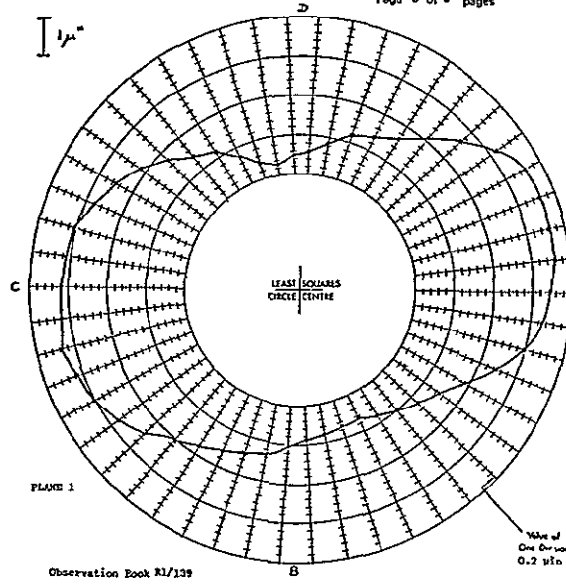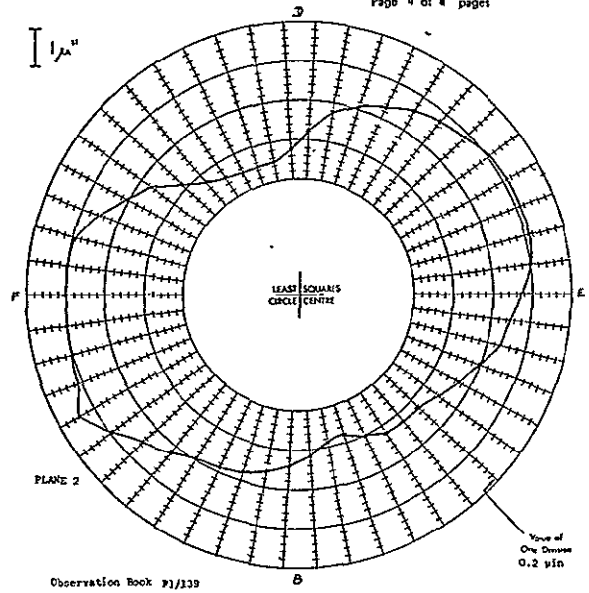
Figure 20: Talyrond BCS Measurements on Gyro Rotor of One Microinch Sphericity

bearing clearances and the position of the parting plane of
the gyro housing to an accuracy of tens of microinches, well
within the requirements defined in Section C (3) (k).

Given the right equipment the metrology of gyro components,
though far from simple, no longer poses any insuperible diffi-
culties. Figure 21 illustrates the gyro rotor set up for
measurement on the Talyrond BCS system.

(h)   Some Reflections

The story of gyro development, needing ten years after the
completion of the spin up calculations to arrive at a satisfactory
design for the quartz gyro housing, is not a happy one, and we as
Principal Investigators accept full responsibility for the mis-
takes that were made. Since the technically ambitious goals
of the Gyro Relativity program have inevitably given the program
an unusual history, we think it may be useful to set down
what we have learned and offer hints for the future.

Broadly speaking gyro development went quite well in the
first three years of the cooperation between Stanford, Honeywell
and Davidson from 1965 to 1968, quite badly for the next four
years and has recovered steadily since 1972. Partial exceptions
to the statement that everything went badly between 1968 and
1972 are the rescue operation with the ceramic housing (1970),
the quartz rotor work at NASA Marshall Center (started 1969)
and the separate work on the quartz telescope by D. E. Davidson,
discussed in Section G.   If we are right in claiming that
things are going well now, why were we unable to make them go
in the right direction during the period 1968 to 1972?

A large company like Honeywell can do useful work at a
small funding level if the task concerned is identical or
almost identical with one it has already performed. The
Honeywell electrical suspension system and Honeywell ceramic
gyro housing were cases in point. The suspension system cost

INT.

S&EXT.

LOCK

ORIGINAL PAGE IS
OF POOR QUALITY

Figure 21: Gyro Rotor Under Measurement on Talyrond BCS
System

$47,000 (somewhat more than was necessary) and the ceramic
housing $33,507; they were delivered expeditiously and ful-
filled important needs in our program. On an entirely novel
task the large company can also do well if funded on a massive
scale. Honeywell's laser gyro begun about the same time as
our cryogenic gyro, has been a success. Where things go wrong
is when one attempts, as we did, piecemeal funding of a task
whose novelty is greater than appears at first sight. We thought
the quartz gyro housing was only a small advance on Honeywell's
existing capability; actually it was a big change and that
for two reasons. The technicians in the Honeywell model shop
had to learn how to work quartz, which is a craft all of its
own, and the design engineers had to take into consideration
problems arising from cryogenic operations and the need to
eliminate magnetic material, concerning neither of which did
they have any intuitive understanding. The issues are simple
enough in themselves, but when, as was the case here, a man is
working on a special task intermittently between heavy bouts of
activity on routine programs he forgets what he has been told.

     An instance where unfamiliarity with the background led one
Honeywell engineer to a bad decision occurred in 1968.
We had requested some experimental work on forming the raised
ridges around the spin up channel by means of a thin layer of
filled epoxy applied to the surface of the quartz. The engineer
tried this, found it promising but not wholly satisfactory, and
then suddenly had the bright idea of cutting a recess in the
housing and machining the entire spin channel assembly from a
massive block of casting epoxy formed in the recess. This might
have worked for a room temperature gyro. For a cryogenic one it
was a disaster, because with the thick block of epoxy (in contrast
to a thin flexible surface layer) differential contraction between
the quartz and epoxy on cooling is enough to destroy the housing.
The engineer exceeded his authority, but far more unfortunate
than the failure in protocol was the failure in understanding which
led to such a mistake.

These remarks will have value only if they are seen in the general context of large company operation, rather than as a specific criticism of Honeywell. The piecemeal funding which was all we could provide was simply not suited to the large company's way of doing business. A manager from another company whose judgement we respect told us after we had recounted some of Honeywell's difficulties that he felt sorry for those guys. Another experienced physicist-engineer from a competitor of Honeywell's told us that his company wouldn't have touched the job with a ten-foot pole.

Why did we go to Honeywell? Why not go to Davidson Optronics, who had experience with quartz work? In the end, in 1976 we did get Mr. Davidson to assist in the design of the simplified quartz housing. The earlier decision had not been taken without forethought; we did, as explained in Section D (1) (a), carefully think about the interface between the Honeywell and Davidson parts of the experimental package and get the Davidson Optronics Company to manufacture the gyro shield assembly: a task we had originally assigned to Honeywell. Our reasoning was based on two considerations. First, Honeywell could claim some knowledge of quartz fabrication: they were doing quartz work on the laser gyro and they informed us that they were beginning to study quartz as a material for electrically suspended gyros. The second consideration was that manufacture of a complete gyro housing involved many processes--sputtering or plating of electrodes, precise roundness measurements, application of readout rings, etc.--for which Honeywell was set up and Davidson Optronics was not. As things turned out, of course, we have had to do many of these processes ourselves. In 1965 we had no sputtering facility in the Stanford low temperature group and no one to do the sputtering if the facility were there. Honeywell seemed the obvious answer.

Good program management reduces in the end to the problem of the particular versus the general. Success in a program like

the Gyro Relativity experiment requires a firmly articulated
overall plan for the experiment and correct insight as to which
particular areas are the ones where progress must be made now.
To rush in with clever solutions to details without the general
understanding may yield little more than a sensational fireworks
display; on the other hand without detailed solutions to some
problems one will get nowhere. Looking back we think we did a
reasonably good job in establishing the overall and intermediate
parts of the experiment plan, but were less successful in identi-
fying short term particularities. Thus three issues we addressed
early in the gyro design were (i) ensuring mechanical stability
by arranging for the quartz parts to be optically contacted to
the telescope, (ii) provision of a mechanically stable super-
conducting magnetic shield for the gyro, (iii) ensuring that the
electrodes and electrical feedthroughs of the gyro had low enough
resistance for the heat dissipation in the dewar from suspension
currents to be negligible. These are all important points
ultimately; none was imminently so in the first gyro operations.
They were the wrong particularities; and indeed we were forced
to accept compromises on all of them to get the gyro working.

On the other hand no compromise was possible on spin channel
design. It was here that the early gyro housing work at NASA
Marshall Center proved less than satisfactory through poor under-
standing of the extent to which the theoretical analysis locked
in the design parameters, and a certain reluctance to consult
Stanford about the design, to which we should have responded
more forcefully than we did.

Wisdom would have seen as soon as the spin up design was
completed in late 1967 that manufacture of these parts in quartz
might be too hard for Honeywell and that a back up ceramic
housing should be started immediately. We did not want to spend
an "unnecessary" extra $30K; Honeywell had already finished the
outer envelope assembly for Quartz Gyro Housing No. 1; the
Honeywell engineers told us what they no doubt believed and we
wanted to hear that the job could be done. One other factor

that helped lead us astray was an experiment we had done at Davidson Optronics in 1967, where a 1 mil thick layer of aluminum was evaporated on a flat quartz test piece and cycled to nitrogen temperatures several times.[39] Since this withstood the differential contraction, we thought all would be well with metal coating on a quartz housing. Putting a uniform coating in spherical geometry is unfortunately a very different story. To get uniformity one has either to plate uniformly or apply a thicker coating which can then be lapped to size. Neither proved to be feasible with the copper-plating techniques which were all that was conveniently available at Honeywell.

Good judgement on the issues to address and good judgement whether people can do what they say: from these fundamental needs of program management there can be no escape. Equally essential is the need to make sure that everyone in the program has enough grasp of the generalities not to stubbornly work solutions to their immediate problem which cause immediate difficulties elsewhere. Here one is in tricky territory because if the difficulties are not immediate the quick intermediate solution is often by far the best one to have since it allows the experiment to proceed.

Finally we have to admit belated rediscovery of one management principle so well known that we are ashamed to mention it: the importance of the <u>written</u> <u>word</u>. Physicists working in their laboratory get so accustomed to living with their apparatus and fixing it as they go along that they fail to appreciate that memory and word of mouth cannot be relied on after a few weeks when collaborating with someone 2000 miles away. We have had to learn some of these lessons the hard way. We hope that others will benefit from our findings and not find, with Oscar Wilde, that "One learns nothing from experience. Experience is simply the name we give to our mistakes."

(2) Gyro Suspension Systems

As stated in D (1) (a) above the original subcontract from
Stanford to Honeywell in January 1965 (Stanford PR 0392) included
the design, fabrication and checkout of an electrical suspension
system for the laboratory version of the London moment gyroscope.
The system closely resembled one supplied by Honeywell to the
U.S. Air Force under another program. Gyro suspension was by
means of 20kHz, 3kV signals applied to the three mutually perpen-
dicular sets of electrodes; the suspension voltages were controlled
by position sensing servos based on measuring the capacitances in
the three axes by 30V signals at frequencies of 1.1 MHz, 1.28 MHz
and 1.43 MHz. To begin with Honeywell offered Stanford (and JPL)
a previously untried support scheme for which the frequencies of
the sensing and support voltages were identical; this did not
work out so at some expense we reverted to the earlier design.
The novel configuration of electrodes in the Stanford gyroscope
called for modifications in the output transformers and some
other parts of the electronics. The suspension was designed to
have two operating levels with preload capabilities for a solid
quartz rotor of 1.1 g and 2.3 g. The preload is defined as the
acceleration applied along a single axis that drives the voltage
or plate to null. With the Honeywell system the maximum accelera-
tions on the gyro under which the electronics could maintain
suspension were about 50% higher than the preloads.

The Honeywell suspension system was delivered to Stanford
in August 1967. Systematic testing and preparation for operation
with the cryogenic gyroscope was begun by J. R. Nikirk in
February 1970 upon his appointment as a Research Associate in
the Stanford Department of Aeronautics and Astronautics. The
work was done partly using "dummy loads," that is the special
set of variable high voltage capacitors obtained from Honeywell,
referred to above, and partly using a gyro housing manufactured
by Honeywell under the GEANS program and made available to
Stanford through courtesy of the U.S. Air Force. The MEG housing

(as it is called) was set up in a small test facility at
Stanford with a .1.5 inch diameter nickel-coated aluminum rotor
purchased specially from Honeywell under the present Grant.
Aluminum is about 10% denser than fused quartz. To match the
weight of the final quartz rotor a cylindrical hole was drilled
and plugged in the aluminum rotor, leaving a small cylindrical
cavity at the center of the sphere. With the MEG set up J. R. Nikirk
measured suspension characteristics of the Honeywell system such
as transient power supply voltage and electronics drift, reporting
warm up times ranging from 30 minutes to two hours during which
the center of suspension shifted by distances ranging from 6 to
10 microinches, or 8 to 13 microinches when scaled to the 65pF
capacitances of the Stanford housing. Movements over further
periods of eight or more hours varied a few microinches around
the mean point. These figures were to be compared with the
clearances of 200 to 300 microinches between the rotor and gas
spin up channels in the Stanford housing.

In 1970 R. Decher of NASA Marshall Center asked Stanford
for help in preparing specifications for a new gyro suspension
system to be purchased for use at MSFC. The original intention
was to purchase the system from industry. Drawing on the exper-
ience with the Honeywell suspension system we took the opportunity
to specify design improvements that would give better sensing
bridges, better centering capability and a control servo with
sufficiently quick response to support the gyro through a
fairly severe earthquake if the suspension system were used at
Stanford. The preliminary design work done while drawing up the
specifications led us to propose to NASA to fabricate the sus-
pension system at Stanford. In May 1971, after considering
other bidders, NASA awarded Stanford Contract NAS8-27333 for
$35K (afterwards extended to $47.3K) to perform this task.
The design was accomplished in the last five months of 1971
by J. R. Nikirk with support from R. A. Van Patten, R. R. Clappier
and a temporary engineer, J. Eccher, hired from Ball Brothers

Research Corporation. Assembly of the first unit was completed at the end of January 1972, at which time systems tests and evaluation began. Regenerative signals were observed, induced first by high preload voltages and then later by the transients that occur during gyro levitation. These difficulties, which caused J. R. Nikirk and R. A. Van Patten much concern, were eventually solved by adding further harmonic suppression filters and increasing the excitation voltage of the position sensing bridge. The package was designed to have about 40% less volume than the Honeywell suspension system so that it could be mounted easily on top of the tiltable laboratory dewar described in Section J (4).

Figure 22 illustrates the suspension system. As compared with the Honeywell system it had greatly improved centering stability and better adjustment capability. Table 8 summarizes performance characteristics.

Table 8: Peformance Characteristics of Stanford Gyro Suspension System

Centering static sag	3.9 microinches
Warm-up drift	<1.0 microinch
Drift under $\pm$ 20° temperature change	<$\pm$3.6 microinches
Centering adjustment	better than 1.0 microinch
Overall bandwidth	640 Hz
Damp out time for small signal step	2.5 mS

The bandwidth was such that the suspension system could support a solid quartz gyro rotor through a Richter 6.5 earthquake five miles away. Any larger earthquake would knock the building down. The dynamic centering capability had been specified as needing to be better than 50 microinches throughout the response range. At frequencies above 30 Hz the performance was right on the
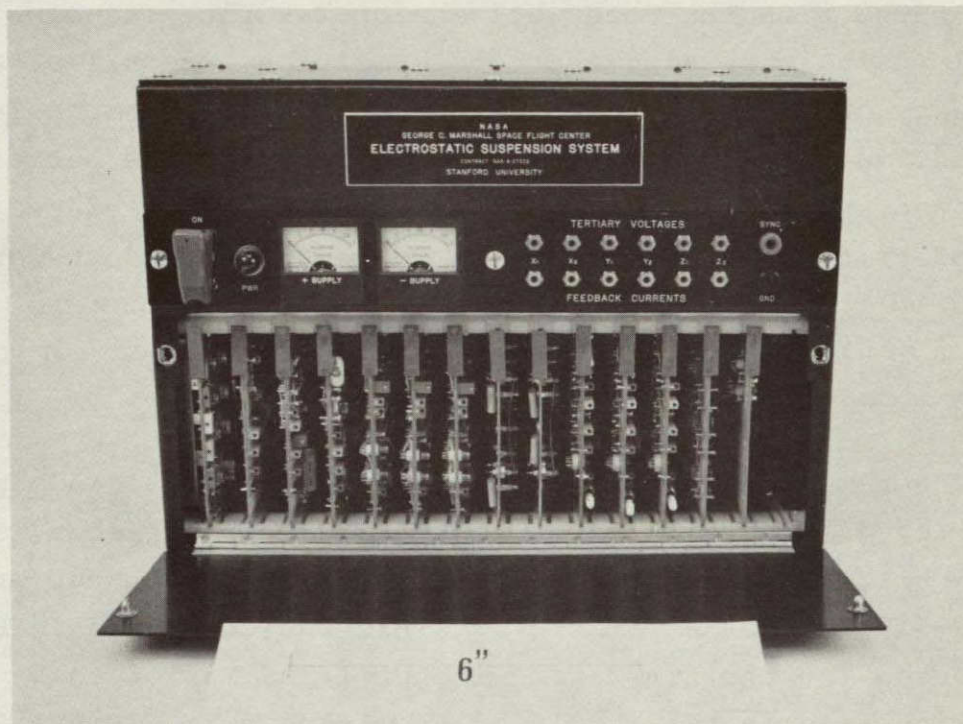
Figure 22:   The Stanford Gyro Suspension System

specification; at lower frequencies it was better than specified, making the dynamic centering in that frequency range closer than 50 microinches.

Another important improvement in the new suspension system as compared with the Honeywell design was that the electric signals used in sensing the rotor position were all at a single frequency of 1 MHz instead of three different frequencies, and the sensing voltage was 20:1 lower. Interference between the gyro suspension and readout was correspondingly reduced: a fact of critical significance in the ensuing readout work (Section D (4) (d). The 1.5 volt operating voltage of the sensing bridges is not far from the level required for the flight electronics system (about 0.3 volts).

The new suspension system was handcarried to NASA Marshall Center by J. R. Nikirk in November 1972. In December 1972 we began building a second box of identical design under Grant 05-020-019 for use at Stanford. This was completed in February 1973, used for the first time in April and May of that year, and used regularly in the gyro runs from then on. A Final Report "On the Fabrication of an Electronics Suspension Subsystem for an Electrostatically Suspended Gyroscope for the Relativity Experiment,"[23] was completed under Contract NAS8-27333 in April 1973, reference to which should be made for further details.

As time went on we made several improvements to the new suspension system following experience of working with a live gyro. One was to increase the range of centering adjustment to allow the gyro to be centered with respect to the spin up lands rather than the electrodes. Another improvement was to make the preload adjustment variable all the way from zero to its maximum value to help in evaluating the 20 kHz pickup between the suspension and readout. In August 1973 J. R. Nikirk discovered a curious problem, which took some time to fix, a small but

annoying 5 kHz oscillation at certain combinations of servo gains and preload setting. These and other changes were made during the difficult period of gyro development described in Section D (4); much care was needed in separating problems inherent to the suspension system from other troubles with the gyroscope.

Documentation of the various changes was forwarded to NASA Marshall Center for incorporation in the MSFC system.

Operations with the Honeywell suspension system continued until May 1973. Several failures occurred, of which the most notable one followed an arc in the gyro during an attempted cryogenic run in April 1973. The incident happened just as we were about to build an automatic shut down system to protect against arcing damage. In fact the parts had already been ordered and had arrived the day before the damage took place. The automatic shut down circuit senses current drawn by the suspension system from its power supply and shuts off the power at a critical threshold. It proved an important addition to the system, minimizing damage whenever abnormal conditions occur.

In October 1972 NASA Marshall Center agreed to fabricate in-house twelve thick film wide band differential amplifiers for use as spares for the MSFC suspension system and for the new Stanford system. Schematics and layouts and details of resistor tolerances were supplied by Stanford to NASA Marshall Center on the basis of earlier experience with a similar amplifier fabricated by the Johns Hopkins Applied Physics Laboratory for the DISCOS drag-free controller. The amplifiers were duly completed in December 1973 and used with excellent results.

Other work related to the suspension systems included completing a new set of capacitative dummy loads for high voltage testing and a modification to the Honeywell suspension system

to increase the range of centering adjustment. Shortly before
his death in March 1975, J. R. Nikirk had completed the design
analysis for an improved laboratory suspension system, having
a factor of ten higher resolution in the capacitance sensing
bridge, simplified design layout, and adjustable capacitances
to aid in tuning the suspension cables. Plans for building
this system had to be dropped after Nikirk's death. The most
recent addition to the suspension system has been a remote
control panel designed by R. A. Van Patten for the new precision
gyro readout experiment described in Section E.

(3)   Magnetometer Development

The plan for mechanizing the gyro readout using a SQUID
magnetometer has been described in Section C (3) and illustrated
in Figure 9 (p. 63) to which reference should be made. The
present section covers development work on the magnetometers
due principally to J. T. Anderson and R. R. Clappier. The
interfacing of the magnetometers with the large laboratory
dewar and elimination of interference between the suspension
system and readout is described in Section D (4) (d). The
process of reducing trapped flux in the gyro rotor and observing
the London moment are described in D (4) (e) and D (4) (f).
For earlier research on vibrating plane magnetometers, reference
should be made to the paper by J. E. Opfer[30] and the 1971
Annual Report on Grant 05-020-019.

In 1971 when the present work began, there were no suitable
commercially available SQUID magnetometers; we had to build our
own. As time has gone by, several cryogenic companies have
marketed SQUIDs and we have gradually been able to take advantage
of the progress by purchasing some or all of the components from
commercial units. In some areas we are disposed to feel, looking
back, that we were a little slow in adapting our thinking to
industrial progress.

Our first operating SQUID was a two hole structure due in design to J. E. Zimmerman. Later we adopted a toroidal configuration having better sensitivity and shielding, with a weak link formed from a pointed niobium screw touching the niobium base of the cavity, adjusted at low temperatures by a long screwdriver. The adjustable toroidal point contact SQUID is shown in Figure 22, along with a non-adjustable toroidal SQUID manufactured by the SHE Corporation, with which we began to experiment in 1974. The SHE unit has excellent mechanical stability: in collaboration with Ball Brothers Research Corporation we demonstrated in 1974 that it passes flight qualification shake tests applicable to either the four stage Scout or two stage Delta vehicles. Details of the shake test are given in the 1974 Annual Report. The original SHE units had cupronickel case and black Stycast epoxy filling, both of which might be expected to have too much residual ferromagnetism to be used near a gyro rotor in which the trapped field has to be kept below 10^{-7} gauss. We had two SHE units made specially with copper casing; these were used along with one of the old adjustable point contact SQUIDs in the London moment observations described below. Recent SHE units have a beryllium-copper casing. The new apparatus to be described in Section E should allow them to be used without generating appreciable trapped fields.

The characteristics of other weak link junction structures were investigated both experimentally and through literature surveys as described in the 1972 and 1973 Annual Reports. Research at NASA Marshall Center to develop better junction structures has been carried on in parallel with the Stanford program by P. Peters, L. B. Holdeman and J. B. Hendricks.[40] We have also carefully followed progress on other types of SQUID developed elsewhere, in particular the thin film double junction d.c. SQUID recently perfected by J. Clarke of the University of California, Berkeley, the properties of which are reviewed in the 1975 Annual Report. The thrust always has to
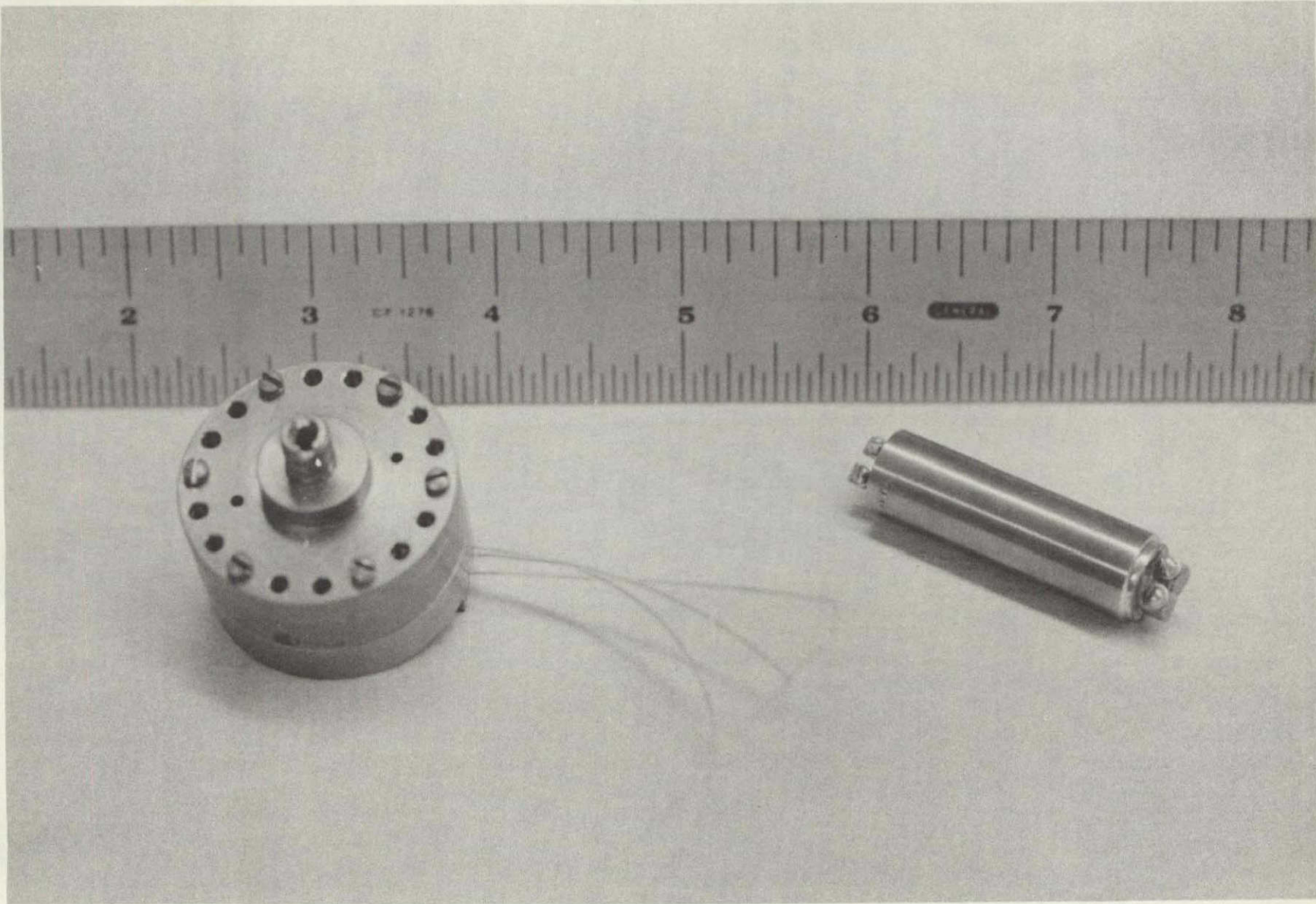
Figure 23: Adjustable and Fixed Toroidal Point Contract
SQUID Unit

be towards reduction in noise and improvements in null stability.
These are achieved either through the development of new SQUID
concepts, operation in a different frequency regime (as in
recent developments of microwave SQUIDs), or evolutionary
changes in electronics design.

Electronics for the SQUIDs used in the Gyro Relativity
program have been developed continuously since 1971. The rf
box was first operated in 1972. It comprised a 30 MHz rf
oscillator to pump flux periodically through the SQUID and
an rf amplifier-detector to amplify the tank voltage to a
useful level and rectify it. Significant features of the rf
signal source were: a crystal controlled oscillator for
frequency stability and low fm noise, a high frequency chopper
for use as a demodulator, two dual-gate MOSFETs for external
electronic control of the rf level, and a tuned filter to
remove higher harmonics from the 30 MHz drive signal and reduce
noise in the SQUID. Significant features of the rf amplifier
were: a low noise cascode input stage with noise figure less
than 1.5 db, a dual gate MOSFET second stage with remote
gain control, an integrated circuit amplifier for additional
gain, a diode detector biased to provide linear detection for
signals as low as 50 mV, and a line amplifier to prevent cable
capacitance from unduly lengthening the response time of the
output circuit. The oscillator and amplifier/detector circuits
were combined with an rf voltage modulator, the rf attenuator
and filter circuit in a single package. Progressive improvements
to the rf circuitry were made after June 1973 with a new 200 MHz
oscilloscope, supplied by NASA Marshall Center, which provided
an analytical capability not previously available, with the aid
of which we gradually discovered and corrected hitherto unnoticed
faults in the system.

To begin with we used magnetometer feedback boards pur-
chased from Develco Incorporated, although their response times
were known to be slower than was desirable. In 1973 we designed

and built a prototype magnetometer feedback board of our own
with superior high frequency performance. Using a 100 kHz square
wave magnetic field modulation and full wave demodulation of
the rf box detector output, the magnetometer could be operated
with unity gain at frequencies as high as 30 kHz, with the very
important consequence that its output responded (at low levels)
to the 20 kHz magnetic field from the suspension system. We
were therefore able to lock the magnetometer with some 20 kHz
signal present and hence obtain a fine trim on the 20 kHz
bucking signals.

As we worked with the prototype feedback card we observed
many areas for improvement. One was that the critical current
of the adjustable toroidal SQUID then in use tended continually
to drift away from the set point making the magnetometer lose
lock unless the rf drive level was adjusted. We developed a
control loop that automatically adjusted the rf level for best
magnetometer operation. Drawing on the experience with the
prototype card we then built an entire new magnetometer unit,
incorporating improvements in every circuit together with a
new magnetometer control panel and a card rack for the new
circuits. The card rack housed: 2 cards for the magnetometer
feedback circuit, 1 card for the new rf level control loop, 2
cards for the trapped flux bucking circuit described in D (4)
(e), 1 card to control the rf box and 1 power conditioning
card. New features on the panel and simplified control
made the magnetometer much easier to use than earlier versions.
The magnetometer was completed and checked out by mid-March 1974
and used in all the gyro readout work up to the detection of
the London moment in March 1975. Figure 24 illustrates the
completed system.

The rf level loop was particularly useful in the early
stages of the work because it increased the range of tempera-
tures over which the SQUIDs would operate without adjustment
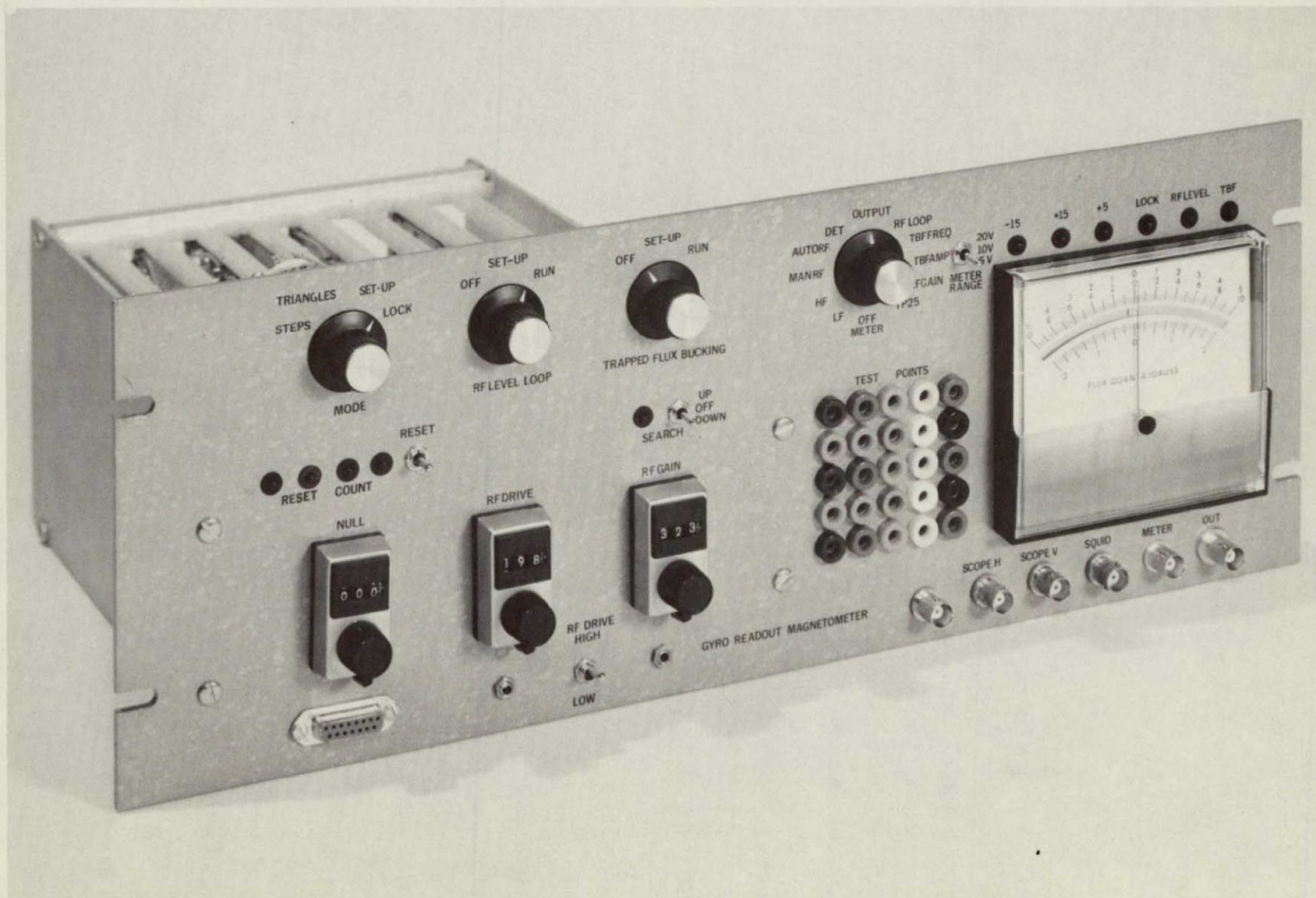
Figure 24: Second Generation SQUID Magnetometer
Electronics (1974)

123

from 0.3K to 1.5K. The temperature cycling required in the field cancellation work described in Section D (4) (e) made vitally important.

In 1975 and 1976 we completed fabrication of a third generation magnetometer for gyro readout. The basic design of the existing magnetometer was preserved, but many small circuit changes were made to improve the drift performance and temperature stability. Changes included a new panel, new control circuits, a new demodulator and new feedback card. The cards were reproduced in printed circuit form; seven units altogether were built for this and other experiments including the Equivalence Principle Accelerometer.   The new magnetometer has roughly a 2:1 improvement in bandwith as compared with the earlier unit: 3dB at 40 to 50 kHz. Drifts in the demodulator due to changes in temperature of the electronics are reduced a factor of 20 from $2 \times 10^{-5}\phi_0$ to $10^{-6}\phi_0$ per ^{O}C. Drifts due to thermoelectric effects in the feedback line have been reduced a factor of 1000 by replacing the voltage source with a current source. With the old unit transient temperature changes, during helium transfer say, could cause offsets as great as $10^{-2}\phi_0$ and there were some drifts even under nominally stable temperature conditions; now all of these effects are negligible. The resolution of the magnetometer is not appreciably altered since it depends on properties of the rf circuitry and SQUID which have not been changed.

To speed up circuit development on the third generation magnetometer we modified a 25 liter storage dewar vessel so that it could accept a probe containing an SHE SQUID. This quickly operated low heat leak installation is a great help when trying to concentrate on electronics development; it allows us to run a SQUID for several weeks without much attention.

Some of the technical problems encountered in developing the third generation magnetometer required fairly sophisticated treatment. The use of current source for feedback, for example, is complicated by cable capacitance which makes current feedback work poorly at higher frequencies. Since stability and drift are low frequency effects, the solution is to use current feedback at low frequencies and voltage feedback at high frequencies. (Actually even the high frequency voltage is converted to a current in the rf box before reaching the SQUID). The use of two different output schemes simultaneously poses interesting control problems, but we were able to develop a satisfactory prototype feedback module, followed by eight printed circuit copies. The basic design gives a full scale output of 10 volts for a 200 ϕ_0 input. We modified one module to give 10 volts for 1 ϕ_0 full scale and three others with 20 ϕ_0 full scale.

Figure 25 illustrates the third generation magnetometer with the rf box.

In late 1976 we purchased a magnetometer unit from the SHE Corporation, which was used in the noise test measurements described in Section F. The resolution of this unit is probably about a factor of five better than earlier magnetometers as a result of improvements in noise matching of the rf head to the SQUID.

One of the key circuits used in the Gyro Relativity Program is a high speed demodulator. The magnetometers use a printed circuit version of this circuit, while the gyro suspension system currently uses a hard-wired version. Both work well in the laboratory, but for flight a smaller more rugged hybrid circuit version would be helpful, especially since a fair number of these circuits are used. Each suspension system and each magnetometer uses one demodulator per axis for each gyro. The Hybrid Circuit group at NASA Marshall
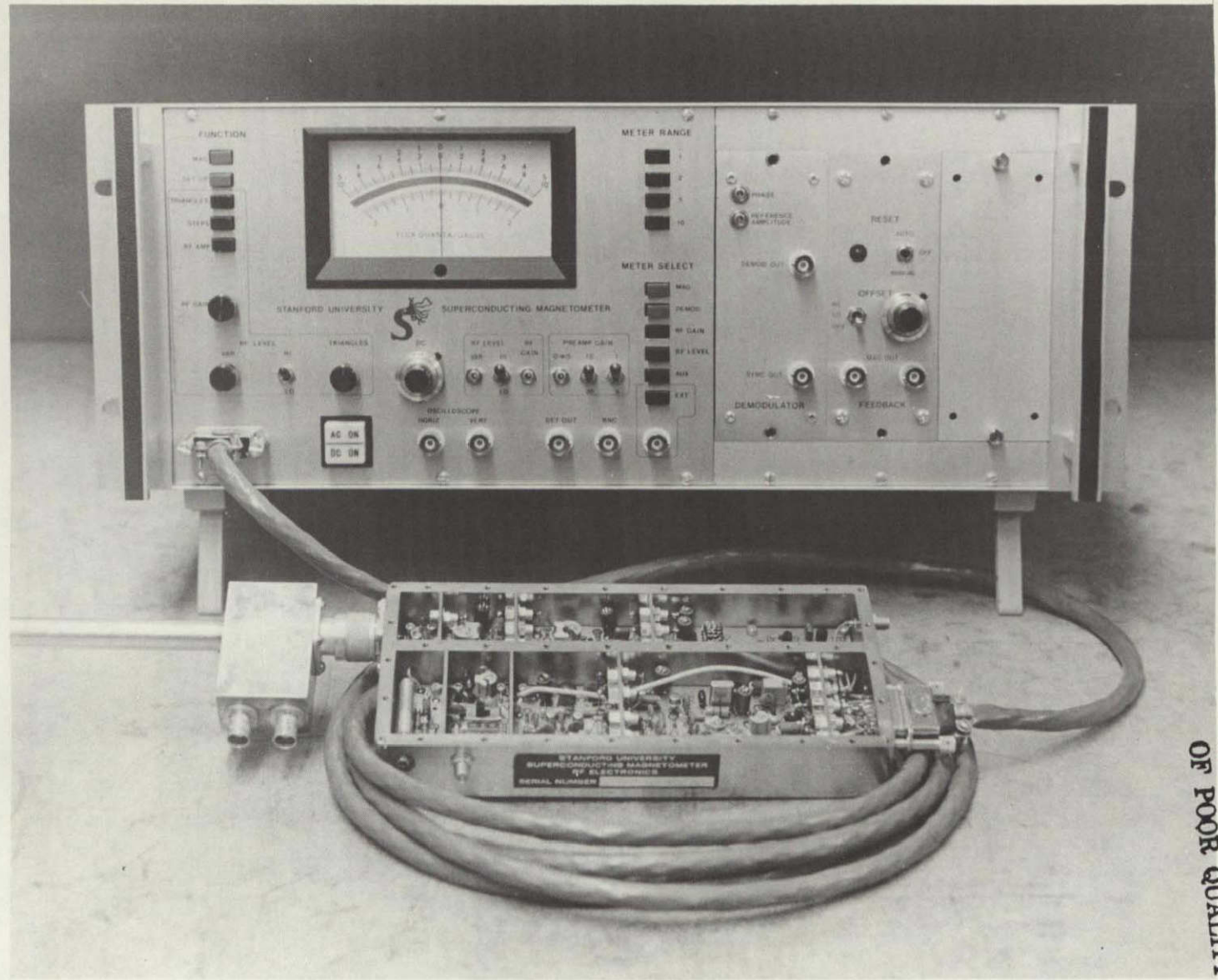
Figure 25:   Third Generation SQUID Magnetometer Electronics
             with RF Box (1976)

Center has been working for over a year on a hybrid version
of the driver section of the Stanford designed demodulator.
The driver provides high speed gate signals for the field
effect transistor (FET) demodulator and utilizes a regenerative
feedback technique to achieve fast switching without consuming
a lot of power. This requires careful circuit layout. The
MSFC group has combined a good layout with a component matching
scheme which has produced circuits that perform very well.
Three of these circuits have undergone preliminary tests at
Stanford.

(4)   Gyro Operations 1971 - 1975

   (a)   General

     This section covers work on the gyro and gyro readout up
to the completion of the first London moment observations with
a live gyro in March 1975. That experiment marked the completion
of a distinct phase in evolution of the Gyro Relativity experi-
ment, following which we began the new precision readout experi-
ments described in Section E. The work reported in the present
section was nearly all done in the large tiltable non-magnetic
dewar designed by C. W. F. Everitt and R. D. Hall between 1965
and 1968, fabricated by AGS Incorporated of Waltham, Massachusetts
and delivered to Stanford in April 1969. This dewar was designed
to fulfil two purposes: (i) to serve as a laboratory test stand
for the gyroscope, (ii) to evaluate our ideas about the flight
dewar by incorporating as many features of the final design as
possible into the laboratory model. Details are given in Section
J (4). In many ways the dewar was a pioneering effort which
has influenced designs of subsequent flight dewars including
those of IRAS and other long-term helium experiments in space.
In retrospect we see that it was in some degree a mistake to
combine the two functions in one apparatus, in that the dewar
did not in fact solve one major problem that it set out to
solve; providing an adequate low magnetic field environment

for the gyroscope, and, being cumbersome to use, it had by 1974
turned out to be not well suited to the gyro tests then in
progress. On the other hand if the two functions had not been
combined we would probably never have gained the experience with
dewar operations that is essential to the experiment, and NASA,
as well as ourselves, would have been the losers.

Before the gyro tests could be run, the dewar had to be
made to work, and this was done during 1969 and 1970 by J. A.
Lipa and J. J. Gilderoy.

(b) Gyro Suspension

The period from March 12, 1971 when the ceramic gyro
housing was delivered to Stanford until June 19, 1973 when the
first time a niobium-coated solid quartz gyro rotor was spun
up at a temperature of 7°K, was a gruelling time in the develop-
ment of the Gyro Relativity experiment. J. A. Lipa and J. R.
Nikirk together fought many severe problems on the gyroscope.
To begin with two months were lost because the gyro rotor was
jammed in the housing. This trouble had been suspected at
assembly. Lipa and Nikirk demonstrated it from capacitance
measurements and traced what was wrong to errors in location
of the alignment pins for the two halves of the housing, as well
as to pimples and machining burrs on the raised copper spin lands.
Honeywell worked out a new alignment procedure using a reference
ball matched in diameter to the cavity, and verified clearances
by means of a special indicator probe that could be inserted
through the spin ports after assembly. The parts were returned
to Stanford on May 19, 1971. After checking clearances and
breakdown voltages Lipa and Nikirk tried to levitate the gyro
in a room temperature test chamber assembled earlier in the
year. Then began a series of electrical breakdown problems.
Levitation first of all failed because of arcing between the
electrodes. After this had been repaired intermittent levita-
tion was achieved for periods of up to five minutes, but a 70 kΩ

short developed between one electrode and the ball. The short was traced to poor adhesion of the gold coating that Honeywell had applied over the sputtered titanium electrodes to reduce their resistance: during levitation the electrostatic stress pulled up slivers of gold from the surface like the leaf in a gold-leaf electroscope. An attempt to clear the short by applying higher currents from a d.c. power supply burned out the connection between the feedthrough and the electrodes.

Before going further we decided to investigate the electrical breakdown problem by experiments on a flat test piece purchased from Honeywell, which had three different kinds of electrode. The breakdown characteristics were substantially improved by having electrodes of titanium only, with no gold coating and with "radiused edges" -- i.e. made with a rounded annular moat about their peripheries to place the sharp edges of the sputtered film further from the surface of the ball. We instructed Honeywell to cut moats and sputter on fresh and thicker titanium electrodes. The work was done in October 1971, yielding some improvement but still far from satisfactory results. Breakdown characteristics in the housing were nothing like as good as they had been in the test pieces. An attempt to understand why, described in the 1972 Annual Report, revealed a correlation between breakdown voltage and the resistance per square centimeter of the electrodes, suggesting that we should go to much thicker electrodes. The pieces were shipped back to Honeywell for yet another recoating. At the same time we had the electrodes recessed at the center where the plate makes contact with the feedthrough pins, since we observed that breakdown was now concentrated in this region, and we ordered a new lightweight hollow beryllium rotor, matched in diameter to the cavity which would let us get on with some gyro work at lower support voltages.

In January 1972 the gyro was reassembled with the hollow
rotor and immediately levitated. However after 2.5 hours
of successful operation the gyro failed. Disassembly revealed
deterioration in the connection between one electrode and its
feedthrough wire. After further experiments with temporary
repairs we took the bull by the horns and sputtered thick
copper electrodes onto the ceramic housing ourselves. Thus
finally in March 1972, one year after delivery of the parts,
we achieved gyro levitation for extended periods with a hollow
beryllium rotor.

All of the foregoing work was done in the room temperature
test chamber. Meanwhile J. A. Lipa had been getting the large
laboratory dewar to work and J. R. Nikirk had been developing
high voltage low heat-leak cabling and high vacuum high voltage
non-magnetic feedthroughs to operate the gyro in the dewar.
Work on these tasks is described in the 1971 and 1972 Annual
Reports. The first gyro levitation in the big dewar was per-
formed in October 1972. For some months we continued to work
with the light beryllium rotor to have margin on the suspension,
but as time went on we gained confidence and after the beryllium
ball had been damaged during the spin tests to be described in
D (3) (c) we reassembled the gyro housing with a full-weight
nickel coated aluminum rotor obtained earlier from Honeywell.
Following some initial problems, due probably to debris in the
housing, we succeeded in December 1972 in levitating the aluminum
rotor for extended periods without incident. In April 1973 we
levitated a copper-niobium coated quartz rotor.

With this, the problem of gyro levitation could be said in
some degree to be solved. It is not entirely solved because one
of the mysteries of the Gyro Relativity program has been that
whereas Honeywell have established a reliability in gyro levita-
tion characterized by a five year mean time between failure, we
at Stanford have suffered continued minor and occasional major
suspension problems. Thus in December 1972 we observed that

whereas levitation of the beryllium rotor had always appeared
stable, the heavier aluminum rotor sometimes displayed anomalous
motions. Long periods of stable operation would be disturbed
by spells of wild behavior, during which large position errors
would occur followed by pulsing and arcing and·a need to shut
down the system. The phenomena seemed to happen mainly when the
ball was not altogether free in the housing. We had reason to
think that in the ceramic housing the copper coating on the
raised spin up lands was imperfect and that small spring-like
flaps stood up from the lands and sometimes touched the ball.
Also the ball seemed occasionally to gain a large static electric
charge; the pulsing phenomenon could sometimes be made to go
away by allowing the potential of the spin up lands to float free
of ground. J. R. Nikirk developed a precise method of centering
the ball by injecting triangle waves into each suspension channel
in turn and looking at the resultant motions in all three channels.
Other difficulties were observed from dirt introduced with the
spin up gas (despite careful filtering) and cryodeposits formed
in the experimental chamber during cooldown. We have gradually
gained enough ad hoc knowledge to fight our way out of the worst
difficulties and achieve periods of a few days trouble free
gyro operation.

Levitation of a niobium coated quartz rotor in Quartz Gyro
Housing No. 2 was achieved in December 1976 and January 1977.

(c)   Gyro Spin Up : ·Comparison of Experiment and Theory

The design calculations on the gyro spin system received
some verification in experiments performed by T. D. Bracken[7]
in 1967 when an aluminum rotor was spun to 125 Hz at 4K in a
gas bearing. The test gave no information on the effectiveness
of the differential pumping system, and the operating parameters
differed appreciably from the final expected values; nevertheless
the results were in good agreement with the predicted maximum
spin speed under those conditions of 150 Hz and the predicted
spin up time constant of 45 minutes.

In order to check the efficiency of the spin up ridges a
flat test piece simulating the housing geometry was made up in
1971. Room temperature tests suggested that the original cal-
culations were a factor of 3 to 6 too optimistic, and on reexam-
ining the calculations we discovered an omission that accounted
for the discrepancy. Since the ceramic housing had already been
fabricated, we left it as it was, but in Quartz Gyro Housing No. 2
and in later housings we enlarged the pump out ports to provide
greater pumping speed and alleviate the problem. The calculated
limiting spin speed with the ceramic housing, allowing for the
omission, was 150 Hz.

The experience in 1967 with the gas bearing spin assembly
disclosed the need for great care to prevent introducing dirt
with the spin up gas. A series of experiments in 1971 showed
that a filter made with Millipore Duralon papers with 0.5×10^{-4}
inch pores would work satisfactorily provided care was taken to
avoid excessive quantities of contaminant which might cause
clogging. A filter holder was made which was non magnetic and
easily cleaned. The whole experimental chamber of the
large dewar was designed to be assembled and sealed in a clean
room before installation in the dewar. The apparatus was
designed to take spin gas from a pipe running to the vapor
above the main helium well of the dewar.

Figure 26 illustrates the assembled large dewar ready for
spin up. The apparatus stood about eight feet high. The main
spin channels were exhausted by a 120 cfm rotary pump connected
by a three inch flexible line to a valve on top of the dewar
and thence to a two inch fiber-glass pipe running down inside
the neck to the spin up channel outlet lines. The differential
pumping channels were exhausted by a ten inch high speed dif-
fusion pumping station, visible in the photograph, connected
via a stainless steel line to the dewar neck-tube and experimental
chamber. A cross-section of the dewar is reproduced below in Figure
68, p. 288. To begin with the differential exhaust pressure (and
therefore spin speed) was limited by the forepump to the high
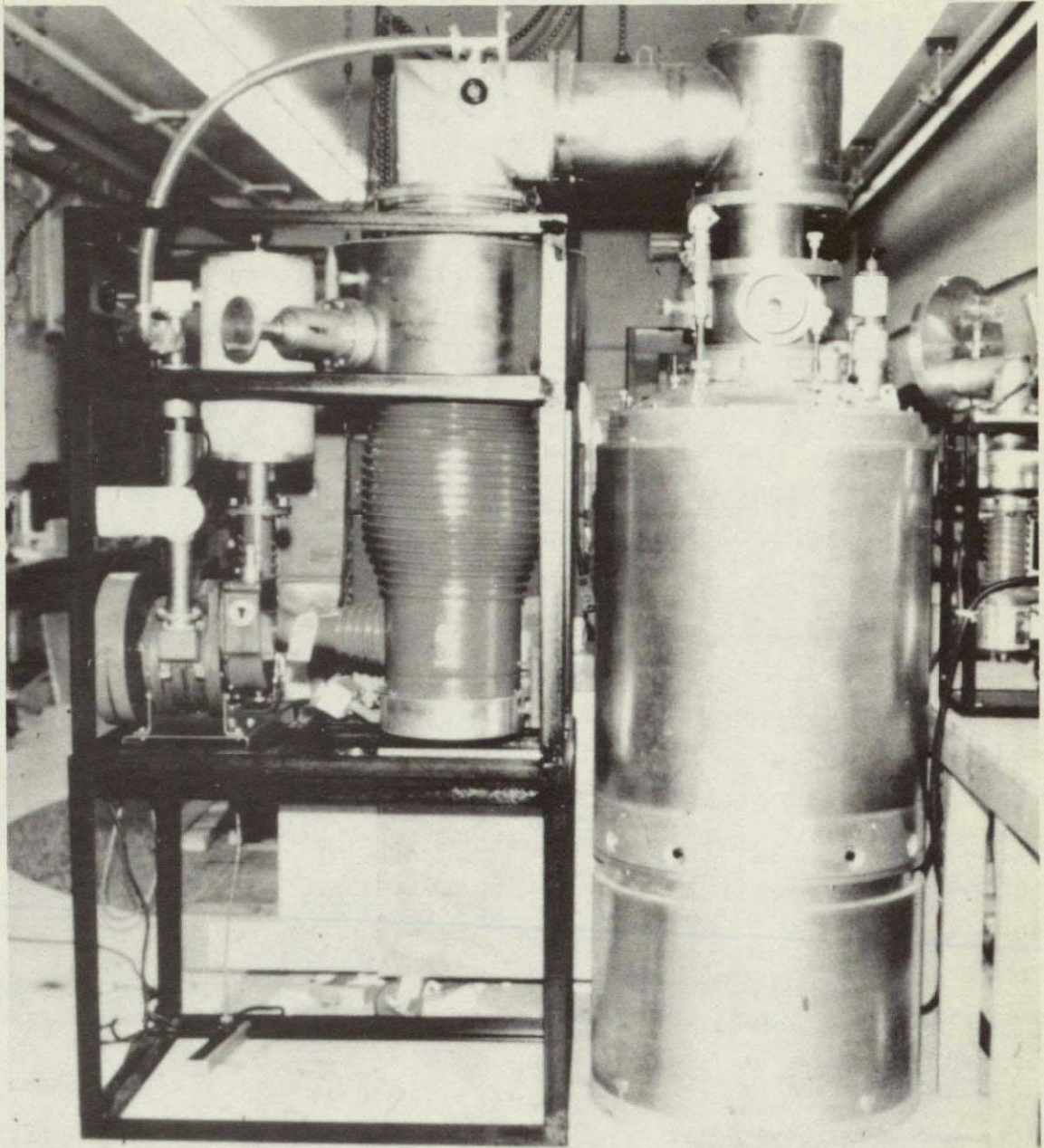
Figure 26: Main Laboratory Dewar and Pumping Station

speed diffusion pumping station, so we modified the foreline
and added a second larger pump in parallel.

The first attempted low temperature spin test with a beryl-
lium rotor was in October 1972. At that time we had no sure
way of telling whether the ball was spinning at room temperature;
the plan was to go straight to liquid helium temperatures and
look at the trapped flux in the spinning ball either with SQUID
magnetometers or a backup fluxgate magnetometer. Difficulties
with the magnetometers made the results inconclusive; our impres-
sion was that the ball was jammed in the housing. On warming up
we ran a spin test at room temperature, hoping to see the spin
from the suspension error signals, since we had learnt from
Honeywell that it is possible to do so at speeds over about
50 Hz. At that time we had no working experience of the char-
acteristics of the gas spin up system. A prolonged application
of gas seemed to generate no spin; the only output from the
suspension was an 800 Hz signal which we attributed to a
mechanical resonance in the dewar structure. Evidently the
ball was still jammed. Disappointed we switched off the sus-
pension system only to hear a horrid clonk; the hollow ball had
been spinning at high speed, possibly 800 Hz, and it had cracked.
Fortunately no great damage was done to the housing. The maxi-
mum gyro spin speed theoretically possible in this test was
estimated to be as high as 1600 Hz.

Our next step was to insert the full-weight nickel-coated
aluminum rotor. On January 4, 5, 1973 J. A. Lipa and J. R.
Nikirk performed the first controlled spin tests just below
room temperature. Readout was by magnetizing the nickel
coating on the aluminum ball and observing the rotating
magnetic moment with the fluxgate magnetometers. Shortly
after this run Nikirk made a very important discovery.
He found, contrary to the experience of Honeywell, that
in a quiet environment the spin of the ball could be read

out from the suspension error signals even at low speeds, indeed even when the ball was slowly tumbling at about 0.1 Hz. The observations were made first with the Honeywell suspension system and later much more readily with the new Stanford suspension system. This discovery was crucial to future gyro operations. It supplied a means of checking ball behavior all the way from room temperature to liquid helium temperatures. We were no longer shooting in the dark. As time went on Nikirk refined the technique until it applied even to much better balanced balls than we originally had.

The first low temperature spin tests were made in June 1973 using fluxgate readout of the trapped magnetic fields in a copper-niobium coated quartz rotor. A spin speed of 16 Hz was reached. Figure 27 reproduces the start of one spin up taken then, showing both the trapped flux signals in the fluxgate magnetometer and the suspension error signals in all three axes from the out-of-roundness of the ball. In later runs the spin speed at low temperatures was raised to a maximum of about 40 Hz.

Figure 28 shows spin up data taken with the ceramic housing at a temperature of about 6K. The upper diagram gives mass flow-rate through the differential pumping system versus the inlet pressure of the gas into the spin channel, the mass flow rate being determined from measurements of the inlet pressure of the high speed diffusion pump. The flow rate over the raised ridges turns out to be close to the predicted value. The lower diagram gives initial spin torque versus inlet pressure. The spin torque may be somewhat higher than predicted, but this depends heavily on the accuracy of the data points at the high pressure end of the scale; more data is needed before a firm conclusion can be drawn. Little data is available at present on the dependence of the drag torque in the housing on spin speed, which is the remaining significant parameter. Our experience at spin speeds up to 30 to 40 Hz is that drag is certainly not a limiting factor
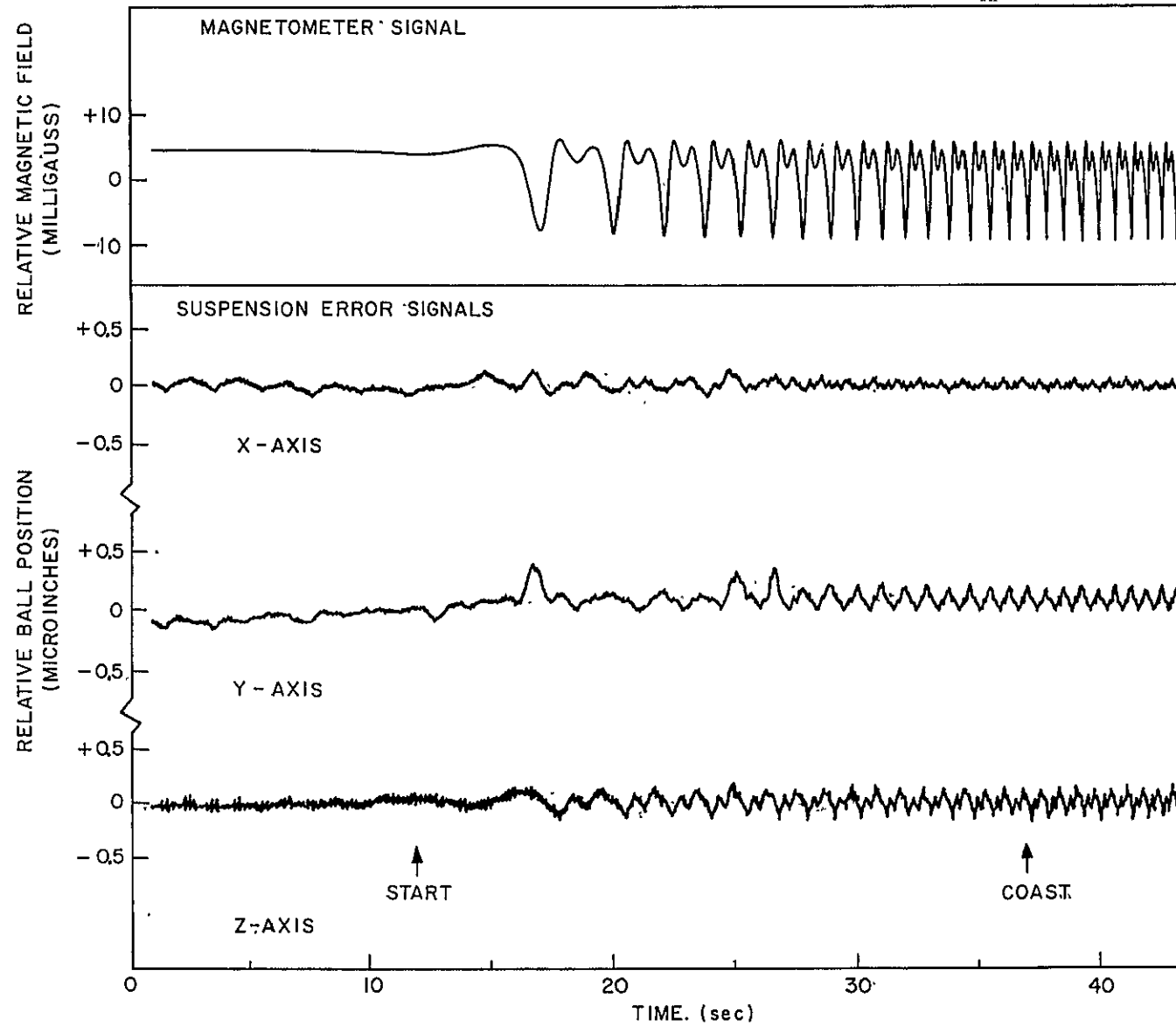
Figure 27: Trapped Flux and Suspension Error Signals
during Low Temperature Gyro Spin (June 1975)
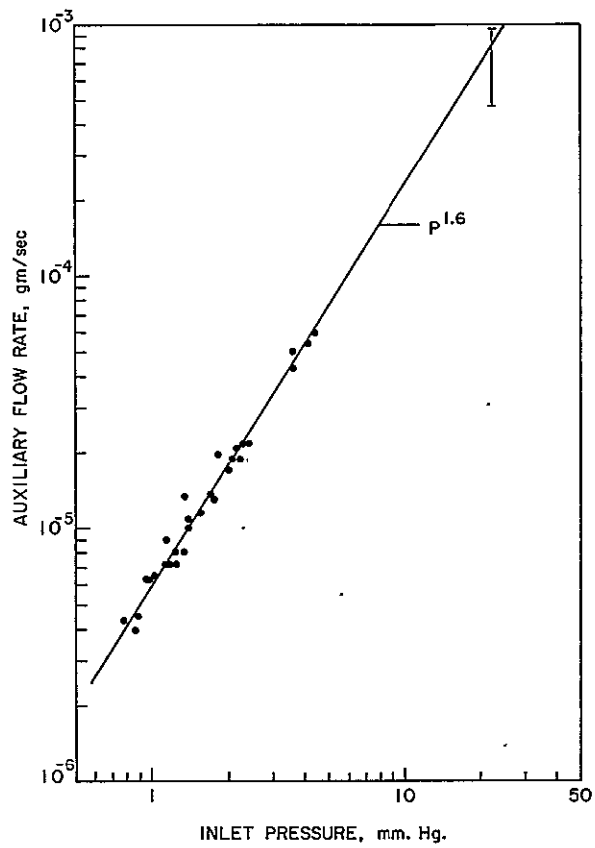
(a)   Auxiliary Flow Rate versus Inlet Pressure
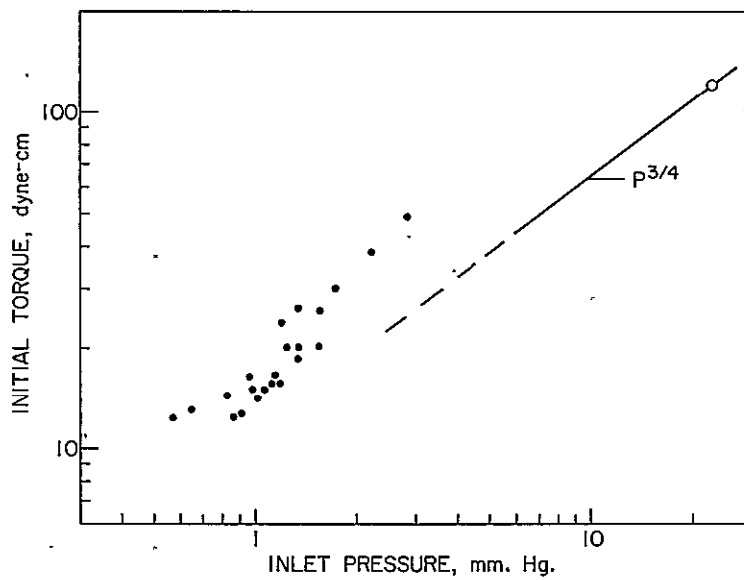
(b)   Initial Torque versus Inlet Pressure

Figure 28:   Data on Spin System with Ceramic Housing

137

to that level. Recent calculations on spin up parameters by
G. Karr[27] of the University of Alabama, Huntsville, imply
that more spin torque may be available than expected from the
Bracken-Everitt theory.

Recently we have begun collecting spin up information
with Quartz Gyro Housing No. 2. The main differences in spin
up design between this housing and the ceramic housing are its
larger differential pumping ports and larger rotor-housing
clearance. The difference in clearance is only temporary: a
better-fitting ball is available and will be used once the
initial operating period in the new test facility is over.
For the quartz housing the initial torques are 30 to 40%
higher than the data from the ceramic housing, a result which
may imply that there is a significant pressure drop in the
ceramic housing downstream from the pressure gauge. The mass
flow rate through the auxiliary channels is at present a factor
of five higher in the quartz housing because of the larger
rotor-housing gap.

Analysis of the spin data is continuing. The results so
far appear to be in substantial agreement with Bracken's pre-
dictions. To date we have limited ourselves to speeds below
40 Hz, but this has been dictated more by caution on our part
than by any limitation of the spin up system. As more gyro
housings become available we plan to increase the operating
speed to 100 Hz and above. High speed spin tests are also
planned at NASA Marshall Center.

(d) Free Running Gyro Performance

After spin up the gyro housing is pumped down to a low
pressure to allow the rotor to spin freely for extended periods.
Since June 1973 we have operated the gyro for nearly 1000 hours
at low temperatures at spin speeds up to nearly 40 Hz. During
low temperature operations we have had periods when levitation
and spin up were virtually impossible; on the other hand we have

had faultless runs of over 24 hours continuous spinning, during which we were able to make observations of rotor dynamics and gyro spin down time.

The gyro precession rate and polhoding period can only be accurately observed using the low temperature magnetometer readout system described in the next subsection. So far it has been most convenient to extract the information from the time dependence of the trapped flux signal. For a gyro without a preferred spin axis both the precession torque and polhode frequency are variables depending on the orientation of the body axes relative to the initial spin axis, so they vary from spin up to spin up.

Our most extensive data was obtained with the ceramic gyro during the London moment observations described in Section D (4) (g). At that time the rotor was deliberately unbalanced to obtain a high precession rate and simplify detection of the London moment. For this rotor the precession rate normalized to 50 Hz spin speed was as high as 5 arc-min/sec, corresponding to an unbalanced torque of 46 dyne-cm. The polhode period corresponded to a moment of inertia ratio $\Delta I/I$ of about 1.4×10^{-4}. For the rotor currently in use in the quartz housing the maximum precession rate observed so far is 1.0 arc-min/sec and the inertia ratio appears to be about 1.3×10^{-3}. The latter result is tentative because only partial observations have been made to date. The high inertia ratio is surprising in view of the rotor-coating method which utilizes a tetrahedral angle deposition sequence.

The observed precession rates are three orders of magnitude higher than is acceptable for a flight mission aimed at doing a 1 milliarc-sec experiment in a 10^{-9} g average environment. The chief requirement is to improve the uniformity and reduce the thickness of the ball coatings. A factor of ten improvement in uniformity seems reasonably straightforward. The present

thickness of about 140 μin is set by the need to withstand electrical breakdown. In space the breakdown problem is much less because arcing is much easier to avoid at the lower suspension voltages. The most dangerous time would be during spin up when the electrodes operate at a few hundred volts, but these voltages are still low enough to be able to run with a thin film without problems. To test a gyro with a thin film coating in the laboratory before launch, a supplementary gas or magnetic bearing can be incorporated in the housing if desired. Another approach is to coat the rotor with a second thick breakdown resistant film having a density close to that of quartz. Probably such a film should be made electrically conducting to avoid static charge build up.

During the free running phase the gyro rotor gradually slows down through gas drag in the cavity. Its speed may also be altered by gas leakage in the spin up plumbing, stray material in the housing, and torques from the suspension system, which, while negligible in space, can be appreciable with an out of round ball and the high support voltages required on Earth. Apart from occasional dramatic disturbances when the rotor hits the wall, the speed perturbations are generally small low-frequency effects. Gas drag has been the dominant factor. From Equation (7), p. 53 we can compute gas pressure in the housing from the observed spin down time. The highest time constant so far observed has been 175 hours at room temperature. This gives a housing pressure of 7×10^{-5} torr. The observed chamber pressure was 1.5×10^{-6} torr. In the low temperature runs made to date we have usually introduced helium exchange gas into the chamber to carry away the heat from the suspension currents. The smaller time constants observed have agreed well with the values calculated from the chamber pressure.

Figure 29 illustrates trapped flux signals showing gyro precession and polhoding in a typical low temperature run.
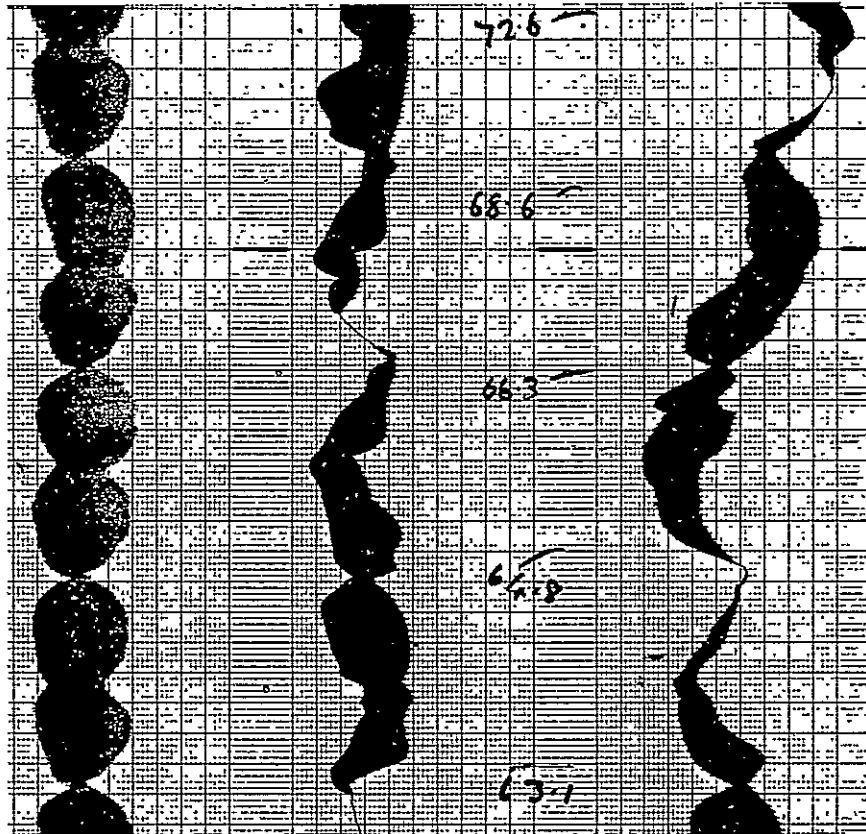
(a)   Spin Speed 15 Hz, 1 min = 2.5 small divisions
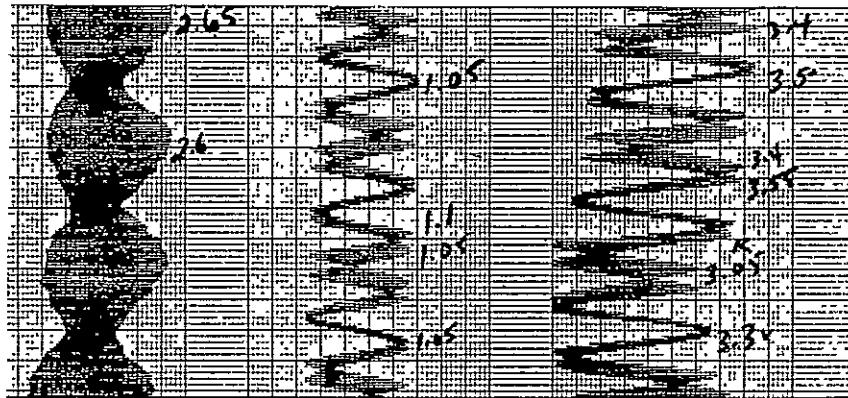
(b)   Spin Speed 0.39 Hz, 1 min = 10 small divisions

Figure 29:   Trapped Flux Signals Observed in Three Axis
             Readout System, Showing Polhoding (Left Hand
             Traces) and Precession (180° between Nulls of
             Center and Right Hand Traces) at Spin Speeds
             of 15 Hz and 0.39 Hz

             Operating temperature ∿ 6K

141

(e) Interfacing of Readout Magnetometer with the
     Dewar and Gyro

The first run with a magnetometer in the large laboratory
dewar was performed in June 1973, concurrently with the first
low temperature spin test. We successfully operated the magne-
tometer with the gyro switched off, but observed large amounts
of pickup as soon as the suspension system was turned on. This
interference was clearly different from the expected magnetic
pickup in the readout loop. It was present whether the SQUID
was acting as a magnetometer at liquid helium temperatures or
as a passive rf load at room temperature. It was evidently
due to imperfect electrostatic shielding between the suspension
cables (and other sources) and the SQUID tank circuit. The
SQUID tank and these amplifiers are tuned to 30 MHz; the
interference resulted from 30 MHz harmonics of the 1 MHz and
20 kHz signals from the suspension system.

. We did extensive tests to see how much interference the
magnetometer could tolerate and to find out how to reduce the
pickup to acceptable levels. Measurements on the normally
operating magnetometer in a small test dewar established that
the shielding must be improved by at least a factor of 1000
for proper operation. We then set up a room temperature sim-
ulation of the dewar cabling on a ground plane, to investigate
which combinations of shielding and ground techniques were most
effective. We tried over a hundred such combinations, some
using a rod antenna as the source of interference and some
using the suspension system with dummy loads. Later we per-
formed interference tests in the dewar itself. Following these
tests we put the SQUID and damping cylinder in a totally
enclosed copper shield, provided triaxial shielded cables with
shielded ends for the rf line from the SQUID up to the con-
nector at the top of the dewar, and carefully dressed this .
cable and all other cables in the neck tube close to the ground

plane provided by the neck tube wall and away from the suspension cables. Thereafter there was no measurable electrostatic interference.

The next problem was magnetic pickup between the suspension and readout. To get rid of pickup from the 1 MHz position sensing signals, and reduce the 20 kHz pickup, we introduced a low pass filter between the gyro readout ring and the SQUID, based on the damping cylinder referred to in Section C (3) (b). A typical SQUID-damping cylinder assembly is illustrated in Figure 30. The readout ring is connected to a coil around the outside of the cylinder; inside the cylinder another coil is connected to the SQUID. The damping cylinder is made of a conducting (not superconducting) material and is typically 0.5 cm in diameter, 4 to 5 cm long and 0.025 cm in wall thickness. At high frequencies reaction currents are damped by the resistance of the cylinder, allowing low frequency signals to pass. The damping cylinder has the second benefit of substantially reducing capacitive coupling between the two coils. We experimented with bandwidths from 5 kHz, which passed too much 20 kHz pickup, to 5 Hz, which was far lower than necessary. The bandwidth depended on resistivity and wall thickness, which were varied both by machining and electroplating the cylinder. Metals used were brass, or copper for plating. The cylinders eventually used in most of the work were made entirely of copper to reduce thermoelectric voltages, which are a source of spurious signals, and had bandwidths of 250 to 300 Hz.

The first successful operation of a magnetometer with the live gyro was during the third cryogenic run of the large laboratory dewar in November 1973, using a damping cylinder of 35 Hz bandwidth For the same run we had built up a 3 axis 20 kHz bucking system, and with the combination of bucking and filtering systems we succeeded in locking the magnetometer with gyro suspended for periods of several hours.
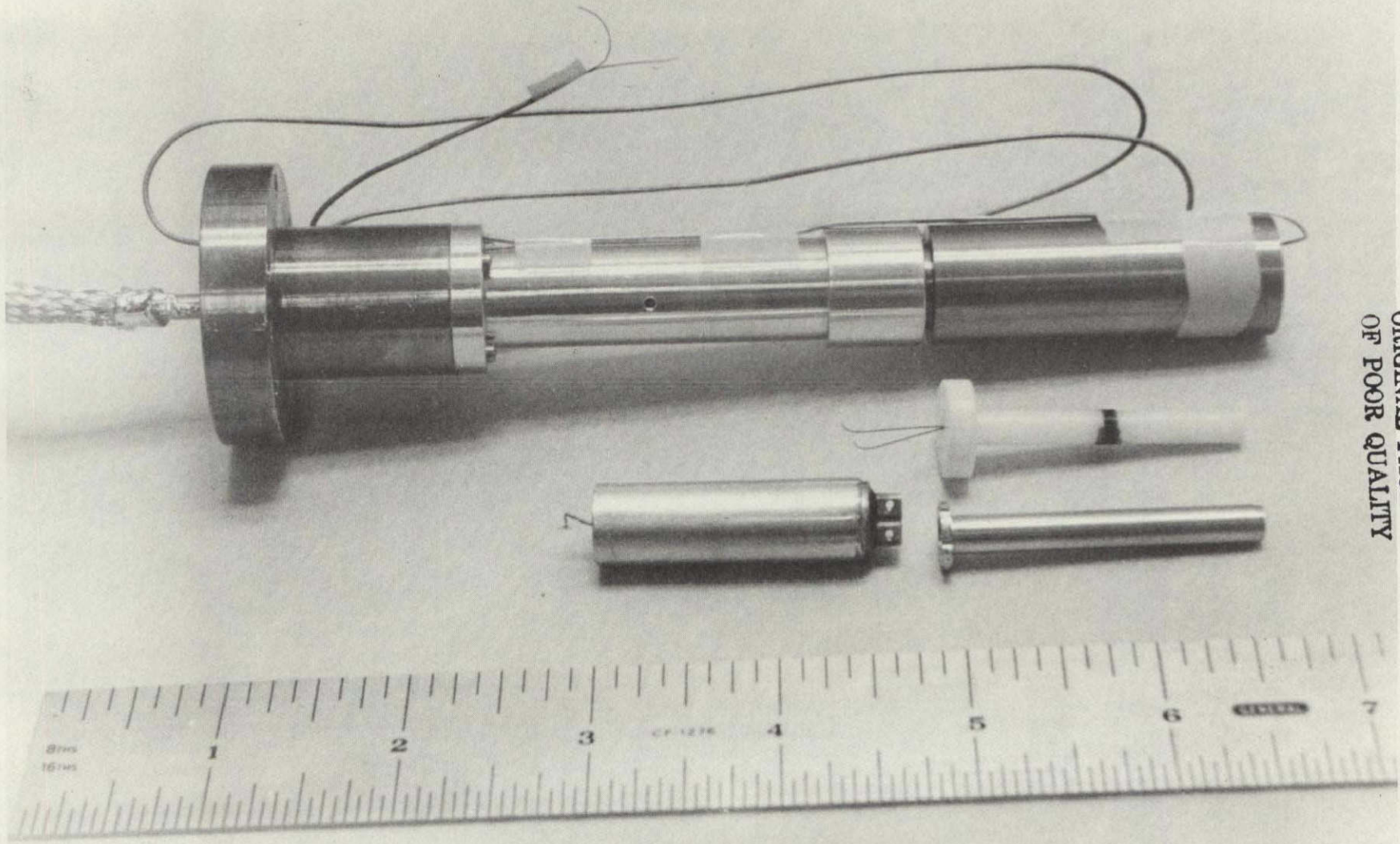
Figure 30: SQUID/Damping Cylinder Assembly

We continued for about a year with the single axis readout while working to reduce trapped fields in the gyro rotor by the methods described in D (3) (f). For the reasons explained in D (3) (g) observation of the London moment required a properly calibrated three-axis gyro readout; this we began building in November 1974. In principle the three axis readout was a logical extension of the single axis readout, but several problems had to be solved before it worked well. One was temperature stability of the SQUID magnetometer. The original SQUID had been attached to the gyro base plate and not well anchored thermally to the helium bath. The rf level loop corrected the problem to the extent of maintaining the right SQUID bias, but temperature gradients generated thermoelectric currents in the damping cylinder, giving rise to readout errors from the charging magnetic fields. The new SQUIDs were SHE units. We improved the heat sinking by attaching their housings directly to the bolt circle of the inner well of the dewar, which was in much closer thermal contact to the bath, and also sought to reduce thermal gradients by applying the dewar-within-a-dewar concept to the SQUID assembly. The damping cylinder was heat sunk at one end and surrounded with a simple dewar that isolated the assembly from external sources of heat. Since there were no significant heat sources inside the shield dewar, thermal gradients, and hence thermoelectrically generated fields, were minimized. Thermal stability of the SQUIDs was substantially improved by these procedures.

By the end of 1974 we had built three magnetometer electronics packages with all the necessary circuits for control of the rf box and with current feedback circuits to read out the magnetic field. Early in 1975 we installed the two additional SQUIDs and damping cylinders in the dewar along with all the necessary cables. At first the three rf boxes interfered electrically with each other but this problem was easily solved by grounding them together. The SQUIDs all worked during the first cooldown of the three axis system in January 1975.

Figure 31 illustrates the gyro assembly in the laboratory dewar in its final form, with ceramic gyro housing, spin up plumbing and filter, high voltage suspension cables, and three magnetometer and damping cylinder assemblies connected to coils wound on the outside of the gyro housing. The single large magnetometer/damping cylinder assembly is the one with the original adjustable point contact toroidal SQUIDs. The other two are the improved housing with the SHE SQUID units. The original SQUID was attached to the readout loop wound on the centering ring at right angles to the parting plane between the two halves of the gyro housing, identified as channel II of the gyro readout. For this we applied a counterwound coil of the type illustrated in Figure 10, p. 76 which cancelled changes in the ambient field by a factor of 10 to 25 and helped considerably in rejecting 20 kHz pickup. Shortage of time and practical considerations dissuaded us from applying counterwound coils in the other two readout channels. When the suspension system was turned on the performance of magnetometers I and III (the new magnetometers), sharply deteriorated, because they were using most of their capability to follow a 20 kHz signal from the suspension, which greatly reduced their margin for other signals. Tests showed that all three damping cylinders were working; however the damping cylinders for channels I and III, being made at a different time from channel II had slightly higher bandwidth. We eliminated the trouble by applying 20 kHz bucking in channels I and III and the three axis readout operated excellently with the gyro suspended.

(f) Reduction of Trapped Flux in the Gyro Rotor

The process of reducing the ambient magnetic field in the large laboratory dewar depended on a combination of Mu-metal shielding and field cancelling coils around the gyro. In many, but not all of the experiments, a superconducting lead shield was wrapped on the outer surface of the experimental chamber in the helium well of the dewar in order to stabilize the field
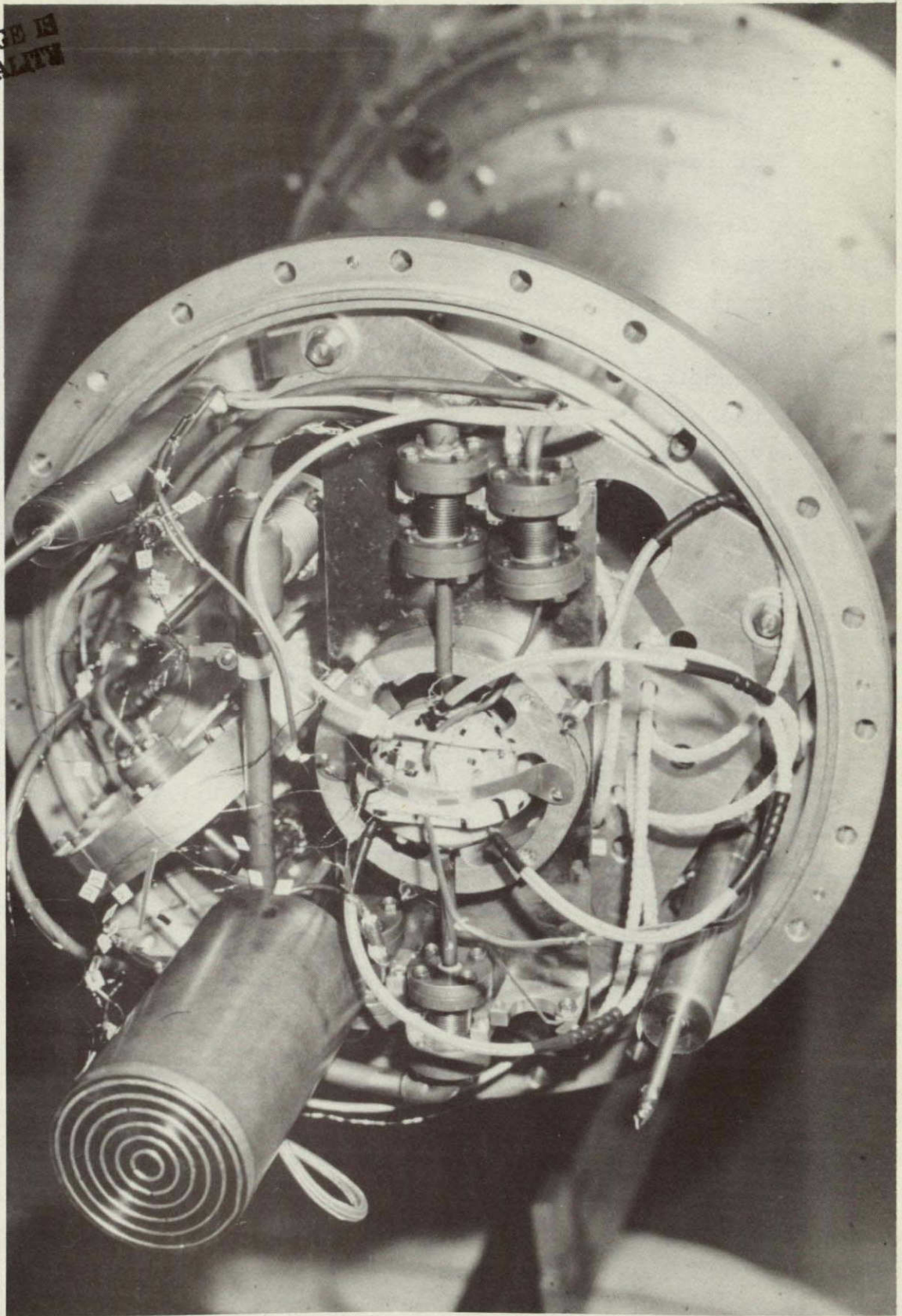
Figure 31:   Gyro Assembly in Main Laboratory Dewar

147

from the Mu-metal shields. The cancelling coils were a set
of three orthogonal coils surrounding the gyro, through which
measured currents were passed to balance out the residual fields.

For the low temperature run of November 1973 during which
a magnetometer was operated for the first time with a suspended
gyro, only the inner Mu-metal shield was available. The field
level observed was 3×10^{-2} gauss, which was large enough to
make the magnetometer lose lock as soon as the gyro was spun
owing to the high slew-rate of the rotating trapped field. In
progressive stages we completed and annealed the outer Mu-metal
shield, removed magnetic materials from the helium well and
experimental chamber, and added degaussing coils and trim coils
to the Mu-metal shields. To measure the field in the experimental
chamber we put in a three-axis flip coil magnetometer with a
fluxgate probe. An important step was to make vacuum sealed
push-rods to manipulate the flip coil, allowing us to make
field measurements with the gyro suspended. By means of the
shields and flip coil we easily reached fields of 5×10^{-4} gauss
or less at the gyro. A limitation of the arrangement was that
the flip coil was 4 inches above the gyroscope, and there were
appreciable field gradients in the inner well. Thus in one
run (October 1974) the field after one test was 4×10^{-4} gauss
at the flip coil and fortuitously lower at the gyroscope,
being only 2×10^{-4} gauss, as measured from the trapped flux
signal.

To go lower we developed a field cancelling procedure which
consisted in applying small known currents to each in turn of
the three field cancelling coils around the gyro and observing
the resultant trapped flux after heating and cooling the gyro
each time. By slow iterations the field was brought down to
about 2×10^{-5} gauss. It is hard to conceive of anything more
tedious. The method did work but between 2×10^{-5} and 5×10^{-5}
gauss the results began to be non-repeatable, with considerable

variations in the amount of flux trapped in the rotor in successive identical cooldowns. This effect was eventually attributed mainly to thermoelectric generation of slowly varying fields in the neighborhood of the gyro through temperature gradients in the various metal components of the gyro support assembly. Experiments by P. M. Selzer[41] at Stanford in 1972 had shown that the Thomson effect can generate large circulating currents in strained metals at low temperatures. The currents from a one degree temperature difference across a copper block at 4K were enough in one instance to produce a magnetic field of 1 gauss at the surface. The consequence of the Thomson effect in strained materials was quite unfamiliar to us, though subsequently we have learned that the equivalent effect at room temperature was a commonplace of laboratory handbooks of the 1900s!   In order to reach fields near 10^{-7} gauss, such as are ultimately needed, all metal parts must be removed from the neighborhood of the gyro. This we have done in the new ultra-low field apparatus started in May 1975 (Section E below). Meanwhile we struggled on with the field cancellation procedure in the old dewar but were never able to go below 10^{-5} gauss. The London moment in a ball spinning at 30 Hz corresponds to 2×10^{-5} gauss. Special procedures were necessary to separate it from the trapped flux signals.

(g) Observations of the London Moment

During 1974 we identified three methods for detecting the London moment in a gyro limited by short running time and appreciable quantities of trapped flux in the rotor. Briefly these were:

(i) unbalancing the rotor to make it precess rapidly about the vertical axis, while at the same time having trapped flux signals sufficiently constant to allow simple subtraction of their d.c. component

(ii) adding gas to make the rotor spin down rapidly, in which case, if there is little precession, the variation of London moment with spin speed may be observable

(iii) computation and correction for trapped flux utilizing data from a three axis magnetometer system.

In March 1975 we obtained the first London moment data by a combination of methods (i) and (ii) using data collected from the three axis readout to prove the stability of the trapped flux signals. Figure 32 illustrates the fundamental task of gyro readout of the London moment and trapped flux signals. The Cartesian reference frame i, j, k is centered on the ball with axes parallel to the readout loop normals. The vector $\underline{\Omega}$ represents an arbitrary spin axis along which lies the London moment vector M_L; the trapped flux vector $\underline{M}$ is inclined at an arbitrary angle θ. The trapped flux signal has a d.c. component $M_{DC} = \underline{M} \cos\theta$ and an instantaneous a.c. component $M_{AC} = \underline{M} \sin\theta$ which links each loop in an amount depending on the direction cosines ω_i, ω_j, ω_k of the spin axis $\underline{\Omega}$. Thus from the ratio of the a.c. signals only we can find the direction of $\underline{\Omega}$ up to an arbitrary sign in the components. Then given the value of $\underline{M}$ determined by some other means we find θ and hence the d.c. components of the trapped flux $\underline{M}_{DC} = (M_{DC}^i, M_{DC}^j, M_{DC}^k)$. This information is all that is needed to determine the components of $\underline{M}_L$ up to an arbitrary constant. Since the quantities M_L^i, M_L^j, M_L^k vary in exactly the same fashion as ω_i, ω_j, ω_k we can make an unambiguous identification of $\underline{M}_L$ if the ball precesses. Such a determination is independent of polhoding action. Depending on the accuracy with which $\underline{M}$ can be determined we can in principle compensate for a large trapped flux signal, provided we have a three axis readout. Figure 33 illustrates signals observed with the three axis readout and a relatively high level of trapped flux in a slowly tumbling gyro rotor.

GYRO READOUT VECTORS
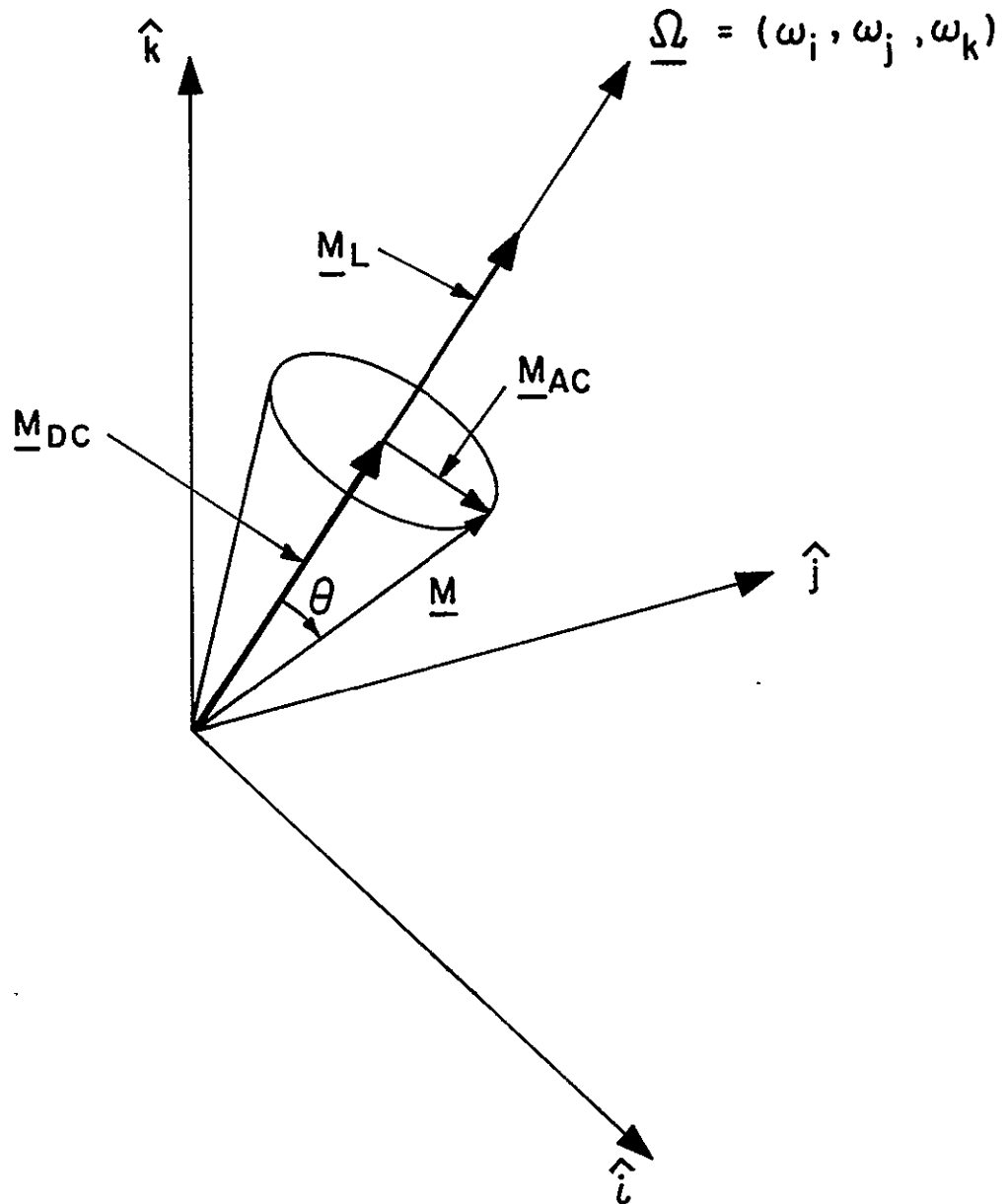
FIGURE I

Figure 32: London Moment and Trapped Flux Vectors in Gyro Readout
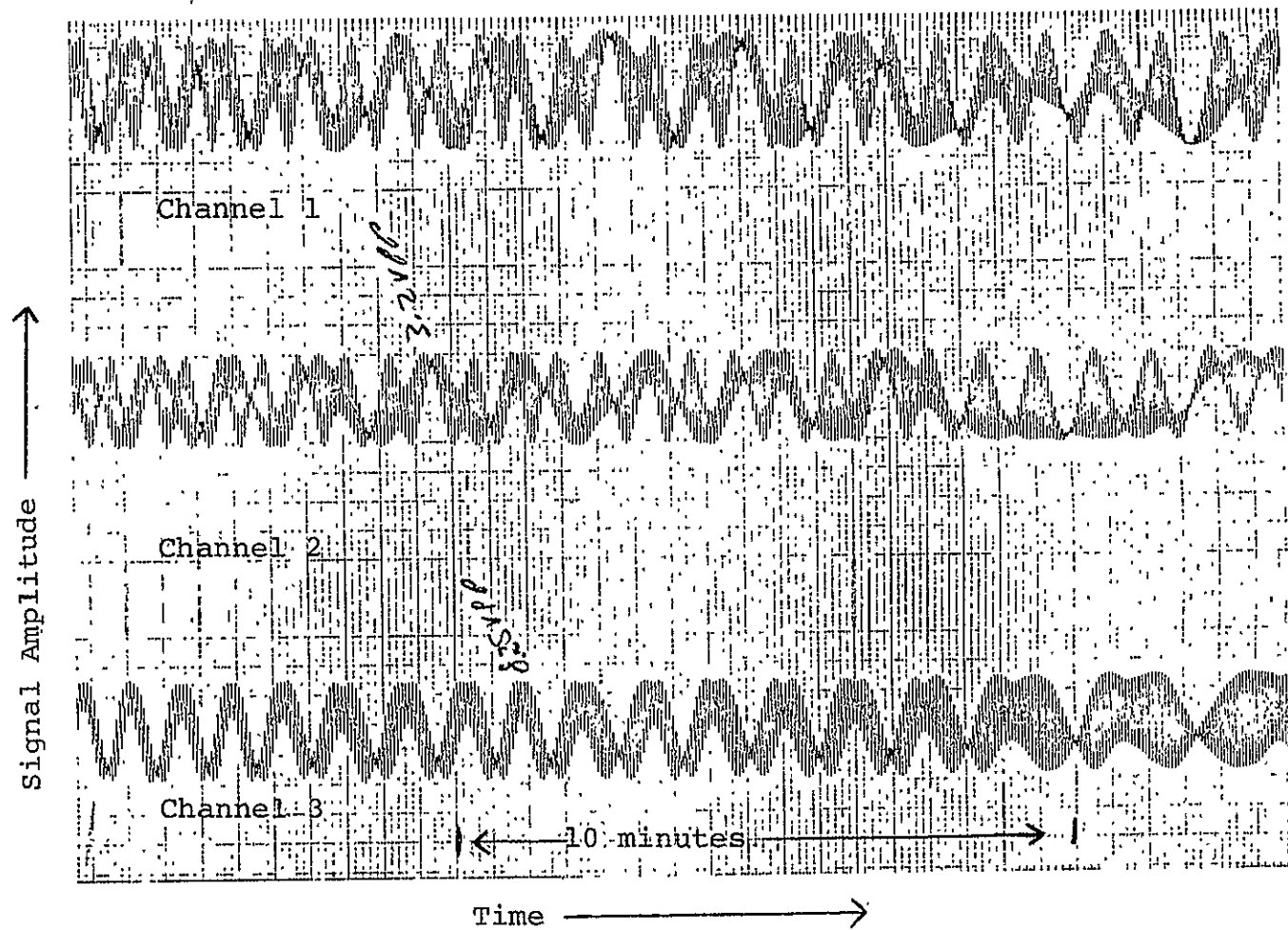
Figure 33 : Trapped flux readout signals obtained with the three axis SQUID
readout system. Spin speed: 0.3 Hz; Temperature: 6K;
Trapped field: Approximately 3 x 10^{-4} gauss.

Even if the trapped field is slowly varying the London moment can be detected in the presence of a trapped field equal to or larger than itself, provided it has simple dipole form. The problem is when the trapped field is non-uniform. When the field in the large dewar was nulled to levels at or below the London moment at 30 Hz, it has gradients which yielded significant components of trapped flux in the ball right up to the sixth harmonic. Not only had we no method of processing such a complex signal, we found also that the strong harmonic content seriously threw off the first order calculation.

Another difficulty was that as the field level was reduced we ran into problems with field changes originating in electrical discharges from the suspension. Often activity that was not enough to make the rotor strike the walls would noticeably alter the trapped flux. The underlying cause of the discharging appeared to be the imperfect quality of the electrodes in the ceramic housing, which had suffered heavy punishment and had many repairs during its four years of use. In the absence of a better housing we could do little but wait for quiet periods or shut down for further electrode repairs.

In these circumstances our technique for observing the London moment was to measure the spin speed dependence of the total magnetic moment parallel to the spin axis (which is in general the sum of the London moment and axial components of trapped flux) and to use transverse flux data to check the constancy of the axial trapped flux.

To facilitate readout we added a three channel signal conditioner for the magnetometer outputs. These preprocessing circuits, which were among the last of J. R. Nikirk's contributions to the program, separated the readout signal from each magnetometer into d.c. and a.c. components and so produced signals that would with appropriate processing isolate the London moment.

·Figure 34 shows the London moment data obtained during an 18 hour run on March 11, 1975. The measurements of parallel flux agree with the theoretically predicted spin speed dependence of the London moment to within the 10% accuracy of the sensitivity calibration of the pick up loop. The data cannot be explained away by attributing the variation with spin speed to a variation of the parallel component of trapped flux. No more than 2 or 3% of the observed signal at most could be so accounted for. Each data point corresponds to a measurement made when the gyro spin axis was normal to the channel II pick-up loop with low d.c. drift characteristic. There was no detectable change in the trapped flux during the data collection period, either from suspension system activity or any other cause. The trapped flux signal did exhibit a high harmonic content, as has been mentioned: efforts to calculate and subtract out the parallel trapped flux component were not very successful. Hence we had to rely on the constancy of the trapped flux to a greater extent than will ultimately be necessary.

The detection of the London moment in a live gyro repre-sented the end of a distinct phase of the Gyro Relativity program. The clear need now was to devise a means of operating the gyroscope in ultra-low magnetic fields, to which problem our attention next turned. Results of the London moment observa-tions were presented in a paper by J. A. Lipa, J. R. Nikirk, J. T. Anderson and R. R. Clappier at the 10th International Conference on Low Temperature Physics held during August 1975 at Helsinki, Finland.[42]

E.   THE PRECISION GYRO READOUT EXPERIMENT

(1) Planning

In reviewing the experimental situation at Stanford during April 1975 after observing the London moment, we concluded the
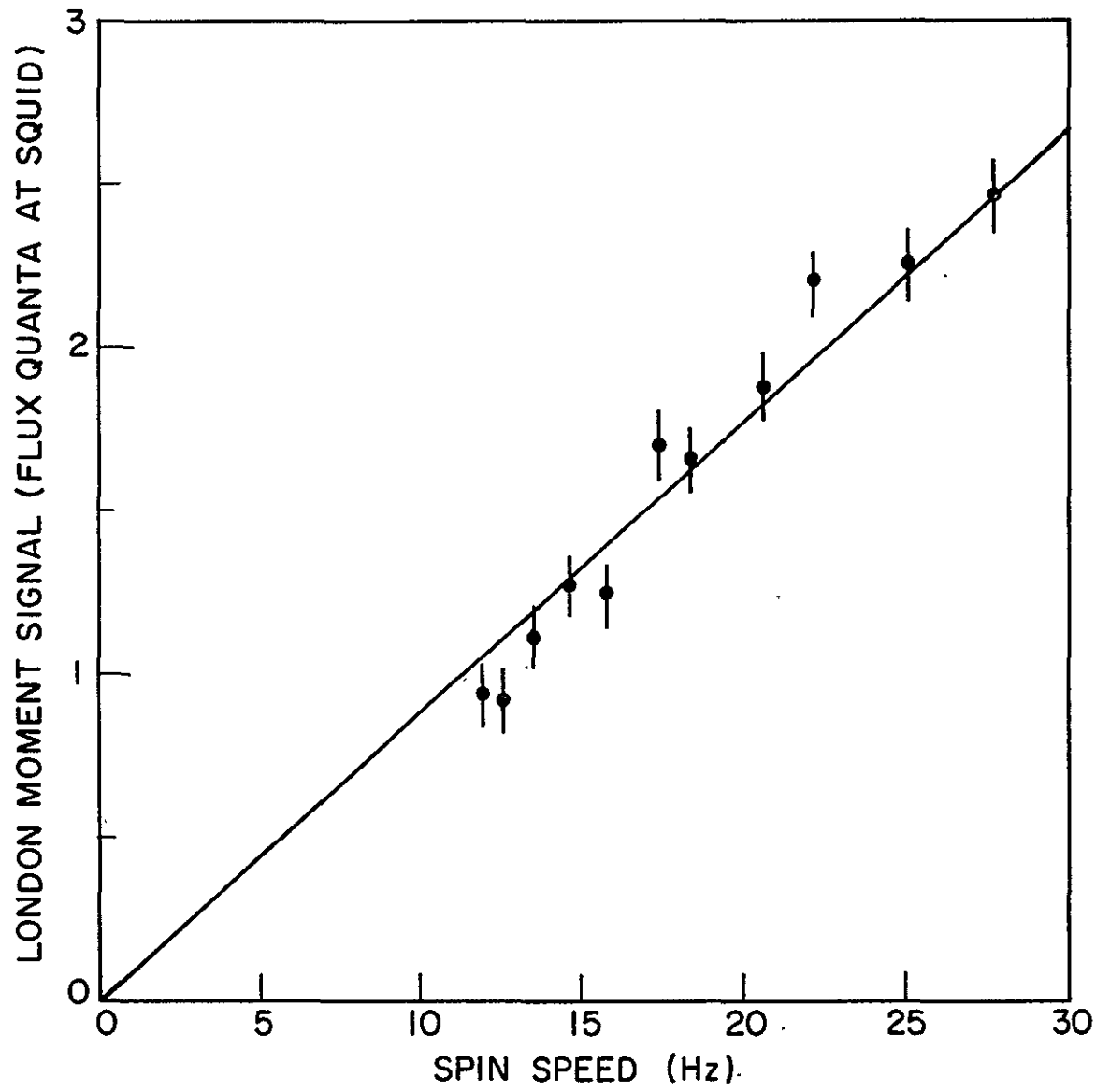
Figure 34:   London Moment in Gyro Rotor as Function of Spin
Speed: Comparison of Experiment and Theory

155

time had come to define a new goal for laboratory research: an all out effort to obtain an angular resolution approaching 1 arc-second in London moment readout on a live gyroscope. Doing this required an entirely new test facility with the gyro mounted inside an ultra-low magnetic field shield, all metal parts and ferromagnetic materials being removed from its vicinity, together with the use of quartz rather than ceramic gyro housings, readout magnetometers of improved sensitivity and stability, and data processing with an on-line mini-computer. We had already started on a quick turn around facility, based on a standard 12 inch dewar, which would provide for gyro development without the long delays encountered in the large laboratory dewar. Our plan was to combine precision readout with the quick turn around facility, using some of the components we had already bought or built. The choice of 1 arc-second resolution as the design goal was somewhat arbitrary: it seemed, however, about the best we would be likely to achieve with a live gyro allowing for gyro drift and limitations on the system due to ground vibrations. A subsidiary goal was to demonstrate readout magnetometer performance in a separate facility to 0.01 arc-sec or better.

The new plan was reviewed at meetings at NASA Marshall Center and NASA Headquarters, May 6, 7, 8, 1975 and summarized in a letter from C. W. F. Everitt to A. L. Schardt dated May 16, 1975. The schedule and management plan was given in a subsequent letter to Dr. Schardt dated June 26, 1975 and in the 1975 Request for Continuation of Support on NASA Grant 05-020-019. During the 18 month period from July 1975 through the termination of Grant 05-020-019 we have worked with unexampled vigor and now have an operating facility in which we have tested both ceramic and quartz housings at low temperatures. An 8 inch diameter ultra-low field shield with field levels of 2×10^{-7} gauss is available for installation in the facility. We have

also completed the independent readout demonstration to an
accuracy corresponding to 0.001 arc-second: a factor of ten
better than the goal established in 1975.

Development of the precision readout experiment has
required close coordination of the work of all members of the
group. Design of the new facility was chiefly the responsibility
of F. J. van Kann and B. Cabrera with support from R. Hacker;
the ultra-low field shield was made by B. Cabrera; broader
aspects of planning and quartz gyro development were due to
J. A. Lipa, magnetometry to J. T. Anderson and R. R. Clappier,
support electronics to R. A. Van Patten, development of the
minicomputer to R. R. Clappier. Fabrication of many of the
parts of the new facility has been due to J. J. Gilderoy, Jr.
and members of the Physics machine shop.

(2)   Ultra-Low Magnetic Field Technology

(a)   Shield Cooling Techniques

One of the special properties of a superconductor is that
in most circumstances the magnetic flux through a closed super-
conducting surface is conserved. During the period 1969 to 1975
under separate funding we developed techniques to exploit this
property and create permanent regions of extremely low magnetic
field by heat-flushing and expanding a series of superconducting
lead shields. We are now routinely able to make shields 4 inches
and 8 inches in diameter in which the fields over a length of
about 30 inches are below 10^{-7} gauss.

Our first idea for obtaining ultra-low magnetic fields
was to cool a tightly compressed sock-like superconducting
shield in a low field and then expand it. Since flux is equal
to field times area, the increase in area will cause a corres-
ponding decrease in field. Figure 35 illustrates the process
schematically. The sock, constructed of pure lead foil is
pleated longitudinally and folded flat as in the left hand
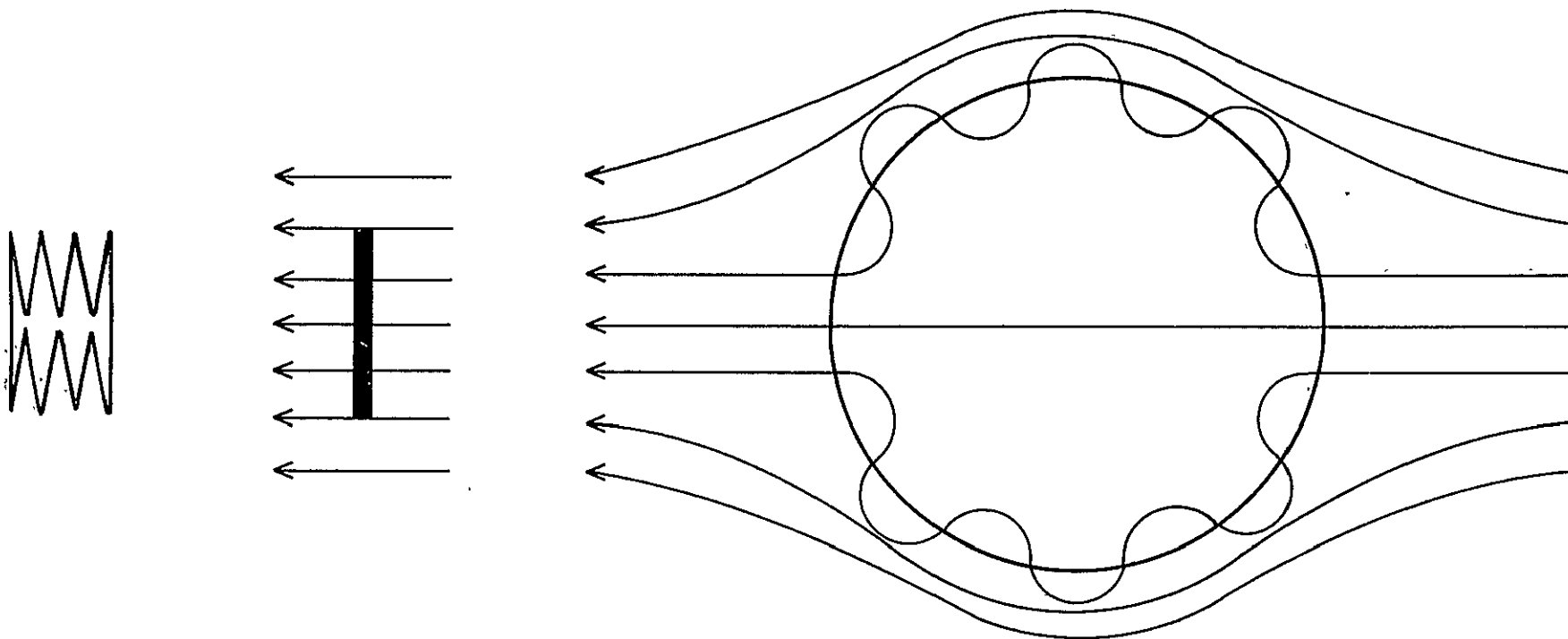
Figure 35: Schematic Representation of Magnetic Field
Before and After the Expansion of a Lead Shield

and middle diagrams, and then cooled through its superconducting transition. Assuming strong flux pinning the field in the direction shown is reduced after expansion in the manner indicated in the right hand diagram. In principle an even greater field reduction than that attributable to the area change might be expected with a tightly folded lead shield as a result of the flux-expulsion property of a superconductor (the Meissner effect). A solid Type I superconductor excludes up to 99% of the magnetic field through the transition temperature, and the tightly folded lead shield might be considered as equivalent to a closed solid. In practice the Meissner effect contributes little to field reduction in such circumstances--probably no more than a 30% improvement over the simple expansion process.

A second method of field reduction is heat flushing. If a temperature gradient is applied along the superconducting sock as it is cooled one end will be superconducting and the other normal, with a transition region in between. Further cooling will make the superconducting boundary move steadily forward, and in suitable circumstances the magnetic field is progressively pushed out of the enclosed volume. Two opposing mechanisms determine the effectiveness of heat flushing:

(i) as the temperature gradient is increased the area of the shield going superconducting at any one time will become smaller, and with constant ambient field the flux through this transition zone will also decrease. Ultimately with a low enough initial field and high enough temperature gradient, the transition zone flux will stay always under half a flux quantum: then no field will be trapped anywhere in the shield as the superconducting boundary moves from one end to the other: one will have a region of zero magnetic field.

(ii) on the other hand the thermoelectric currents described in Section D (3) (e), due to the Thomson effect in a strained metal, generate magnetic fields proportional to the temperature gradient across the cooling shield. Since the current depends on thermopower divided by the resistance

of the material, the magnetic fields created during
heat flushing can be reduced by working with thinner
shields. Requirements of mechanical strength and (43)
other practical considerations reviewed elsewhere
make the thinnest useful shield material at present
a 2.5 mil lead foil.

The procedure we have developed for making 10^{-7} gauss
shields combines the expansion and flushing techniques. To
avoid trouble with thermoelectrically generated fields, the
ambient field is lowered in steps by cooling a series of
three or more shields successively one inside the other,
reducing the temperature gradient used in heat flushing
at each step. The applied gradient should not be smaller
than the characteristic temperature fluctuations in the
material, however, since the fluctuations would then produce
local superconducting paths enclosing normal regions and
trapping magnetic flux.

Figure 36 illustrates the cyclic procedure in which a
lead shield of given diameter is cooled and expanded inside
another shield of the same, or in some instances smaller
diameter. Stage (a) shows an open sock-like shield in a
dewar vessel, the shield having already been cooled and
expanded in a low magnetic field (the first sock is cooled in
a field of about 10^{-4} gauss provided by conventional Mu-metal
shields). A typical sock is 4 inches in diameter and 36 inches
long, welded from 2.5 mil lead foil and suspended from the
top plate of the dewar by a cloth cylinder glued to the upper
end of the foil. Stage (b) shows the second sock, pleated as
on the left hand diagram of Figure 35 into a strip 36 inches
long and 1.5 inches wide, inserted into the first shield
and maintained above its superconducting transition tempera-
ture by being enclosed in a double-walled glass tube (a dewar)
like a diving bell, to which an overpressure of helium gas
has been applied to drive the helium liquid level to a point
below the bottom of the sock. Stage (c) shows the sock after
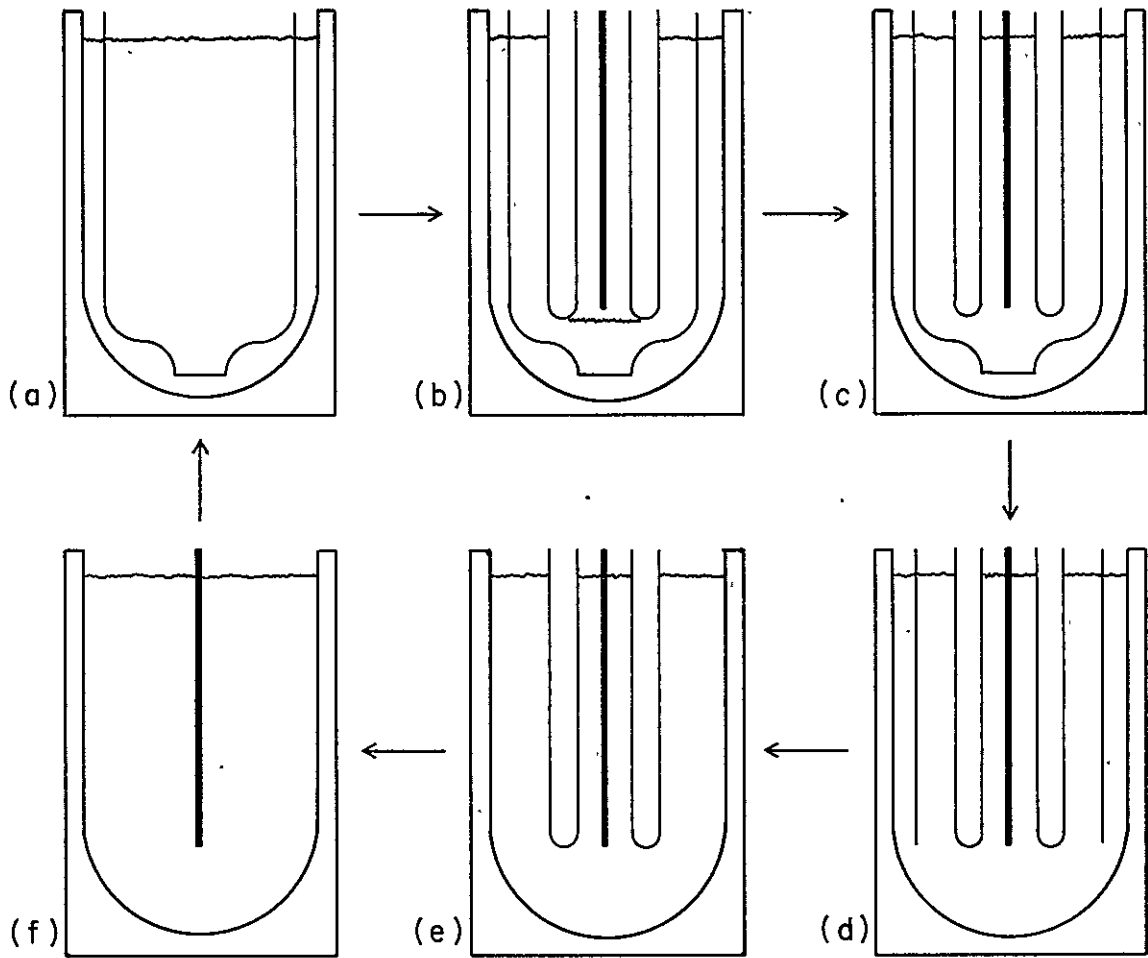
Figure 36: Shield Cooling Cycle for Generating Ultra-Low Magnetic Fields

(a) Expanded lead bag (b) Second lead bag inserted, folded and warm (c) Second bag cooled (d) Hole torn in bottom of first bag (e) First bag removed (f) Second bag ready for expansion

cooling below its superconducting transition temperature, with the helium level in the double-walled glass tube now back up to the same level as in the rest of the dewar. Details of the heat flushing procedure are described below. The next two stages (d) and (e) consist in tearing out the bottom of the outer lead shield by means of a special tool and removing it from the dewar. Stage (f) is to lift away the double-walled tube from around the inner lead shield, which is now ready for expansion to stage (a), after which the cycle may be repeated by introducing and cooling another folded shield.

For the present work all the shields used in field reduction are of 4 inch diameter, except the last which is of 8 inch diameter but capable of being folded small enough to fit inside the 4 inch shield and double-walled glass tube.

Our original heat flushing procedure was a quasi-static one. The helium level was allowed to rise very slowly around the folded shield over a 12 hour period, the motion being controlled by cutting back the gas flow and venting through the upper end of the double-walled glass tube. More recently we have avoided this time consuming procedure by introducing a calibrated helium gas leak into the vacuum space of the tube so as to provide transverse heat flow along the entire length of the shield. The new method has three advantages (i) the heat flux across the whole length of the tube reduces the temperature gradient in the shield and hence also reduces the gradient induced magnetic fields (ii) the small temperature gradient ensures that the liquid level will not oscillate, allowing faster cooldown (iii) the apparatus no longer has to be constantly monitored to reduce the gas flow while preventing oscillations.

(b)   Magnetic Fields in an Empty Superconducting Shield

Before a superconducting shield is cooled the ambient field must be reduced to a level below that at which any point

on the surface sees the critical field H_c; otherwise flux may penetrate the shield. In bulk superconducting lead at 4.2K, H_c is about 550 gauss, but the maximum external field allowable with a thin-walled hollow shield is much less than 550 gauss for two reasons. The first concerns the thermodynamic state of the shield. The question is whether the Gibbs free energy is less in the intermediate state where the flux penetrates the shield or the Meissner state where it is excluded. Expressions for the Gibbs free energy of cylindrical and spherical shields have been derived by B. Cabrera,[44] who finds that with an 8 inch diameter lead cylinder of 2.5 mil wall thickness at 4.2K, the "effective critical field" $(H_c)_{eff}$ above which the field penetrates is about 14 gauss rather than 550 gauss.

The second important limitation on the external field which a hollow superconductor can withstand is from the effects of self-demagnetizing fields near the sharp edges of a folded or crinkled balloon. Provided the condition from Gibbs free energy is satisfied the shield will normally exclude most of the flux even if nucleation sites do exist where $(H_c)_{eff}$ is less than the ambient field, but even local penetrations of the field at nucleation sites are often irreversible and thus undesirable. Limits on the field from the standard self-demagnetizing factor for an ellipsoid have been calculated by Cabrera, who finds both empirically and theoretically that a single Mu-metal shield giving an ambient field of a milligauss is sufficient to guard against unstable local penetrations as well as the free energy effect. In one instance an irreversible field penetration occurred in the lower part of a lead shield transported through the Earth's field (0.5 gauss). This can be attributed to unstable changes initiated by the self-demagnetizing fields at the sharp edges of several small holes along a seam towards the bottom of the shield.

Once a shield is in the Meissner state there are three
major sources and several possible minor sources of remanent
field in it, as follows:

(i) trapped flux in the shield wall is the dominant
contribution to the field until enough shields
have been cooled to eliminate flux from the last
shield. In the best shields produced so far
there is less than one unpaired quantum of flux
for every 20 cm^2 of surface area, which corres-
ponds to a residual field of 4 x 10^{-8} gauss at
the center of the shield.

(ii) With a cylindrical shield having an open top the
external field comes in through the opening. For
uniform fields applied in the axial and transverse
directions the residual fields at a distance z
below the top are proportional to $e^{-3.83\ z/a}$ and
$e^{-1.84\ z/a}$ respectively, where a is the radius of
the cylinder. In general the attenuation for any
localized magnetic field either inside or outside
a cylindrical shield must be at least $e^{-1.84\ z/a}$.
We have verified this result to 1% for a half inch
diameter shield.[45]

(iii) the fall-off of an external axial field through a
small hole in the wall of a cylindrical shield has
also been studied. The attenuation at the center
is approximately proportional to $(r/a)^3$ where r is
the radius of the hole and a again the radius of
the cylinder. This result has also been verified.[46]

Other sources of field in an empty superconducting shield
too small to detect at present are the London moment from the
Earth's rotation, which produces a uniform field of 8.3 x 10^{-12}
gauss, and an effect predicted by V. L. Ginzberg and others in
which magnetic fields are generated by temperature gradients
across anisotropic superconducting material. During prolonged
use of a superconducting shield substantial amounts of frozen
air are condensed as a result of repeated insertions and removals
of apparatus from the cold dewar. To check whether solid air
had remanent magnetization we brought 10cc of it within 3cm
of the flip coil of a magnetometer capable of measuring 10^{-8}
gauss. There was no measurable change in field. Thus although
solid oxygen is paramagnetic it exhibits no appreciable ferro-
magnetism at 4.2K.

(c) Fields Associated with Apparatus Inside the Shield

Given an ultra-low magnetic field region the next problem is to avoid generating fields in the apparatus that goes into it. There are three contributions, two of which have already been discussed: the remanent magnetization of materials, their susceptibility and thermoelectric effects.

Table 9 summarizes measurements made by B. Cabrera in 1974 and early 1977 on the remanent magnetizations of commonly used construction materials at 4.2 K. The apparatus comprised a shielded pickup loop surrounded by an 0.5 inch diameter, 4 inch long superconducting shield. The change in flux when a sample passed through the coil was recorded; there was also a calibration solenoid on the apparatus. The shield provided a stable ambient field of about 10^{-6} gauss and rapidly attenuated the fields from the samples as they were moved away from the detection coil. All but a few measurements were based on standard samples 3/16 inch diameter by 1 inch long. Figure 37 presents the same data in graphical form. For each individual sample the error was less than the diameter of the point on the diagram. The scatter from sample to sample of different batches of material was less than an order of magnitude. Typical cases are measurements for G-10 and manganin wire.

Susceptibilities become significant where stable uniform fields are needed inside the shield. There are two clearly separable cases. In normal materials, with paramagnetic and diamagnetic susceptibilities below 10^{-5}, the effects are only important when applied fields are more than 10^5 times instrument sensitivity. In superconductors, with a perfect diamagnetic susceptibility of $-1/4\pi$, they can produce significant distortions in any field.

Thermoelectric effects in the large laboratory dewars were described in Section D (3) (f). Normal metals can generate large fields as they are cooled and hence cause large

Table 9: Magnetic Remanent Magnetization of Construction Materials at a Temperature of 4.2K

Material	Source	4πM (gauss)	Vol. (cm³)
I. Ceramics and Glass:			
Blue alumina (cobalt trace)	Honeywell, St. Petersburg, FL.	1.5×10^{-4}	0.0386
Fused quartz	Englehard, Hillside, N.J.	$<5.9 \times 10^{-8}$	0.201
*Macor (machinable glass ceramic)	Corning Glass	$<1.1 \times 10^{-7}$	0.113
Pyrex	Corning Glass	1.6×10^{-7}	0.201
White alumina AL300: #1 (1968)	Western Gold & Platinum	4.3×10^{-5}	0.0775
#2 (1968)	Belmont, CA	5.8×10^{-6}	0.0914
#3 (1973)		$<7.9 \times 10^{-8}$	0.100
II. Epoxies and Resins:			
Epibond 100A	Furane, L.A., CA	2.6×10^{-5}	0.097
Epocast 121	Furane, L.A., CA	6.9×10^{-7}	0.114
Epoxy 907	Miller-Stephenson Chemical, L.A., CA	9.0×10^{-5}	0.113
G-10· rod stock	Unknown	4.1×10^{-5}	0.201
tube #1	Synthane-Taylor, LaVerne, CA	4.2×10^{-5}	0.0415
tube #2	Synthane-Taylor, LaVerne, CA	2.2×10^{-5}	0.0391
Hysol XCA-570	Dexter Corp., Olean, N.Y.	3.4×10^{-5}	0.113
Phenolic (cloth filled)	Unknown	1.6×10^{-6}	0.113
*Plybond #43-2	GC Electronics	9.6×10^{-6}	0.0063
RTV 3110	Dow Corning	1.6×10^{-6}	0.0737
Stycast 2850-FT	Emmerson & Cummings	1.1×10^{-3}	0.121
*Stycast 1266	Emmerson & Cummings	6.0×10^{-5}	0.030
Torr Seal	Varian Associates	2.8×10^{-5}	0.113
III. Metals:			
Aluminum 6061-T6· rod stock	Alcoa	4.7×10^{-7}	0.201
anodized sheet[1]	Alcoa	$<2.1 \times 10^{-7}$	0.037
*Beryllium copper sheet	Unknown	1.6×10^{-3}	0.055
Brass: rod #1[2]	American Brass & Copper, Oakland, CA	9.7×10^{-4}	0.113
rod #2[2]	American Brass & Copper, Oakland, CA	7.5×10^{-5}	0.0238
4-40 screw[2]	Sloss & Brittain, S.F., CA	1.0×10^{-6}	0.039
Copper: OHFC rod[3]	American Brass & Copper, Oakland, CA	6.3×10^{-6}	0.201
99.999% rod[3]	Atomergic Chemetals, L.I., N.Y.	1.5×10^{-6}	0.201
*Cupronickel tubing (70% Cu/30% Ni)	Uniform tubes	3.3×10^{-3}	0.0151
Phosphor bronze	R. J. Leahy Co., S.F., CA	1.4×10^{-3}	0.0238
Steel: 304 stainless tube[4]	Superior Tube Co.	4.4×10^{-3}	0.0227
soft steel rod	Unknown	1.9×10^{-1}	0.00036
Titanium: rod	Unknown	6.5×10^{-5}	0.0238
4-40 screw	Surplus from Lockheed	1.5×10^{-5}	0.039
IV. Plastics:			
*Dacron string, Micron 30 lb. test	Cortland Line Co., Cortland, N.Y.	4.4×10^{-6}	0.021
Delrin	Dupont	2.7×10^{-7}	0.201
HMW polyethylene	Dupont	3.3×10^{-6}	0.201
Kapton sheet	Dupont	$<4.5 \times 10^{-7}$	0.0174
Mylar	Dupont	$<6.4 \times 10^{-7}$	0.0124
Nylon: natural	Dupont	1.6×10^{-7}	0.201
black[5]	Smith, Inc., Brooklyn, N.Y.	3.7×10^{-5}	0.046
*Shrink tubing HTX	ICO Rally, Palo Alto, CA	3.7×10^{-4}	0.033
Teflon: rod stock	Dupont	3.6×10^{-6}	0.201
#20 spaghetti	ICO/Rally, Palo Alto, CA	$<2.1 \times 10^{-7}$	0.038
V. Solder:			
Indium[9]	Indium Corp.; Utica, N.Y.	2.4×10^{-6}	0.0322
Silver solder[6]	Handy & Harman	1.8×10^{-3}	0.0503
157-B eutec rod[9]	Eutectic Corp., Flushing, N.Y.	$<1.6 \times 10^{-7}$	0.0503
VI. Wires:			
*Chromel 1-P[10]	Sigmund Cohn, Mount Vernon, N.Y.	>6.3	0.00097
*Coax cable 293-3908-0000	ICO/Rally	3.4×10^{-6}	0.090
Copper #33 formvar ins.[7]	Belden, Chicago, IL	3.3×10^{-5}	0.00525
*Copper-Constantan GG-T-30[10]	Omega, Stamford, CT	1.6×10^{-1}	0.024
*Copper Nickel Alloy 3-01[10]	Driver-Harris, Harrison, N.J	6.3×10^{-4}	0.0083
Evanohm #28 silk ins.[7]	Driver Co. Newark, N.J.	5.2×10^{-5}	0.0083
*Gold – 0.07% Fe[10]	Sigmund Cohn, Mount Vernon, N.Y.	1.2×10^{-4}	0.00048
Manganin #30 forex ins. folded[7]	Magnet Wire Supply, Chatsworth, CA	1.7×10^{-5}	0.0125
cut[7]	Magnet Wire Supply, Chatsworth, CA	2.1×10^{-5}	0.0125
#40 folded[7]	Magnet Wire Supply, Chatsworth, CA	6.9×10^{-6}	0.0057
VII. Miscellaneous			
*Capacitors (ceramic chip):			
Type 100B-100-J-CX, 68pf	American Technical Ceramics, Huntington Station, N.Y.	8.9×10^{-6}	0.0170
Kemet NPO, 470pf	Union Carbide	4.3×10^{-5}	0.0141
*Connectors:			
BNC pin UG-604/U[11]	Amphenol	1.3×10^{-4}	0.028
Pin #450-3750-01-03	Cambion, Cambridge, MA	2.5×10^{-2}	0.014
*Germanium thermometer #SP2401E	Solitron, Riviera Beach, FL	8.5×10^{-4}	0.028
Pencil lead 4H[8]	Koh-i-noor 4H	1.8×10^{-3}	0.0196
Resistors: 1/2W	Spear	1.9×10^{-3}	0.051
1/4W	Allen-Bradley	3.1×10^{-3}	0.0176
1/10W	Unknown	1.9×10^{-3}	0.0079
assembly for heat switch		4.1×10^{-3}	0.0503
*1/4W 1KΩ 5% #1	Ohmite	4.3×10^{-4}	0.028
* #2	Ohmite	1.6×10^{-4}	0.028
*1/4W 10KΩ 1% RN60D	Corning Glass	5.1×10^{-7}	0.059
Silicon grease	Dow Corning	$<7.0 \times 10^{-7}$	0.113
*Tape: Blue Cross (Black)	Hampton Mfg., New Rochelle, N.Y.	1.9×10^{-5}	0.125
Masking	Scotch	4.9×10^{-6}	0.113

*Measured April 1977, all others measured September, 1974.
[1] Cutting with steel scissors produced magnetic contamination, so that the sample was re-etched.
[2] Magnetization here partially due to superconducting inclusions, producing highly variable results.
[3] Signal due to surface oxide layer.
[4] Bigger on ends where cuts were made.
[5] Many pigments appear magnetic (especially black).
[6] Contains nickel.
[7] Seems to come from insulation.
[8] Possible to use as home-made resistor.
[9] Does not superconduct at 4.2° K.
[10] Thermocouple wire.
[11] Center pin from a female connector.
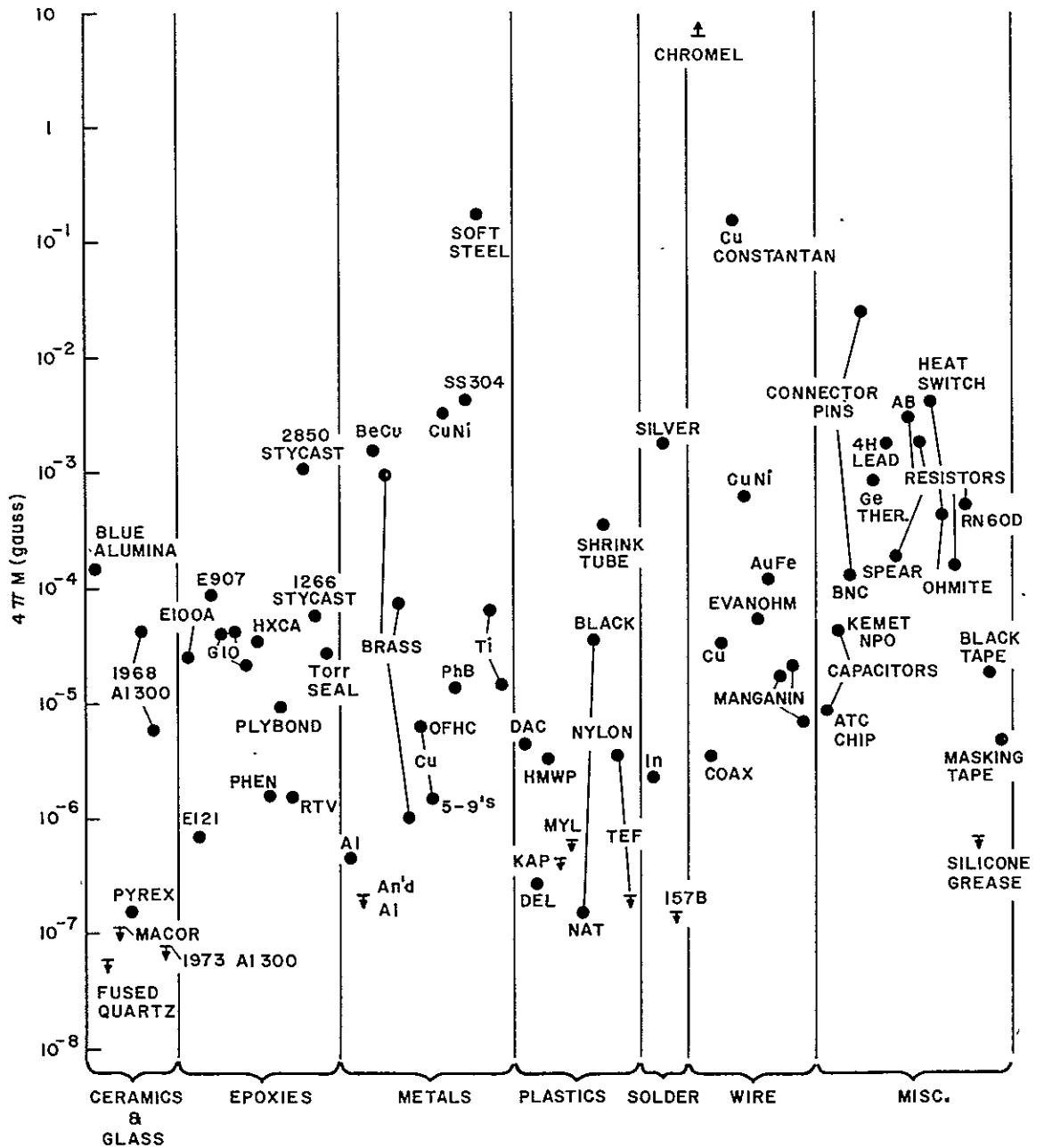
Figure 37: Graphical Representation of Remanent Magnetism Data for Cryogenic Construction Materials

amounts of trapped flux in the superconducting parts of the apparatus. A study of one test sample by B. Cabrera yielded fairly good agreement between theory and experiment. The only way is to cool carefully and have as little normal metal as possible near the gyroscope during cool down.

All of these effects have had to be taken into account in designing the probe for the 1 arc-second gyro readout experiment and the magnetometer for ultra-low field research.

(d) Magnetometer for Ultra-Low Field Research

Measurements of the magnitude and direction of the field inside an ultra-low field shield require a sensitive SQUID magnetometer connected to a flip coil capable of being turned to known angles about a horizontal axis on a probe that can be turned to any position about the vertical axis. The probe and flip coil assembly should be non magnetic. The magnetometer used for most of the development in ultra-low field technology was far from satisfactory. The SQUID was a home built Beasley type double point contact unit, while the flip coil and probe were of aluminum and subject to magnetic contamination and the thermoelectric effects just discussed. The absolute field sensitivity was limited to about 10^{-8} gauss.

During 1976 we replaced the original magnetometer with a greatly improved version which gave a factor of 100 improvement in absolute field measurement capability. The aluminum flip coil assembly was replaced by one of simplified design made of pure quartz tubing. The double point contact SQUID was replaced by an SHE toroidal unit with the Stanford third generation electronics system. Figure 38 illustrates the flip coil assembly. The only metal parts are the niobium wires for the flip coil and Helmholtz coils used in field calibration, these wires being threaded through the fine quartz tubes from which the structure is made. The new magnetometry reduced by a factor of 1000 the sensitivity of the SQUID itself to changes in the external field and increased by a factor of three the relative sensitivity. Once initial difficulties had been overcome the new magnetometer was decidely more reliable than the earlier
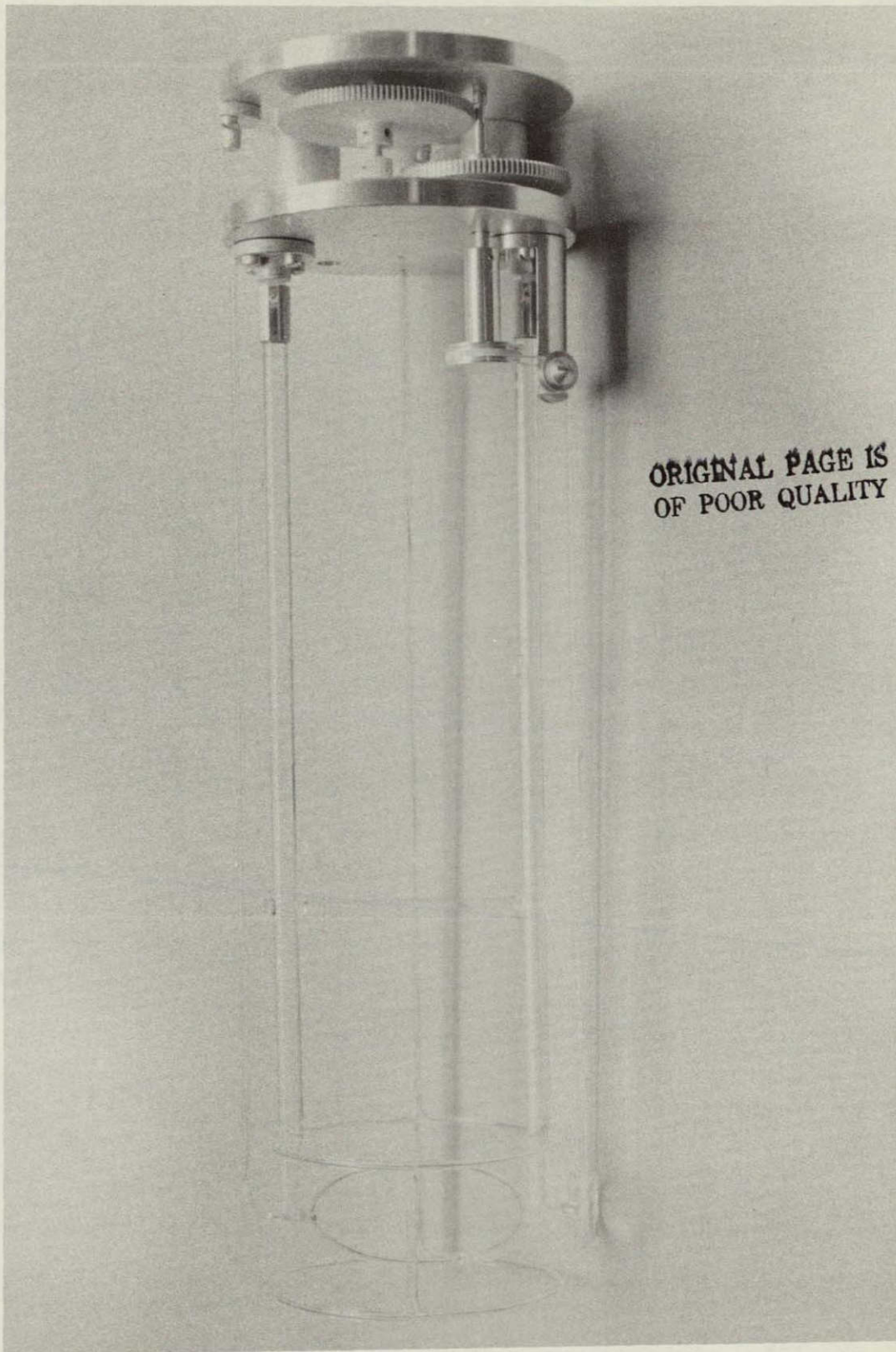
Figure 38: Magnetometer for Ultra-Low Field Research

169

one.   These improvements have given a background field below 10^{-8} gauss and an instrument sensitivity of 10^{-10} gauss.

(e)   Production of a 2 x 10^{-7} Gauss Magnetic Shield for the New Apparatus

Before starting the precision gyro readout experiment we had purchased a 12 inch superinsulated dewar vessel for the quick turn around gyro test facility. Our first thought was to use this dewar with a 12 inch ultra-low field shield for the new apparatus. However, although some of the upper parts of the new dewar probe do have to be 11 inches in diameter, the diameter of the 38 inch long cylindrical vacuum chamber at the lower end, in which the gyro is mounted, needs only to be 7.5 inches. We decided therefore to restrict ourselves to an 8 inch ultra-low field shield, reducing in that way the length of shield needed to attenuate the leakage field through the top of the superconducting shield.

For reasons discussed in E (3) (a) we purchased a second 12 inch dewar for ultra-low field operations. The dewar assembly comprises a slightly modified Cryogenic Associates model SD-10 dewar of 12 inch diameter, surrounded by a 17.5 inch diameter, 78 inch long Mu-metal shield, which provides a 10^{-3} gauss region in which to make the ultra-low field shield. Mounted in the bottom of the dewar is an 8 inch diameter 40 inch long aluminum well (identical in fact with the inner well of an 8 inch dewar) within which the ultra-low field shield is made. For practical reasons the ultra-low field shield is made in one laboratory and transported with the dewar and 17.5 inch Mu-metal shield to the main facility, where the whole assembly is inserted into a second Mu-metal shield, 23.5 inches in diameter and 88 inches long, permanently mounted there. The combination of the two Mu-metal shields reduces the ambient field from 10^{-3} to 10^{-4} gauss, ensuring that the leakage field through the open top of the ultra-low field shield is alternated below 10^{-7} gauss at the level where the gyro sits.

Production of the ultra-low field shield was begun in June 1976 and completed in October 1976. Most of the

paraphernalia used was already available from an earlier experiment. New items included an adapter top plate going from the 12 inch opening of the dewar to an existing 8 inch top plate, a new baseplate to anchor down the dewar, and a large transport cart to allow the dewar full of helium and containing the ultra-low field shield to be tilted at 45° and wheeled through doorways to the main facility. The new quartz flip coil magnetometer described in E (2) (d) was used throughout the work.

To provide a controlled heat leak through the double-walled glass tube surrounding each folded lead sock during cooldown a new helium gas leak was designed and constructed. The helium diffusion path was a teflon diaphragm 3/4 inch in diameter and 5 mil thick. This was attached to an atmospheric pressure chamber and the desired leak rate into the vacuum space of the double walled tube was established by mixing the right proportions of helium and air in the pressure chamber. The best cooling rates for the shield were obtained by combining a set helium leak rate of 4×10^{-7} atom cc/sec into the vacuum space with a vent rate of 30 cc/min at STP out of the inner helium chamber containing the shield.

Expansions of the shields were performed by inserting a spherical plunger, made from a cut down aluminum kitchen colander, into each bag after cooldown and removal of the outer bag and double-walled glass tube.

The final 8 inch ultra-low field shield was cooled overnight on October 6, 1976 after three successive expansions of 4 inch bags on September 16, September 22 and September 28. An earlier successful expansion of a 4 inch bag in June 1976 had been followed by setbacks through magnetometer troubles and the loss of a second lead bag early in September. Figure 39 illustrates five stages of field reduction. Curve 1 shows the initial field in the 17.5 inch diameter Mu-metal shield

8" diam LEAD SHIELD

MUMETAL SHIELD

• GYRO POSITION

4" diam LEAD SHIELD POSITION

1.2
0.8
0.4
0
× 10⁻³ GAUSS

(6-8-1976)

MAGNETIC FIELD INSIDE MUMETAL SHIELD

1.2
0.8
0.4
0
× 10⁻⁴ GAUSS

(9-16-1976)

MAGNETIC FIELD INSIDE FIRST 4" LEAD SHIELD

1.2
0.8
0.4
0
× 10⁻⁶ GAUSS

(9-22-1976)

MAGNETIC FIELD INSIDE SECOND 4" LEAD SHIELD

2.4
2.0
1.6
1.2
0.8
0.4
0
× 10⁻⁶ GAUSS

(9-28-1976)

MAGNETIC FIELD INSIDE THIRD 4" LEAD SHIELD

1.2
0.8
0.4
0
× 10⁻⁶ GAUSS

(10-6-1976)

MAGNETIC FIELD INSIDE FINAL 8" LEAD SHIELD

0 5 10 15 20 25 30 35 40 45 50
INCHES

Figure 39:   Five Stages of Magnetic Field Reduction in Preparing 8 inch Ultra-Low Field Shield

172

with a peak value of about 10^{-3} gauss 30 inches above the bottom of the shield. Cooldown of the first 4 inch lead shield was impaired when the glass cooling tube was accidentally cracked, but the field level as shown in curve 2 was·below 10^{-4} gauss. The cooldown rate of the next shield was close to but slightly faster than optimal, yielding a maximum field of 0.8×10^{-6} gauss as shown in curve 3: an improvement factor of about eight. Curve 4 shows the field of the third 4 inch shield. The large peak at the 22 inch position is due to a tear in the lead bag which we discovered when the shield was removed from the dewar after cooling the final 8 inch shield. Although the leakage field through this hole was five times larger than our goal of 5×10^{-7} gauss for the shield,·we decided to go ahead and cool the 8 inch shield next. The field level in the third 4 inch bag was still adequate to reach a final field of a few times 10^{-7} gauss, and it seemed best to have this rather than consume time making another 4 inch shield which would allow a reduction in the final field to 5×10^{-8} gauss.

To minimize the possibility of tearing the seams in the 8 inch shield we made a new tool to partially open the shield before inserting the standard spherical shield-expansion plunger. Final expansion was done satisfactorily on October 8, 1976.

The cloth top of the shield was next successfully removed using strings which had been preattached to each tab glued around the top of the shield. A four-inch long expansion clamp was then inserted at the top of the shield to prevent damage during insertion of the probe. We encountered some difficulty in sizing the clamp, having to remove it from the dewar twice and trim the material before achieving a satisfactory fit.

Curve 5 of Figure 39 illustrates one field profile for the 8 inch bag taken soon after its completion. Figure 40 is a more complete plot of orthogonal field components along the axis of the shield. Figure 41 illustrates the absolute
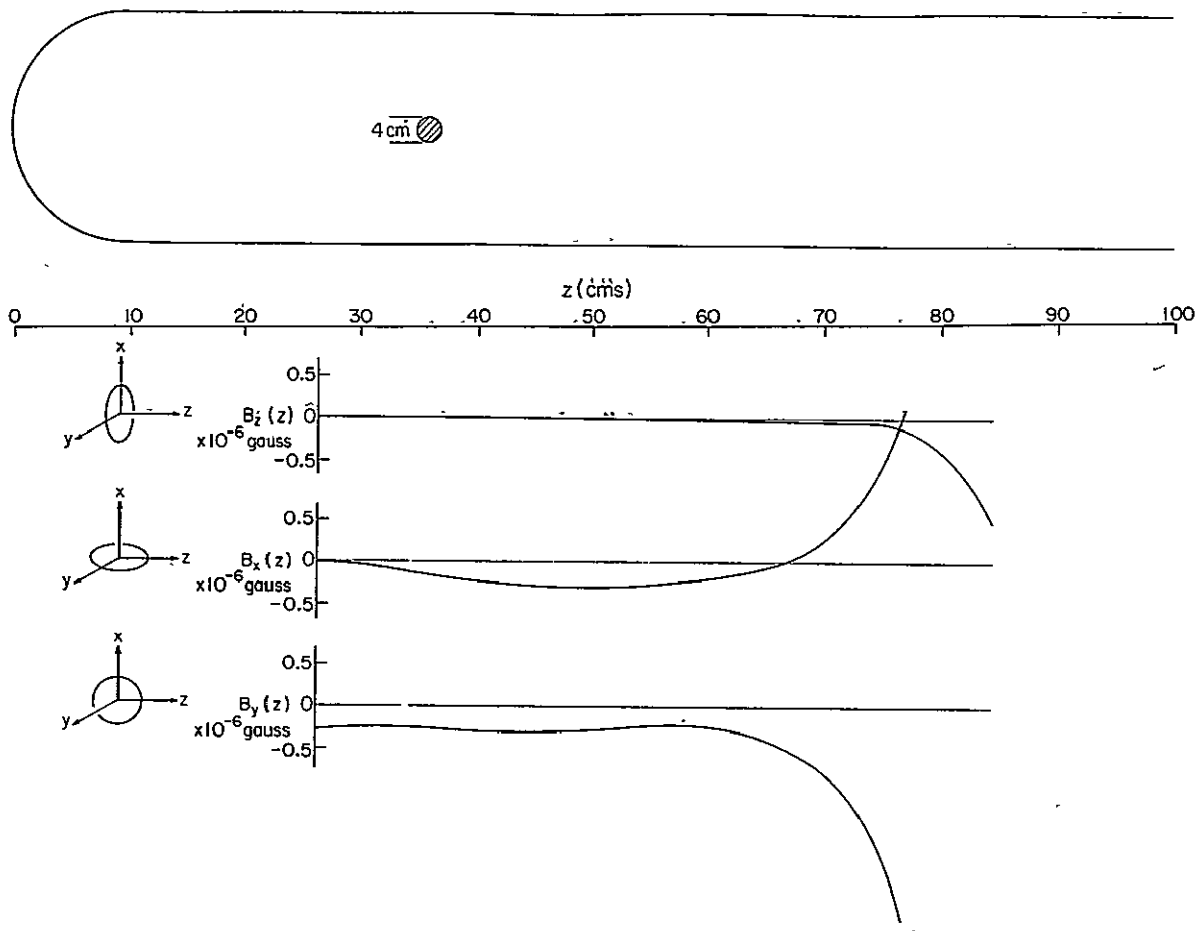
Figure 40: Magnetic Field Components Along Axis of 8 inch
Ultra-Low Field Shield
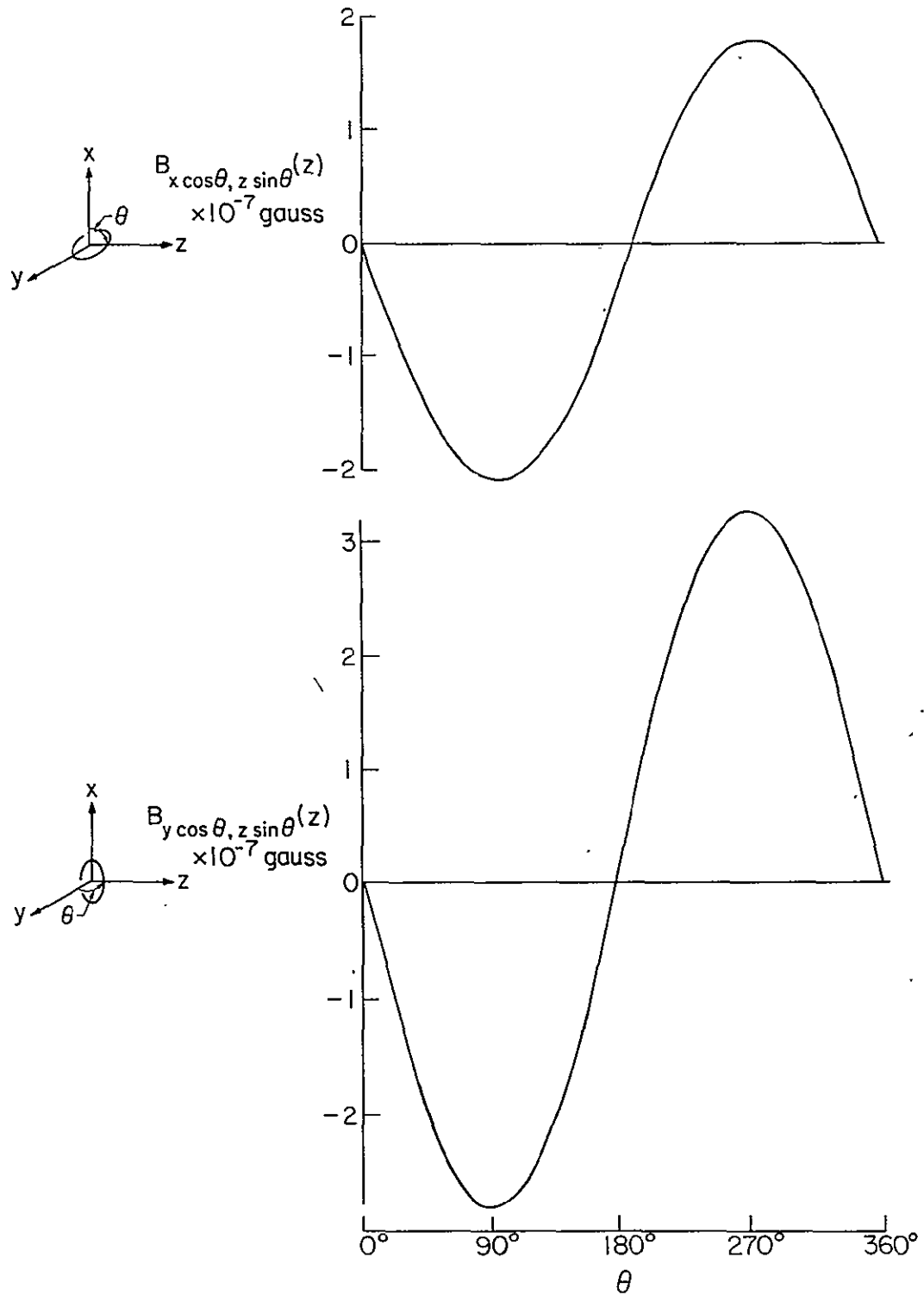
Figure 41:   Absolute Magnetic Field Measurements in Ultra-
Low Field Shield at Gyroscope Position

175

magnitudes of the field at the gyro position obtained by
rotating the flip coil with its axis in two orthogonal
directions. The absolute field magnitude is 2.3×10^{-7}
gauss. We are of the opinion that our improvement of
one order of magnitude in field reduction can be obtained
fairly straightforwardly in a future cooling cycle by
carefully annealing the shields and avoiding seam tears.

An automatic telephone dialler system coupled to the
low limit relay of the helium level sensor was connected to
the ultra-low field dewar shortly after completion of the 8
inch shield. If the helium level should drop to where the top
of the shield were in danger of going normal the system will
automatically telephone a warning message to group members either
at home or in their offices at any hour of the day or night.

Figure 42 is a view into an 8 inch ultra-low magnetic
field shield after completion.

(3) Design of the Gyro Test Facility

The new facility has to allow reasonably high spin speed
of the gyro (at least 100 Hz) in an ultra-low magnetic field.
The turn round time between runs has to be short and the
apparatus should be constructed as far as possible using known
technology and existing or commercially available components.
The design has to be worked out in such a way that the probe
containing the gyro can be inserted into and removed from the
dewar containing the ultra-low field shield without sudden
changes in helium level that would cause any part of the shield
to go normal.

We gave considerable thought to the layout of the laboratory.
The requirements to assemble the apparatus at a clean bench and
test it first at room temperature, then liquid nitrogen tempera-
ture and finally at liquid helium temperature poses interesting
problems of logistics and room layout. As Figure 43 shows, the
assembled apparatus is mounted above floor level and is surrounded
by electronics and other support equipment, including the clean
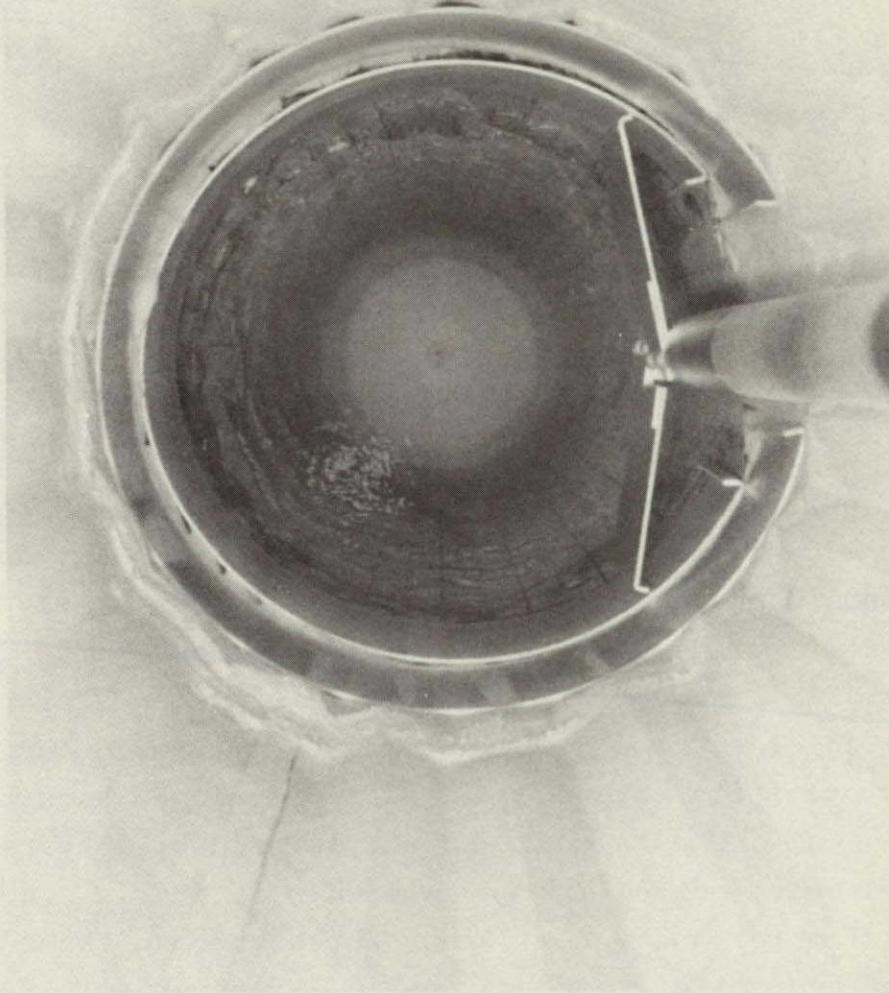
Figure 42:   Looking Down into an 8 inch Ultra-Low Field
Shield

bench, protected from dirt in a nearby alcove. Traditional cryogenic practice is that in a small apparatus the probe is held fixed and the dewar is raised and lowered around it, while in larger apparatus the dewar is fixed. After much discussion we concluded it was best to make the dewar movable and the probe fixed in a rigid frame but detachable and transportable to the clean bench.

Figure 44 illustrates the planned apparatus with the assembled probe and dewar. The probe assembly is about 6 feet long and is bolted with its top plate 6.5 feet above floor level to a rigid aluminum tripod with slightly splayed legs formed from tubular columns over 8 inches diameter, anchored to a 10 foot diameter 5 foot thick concrete pad located with its top surface one foot below floor level and physically isolated from the building structure. Two interchangeable dewar assemblies are used: (i) the 12 inch inner diameter dewar described in Section E (2) (e) which contains the ultra-low field shield and is enclosed in the tight fitting 17.5 inch diameter Mu-metal shield, (ii) the nearly identical 12 inch dewar originally purchased for the quick turn around gyro test facility, used without extra superconducting or Mu-metal shields. The dewar assemblies fit inside an 18 inch diameter precision bore foam insulated airlock which is open at the bottom. They are raised and lowered by a hydraulic lift, and accommodated in the lowered position in a hole 3.5 feet in diameter and 9 feet deep, bored through the concrete pad. The hydraulic cylinder goes in a further hole 9 inches in diameter and 9 feet deep under the center of the main hole. Either dewar assembly may be attached to the hydraulic piston by means of a bayonet mount mechanism similar to a camera lens. Six Teflon rollers, which slide on three vertical guide rails on the probe frame, are attached to the outer shell. When the cold dewar is raised or lowered around the probe air is prevented from entering the dewar well by an 18 inch diameter piston seal, located at the dewar mouth, which slides inside the airlock cylinder.

NOVA 2/10

DEC WRITER

DESK

COMPUTER

PUMPING STATION

BENCH

CLEAN BENCH

HOLE IN FLOOR

ELECTRONIC RACKS

ROOM TEMPERATURE GYRO TEST STAND

ULTRA LOW FIELD GYRO TEST APPARATUS
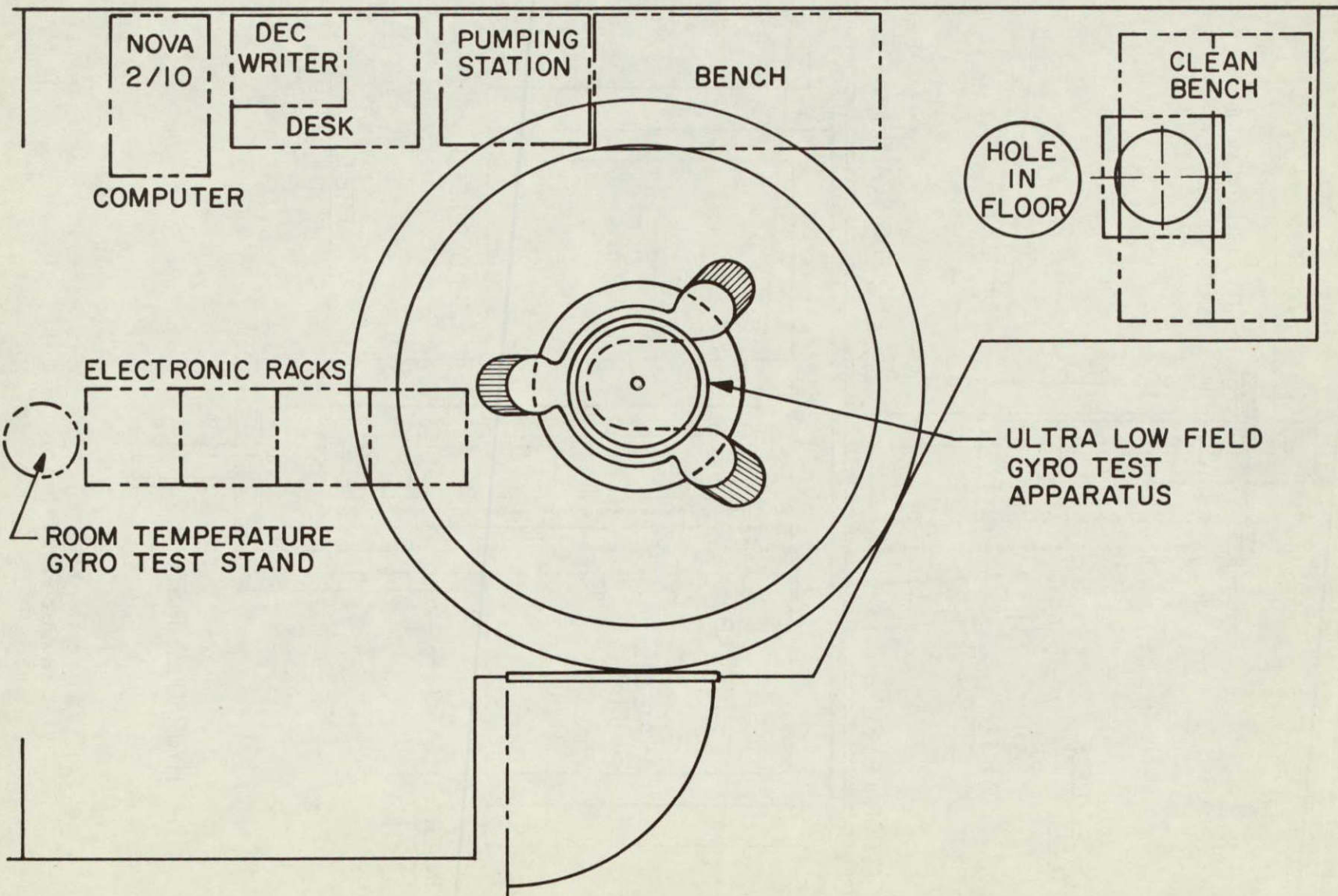
Figure 43: Floorplan of Laboratory for Ultra-Low Field
Gyro Test Facility

TO HIGH VACUUM
PUMPING STACK

PROBE NECK
TUBE

GYRO

AIR LOCK

FLOOR LEVEL

SLIDING SEAL

DEWAR

MUMETAL
SHIELD

CONCRETE
BLOCK

LEAD SHIELD

INSERTED GYRO
POSITION

FEET

0   1   2   3

HYDRAULIC PISTON
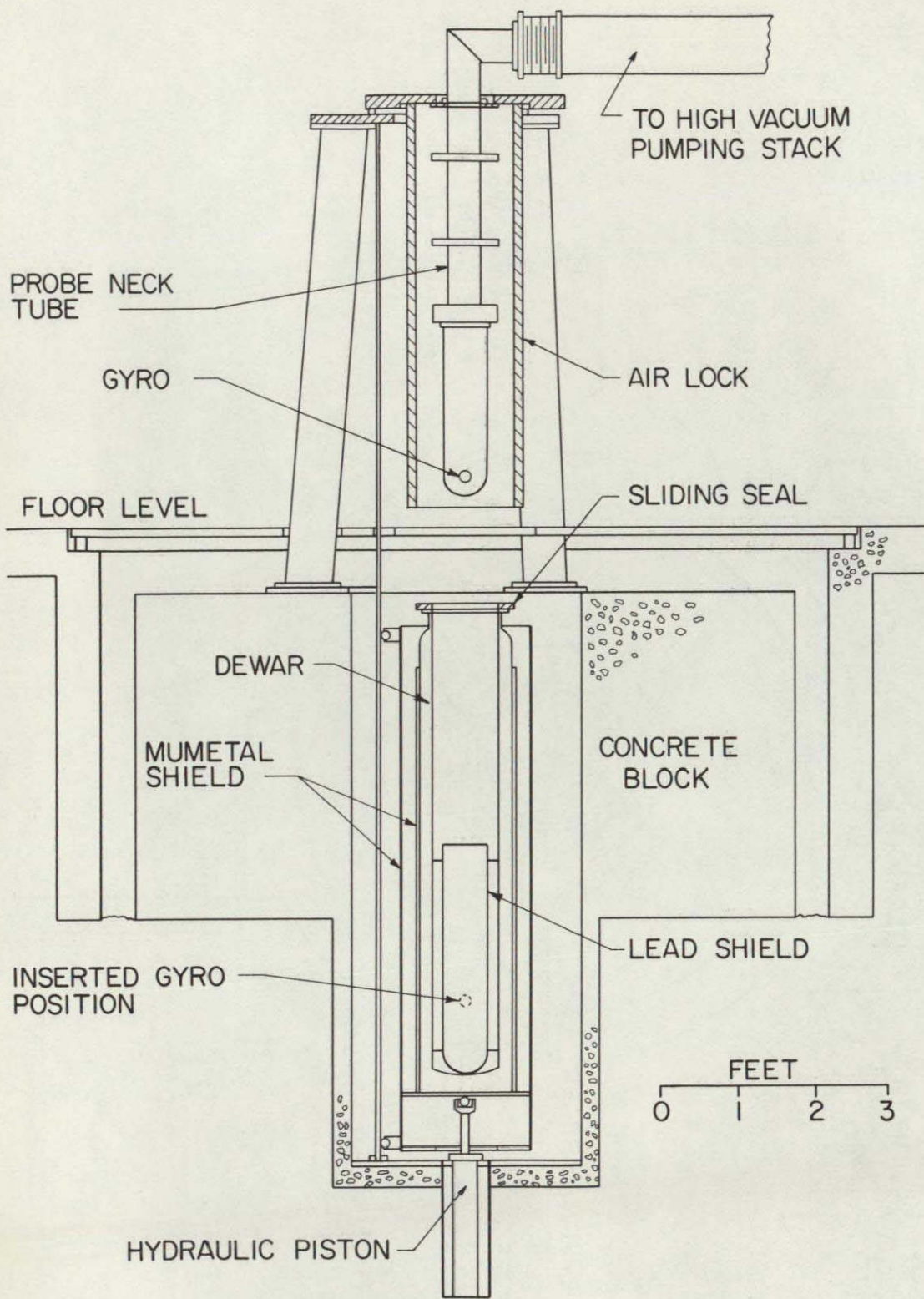
Figure 44: Cross Section of Gyro Test Facility with Dewar
in Lowered Position

180

The use of two interchangeable dewars has several advantages. The two crucial and sophisticated tasks of preparing the ultra-low magnetic field shield and testing the dewar probe proceed independently in different laboratories, minimizing schedule conflicts. Further when the ultra-low field dewar is not being used with the test facility it is available for other work, including measurements of remanent magnetizations of probe components. It was used for example in the readout noise measurements described in Section F. The presence of the outer Mu-metal shield means that the gyro is in a moderately low magnetic field--about 10^{-3} gauss--even when it is cooled down in the non-shielded dewar.

Figure 45 shows the completed facility.

The probe vacuum shell consists of three sections, a 3 foot long necktube section, a double-walled precooling chamber and a main vacuum chamber. The neck tube is constructed from G-10 low thermal conductivity plastic, and consists of a 6 inch diameter high vacuum pumping line surrounded by several 2 inch diameter tubes which contain all the electrical and other feed-throughs. These tubes are self-contained and readily detachable to facilitate their assembly independently of the probe itself. The outer diameter of the neck assembly is 11 inches. The precooling chamber at the bottom of the neck has two main functions: (i) the probe can be precooled by circulating liquid nitrogen through the space between the double walls, (ii) it also allows the use of a 7.5 inch diameter vacuum chamber to contain the gyro, and hence, as explained in Section E (2) (e), the use of a smaller 8 inch diameter ultra-low field shield.

Interconnections between the feedthrough tubes, the gyro and the magnetometer are made inside the precooling chamber. The magnetometers are in separate housings bolted to the bottom around the vacuum can. Two vacuum cans, about 30 inches long are used interchangeably with the probe. One is made of pyrex and is used to get the lowest magnetic field
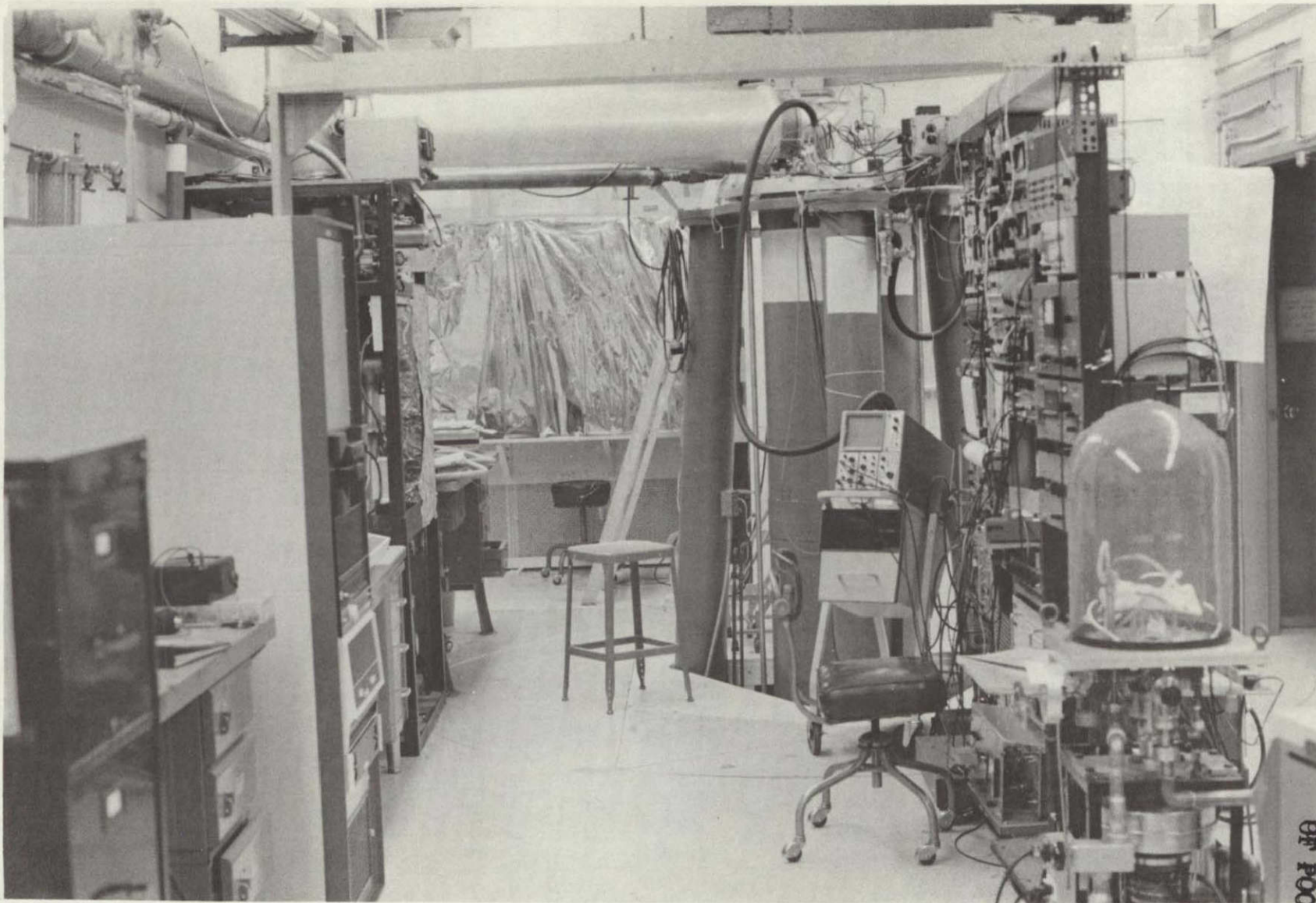
Figure 45:   The Ultra-Low Field Gyro Test Facility

environment. The other is of aluminum and being more robust is used whenever the field requirements are not critical.

The gyro is mounted with its center about 4 inches from the bottom of the vacuum chamber. It is held in a teflon fixture which is attached to a rigid G-10 tube hanging from the bottom of the precooling chamber. Two interchangeable mounting fixtures are available. One holds the gyroscope in an orientation such that its initial spin axis is parallel to the Earth's axis and the rotor supported entirely by two electrodes, which happens to be the best that can be arranged at the latitude of Stanford. The other fixture holds the gyro-scope with its weight equally supported by all three electrodes and its spin axis horizontal. The latter is the fixture presently installed and used for all the tests made to date. The spin up plumbing and other parts used in the low field region were made of carefully selected contaminant free non-metals. Figure 46 illustrates the completed probe.

Time was saved in making the new apparatus by adapting the 10 inch high speed diffusion pump used in the earlier apparatus to evacuate the probe. We were able also to incor-porate the low heat leak high voltage glass tube suspension cables from the old apparatus in the new probe. They are connected to the gyroscope by commercially available teflon dielectric co-axial cables.

Great pains were taken in designing the probe to minimize the heat leaks. This led among other tasks to a detailed study of the thermal design of rf transmission lines for the SQUID readout magnetometers. The primary electrical consid-eration is that the lines have low attenuation to maximize the signal to noise ratio. To minimize the magnetometer null drift that accompanies a drift in rf bias level, the attenuation should be independent of temperature. Low attenuation and low heat leak are contradictory properties because the current carrying electrons in the metal line also
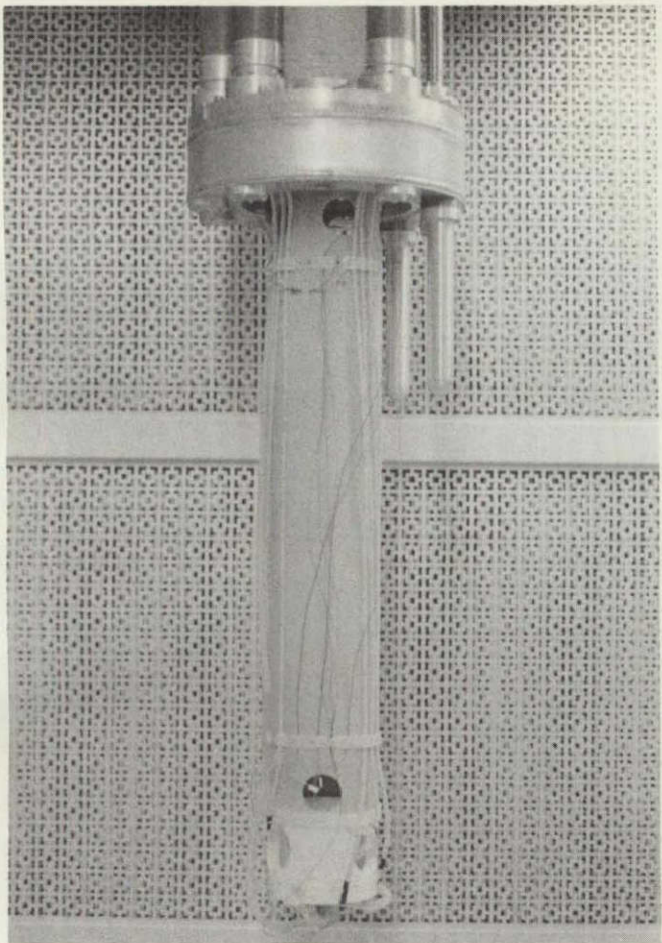
(a) View from Precooling Chamber Downwards
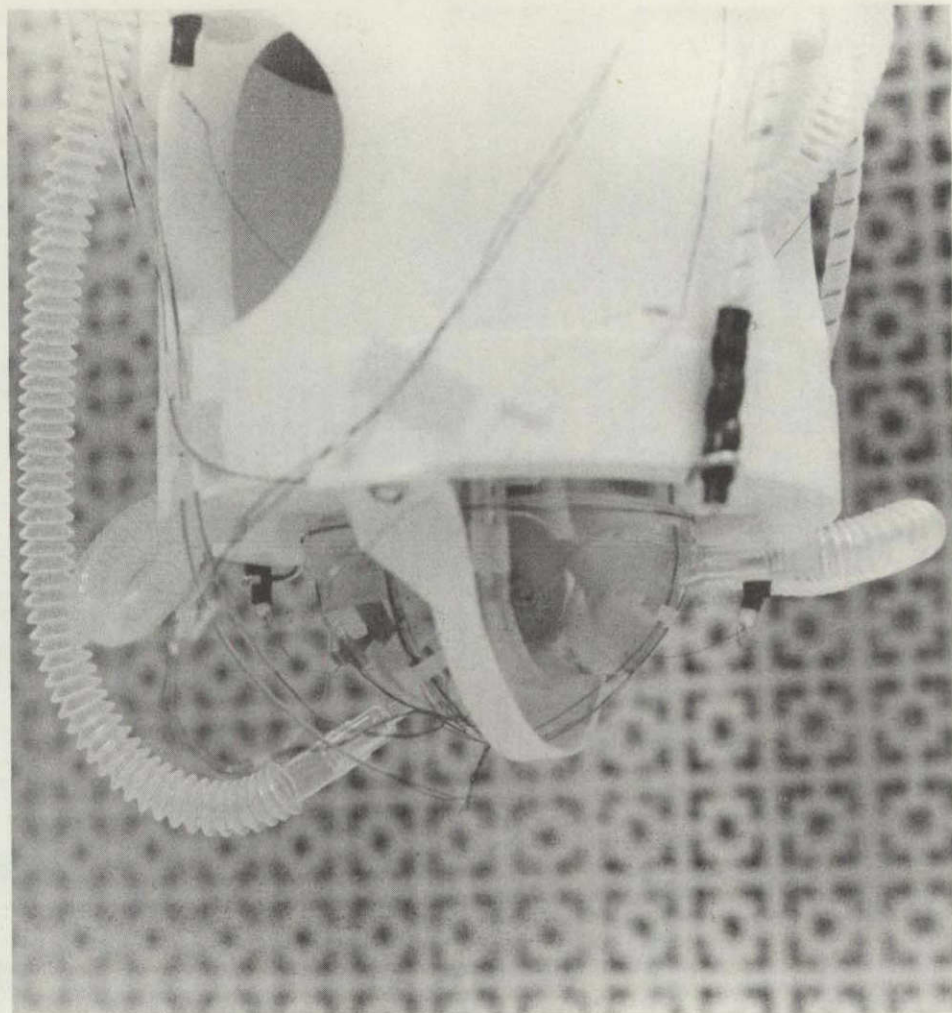
(b) Gyro Fixture

Figure 46: Probe for Ultra-Low Field Gyro Test Facility

large laboratory dewar, but during 1976 we put together a few
useful additional items.

One was a filter panel for use with the 8 channel recorder.
The panel design allows selection of 1 Hz, 10 Hz filters or
flat response for any of the eight channels. The unity gain
low pass active filters are of a three pole Butterworth type
implemented with high-grade monolithic operational amplifiers.
Common mode rejection is provided for all bandwidths, with the
option of a floating or grounded output shield termination.
Any of the filters can be bypassed by plugging in a special
hardwire card, if required, to take advantage of the high
performance recorder plug-in units. The filter panel will
be used with magnetometer, suspension and other analog data
channels.

Another important development was an automatic gyro spin
speed monitor based on trapped flux signals. Our previous
apparatus had a semi-automatic spin speed monitor, which
locked on to the output of a single readout channel, but it
would lose lock and have to be reset manually whenever the
signal from the polhoding ball passed through a null. The
new monitor locks into the fundamental component of the three
trapped flux signals separately and compares them. Most of
the time all three channels will have good signals. When one
channel does go through null, the anomalous signal is detected
by a voting technique by reference to the other channels.
The geometry of the problem is such that only one channel goes
through null at a time, except on very rare occasions when
all three may go together (in which case the speed monitor
has to be reset by hand). A manual select mode allows the
operator to switch to any channel at will. The automatic
select mode switches the spin speed counter to a good phase
lock loop whenever the signal from the current primary loop is
more than a fixed amount in error. The completed instrument
allowed us to lock on and track signals with 10mV amplitudes

from 1 Hz to 90 Hz. It was designed so that as magnetic field
reduction techniques are improved, the sensitivity can easily
be increased to operate with smaller trapped flux signals.
When the gyro spin speed is raised above 90 Hz, the upper
frequency limit of the monitor can also easily be raised.

A remote control panel was built for the existing gyro
suspension system. Its purpose is to allow many of the suspen-
sion functions to be controlled from a convenient location
while the suspension system itself sits on top of the tripod
mount for the new probe. A few simple modifications to the
suspension system were also made. The remote control panel
has proved a great aid to the experiments.

The last major new item, other than the computer develop-
ment described in Section E (6) below, was electronics for
precision biaxial tiltmeters. The sensing elements of the
tiltmeters were obtained from the Autonetics Division of
Rockwell International. The completed units will be used for
recording motions of the ground and dewar stand during gyro
tests and also for certain experiments with the Star/collimator
unit (Section G).

(5) <u>Requirements for Precision Gyro Readout</u>

The goal of a one arc-second readout puts much more
stringent requirements on magnetometer performance than does
just seeing the London moment. The magnitude of the London
moment as observed in March 1975 corresponded to measuring a
few flux quanta at the SQUID magnetometer. A one arc-second
readout at 50 Hz spin speed corresponds to $10^{-2}\phi_0$ at the ball,
and far less, probably only a few times $10^{-5}\phi_0$ at the SQUID.
The exact quantity of flux at the SQUID corresponding to 1
arc-second gyro displacement depends, as explained in Section
C (3) (d), on the inductance ratios in the readout circuit
and the coupling efficiency between the gyro and the SQUID.
In the London moment observations there were losses because

down when the flow becomes critical velocity limited. In an ideal plug that occurs at about 2.1K in the region just below the λ-point where the critical velocity is a rapidly decreasing function of temperature. The theoretical performance curve should therefore approximate to the dotted line in Figure 67, p.

If $\dot{Q}$ max is the maximum expected heat input into the dewar and p_{crit} is the operating pressure at the temperature where $\dot{m}$ begins to decrease, then Equation (36) may be transposed into an inequality governing the design parameters for a plug intended to operate below the λ-point:

$$\frac{kA'}{t} > \frac{\rho S \dot{Q}_{max}}{(p_{crit} - p_0)} \tag{37}$$

Numerical substitution into Equation (37) establishes the need for a plug of high thermal conductivity. Applying this result we designed the plug shown in Figure 65. It was made from a commercially wound roll of 0.5 mil aluminum foil, about 200 turns on a 1-3/8 inch mandrel, tightly held by another aluminum ring. The parts were assembled in a cylindrical bakelite fixture, after simultaneously heating the outer ring to 600°C and cooling the aluminum roll to liquid nitrogen temperatures. The mean spacing between layers of the finished plug, calculated from measurements of the gas flow rate through it at room temperature was about 10,000 Å. We used the plug illustrated in Figure 65 in all the research at Stanford; afterwards it was transferred to NASA Marshall Center for further experimental work there by E. Urban. Subsequently Dr. Urban showed that plugs of sintered metal or ceramic would work equally well provided the pore sizes are correctly chosen. This important result, discussed below, was confirmed by W. B. Davis of Ball Brothers Research Corporation and by members of the JPL group. There is some irony in that our first experiments had been with a sintered silver plug, which failed to work: a failure which we were able to "explain" convincingly by Equation (37); and that was why we adopted the wrapped foil design. Sometimes one can know too much.
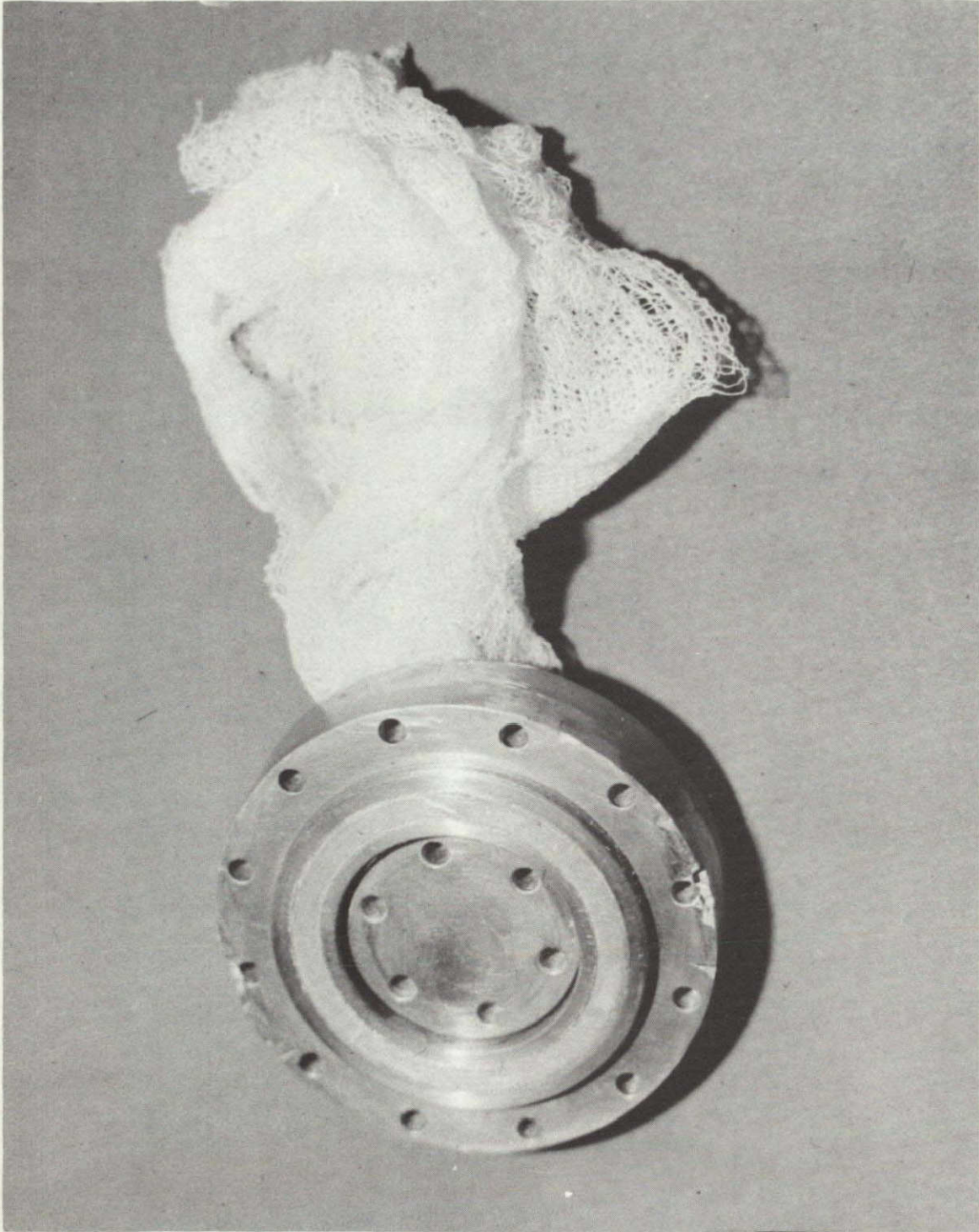
Figure 65: High Thermal Conductivity Porous Plug with Wick

When the porous plug is used for normal liquids the flow-rate is controlled by viscosity. In these circumstances both liquid and gas pass through the pores. For operation to be effective the pores must be large enough to allow sufficient quantities of liquid to pass at reasonable working pressures, yet small enough to prevent significant quantities of liquid being blown away from the outer surface of the plug by the expanding gas before evaporation can occur. For the wrapped foil plug the inequality governing the minimum width between layers is found from the viscosity equation, and for laminar flow conditions is

$$w_{min}^3 > \frac{128\,\eta t}{\pi\rho\ell}\frac{\dot{m}}{(p_{max} - p_o)} \tag{38}$$

where η is the viscosity of the liquid and ℓ the total circumferential length of the layers. For a typical large dewar operating at about 4K, w_{min} has to exceed 6000 $\overset{o}{A}$.

The condition for preventing liquid expulsion from the plug operating in the normal regime is less easy to decide. A sufficient condition is that the operating pressure should not exceed the surface tension force at a boundary between a gas bubble and the escaping liquid. However, the resultant inequality $w_{max} < T/p_{max}$, though possibly applicable for some liquids, leads for helium to a limit where the motion of the gas itself would be restricted by viscosity rather than surface tension. The correct limit has to be determined by comparing the liquid evaporation rate at the surface with the gas velocity, and this is difficult to model.

To test the plug on Earth we built a small invertible dewar illustrated in Figure 66, holding about one liter of liquid helium. The dewar was superinsulated, with two gas-cooled shields, and had two cryogenic valves operated externally, which were opened during the fill period for transfer of the liquid and venting. After filling the valves were closed and the helium vented solely through the plug. The wrapped-foil
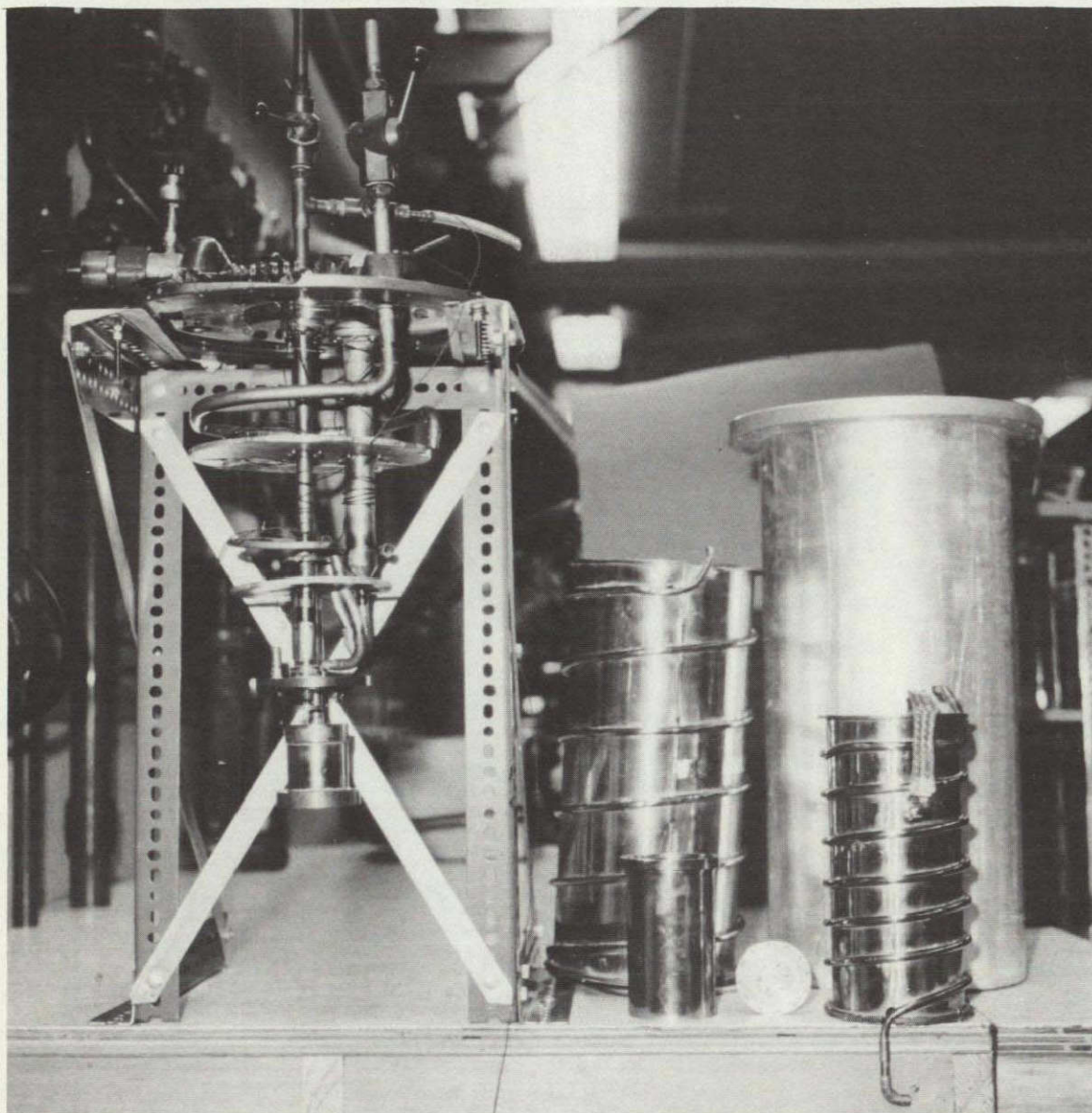
Figure 66:   Invertible Helium Dewar for Testing Porous Plug

plug described above was sealed into the helium well with compressed indium O-rings. For operation on Earth a wick was placed in the helium to help carry liquid to the plug when the dewar was upright; in space where the helium film is thicker the wick is probably unnecessary.

Stable operation was achieved with the dewar in both upright and inverted positions, without appreciable variation in boil-off rate. Figure 67 shows the complete operating curve in the upright position, the temperature being varied by an auxiliary heater. Also shown is the theoretical curve based on Equation (35), using the calculated pore dimension from the gas flow measurements. Over most of the temperature range the agreement between theory and experiment is good. The unstable regime set in at 1.8K rather than around 2.1K. The explanation of the discrepancy remains uncertain; it did not occur in Dr. Urban's research on sintered metal plugs.

The success of the device under negative-g conditions, confirmed in many later experiments at NASA Marshall Center, Ball Brothers Research Corporation and JPL gave good confidence that the plug would work in zero-g also. This was confirmed in the JPL zero-g airplane and rocket flights. An important difference for space operation that at first gave us concern was that the equilibrium thickness of the creeping helium film is likely to be several orders of magnitude greater in space than on Earth. Large heat losses might occur if such a film formed in the vent-tube of the dewar, and it is essential to make sure that the helium really does evaporate at or near the plug. The following calculation made in 1970[53] helped calm earlier fears. The evaporation rate from a liquid surface of area A exposed to vacuum is $\rho_v A \bar{v}$ where $\bar{v}$ is the mean molecular velocity at the surface temperature. Assuming that the helium emerging from the plug spreads over a uniformly heated surface at temperature T, there is a minimum area for evaporation given
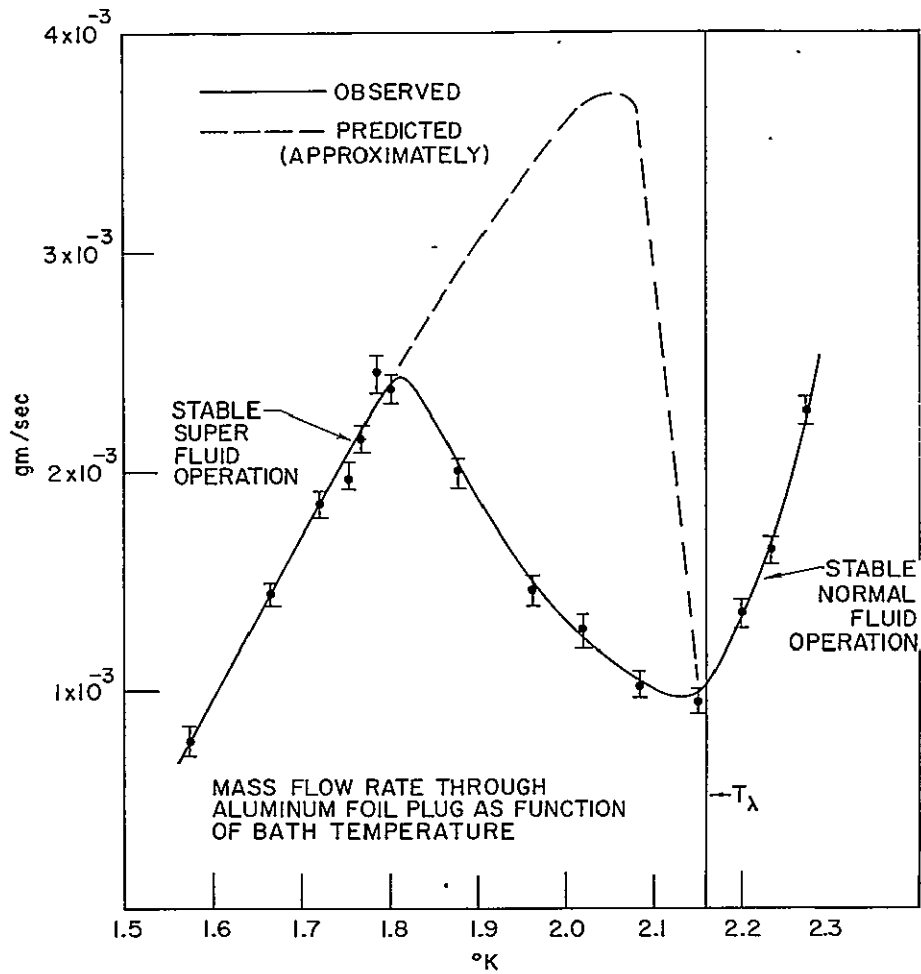
Figure 67: Porous Plug Operation: Comparison of Experiment with Theory

by

$$A_{min} \sim 4 \times 10^{-2} \frac{\dot{m} \sqrt{T}}{p_v (T)} \tag{39}$$

where p_v is the saturated vapor pressure at T. With reasonable guesses for $\dot{m}$ and p_v for a large dewar A_{min} is about 1 cm^2. Thus evaporation should be immediate as the helium leaves the plug.

A few remarks are appropriate on the research which shows that a plug of high intrinsic thermal conductivity is not needed. Besides the work of Urban,[54] Davis,[55] and Mason, Petrac and Wang,[56] there are a number of extremely useful papers by A. Elsner[57] of the Max Planck Institute, Munich, West Germany on a rather different application of flow through thick porous plugs. Our original view was that the pores would have to be so fine that the normal fluid would remain locked to the walls, and that meant that since superfluid carries no entropy there would be no heat conduction through the liquid. Actually the porous plug works even when the pores are coarse enough to allow some circulation of normal fluid; consequently one can take advantage of the enormous apparent thermal conductivity of the superfluid film. Experiments by E. Urban demarked the region of pore size over which a plug of low intrinsic conductivity would work.

The next question is how a low thermal conductivity plug can work in the normal regime. The experiments showed that while there were some circumstances in which a plug seemed not to work above the superfluid transition temperature, in others the operation was perfectly successful. Some questions still remain, but in general terms the answer seems to be given by Elsner's investigations. He found that on pumping across a porous plug from a bath above the λ-temperature, the helium at the outer surface would cool and in fact there was a normal/superfluid transition taking place inside the plug. The boundary moved to a position where stable flow conditions could be set up.

If the foregoing interpretation is correct a plug of high
intrinsic thermal conductivity is unnecessary for controlling
either normal or superfluid helium, but is still needed in
applying the method to controlling other liquids in space.

(3) Thermal Design of Superinsulated Dewars

(a) General

The approach to dewar design followed by several aerospace
companies has been to choose more or less arbitrarily a partic-
ular configuration of the dewar, develop an elaborate computer
program that will model every aspect of the thermal design,
and then attempt to improve performance by a succession of
design changes, rewriting the computer program with each change:
a scenario that usually has the unfortunate computer expert
working with increasing frenzy as the due date of the final
report draws near. This approach can produce a successful dewar
if the design engineer has insight and the approximations in the
computer model are realistic. Unfortunately no complete set of
design guidelines for dewars is available yet to the engineer,
and programmers seem often more concerned with computing ingenu-
ities than dewar design.

Our own approach has been to establish the physical princi-
ples basic to a class of dewars and then optimize the dewar
parameters. The design can be refined if desired by developing
a complicated computer model, but the resultant modifications
must not violate the principles. The dewar we have built (see
Section J (4)) is still a long way from its design performance.
Nevertheless it has brought home the need to understand principles
and exposed some shortcomings of other designs. We summarize
here considerations we have found useful in analysing thermal
design of flight dewars, many of which are not widely known.

(b) Effects of Size of Dewar

Consider the simplest idealized case of a spherical super-
insulated dewar, which has no penetrations, no mechanical supports,

no sources of internal heat dissipation and no provisions to recover the sensible heat from the helium boil-off gas. Let the radius of the helium well be r_o and that of the outer shell r_s, and let their temperatures be T_o and T_s. Assume that the behavior of the superinsulation can be represented by a temperature dependent thermal conductivity $K(T)$. For such a system the maximum hold-time t_{max} occurs when $r_o = \frac{2}{3} r_s$ and is given by the equation

$$t_{max} = \frac{4}{81} \frac{\rho L r_s^2}{\int_{T_o}^{T_s} K(T) dT} \tag{40}$$

where ρ is the density of the helium and L its latent heat per gram. For a dewar utilizing the sensible heat of the boil-off gas the hold-time t_{max} is given by the same equation multiplied by a "gain factor" G, which may be as high as 20 to 25, as discussed in Section J (3) (d).

Equation (40) shows that the hold-times of similar ideal dewars scale as the square of their diameters. Size is therefore a powerful aid in attaining long hold-time. At first the dependence on r_o^2 may seem surprising since one tends to think of the problem as determined by the ratio (volume/area): actually it is just what one should expect since the heat conduction equation is dimensional with respect to (area/length), so the hold-time should depend on $\frac{V}{(A/\ell)}$. In fact if the hold-time of any dewar, however complex, does not scale as the square of its linear dimensions, one must suspect that something has gone wrong. At least one should critically examine the practical considerations that prevent it from fulfilling the natural scaling law.

If there is heat dissipation internal to the helium vessel, the optimization with respect to the diameter of the inner well changes. We have derived the appropriate formula. It shows what common sense would lead one to expect, that when there is internal dissipation r_o should be greater than $\frac{2}{3} r_s$.

Obviously when the internal dissipation is overwhelmingly large
the best that can be done is to make r_o very nearly equal to r_s.

(c) Thermal Considerations in the Mechanical Support
of the Inner Well

The helium well of the dewar has to be supported. Ground-
based dewars are usually supported from a cylindrical neck-tube;
designs for flight dewars usually show fiberglass rods or straps
in tension or compression. Sometimes retractable members are
planned into the design for extra support during launch.

Important quantities in the design are the resonant
frequencies, which are fixed by the masses and moments of
inertia of the inner and outer wells and the elastic properties
of the supports. For the Gyro Relativity experiment -- and any
experiment requiring accurate pointing of an inner package --
the resonant frequencies determine the design and performance
of the spacecraft attitude control system. They should in
general be made as high as possible: the supports should be
stiff: and since stiff supports mean large heat leaks the
requirements of attitude control manifestly compete with the
requirements for a long hold-time dewar.

It is tempting to think that the heat leaks can be reduced
by increasing the length of the support straps, or by tricks
such as making the neck-tube structure of the dewar re-entrant.
Particular design problems may be solved by tricks, but in
general the advantage of longer support members is illusory.
The heat leak and the elastic restoring force both scale as
(area/length); the ratio of resonant frequency to hold-time
of the dewar is unaffected by a change in dimensions of the
support. More generally, for any dewar in which the dominant
heat leak is through the supports, the resonant frequency ω_m
associated with a particular vibrational mode m of the dewar
is related to the hold-time t_{max} by the expression

$$\omega_m^2 = C_m \frac{ELG\, t_{max}}{\int_{T_O}^{T_s} K(T)\, dT} \tag{41}$$

where E is the elastic modulus of the support, L the latent heat of helium, G the "gain factor" from Section J (3) (d), and K(T) the temperature dependent thermal conductivity of the support material. In every mode the coefficient C_m is independent of the lengths of the support members for a dewar of given size and independent of size for a dewar of given geometry. Thus the only latitude one has is to choose a material with the most favorable ratio of elasticity to integrated thermal conductivity $EG[K(T)]/ \int_{T_O}^{T} sK(T)\, dT$. (The gain factor may in principle affect the choice of material since it is a function of the temperature dependence of the thermal conductivity).

There are exceptions to the foregoing general statement. If tensile strength in the supports is important (as it may be to withstand launch stresses) the ratio (tensile strength/heat leak) can be improved by using longer straps of large cross-section. Again by making the support a hollow helical coil spring the ratio (heat leak/spring constant) can be made to depend on dimensions, since heat leak is proportional to rt/ℓ and spring constant to $r^3 t/R^3$, where r is radius of the tube, t its wall thickness, ℓ it length and R the radius of the turns. For a superinsulated dewar, however, the awkwardness of wrapping the insulation makes the idea curious rather than useful.

(d) Optimization of Heat Exchanger Locations

The sensible heat of helium vapor warmed from 4K to 300K is, as stated above, about seventy times the latent heat of the liquid. This refrigeration can be applied to intercept heat entering the dewar from outside by cooling a series of heat shields located in the superinsulation or attached to the dewar neck-tube or other supports. If all the cooling power were used ideally the hold-time t_{max} of the dewar would increase correspondingly: the gain factor $G[K(T)]$ would approach 70.

In practice even if the refrigeration is transferred with perfect efficiency to each heat shield there is no way of making use of all the cooling power. Take the case of a single heat shield. One can easily show there is an optimum working temperature for the shield, which is typically around 70K. Evidently the refrigeration available on warming from 70K to 300K will be lost; furthermore, since the shield is not at the surface of the inner well but about 35% of the way out, the heat load on it is greater than on the inner well of an unshielded dewar and the gain factor is still further reduced. In fact for one typical superinsulation material the gain factor with a single optimally located shield is 11.1. Though much less than 70 this is an impressive gain. The corresponding gains for two and three ideal optimally spaced shields are 19.9 and 25.5. Beyond three shields one reaches a stage of diminishing returns.

The present section reviews the optimization procedure; the problem of getting all the refrigeration out of the gas and into the shield is discussed in Section J (3) (e).

We have considered dewars incorporating up to three heat exchanges in linear, cylindrical and spherical geometries. In practice most dewars are cylindrical; the linear geometry applies in heat sinking the support and other penetrations. For a material with given K(T) the optimum temperatures are independent of the geometry; simple scaling laws relate the optimum positions in the different geometries. As an example we give below the theory for two heat exchangers in linear and cylindrical geometries:

Helium gas flows from the inner chamber (position x_0, temperature T_0) and is in thermal contact with two heat exchangers (x_1, T_1), (x_2, T_2) and escapes at position x_3 at temperature T_3. For linear geometry, x is the distance measured parallel to the axis and for cylindrical geometry x is the radius. Heat is

transmitted along the insulating material which has thermal conductivity $K(T)$. Let $\dot{Q}_0$ be the heat flow between stages 0 and 1, $\dot{Q}_1$ between 1 and 2, $\dot{Q}_2$ between 2 and 3.

Then from the definition of latent heat:

$$\dot{m} = \dot{Q}_0 / L \tag{42}$$

where $\dot{m}$ is the boil-off rate and L is the latent heat.

From the definition of specific heat and heat balance at the heat exchangers:

$$\dot{Q}_1 = \dot{Q}_0 + C\dot{m} \, (T_1 - T_0) \tag{43}$$

$$\dot{Q}_2 = \dot{Q}_0 + C\dot{m} \, (T_2 - T_1) \tag{44}$$

where C is the average specific heat of the helium gas.

From the definition of thermal conductivity we also have:

$$\dot{Q}_0 = \int_{T_0}^{T_1} K \, dt \Big/ \int_{x_0}^{x_1} dx/A(x) \tag{45}$$

$$\dot{Q}_1 = \int_{T_1}^{T_2} K \, dt \Big/ \int_{x_1}^{x_2} dx/A(x) \tag{46}$$

$$\dot{Q}_2 = \int_{T_2}^{T_3} K \, dt \Big/ \int_{x_2}^{x_3} dx/A(x) \tag{47}$$

where $A(x)$ is the cross-sectional area at position x.

Also we have the boundary condition:

$$\int_{x_0}^{x_1} dx/A(x) + \int_{x_1}^{x_2} dx/A(x) + \int_{x_2}^{x_3} dx/A(x) = \int_{x_0}^{x_3} dx/A(x) \tag{48}$$

The right hand side of (48) is independent of the positions of the heat exchangers.

Equations (45), (46), (47) and (48) are rewritten to give:

$$\dot{Q}_0 = K_{01}/A'_{01} \tag{45'}$$

$$\dot{Q}_1 = K_{12}/A'_{12} \tag{46'}$$

$$\dot{Q}_2 = K_{23}/A'_{23} \tag{47'}$$

$$A'_{01} + A'_{12} + A'_{23} = A'_{03} \tag{48'}$$

Equations (42), (43), (44), (45'), (46'), (47'), (48') are easily solved to give:

$$A'_{01} = A'_{03} \left\{ 1 + \frac{K_{12}}{K_{01}(1 + C(T_1-T_0)/L)} + \frac{K_{23}}{K_{01}(1 + C(T_2-T_0)/L)} \right\}^{-1} \tag{49}$$

$$A'_{12} = A'_{01} K_{12} \left| K_{01}(1 + C(T_1 - T_0) L) \right|^{-1} \tag{50}$$

$$A'_{23} = A'_{01} K_{23} \left| K_{01}(1 + C(T_2 - T_0) L) \right|^{-1} \tag{51}$$

$$\dot{m} = \frac{1}{A'_{03}} \left\{ K_{01} + \frac{K_{12}}{1 + C(T_1 - T_0)/L} + \frac{K_{23}}{1 + C(T_2 - T_0)/L} \right\} \tag{52}$$

It can be seen from (52) that the values of T_1 and T_2 which minimize $\dot{m}$ are independent of the positions of the heat exchangers.

For linear geometry:

$$\int_{x_i}^{x_j} dx/A = (x_j - x_i)/A \tag{53}$$

where A is the cross-sectional area.

For cylindrical geometry, the cross-sectional area at radius x is given by $(2\pi x^2 + 2\pi x \ell)$ where ℓ is the length of the cylinder. By treating the ends as an extension of the cylindrical wall we

make an approximation which is good in the limit of large x_0 and relatively thin total insulation thickness. In this approximation the cross-sectional area at radius x is given by

$2\pi x \, (\ell + \bar{x})$, where $\bar{x} = (x_0 + x_4)/2$

$$\text{and} \quad \int_{x_i}^{x_j} dx/A = \frac{\ell n \, x_j - \ell n \, x_i}{2\pi(\ell + \bar{x})} \tag{54}$$

Using (49), (50), (51) and (53) or (54), x_1 and x_2 can be expressed as functions of T_1 and T_2 and the optimum positions may then be calculated from the optimum temperatures.

Computer programs based on the foregoing procedure were developed by B. J. Lipa. An inverse procedure was used earlier by C. W. F. Everitt, based on optimizing the locations of the heat-exchangers in terms of the "reduced lengths" $\int dx/A(x)$ and determining from them the optimum temperatures. The results of the two methods are, of course, identical. Everitt's method consisted in first guessing the position of one heat exchanger, then applying the equations to determine the optimum location of the other exchanger, using the result as the basis for optimizing the first heat exchanger, and proceeding iteratively until the results converged to the desired accuracy. With three heat exchangers the locations of the middle one was guessed first, the others were then optimized, next their locations were used to determine an improved location for the middle one, and so on.

Table 14 summarizes optimized performances for systems of one, two and three heat exchangers in a particular superinsulation, assuming the internal heat load is negligible. The skin temperature of the dewar was taken as 300K.

Table 14: Optimization of Heat Exchangers for a Typical
Superinsulation

Number of Shields	Gain Factor	Temperatures in $^{\circ}K$		
n	G	T_1	T_2	T_3
One	11.1	62.5		
Two	19.9	41	128	
Three	25.5	25.5	87.5	185

For two shields the optimized locations corresponding to T_1, T_2
are 0.15ℓ and 0.45ℓ where ℓ is the total thickness of superinsulation.

Table 14 was obtained for a superinsulation in which K(T)
was equal to AT^2 at low temperatures smoothly fitted to $B(T-T_c)$
at temperatures above 40K. The more rapid the variation of K
with temperature the greater the gain factor for a given dewar
skin temperature; collaterally the higher the skin temperature
the greater the gain factor, since more sensible heat is available.
The relation of dewar performance to skin temperature is discussed
in Section J (3) (f).

The performance is surprisingly insensitive to the locations
of the shields. Optimally located shields usually give only 10
to 20% better performance than equidistant shields. For a
material with K independent of temperature equal spacing is
optimal; for all real materials the thermal conductivity decreases
at low temperatures and the optimum locations are always nearer
the cold wall than the equidistant locations.

So long as there are no internal sources of heat the optimi-
zation discussed in Section J (3) (b) of dewar performance with
respect to the size of the inner well can be partitioned off
from the optimization with respect to the locations of the heat
exchangers. For a spherical dewar the first optimization requires

the diameter of the inner well to be two-thirds of that of the
outer shell; the second requires maximization of the gain factor
G by one of the two methods just described. If there are heat
sources in the helium well the optimizations of r_o and G are
no longer separable. We conjecture that the separation which
occurs when there are no heat sources may be utilized in iterative
solutions of cases where dissipation is present, but since the
optimization with respect to G is so insensitive one does not
in practice need to be too concerned with such niceties.

(e) Transfer of Heat from the Shield to the Gas and Heat Leaks down the Vent-Lines

The calculations of the previous section are for ideal heat
exchangers of negligible thickness, at uniform temperature,
which utilize all the refrigeration available in warming the
gas to that temperature. In reality the gas has to be brought
up a vent-line which has some heat leak down it, and then passed
through a pipe wound in some suitable manner over the heat shield,
long enough to ensure that the shield is properly cooled.

Common sense dictates that the heat leak down the vent-line
joining two heat shields, as calculated from thermal conductivity
and dimensions before taking gas cooling into consideration,
should be made small compared with the heat leak through the
superinsulation. If not one will throw away most of the advan-
tage of gas cooling. Obviously if the uncompensated heat leak
down the vent-line were ten or twenty times the heat leak through
the superinsulation, one would spend all the refrigeration over-
coming it and gain nothing for one's trouble. However it is
not difficult to make the uncompensated heat leak of the vent-
line negligible by making the tube of thin-walled titanium or
some similar material. It follows that the gas will not warm
up much on passing through the vent-line; its temperature on
entering the pipe attached to the upper shield will be more or
less the exit temperature for the lower shield.

The non-critical character of the heat-shield optimization means that temperature differences of a few degrees between different parts of the heat exchanger itself do not much matter. Given a shield with a reasonable thickness of copper or aluminum (30 to 50 mils, say) one can rely on conductivity through the material to keep the temperature more or less uniform. On the other hand proper transfer of heat between the cooling coil and heat shield or other source of heat input is important. In the experimental laboratory dewar, for example, we had trouble with heat conduction between the cooling coils and neck-tube. See Section J (4).

Consider now a pipe at temperature T_p, into which a slug of gas enters at uniform temperature T_o. Assume the mass flow-rate in is low enough for flow to be laminar rather than turbulent and the velocity to be well below the velocity of sound, both of which conditions are fulfilled in all practical cases. After travelling a certain length ℓ_c (the cooling length) the gas will have warmed to a temperature T_i within one exponential factor of the temperature difference $(T_p - T_o)$. The requirement for adequate transfer to the heat shield is that the pipe be a few times ℓ_c long and that it be in adequate thermal contact with the shield.

Standard engineering formulae exist for heat exchange with a pipe. The rigorous expressions are complicated by corrections for the temperature dependences of the viscosity and thermal conductivity of the gas, and should take into account the conductivities of the heat shield and vent-tube. In the limiting case when $T_p - T_o \ll T_p$ the cooling length in first approximation is given by

$$\ell_c = 0.1 \, \frac{\dot{m} C_p}{K} \tag{55}$$

where C_p is the specific heat per gram of the gas at constant

pressure, K its thermal conductivity and $\dot{m}$ the mass flow-rate.
Note that the cooling length is independent of the diameter
of the pipe. This result follows from a cancellation of two
factors: (i) the smaller the diameter of the pipe the higher
the velocity of the gas, (ii) the smaller the diameter the
shorter the conduction path from the wall to the center of
the gas.

Numerical substitution gives a cooling length of 5 cm for
a heat shield at 40K and a dewar operating with 80 mW heat input
(corresponding to an 800 liter dewar lasting one year). Since
the thermal conductivity of helium gas is proportional to $T^{0.74}$,
where T is the absolute temperature, ℓ_c is less at higher
temperatures.

The relatively short cooling length is consistent with
experience of other workers. For small storage dewars a model
assuming perfect contact between the gas and the vent-tube has
been found to work well. For another program we investigated
the vent-tube problem for larger dewars and found that the
resultant heat leaks were within about 20% of those based on
the simpler model of perfect contact. Significant departures
only occurred with very short, large diameter tubes.

We also applied the perfect coupling model to explore the
situation where the heat leak down the vent-tube is comparable
with the radiation heat leak. This can happen between the inner
shield and the helium both if the dewar design is severely
weight or size limited. The location of the coupling point
of the tube to the shield can then be optimized in a similar
fashion to the optimization of the heat shields described
in Section J (3) (d). In this case the tie point of the tube
is best located closer to the warm end of the tube.

Assuming a heat shield of high thermal conductivity with
which cooling coils are in good thermal contact, all the refrig-
eration will be extracted from the gas in a few cooling lengths

(say three) which means that for an 800 liter one year lifetime dewar 20 cm of cooling coil is ample. Various arrangements of manifolding or distribution of thermal contact are possible to increase this length if thought necessary.

The HEAO dewar designed by Ball Brothers Research Corporation some years ago had 46 m. of cooling coil. It is not quite clear why. Perhaps the designer thought that piping the gas around the shield to intercept heat would result in a less massive shield.

(f) Effects of Dewar Skin Temperature

The hold-time τ of the dewar is a function of the temperature dependent thermal conductivity $K(T)$, the gain factor $G[K(T)]$ and the difference $(T_s - T_o)$ between the skin temperature and the temperature of the inner well. No general solution of the variation of hold time with skin temperature can be given but a useful insight is gained by treating $K(T)$ as a simple power function of T: $K = A_n T^n$. Even with this simplification the general expression for G is too complicated to be worth writing out; but by throwing away terms which contribute corrections less than about 20% one can obtain an instructive first approximation to the functional dependence of hold-time on skin temperature for a dewar vessel having one or more heat exchangers in the insulation space. It is

$$\tau \propto T_s^{-(n+1)^2/(n+2)} \tag{56}$$

For n = 0 (that is, conductivity independent of temperature), τ is proportional to $T_s^{-1/2}$ (rather than T_s^{-1} which is what it would be if there were no heat exchangers). For n = 1 (which is a fair fit for many materials) τ is proportional to $T_s^{-1.33}$. For n = 2 τ is proportional to $T_s^{-2.25}$. For n = 3 (which corresponds to free-floating radiation shields) τ is proportional to $T_s^{-3.2}$. The last expression, for free-floating shields with heat exchangers, should be compared to the case without heat exchangers, which of course obeys the Stefan-Boltzmann formula and thus makes $\tau \propto T_s^{-4}$.

Thus although dewars having an insulation whose thermal conductivity is a strong function of temperature gain more from recovery of sensible heat, their hold-times are highly sensitive to skin temperature, and this sensitivity is only slightly reduced by the presence of the heat exchangers.

(g) Transient Response of Dewars

It has been known for many years that thermo-acoustic oscillations sometimes occur in long thin pipes with closed upper ends, extending down into the helium wells of dewars. These often cause a dramatic increase in heat input into the helium. It is best to remove the pipe; if that is impossible schemes exist for damping the oscillations.

Rumors have been going around the cryogenic engineering community for the past year or so of another strange instability occasionally seen in dewars containing gas cooled shields. The temperatures of the shields are said to swing up and down over ranges of many degrees with a period of several days. No explanations of the oscillation have been offered; the tendency has been to keep quiet about them. We have recently discovered a potential cause of such instabilities, attributable to the combined effect of the temperature dependence of the viscosity of the gas and the reaction of heat shield temperature on the boil-off rate of the dewar. The instability has not to our knowledge been discussed before; it is analogous, however, to an instability seen in the cooling of charging leads for superconducting magnets.

We analysed a model in which the impedance of the gas vent-tube was concentrated in a single cooling coil and the heat input into the dewar was from radiation from the heat shield. The gas is driven through the heat-exchanger cooling coil by the difference in pressure between the helium tank and the outside. Starting from arbitrary heat shield temperatures and tank pressures we traced the time variation of dewar parameters and their ability to settle to a steady state. Settling is quite rapid for most coils owing to the relatively

high thermal capacity of the heat exchanger and the low flow
rate and low viscosity of the gas. With small pipes, however,
(typically pipes below 70 mil inner diameter and lengths of a
few meters) bad instabilities can occur in dewars of 100 liter
to 3000 liter capacity. Boil-off rates may fluctuate by up to
two orders of magnitude, with oscillation periods typically about
50 hours. The characteristic form of the gas flow is a sharp
peak of high flow rate with long intervals of very low flow rate
between the peaks.

We do not have enough information to know whether the
effect we have investigated is indeed the cause of the rumored
oscillations in experimental flight dewars. The pipe diameter
needed would seem too small. However our results suggest the
need for caution. Where weight is a constraint dewar designers
may be tempted to cut pipe diameters. The 3000 liter HEAO dewar
proposed some time ago may also face similar constrictions since
most of the cross-section of the vent-tube is taken up by
electrical leads. The proposed vent-tube was an 0.062 inch
annulus, of 0.31 inch outer diameter and length 20 meters.

For dewars with more than one heat exchanger the oscillation
just described is damped and should be no problem. However if
the inner shield were used as a "boiler" as proposed in some
dewar schemes[58] the impedance of the first heat shield would
be negligible and the system might in fact operate like a single
shielded dewar. With the boiler system there is another kind
of instability that might cause trouble: the "Ledinegg insta-
bility."[59] This instability is an oscillation in the location
of the liquid-vapor interface in a heated pipe in which boiling
occurs.

Returning to the long-period oscillations in the temperature
of heat shields we conclude that if such oscillations were to
prove a problem in a particular space dewar, the problem could
be fixed during ground testing by inserting a relatively large
impedance at either end of the vent-pipe at a point where it
may be anchored to a constant temperature surface.

(4) Experimental Laboratory Dewar

The large experimental dewar was designed to fulfil two functions:

(i) to provide a cold chamber for the complete laboratory model of the Gyro Relativity apparatus, incorporating one or more gyroscopes, the cryogenic telescope, super-conducting actuators for the fine-pointing servos if required, and other special features of the experiment. For this purpose the dewar had to be capable of working in any position between horizontal and vertical, and in particular had to be made capable of operating for extended periods when tilted at 37° above the horizontal, parallel to the Earth's axis at the latitude of Stanford. A long hold-time was considered essential to conduct uninterrupted gyro tests over periods of several weeks.

(ii) to give practical information for use in designing a flyable dewar for the Gyro Relativity experiment with lifetime approaching one year.

These aims demanded a high performance dewar, designed with careful attention to the problems of assembly and disassembly of the apparatus, and the requirements of low magnetic fields at the gyro. The restrictions placed in 1966 on the choice of materials for magnetic materials seemed at the time severe. Brass and "non-magnetic" stainless steel were excluded; we limited ourselves to aluminum, titanium, copper and certain plastics. For the reasons already explained in Sections D (4) (f) and E (2) (c) even these were far from the final requirements, but in 1966 we had no experience of thermoelectric phenomena at low temperatures and only glimmerings of ideas about how to create regions of ultra-low magnetic field. With two Mu-metal shields the dewar did just give the field isolation needed to complete the initial London moment observations.

The aim of making the dewar a preliminary to a flight dewar led to a design with heat-exchangers rather than a nitrogen shield, built with a provision to incorporate a porous plug, and extensively instrumented to check the validity of the thermal design. Two compromises caused by the need for an apparatus that

would hold the laboratory experiment were (i) stiffening members were added to prevent the helium well from sagging unduly in the tilted position, (ii) the outer diameter was made less than 30 inches to be compatible with the option we then had of reaching ultra-low magnetic field by lowering the dewar into a huge low field annular dewar.

Figure 68 is a cross-section of the completed dewar. It comprises three separate vacuum chambers containing the apparatus, the cryogen and the insulation. The experimental chamber is a narrow cylinder of maximum diameter 15 inches and length 64 inches, one end being at room temperature and the other at liquid helium temperature. The cold end is an aluminum chamber housing the gyro-telescope package. It is connected to the warm end by an 18 inch long, 9 inch diameter, 0.2 inch wall thickness fiberglass/epoxy tube, which, besides being the low heat leak connection to the outer world, serves the dual function of providing the line of sight for the telescope and the exhaust line for the low pressure (10^{-3} torr) gas drawn through the differential pumping ports of the gyro during spin up. The high pressure (5 to 10 torr) gas is taken up a separate 1.25 inch diameter line inside the neck-tube and out through a valve on the side of an extension tube on top of the dewar. The low pressure gas is exhausted through a removable 10 inch diameter stainless steel elbow attached to the warm end of the experimental chamber. A specially designed valve, operated through the elbow, may be used to close off the experimental chamber after spin up. The valve is designed to incorporate a quartz window: when it is closed the elbow may be removed leaving a clear line of sight through the window for the telescope. Low pressure is then maintained by a separate small high vacuum pump, which may, for example, be an ion pump mounted on the side of the exterior pieces at the warm end of the experimental chamber.

Three optimally spaced cooling coils are attached to the outside of the fiberglass/epoxy neck-tube. Each is made of
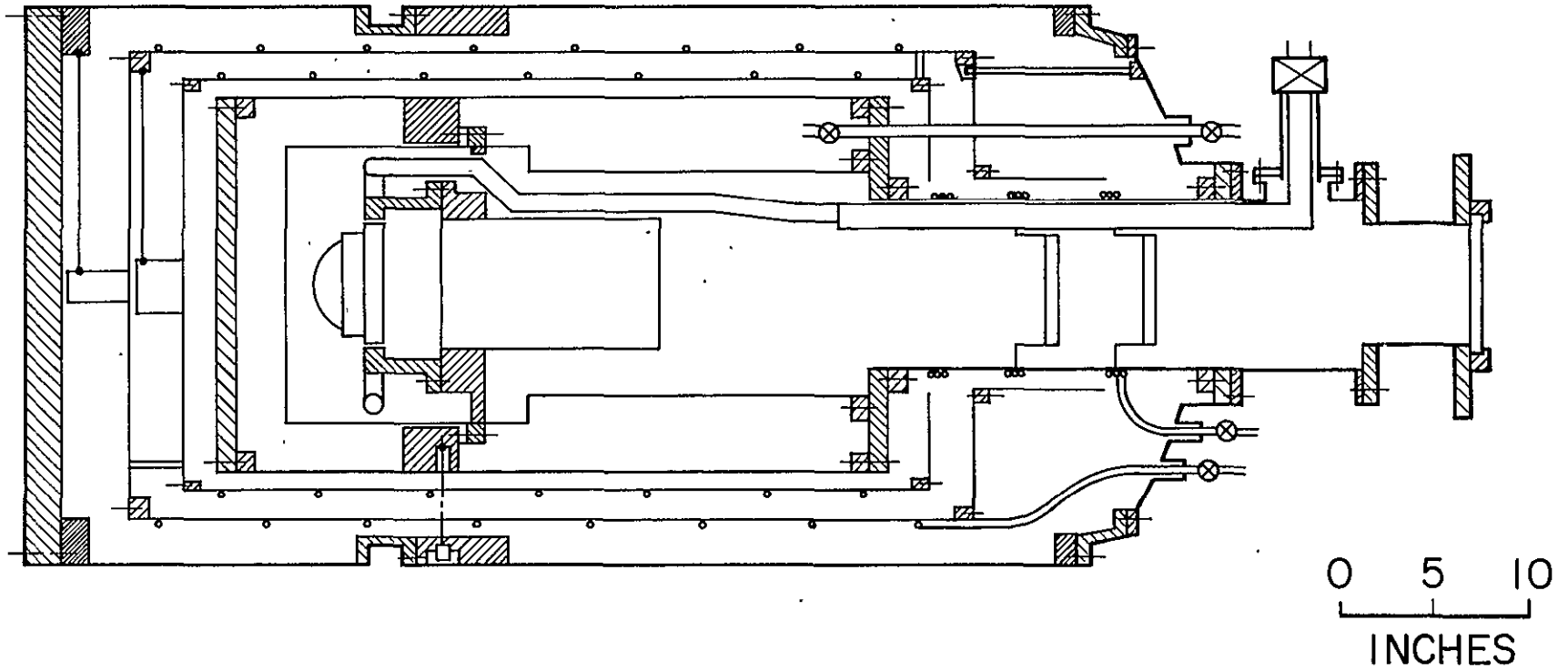
Figure 68: Cross-Section of Large Laboratory Dewar

three turns of copper and joined to the next by a thin-walled
low heat leak titanium alloy tube. A proportion of the helium
boil-off gas from the dewar is passed through the coil. To
reduce the radiative heat load into the experimental chamber,
two quartz windows, heat sunk to the copper cooling coils, are
mounted inside the fiberglass/epoxy tube. Their undersurfaces
are coated with a layer of gold about 500 Å thick. Spectrophoto-
metric data reproduced in Figure 69 shows that a gold film of
proper thickness has about 50% transmission in the visible range
of the spectrum while maintaining an emissivity of about 0.05
in the infra-red. Thus the radiative heat load is reduced to
a negligible value without much loss in telescope performance.

Figure 70 illustrates the cold end of the experimental
chamber and the lower section of the fiberglass/epoxy tube.
The various low temperature vacuum seals through the apparatus
are formed with indium wire in tongue and groove joints of
special design.

Surrounding the lower portion of the experimental chamber
is the 100 liter helium tank shown in Figure 71. It has titanium
fill and vent lines, which are closed at the lower end by two
cryogenic valves when the dewar is operated in the tilted position.
During this phase of operation the helium is vented through the
porous plug described earlier. The plug has not yet been used
in the large dewar. Provision has been made to locate it on a
separate vent-line which directs the boil-off gas through the
cooling coils on the neck and the heat exchangers described below.

Between the helium tank and the outer vacuum shell is the
insulation space, which contains multi-layer insulation and two
copper heat exchangers cooled by the boil-off gas. The heat
exchangers are suspended from the outer shell of the dewar; they
are shown in Figure 72. The positions of the heat exchangers,
like those of the cooling coils on the neck, are optimized for
maximum cooling efficiency by the method of Section J (3) (d).
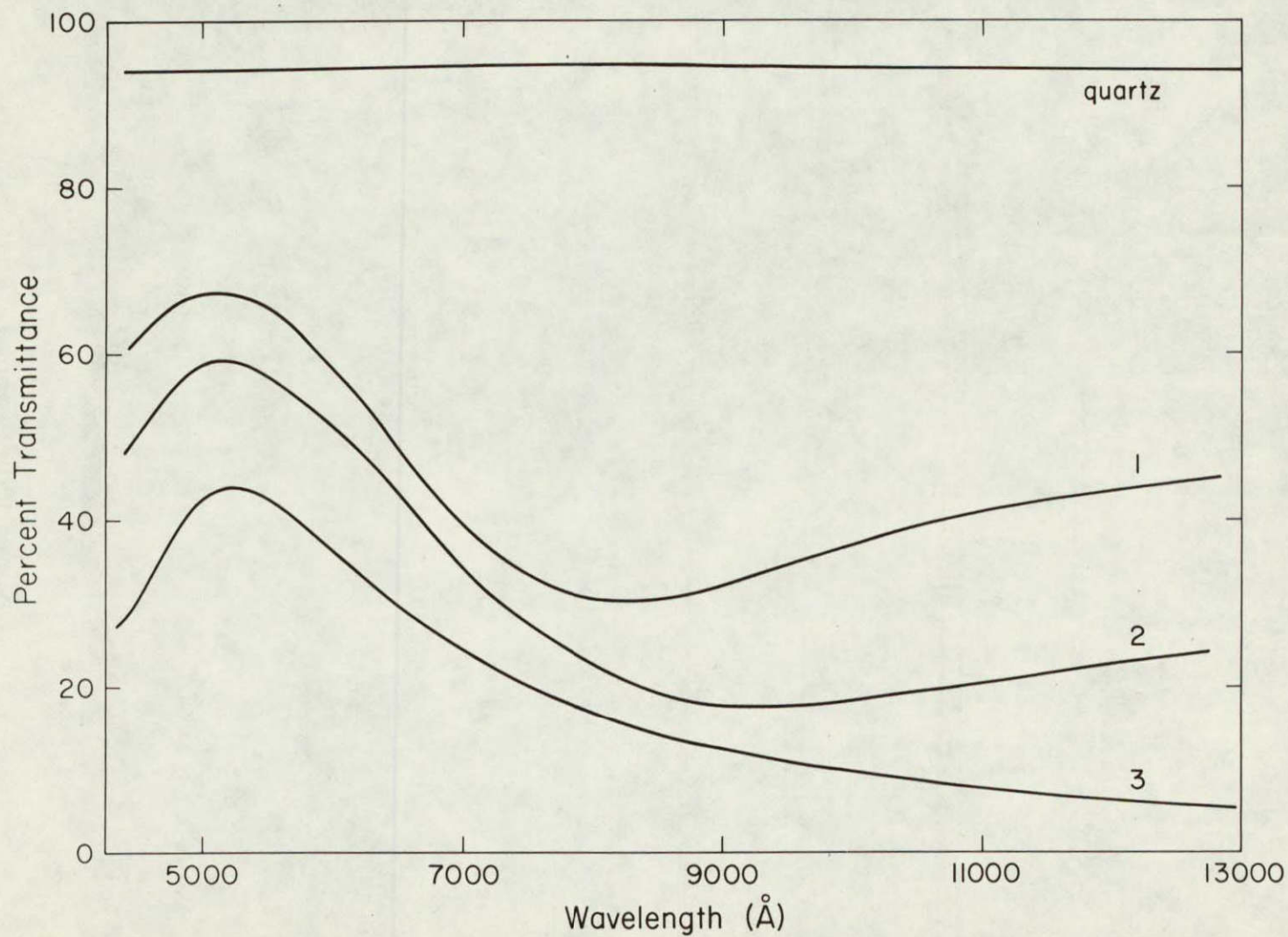
Figure 69:   Transmission of Radiation Through Gold Coatings
on Quartz Plate
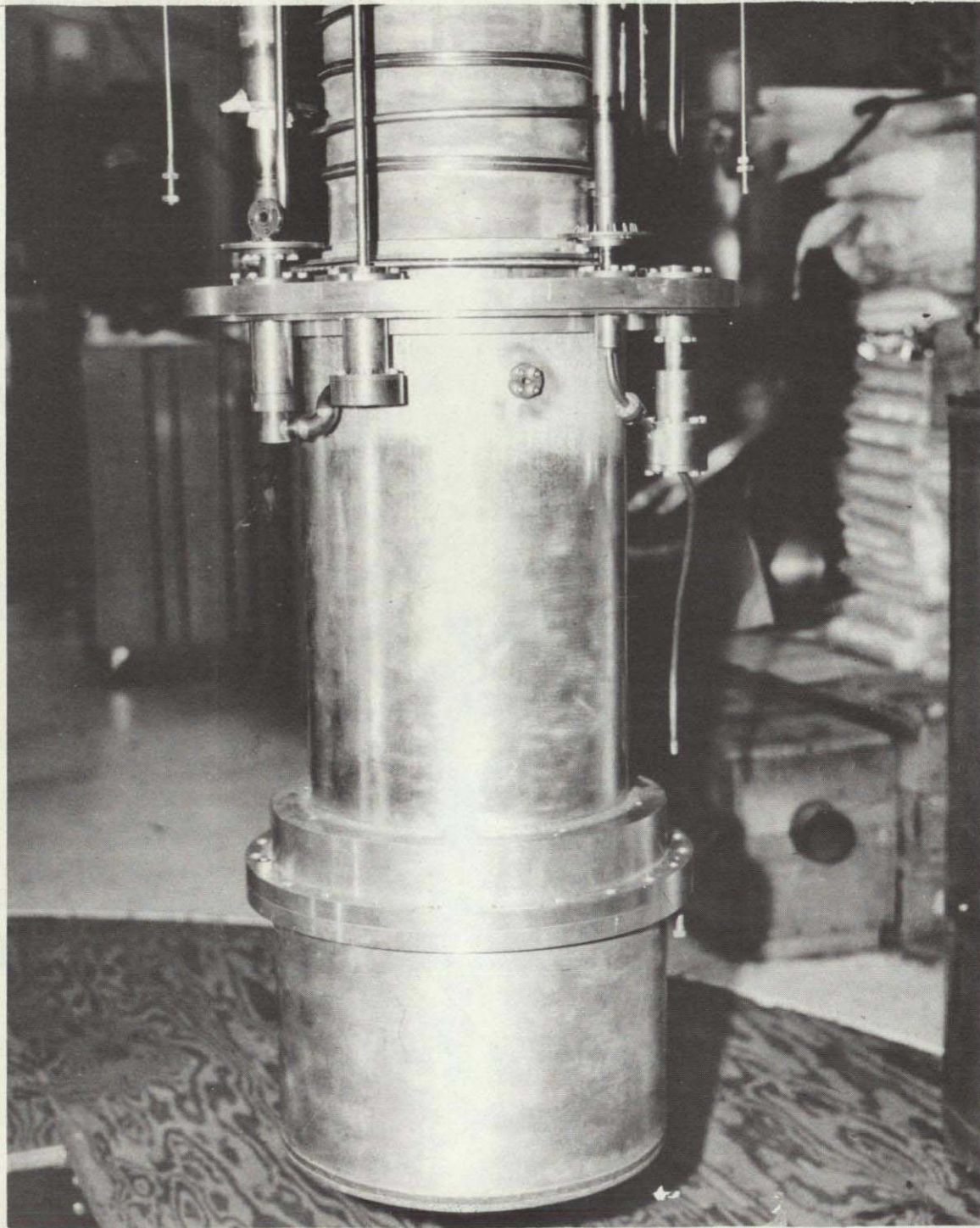
Figure 70: Dewar Experimental Chamber
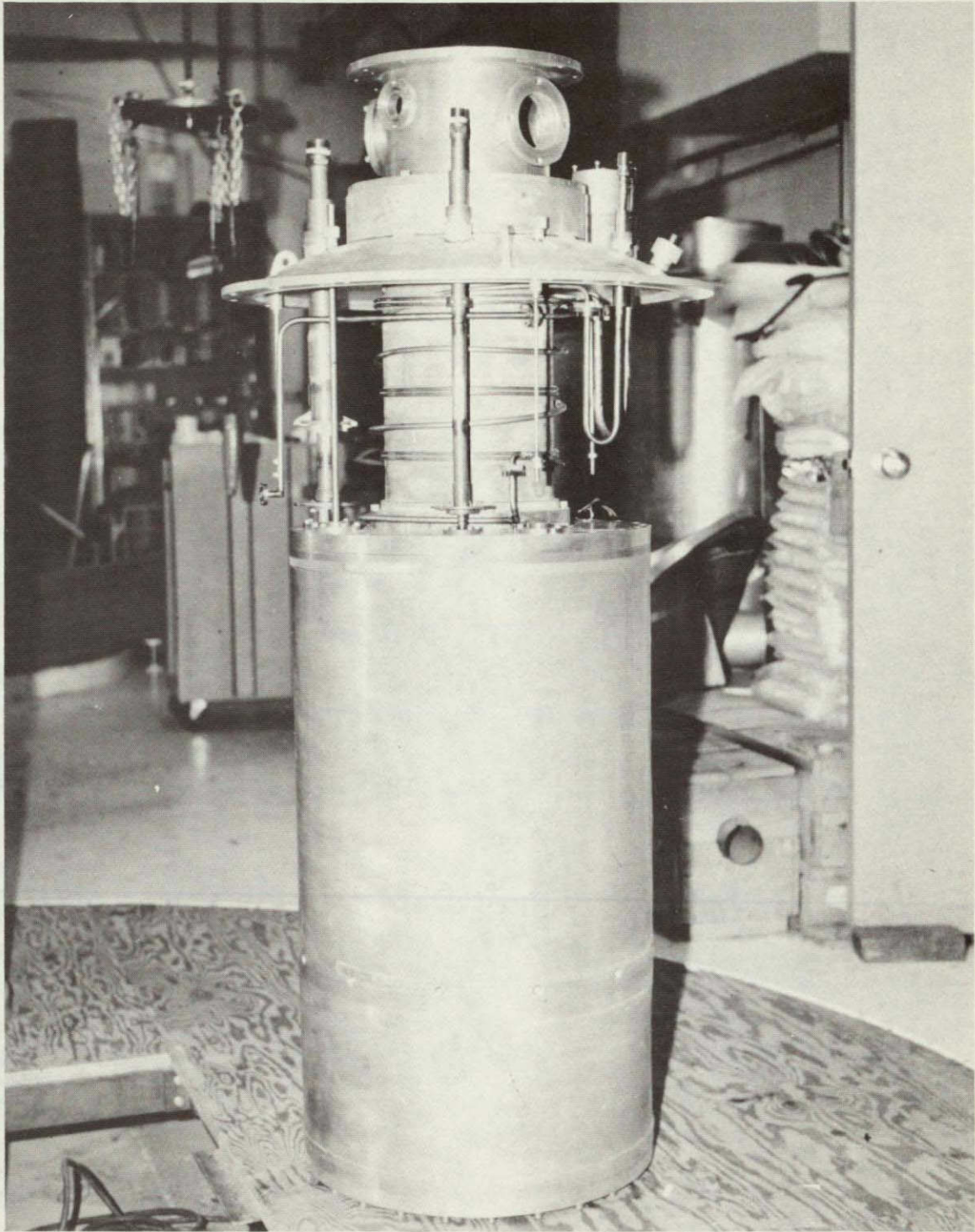
Figure 71: Dewar Helium Well, Neck Tube and Top Plate

Figure 72: Dewar Heat Exchangers

An important feature of the design is that the two gas cooling
systems are run in parallel, the proportions of gas for the two
paths being adjustable at will by two throttle valves at the
room temperature ends of the vent-lines. The variability gives
freedom to optimize the dewar performance under actual working
conditions and equally important provides a diagnostic tool
when things go wrong. One varies the flow rates and watches
the changes in temperature at different points on the neck and
heat shields.

The space between the helium tank and the first heat exchanger
contains no insulation. The remaining two spaces each contain
about 20 wraps of multilayer insulation. To date NRC-2 insulation
has been used, other types could be tried in the future. All
penetrations through the chamber are thermally anchored to each
heat exchanger.

In designing the apparatus we had in mind doing some experi-
ments with the dewar rolling slowly about its axis in the tilted
position. This mode of operation poses severe problems for
alignment of the telescope to the reference star. To help counter-
act the sagging of the helium tank, there are six titanium alloy
tie-rods which penetrate the insulation chamber from the outer
vacuum shell. They were placed deliberately some distance below
the center of gravity of the well, to give a bending moment which
approximately balanced the bending moment from the neck-tube.
This configuration was chosen to constrain displacements as far
as possible, to the lateral plane, the telescope being unaffected
by lateral motions. The tie-rods are one of the major sources
of heat leak. Their location is seen in Figure 73 which shows
the assembled dewar.

Table 15 gives the original calculated breakdown of heat
inputs into the dewar. The heat load of 71 mW corresponds to
a boil-off rate of 2 liters/day at 2K, that is a hold-time of
50 days. Much the largest expected contribution was from the
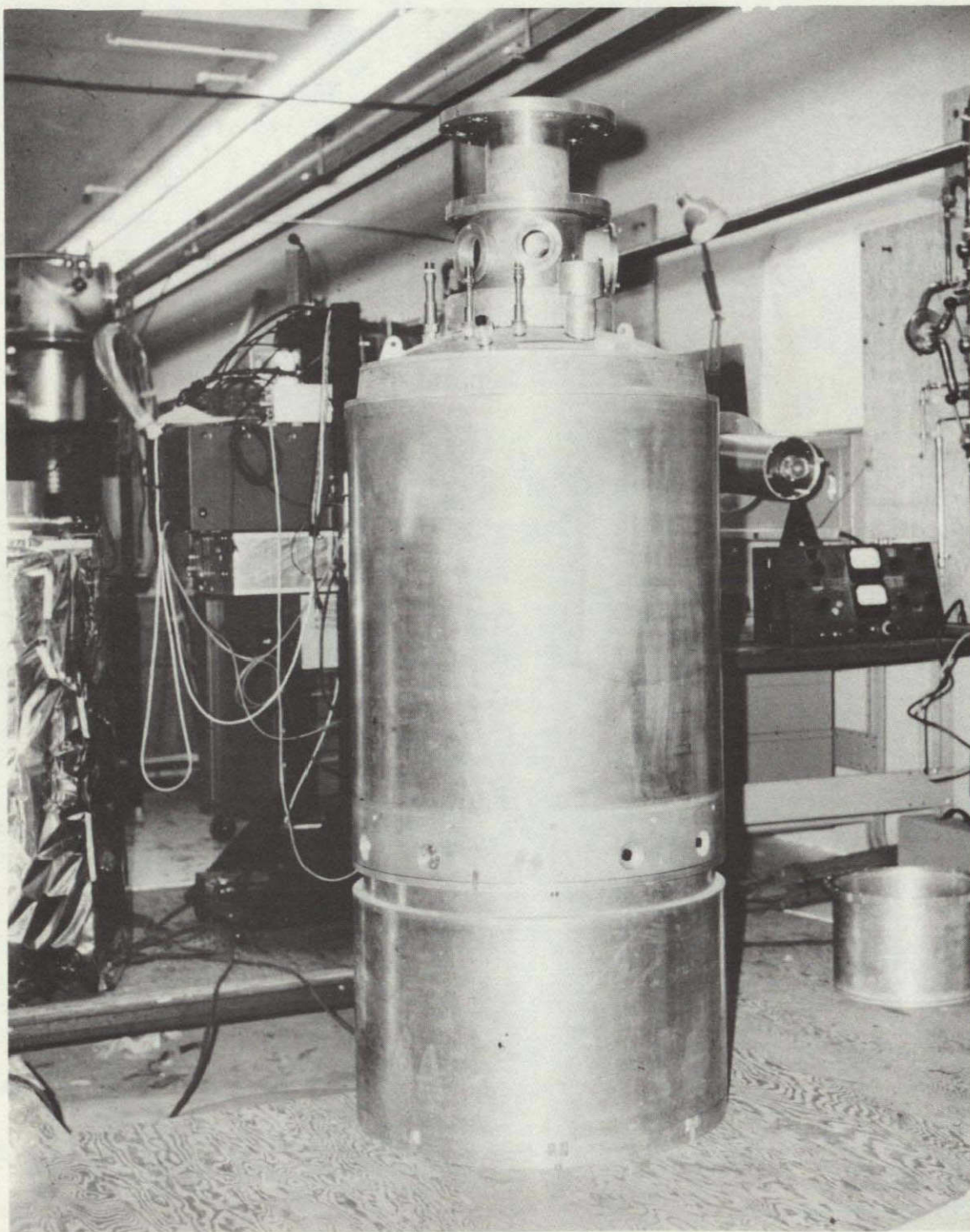
Figure 73: Large Laboratory Dewar Assembled

Table 15: Calculated Heat Leak Budget for Large
Laboratory Dewar

Heat Leak Source	Estimated Heat Leak (Milliwatts)
Superinsulation	5
Neck-Tube Conduction	9
Neck-Tube Radiation	8
Titanium Support Rods	34
Fill/Vent Penetrations	14
Miscellaneous	1
Total	71

titanium tie rods; the option exists for replacing them with
fiberglass straps, and reduce their heat load to about 10 mW.
With further minor improvements, notably in the design of the
fill/vent penetrations, the heat load may in principle be reduced
to 30 mW, making a hold-time of about 120 days.

The boil-off rate is still a long way from the design goal.
The best hold-times achieved so far correspond to about 10 to
15 days, and even that figure has to be qualified. What happens
is that the boil-off is rapid when the dewar is full and then
drops as the helium level drops, especially after the level has
fallen below the bottom surface of the experiment chamber.

To begin with dewar operations were hampered by a failure
at low temperatures of one of the vacuum seals on the fiberglass/
epoxy neck-tube, as the result of a design error. We replaced
the plastic tube temporarily by a stainless steel tube, that
was known to have considerably higher thermal conductivity, and
found as expected that performance was limited by extremely
high losses -- about 380 mW -- down the neck. After modifying
and reinstalling the plastic neck-tube, we observed an improve-
ment, but still nothing like as good as it should have been.
We were still dissatisfied with the neck-tube design, especially
with the heat-sinking of the cooling coils, which were simply

epoxied to the outside of the plastic and were therefore in
poor thermal contact with the radiation shield inside the neck.
We built a new neck-tube with better geometry, having the coils
attached to aluminum rings sealed into the plastic to provide
a conduction path to the inside. Shortage of manpower has
prevented us from trying the new neck-tube, but we hope during
1977 to get the time to run long hold-time tests on the dewar.

We are puzzled by the odd behavior that makes the heat
leak such a strong function of the depth of helium in the
inner well. This should not be. To some extent the improve-
ment that occurs when the liquid level falls below the bottom
of the experiment chamber can be explained away as a reduction
in radiative heat input into the helium, but the relative con-
ductivities of aluminum and plastic, combined with the presence
in the helium well of helium gas, which serves as an excellent
exchange gas, make us suspect that something else is going on.
Further investigations are planned.

The experiments done so far confirm the theoretical analysis
of the heat-exchanger performance in the superinsulation space.
The shields operated near the predicted temperatures and the
changes seen on varying the proportions of gas flowing through
the neck-tube coils and the heat exchangers were reasonable.

The hard knocks of experience encountered in running
the laboratory dewar have been trying. Besides learning the
problems of ultra-low magnetic field operation, we have been
forced to grapple with the difficult problems of neck-tube
design: problems that are crucial in the Gyro Relativity
experiment and in several other experiments requiring a
liquid helium dewar in space.   The neck-tube issue has not
to our knowledge been properly addressed by anyone. Besides
unexpected difficulties we have also had the not uncommon
experience of finding other problems by which people are scared
to be illusory. One instance concerns low temperature vacuum

seals. Doubts are often expressed about the feasibility of making large low temperature seals. The tongue and groove indium seal that we designed has proved simple and reliable. In every case a seal that was leak tight at room temperature has remained so under repeated temperature cycling. It must be remembered however, that these seals can be mis-designed, as both ourselves and many others have found, on other apparatus. Also, differential thermal contraction between the dissimilar materials, aluminum, copper, titanium, need not cause difficulty with joints of 2 inch diameter or less. For the larger seals it is essential to include jacking bolts to get the seals apart. Finally in another design area where doubts are often expressed, the cryogenic high vacuum valves used in the laboratory dewar have been operated successfully on many occasions.

(5) Design of Flight Dewars

The investigations described in the preceding section indicate that a dewar appropriate to the Gyro Relativity experiment can be built to hold helium for a year. The general layout has been shown in Figure 1, p. 13. The dewar would be constructed of aluminum with fiberglass supports and a neck-tube of appropriate design, and would contain about 800 liters of superfluid helium. Dimensions would be about 60 in. diameter by 50 in. length. The superin-- sulation space would contain three gas-cooled radiation shields. Control of the helium would be by a superfluid plug; the gas would be vented to space through the proportional thrusters described in Section K (2) (d). The operating temperature would be about 1.8 K. Critical issues would be the "dewar-within-a-dewar" concept, the design of the neck-tube, and the control of helium sloshing. An important question for NASA would be whether the dewar should be made reusable for later applications in other Shuttle-borne cryogenic gravitational experiments, for example, the free fall Equivalence Principle experiment proposed by Everitt and Worden. Comments on a few

general points are grouped here as background to design of the flight dewar:

(i) <u>Advantages of superfluidity</u>: The use of superfluid rather than normal helium has several advantages. In the first place the creeping film guarantees thermal equilibrium. Although such extreme equilibrium is not required for the Gyro experiment, since even normal helium can maintain sufficient uniformity to ensure the mechanical stability of the gyro-telescope package it nevertheless has other merits. Superfluidity probably eliminates the problem of stratification of gas and liquid in zero-g and also disturbances due to bump-boiling. The superfluid offers an advantage of about 25% in refrigerative capacity per unit volume. Finally its very high specific heat near the λ-point means that the dewar may be sealed off for appreciable periods without significant temperature rise, during launch for instance.

(ii) <u>Helium sloshing</u>: An important question discussed in Section K (2) (b) is the disturbances to attitude control generated by tidal motions of the liquid in the Earth's gravitational field. Should sloshing prove a serious issue a straightforward solution to it, suggested by R. D. Woolley of Ball Brothers Research Corporation is to exploit surface tension effects in a series of graduated compartments inside the helium well. Another possibility to which we have given consideration is to utilize the fountain pressure of the superfluid helium between compartments separated by porous plugs. The analysis of Section K makes sloshing unlikely to be a problem in the Gyro Relativity experiment; however it is in the Equivalence Principle experiment.

(iii) <u>The BBRC test dewar</u>: Between 1972 and 1976, following the first Mission Definition Study[12] of the Gyro Relativity program, Ball Brothers Research Corporation built and tested a 650 liter liquid helium vessel embodying many features of the flight dewar for the experiment. The outer diameter was

54 in. and the length 56 in.; the helium well had dimensions
40 in. diameter by 50 in. long and contained an experiment
chamber of 18 in. diameter and 40 in. long. The inner
vessel was supported by six fiberglass tension members formed
in continuous flat loops; there were also six retractable
titanium supports attached to the outer shell. The insulation
system comprised four multilayer blankets of aluminized nylon
and dacron net, spaced by three vapor cooled shields supported
from the fiberglass straps. There was no neck-tube. In addition
to the thermal model, Ball Brothers built a second model without
insulation for shake-testing.

Construction of the Ball Brothers dewar is described in
the October 1975 "Dewar Technology Study" (BBRC Report F75-20).
The hold-time achieved so far is about six months; the vibration
model has undergone flight qualification test for Thor-Delta
launch. In summary the BBRC dewar satisfies requirements
for the Gyro Relativity experiment in
- shake tests
- hold-time
- compatibility with attitude control system

but fails to address two problems:
- neck-tube design
- requirements for ultra-low magnetic field technology

Section 3 of the BBRC Report just cited (F75-20) contains
preliminary thermal and mechanical analyses of neck-tube designs,
which are of some value in supplementing the work on our exper-
iment laboratory dewar described in Section J (4).

(iv) <u>Dewar-within-a-dewar</u>: We conceived the "dewar-within-
a-dewar" principle in 1971 to provide a clear interface between
the flight dewar and the experiment package, and to reduce the
difficulties of establishing ultra-low magnetic fields at the
gyros. Our original plan was to mount the gyro-telescope
package in an 18 inch diameter vessel, which could be lowered

into a separate low field facility made as an annular helium
dewar containing superconducting ultra-low field shields. The
diameter of the central warm hole of the annular dewar would
be about 20 inches. The inner dewar would be lowered into it,
cooled to liquid helium temperatures, trapping a field of 10^{-7}
gauss or less in the spherical superconducting shields around
the gyros, and then be removed from the facility and inserted
into the main satellite dewar. Initially the main dewar would
be warm; thermal contact between it and the inner dewar would
be established by indium seals made up as the parts were
assembled or by pressure joints formed by shrinkage of the
main dewar on cooling. After cooldown of the main dewars
exchange gas would be let into the insulation space of the
inner dewar. Other intermediate dewars could be developed if
necessary to hold the inner dewar during ground testing.

Since 1971 our ideas on the "dewar-within-a-dewar" have
advanced in several ways. First, an inner dewar diameter
considerably less than 18 inches is acceptable: probably 12 inches
would be enough. This simplifies the ultra-low field facility
because our existing equipment is adequate to make 12 inch
diameter lead bags. Second the ultra-low field facility can
be simplified by using a conventional dewar in air lock, as in
the laboratory facility described in Section E (3) in place of
the annular dewar. Third, our experience with gyro operations
(Section D (4) (f)) suggests making the inner dewar principally
of glass or other non-magnetic material.

A more radical question is whether the "dewar-within-a-
dewar" principle can be dropped altogether by having a single
flight dewar with a lead bag, similar to the present ultra-low
field gyro facilty. One early objection to that was from the
magnetic torques that would be created on the satellite through
the interaction of such a large diamagnet with the Earth's field.

Obstacles of this kind could be circumvented without undue difficulty. Advantages of the approach might be a simplification of neck-tube design and dewar insertion. Disadvantages would be great complexity of the satellite dewar and a more cumbersome airlock.

(v) Inexpensive flight dewars: Our experience in designing the ultra-low field test facility led us in 1976 to suggest an approach to designing inexpensive cryogenic systems that might be used in testing the gyro-telescope package or other experiments requiring hold-times of a few weeks. The principle is to use a standard laboratory dewar of conventional design, possibly strengthened slightly, with a dewar probe having the helium well and porous plug attached to it rather than to the dewar. Cooling coils are attached to the probe and heat sunk to the neck-tube during assembly. One may thus envision an experiment operating for reasonable periods in zero-g with a standard dewar costing little more than $10,000 to $20,000.

This suggestion, due to C. W. F. Everitt, was incorporated in the joint University of Washington/Haverford/Stanford/Rome proposal to NASA for an experiment on Spacelab 2 to measure the anisotropy of cosmic background radiation.

K. DRAG-FREE CONTROL AND ATTITUDE CONTROL TECHNOLOGY

(1) Preliminary

The Gyro Relativity experiment requires pointing control of the telescope with a precision of ± 0.05 arc-seconds and translational control to reduce the average drag on the spacecraft (and hence the average accelerations on the gyroscope to $10^{-9}g$). Thrust for spacecraft pointing and drag-free control is supplied by boil-off gas from the helium dewar, passed through proportional thrusters of novel design. Research on the control systems has been the responsibility of the Guidance and Control

Laboratory of the Stanford Department of Aeronautics and Astro-
nautics directed first by R. H. Cannon and then by D. B. DeBra.
Under the original proposal for Grant NSG-582 (later NGR 05-020-019)
the research on drag-free control was initiated first and was
carried on semi-independently for several years, before giving
birth to a number of fully independent programs such as DISCOS.
In addition to the work under the present Grant, this section
briefly describes drag-free research supported through other
programs.

For convenience of exposition we depart from chronological
order and describe first (Section K (2)) research on the attitude
control and telescope pointing system of the Stanford Gyro Rela-
tivity experiment. Drag-free control technology is described in
Section K (3).

(2)   Attitude Control and Telescope Pointing System

(a)   Background

Attitude control studies were begun by D. B. DeBra and
C. W. F. Everitt in 1965. The first investigations assumed a
satellite of mass 300 kg and length 1.5m, with moment of inertia
80 kgm^2, containing 230 liters of liquid helium (30 kg at 4.2k).
The heat load into the cryogenic region was assumed to be 20 mW,
10 mW from internal dissipation in the vibrating plane magne-
tometers then being considered for gyro readout and 10 mW from
external sources, giving a dewar life-time of one year. In
later studies the satellite mass was increased to 600 kg, the
length to 1.65m, the diameter to 1.23m, making a total moment
of inertia of 330 kgm^2. The volume of liquid helium was increased
to 900 liters (135 kg at 1.6K) and the allowed heat input into
the dewar was assumed to be about 70 mW.

The preliminary analysis of DeBra and Everitt was reported
in May 1966 in the Fifth Semi-Annual Progress Report on the
Physics portion of the program. Several notable conclusions were
then reached. In the first place the dominant external torques

on the 1.5m long satellite in a 500 nautical mile orbit were
from gravity gradients (125 dyne-cm peak value assuming a
$\Delta I/I$ of 10%) and the action of the Earth's magnetic field on
the residual moment of the spacecraft (250 dyne-cm assuming a
moment of 500 gauss-cm^3). Both of these terms are doubly
periodic with the orbit. The next largest term, from aerodynamic
drag, was 15 dyne-cm (assuming the center of pressure and
center of mass to be separated by less than 5% of the diameter
of the spacecraft). By contrast with these relatively modest
external torques the torque produced in getting rid of the
helium boil-off gas from the dewar was enormous. The mean
value (not the peak) calculated for a single jet at 30 cm
moment arm and a helium exit temperature of 200K was 600 dyne-cm:
twenty to forty times the peak value from the gravity gradient
or magnetic terms.

Investigations of gas jet performance quickly showed that
conventional on-off valves for attitude control, whether operated
in bang-bang or pulse-width pulse-frequency modes, would not be
a good idea in the Gyro Relativity experiment. To point the
satellite to within +5 arc-seconds (the design goal we had set
ourselves at that stage) would require some 10^7 firings of the
valves in one year: one firing every three seconds. Reliability
problems were alarming, and would have become more so, had we
persisted on these lines, as constraints on pointing were
tightened. It then dawned on us that the control problem for
a spacecraft carrying liquid helium is different from that for
any ordinary satellite. Normally the control engineer's task
is to put on-board a controller with minimum weight, which means
for a gas system, one with minimum-sized gas tanks. Here we
have a virtually unlimited supply of gas; the problem is how to
get rid of it. The obvious answer, once the question has been
articulated, is to use proportional thrusters to divide the gas
into the opposing streams of variable flow-rate. The result is
an extraordinarily smooth controller, far less liable to failure
than an on-off system, and capable of much closer pointing.

0.001 arc-sec-sec white noise in the hardware electronics of the signal integrator.

Structural noise includes disturbances from sources such as

(i)   thermal expansion and contraction of the outer satellite

(ii)   structural stress relief

(iii) "crinkling" of superinsulation

(iv)   random "twitching" of fiberglass supports and dewar plumbing

(v)   vibration from the telescope chopper wheels.

There was great uncertainty in estimating any of these disturbances. In order to be able to make some investigation of their effect, Bull modelled the total of all internal structural disturbances as white process noise torques with a covariance of $(100)^2 (dyne\text{-}cm)^2$ sec between the satellite structure and the inner well of the dewar and $(6)^2 (dyne\text{-}cm)^2$ sec between the helium well and the gyro-telescope package. These were considered conservative engineering guesses.

The control noise depends on fluctuations in thruster pressure and inner actuator force. For the enlarged dewar, chosen in 1971 at the time of the first Ball Brothers Mission Definition Study, the heat input was 70 mW and the mean thrust capability of the boil-off gas issuing from a 230 K nozzle at 60 cm moment arm, assuming a one year dewar lifetime was 42,000 dyne-cm, or 7000 dyne-cm per thruster. Assuming a 1 dyne rms fluctuation in thrust at 1 rad/sec bandwidth, the torque fluctuations are 60 dyne-cm* at 1 rad/sec. The inner actuator torque depends on the natural frequency of the gyro-telescope gimbals, which was taken by Bull as 25 rad/sec. With this figure assuming an rms noise level equal to 1% of the rms control torque Bull arrived at a value for the torque fluctuations on the inner actuator of 8 dyne-cm in 1 rad/sec bandwidth.

Table 16 summarizes the external torques acting on the spacecraft, with the principal parameters used in making the calculations,

---

*J. S. Bull used the figure 200 dyne-cm rms torque at 1 rad/sec bandwidth.

again assuming the enlarged dewar of 1971 rather than the one originally studied by DeBra, Everitt and Witsmeer. More details. of the calculations are given in Bull's doctoral dissertation;[63] the figures used by Bull have been revised in light of subsequent information.

Table 16:   Satellite Torque Environment

Torque Source	Body	Peak torque (dyne-cm)
Gravity gradient	spacecraft/dewar shell	250
	helium well	10
	gyro-telescope package	20
Magnetic	spacecraft/dewar shell	220
	helium well	<2
	gyro-telescope package	<2
Solar radiation pressure	spacecraft/dewar shell	250
Atmospheric drag	spacecraft/dewar shell	800
Total probable worst case torques	spacecraft/dewar shell	500
	helium well	60
	gyro-telescope package	15

Moments of inertia -- gyro-telescope package I_1 - 4 kg-m^2 helium well I_2 $\sim$ 75 kg-m^2, spacecraft/dewar shell I_3 $\sim$ 250 kg-m^2 •

Mass -- 600 kg
Magnetic moment of spacecraft/dewar shell $\sim$ 500 gauss-cm^3
Maximum projected surface area $\sim$ 12 m^2
Distance - center of mass to center of pressure - 20 cm
Orbit altitude $\sim$ 730 km   (400 naut. miles)

The disturbances from micrometeorite impact were also studied. For a satellite of 12 m^2 projected area there is about a 4% chance of encountering a micrometeoroid of mass 3 x 10^{-4} gm during one year in orbit. The resultant probable torque impulse is 900 dyne-cm sec, impacting an instantaneous change in angular velocity to the satellite outer structure of 8 arc-sec/sec.

A further source of disturbance treated separately was the tidal sloshing motion of the liquid helium.

The mean torque capability of the boil-off gas was, as just stated, 7000 dyne-cm per thruster.

(c) Mechanization of the Two-Loop Attitude Control System

Three alternative mechanizations of the two-loop attitude control system were studied: (i) the classical approach suggested by R. A. Van Patten, which depends on spectral separation of the inner and outer loops, (ii) a system based on arbitrary dynamics with coupled inner and outer loops, (iii) quadratic synthesis of an optimal controller.

The classical approach utilizes the spectral separation of the inner and outer loop to partition the design into two models for which separate classical compensation networks can be built. The slow outer loop is closed about the fast inner loop by making the thrust a function of the rate and position of the cryogenic actuator, taking into account the resulting 90° phase lag.

A control system is said to have arbitrary dynamics if the designer can choose parameters which enable him to give the system an arbitrary set of eigenvalues (roots of the characteristic equation). These parameters may be physical parameters of the system (moments of inertia, spring constants, damping coefficients, etc.) or gains in a control law. There must be as many parameters available as there are roots to be assigned and each must affect all the roots: then an arbitrarily chosen set of roots determines the parameters and gains. When extra parameters are available the solution is not unique. Thus for a single control in which only feedback gains are available all states must be fed back to obtain arbitrary dynamics, but if two controls are available (as in the case under consideration) only half the states may be needed or the roots do not uniquely determine the gains. Since the control system for the Gyro Relativity satellite has two controllers, and at the same time the natural frequency ω_{γ} between the gyro-telescope package and experimental chamber can be chosen by the designer, it is possible to use arbitrary dynamics while feeding back only the

telescope angle θ and its derivative $\dot{\theta}$ and integral $z_1 = \int \theta dt$.
The result, as discussed below, is a system with a seventh order
characteristic equation but eight quantities available for
adjustment, giving the designer some latitude for optimizing
the control and state amplitudes.

Additional information on the system states can be obtained
by having extra sensors besides the telescope: for example a
device to measure the angle α between the experiment chamber
and dewar shell, together with the corresponding rates, etc.
Alternatively an "estimator" may be introduced into the control
system to model the plant and estimate the unmeasured states.
In the limit when all states are fed back to two controls
there are twice as many gains as needed to determine an arbi-
trary set of roots. Advantage can be taken of the additional
information by applying the method of quadratic synthesis,
in which the control law is chosen to minimize the integral of
a positive definite quadratic performance index, sometimes
called the "cost function." The weighting factors of the per-
formance index may be thought of as expressing the designed
ratio between state amplitude and control effort. The result
is an "optimal controller."

An optimal controller is optimal in the practical sense
that it minimizes the state and control amplitudes for any
particular desired ratio of state amplitude to control effort:
it will, for example, specify the design to give simultaneously
sufficient pointing accuracy and minimum consumption of helium
gas. Quadratic synthesis of an optimal controller with constant
gains requires steady state solution of the control Riccati
matrix differential equation, which for a system as complex
as the Gyro Relativity satellite demands a digital computer
program. However the reduction in sensitivity to variations
in system parameters and more efficient use of control effort
may justify the extra complexity. We were urged in this direc-
tion by the surprising sensitivity to parameter variations
exhibited in the classical and arbitrary dynamics approaches.

The classical controller requires (as Van Patten had pointed out) a high level of natural damping in the dewar structure to prevent the system from becoming unstable. Dashpots probably have to be added to the fiberglass supports. Bull concluded that integral control terms should probably be added to both inner and outer loops to obtain high gain at the low frequencies corresponding to orbital disturbances without unduly degrading the short period response. Bull retained double integral control through his later studies of the optimal controller/estimator.

The arbitrary dynamics approach couples the inner and outer loops without requiring the spectral separation of the classical controller, and also allows some of the damping for the outer loop to be provided from the integral of the telescope signal. This unusual by-product of integral control is possible because of the dynamic coupling of the inner actuator control torque through the middle body into the flexible outer mode of the dewar. The characteristic equation is seventh order having a state vector with components z_i, θ, $\dot{\theta}$, γ, $\dot{\gamma}$, α, $\dot{\alpha}$, where z_i is the integral of the telescope measurement, θ the telescope readout angle, γ the angle between the gyro-telescope package and the experimental chamber and α the angle between the experiment chamber and the dewar shell. On the other hand, eight quantities -- six control gains, when z_i, θ and $\dot{\theta}$ are fed back to both actuators and the two natural frequencies ω_γ and ω_α of the inner and outer structures -- are available for adjustment. Relying on a general knowledge of bandwidth requirements in various modes of the system, Bull was able to choose pole locations for the characteristic equations and still keep one parameter free for optimizing the state and control amplitudes. With the resultant suboptimal system small changes in ω_α called for very large changes in ω_γ to maintain the same pole locations. The best natural frequency for the outer loop when closed around a 25 rad/sec inner loop was 5.02 rad/sec. Under these conditions an rms telescope pointing accuracy of 0.12 arc-sec could be

achieved with 4000 dyne-cm rms thrust level and 66,000 dyne-cm rms torque on the inner actuator. The range of motion of the outer satellite was 0.68 arc-sec.

The parameter sensitivity of the suboptimal system led us to give serious consideration to modern control methods. The matrix equations describing the three body system with an estimator are

$$\dot{x} = Fx + Gu + w$$

$$z = Hx + v$$

$$\dot{\hat{x}} = F\hat{x} + G\hat{u} + K[z - \hat{z}]$$

$$\hat{u} = -C\hat{x}, \quad C = B^{-1}[N^T + G^TS], \quad K = [PH^T + T]R^{-1}$$

$$\dot{S} = -F^TS - SF - A + CBC^T$$

$$\dot{P} = FP + PF^T + Q - KRK^T$$

(57)-(62)

where w and v have zero mean and spectral densities QT and T^TR

$$E\left|w(t) \quad w^T(\tau)\right| = Q \quad T \quad \delta(t - \tau)$$

$$E\left|v(t) \quad v^T(\tau)\right| = T^T \quad R \quad \delta(t - \tau)$$

and the following are vector quantities

  u - state space control vector (dimension $m = 2$) incorporating the control torques for the cryogenic actuator and helium thrusters

  v - state space measurement noise vector (dimension $p = 2$)

  w - state space process noise vector (dimension $p = 2$)

  x - state space state vector (dimension $n = 7$), incorporating the orientations of the three bodies (θ, γ, α) and their rates ($\dot{\theta}$, $\dot{\gamma}$, $\dot{\alpha}$) and the integral z_i of the telescope measurement

  z - state space measurement vector (dimension $p = 2$) incorporating the telescope angle measurement and the output of the amplifier integrating the measurement

The vectors $\hat{u}$, $\hat{x}$ and $\hat{z}$ are the estimated values of u, x, z included in the estimator.

The following quantities in Equations (57) to (62) are matrices

A - state penalty matrix (dimension n x n)

B - control penalty matrix (dimension m x m)

C - control gain matrix (dimension m x n)

F - natural dynamics matrix (dimension n x n), incorporating combinations of spring constants and moments of inertia

G - control distribution matrix (dimension n x m)

H - measurement distribution matrix (dimension p x n)

K - estimator gain matrix (dimension n x p)

P - estimated state error covariance matrix (dimension n x n)

Q - process noise covariance matrix (dimension n x n), which combines the terms Q_u and Q_w:

$$Q - Q_W + GQ_u G^T, \text{ where}$$

Q_u includes the inner actuator and thruster white noise torques

Q_w includes the model of random structural noise discussed on p. 308 above

R - measurement noise covariance matrix (dimension p x p) incorporating photon noise in telescope readout and white noise in the integrator hardware (see p. 308 above)

S - Riccati control matrix (dimension n x n)

T - cross-correlation noise matrix (dimension n x p) (actually there is in the Gyro Relativity system perfect correlation between the noise in the telescope angle measurement and the process noise during the integral of the measurement)

where again m = 2, n = 7 and p = 2.

With the above equations synthesis of the controller proceeds iteratively in the following general sequence:

(i)   a digital computer program is applied to select natural dynamic parameters that will yield a reasonable error amplitude in the estimator and keep down the sensitivity of the system to white sensor, process and control noise.

(ii)   The estimator design is iterated, using digital computer programs, on the basis of sensor, process and control noise.

(iii)   The design of the controller is iterated, also on the basis of sensor, process and control noise, and through digital computer programs.

(iv)   Digital and analog computers are applied to iterate the integral control gains to obtain satisfactory response to low frequency torques.

(v)   The performance of the controller/estimator is simulated on an analog computer to investigate transient response and the sensitivity of the system to gain changes.

Hardware fabrication can then begin.

Details of the iteration procedure are given in J. S. Bull's doctoral dissertation. Initial choices for the desired rms values of the components of the state vector were: telescope pointing angle θ - 0.03 arc-sec, null offset γ between gyro-telescope package and experimental chamber - 1 arc-sec, null offset α between inner and outer shells of dewar - 0.1 arc-sec, with the values for $\dot{\theta}_d$, $\dot{\gamma}_d$ and $\dot{\alpha}_d$ being made extremely large in order to produce very small penalties on these state elements. The rms thruster torque was chosen at 1000 dyne-cm (6% of saturation for two thrusters on opposite sides of the spacecraft*). The time constant for the integrator was chosen at 50 seconds, which is short compared with the period of torques at twice orbital frequency and gives a reasonable settling time for the system on reacquiring the star. Following the iterations the

---

*In Bull's analysis this was equivalent to 10% of saturation.

rms pointing accuracy was improved to 0.017 arc-sec; the thruster
torque levels became 1070 dyne-cm. Results are summarized in
Tables 8.8 through 8.12 of Bull's thesis. Table 17 here, cor-
responding to 8.13 in Bull's thesis, compares performances of
classical, suboptimal and optimal controllers based on the
parameters used by Bull. We must emphasize that these figures
are based on the very conservative assumption that the resonant

Table 17:   RMS Performance of Controller/Filter Combinations

Controller Filter	Pointing Accuracy θ (arc-sec)	Torque Level on Cryogenic Actuator (dyne-cm)	Torque Level on Helium Thrustors (dyne-cm)
Classical	0.120	66,000	4,000
Suboptimal based on arbitrary dynamics	0.080	45,000	1,800
Optimal Estimator	0.017	9,070	1,070

frequency of the inner well with fiberglass supports is about
5 rad/sec. In reality we may expect a resonant frequency of
50 to 100 rad/sec, a charge which should considerably ease the
requirements on the final design.

Engineering comments on the selection of estimator penalty
matrices (Q, R, T) and controller penalty matrices (A, B, N) are
given on pages 107 - 112 of Bull's thesis together with comments
on four different mechanizations of integral control. The
answers are not clear cut. In general the type of control most
likely to do the best job of driving the state to zero at low
frequency is "output integral control fed back into the estimator
plant model."

The first optimal controller design was quite sensitive to
variations in system parameters. With an outer mode resonant

frequency ω_α fixed at its nominal 5 rad/sec, the range of frequencies in the inner mode ω_γ allowing stable operation was 23.0 to 32.0 rad/sec, while with ω_γ fixed at 25.0 rad/sec, the range on ω_α was 3.0 to 7.0 rad/sec. Although considerably wider than the nominal changes in frequency to be expected from the change in mass of the middle body with helium boil-off, these limits were too close for comfort. Under separate support, Z. Hadass developed a method for sensitivity reduction based on an extension of optimal design procedures.[64] The aim was to reduce the sensitivity to changes in natural frequencies and thruster torque by adjusting other parameters within the command of the designer, for example the estimator and feedback gains in the controller. The result was a slight loss in pointing precision and a slight increase in gas expenditure, but that was acceptable in view of the performance margins.

The analytical approach was to incorporate variable parameters in the dynamic matrices describing the system, treated as gaussian random variables and represented as a variable parameter vector, with mean at the nominal values of the parameters and with known covariance.

Use is then made of a modified cost function I which represents effects of both random processes acting on the state of the system and the random parameters. If the state is represented as the sum of nominal and perturbed states $x = x_n + \delta x$, the performance index may be written as

$$I = \text{trace } (A + C^T B C) (X + \epsilon \delta X) \qquad (63)$$

where X is the covariance matrix of the nominal system, δX is the addition to the covariance due to the variable parameters and ϵ is a sensitivity weighting coefficient, selected by the designer, which determines the extent of the sensitivity reduction in a given design.

The method was implemented as a computer program and then applied to the controller for the Gyro Relativity experiment. A series of designs were investigated with different degrees of

desensitization. The table compares one such design with the original optimal design. A 3 to 1 increase in the range of stability is gained at the expense of an acceptable loss in pointing accuracy (2.4 to 1) and a negligible increase in gas expenditure.

A comparison of results from the optimal and desensitized designs is presented in Table 18.

Table 18:   Pointing Control System Parameter Sensitivity

		Optimal design	Densensitized design
Range of stability (rad/sec)	Stiff spring (inner)	23.0 - 32.0	17.7 - 102.5
	Stiff spring (outer)	3.4 - 6.6	3.1 - 11.0
Pointing precision (arc-sec)		0.017	0.041
Control effort on inner servo (current to cryogenic actuator) (dyne-cm)		9070	13,000
Control effort on outer servo (gas expenditure) (dyne-cm)		1070	1091

The degree of desensitization may be adjusted to intermediate values if desired.

(d)   Development of Proportional Helium Thrusters

Upon recognizing the merit of proportional control for the Gyro Relativity program we examined a number of approaches to designing the thruster. J. Mathiesen conceived two mechanical devices -- one with a translating pintle and the other with an eccentric rotary valve -- each of which provided differential

flow out of two opposed nozzles. We also examined techniques for modulating the flow without moving mechanical parts.

The research on thrusters having no moving parts was initiated by F. Rehsteiner, who had earlier been responsible for the analysis to be be described in Section K (3) (b) on the gas-bearing for the drag-free simulator. The first idea, due partly to R. A. Van Patten, was for a directional thruster based on the Coanda effect, that is the phenomenon whereby a jet of fluid tends to remain attached to a curved wall over which it is flowing. The breaking angle depends on the curvature and surface temperature of the wall, so by heating the curved surface the direction of the jet stream, and hence the direction of thrust, can be varied. A straightforward application of the Coanda effect turns out to be complicated by shock wave phenomena in the gas issuing into the vacuum of space and the range of directional variation is too small for efficient use of helium as a propellant. An alternative is to apply the effect in directing a jet towards a dividing vane between a pair of recovery chambers going to opposed nozzles. The flow rate from the two thrusters is then varied by deflecting the jet. This scheme appeared to work in principle but was affected by changes in environmental temperature as well as the control temperature. Rehsteiner next developed a more sophisticated design, based on a differential Coanda effect in which two gas streams impinged on each other. Any change in the common temperature of the system would change the distance to the meeting point but not the net direction of the combined stream produced by confluence of the two jets.

At this point Jean Noel Aubrun joined the team and suggested a method of making the flow phenomena visible by striking an electric discharge in the helium gas. Working together Rehsteiner and Aubrun built an apparatus in which they could verify experimentally the mathematical model they had developed for the flow. The conclusion of the research was that a Coanda

effect valve of this type would work well at Reynolds numbers above 1000, but became marginal at a Reynolds number of 100. Since the Reynolds numbers corresponding to the average boil-off rate of the dewar were in the range 20 to 50, we were forced reluctantly to drop this promising scheme.

The idea of a valve with flow rate modulated by temperature remained attractive. Rehsteiner's next approach was to exploit the temperature dependence of the viscosity coefficient. The gas was passed to the opposed thrusters through two long capillary tubes, and by heating these differentially the flow rates could be varied. This design had two shortcomings. The range of temperature variations was limited so that the range of modulation of thrust was less than was desirable. Second, in order to get rapid response to heating and cooling the capillary tubing had to have extremely thin walls. Some prototypes were made by depositing electroless nickel on a wax mandrel. Rapid heating was effected by passing an electric current through the wall and the gas would quickly cool it down when the current was stopped. While the idea seemed promising the process was delicate and the apparatus was hard to assemble even after tubes had been successfully manufactured.

After considerable thought about other techniques for differentially controlling the gas flow we reverted to the mechanical design. The design was worked out by J. S. Bull and J. Mathiesen. A pintle was supported on a translational spring and driven by coils acting on a ferromagnetic section in the center of the pintle. Figure 74 is an "exploded" view of the disassembled thruster. Its size was chosen as a compromise between low power (power consumption gets less as the volume of copper used in the coil is increased) and a reasonable size for putting on the satellite.

With a thruster developed Bull undertook a careful evaluation of its performance. The chief questions concerned the performance at very low Reynolds numbers and boundary layer effects. Since thrust levels of the order of 1 to 10 dynes were expected, Bull
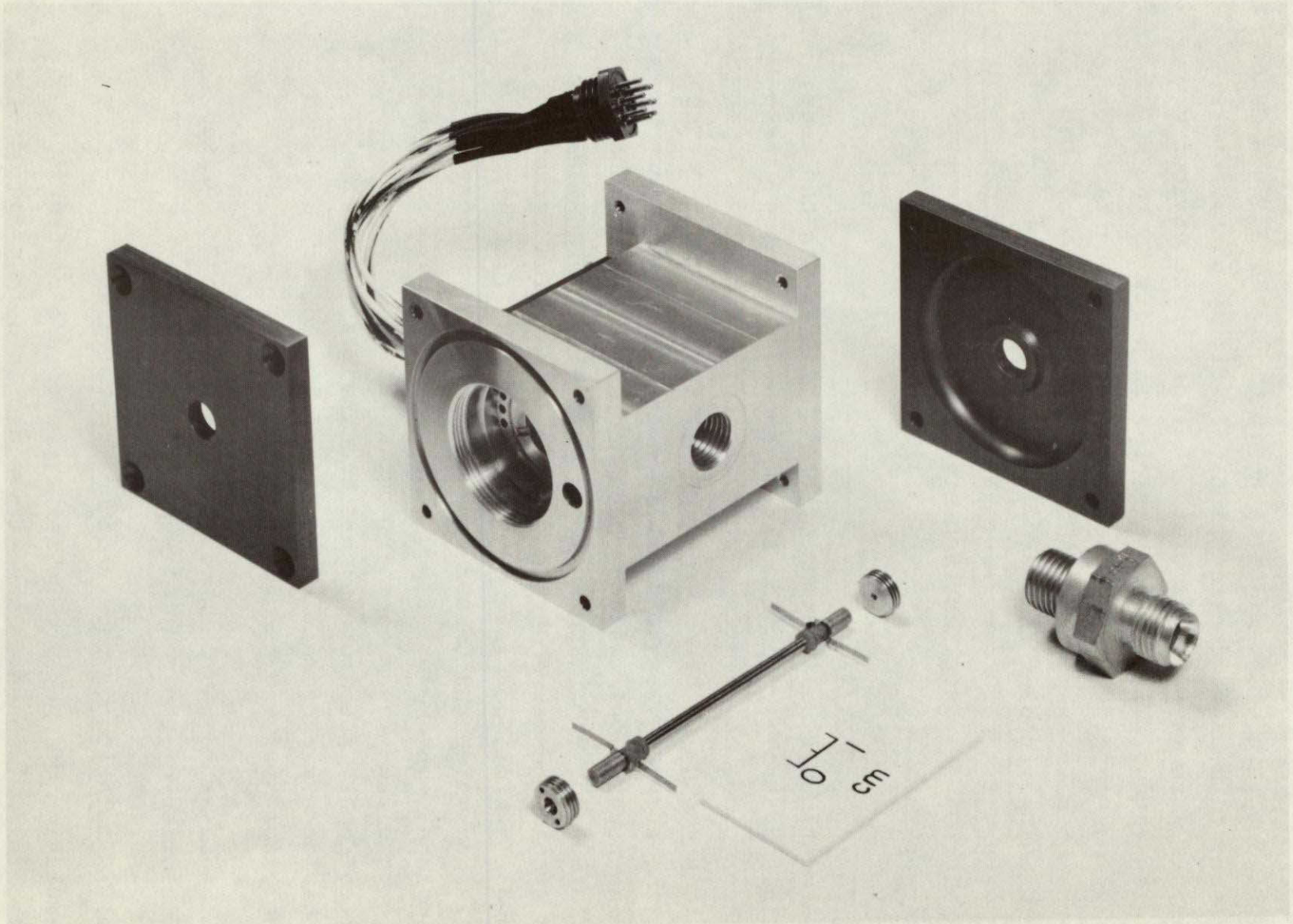
Figure 74: Proportional Thruster: Exploded View

built up the thrust stand illustrated in Figure 75 using a Cahn
microbalance to measure the reaction. Initially steady state
measurements were made to calibrate the nozzles at various
helium flow rates. Figure 76 shows that in spite of the
extremely low Reynolds numbers in the throat (R_e on the order
of 10) the loss in specific impulse is only about 15 to 20%.
Furthermore concern over boundary layer build up at low pres-
sures of a few times 10^{-4} torr proved unfounded. The data show
high resolution and excellent repeatability for measurements
of thrust at such low levels.

The continuous calibration of the thrusters was the first
step. In a control system the thrust has to be changed abruptly.
While theoretical calculations were encouraging they were per-
formed at Reynolds numbers for which little data exists. The
mass of the thruster was so great that its reaction to any
change in thrust level would be slow and far too demanding
in resolution for the response to be evaluated by conventional
sensors. Bull therefore developed a novel reaction thrust
measurement system, consisting of an extremely light system
of baffles on which the thrust from the two opposed nozzles
would impinge. The material was balsa wood, which meant one
day to outgas the vacuum chamber, but which taken together with
a modification to the microbalance electronics, yielded a
device having a measurement bandwidth of 20 rad/sec, a figure
acceptable for studying the satellite dynamics.

The test stand was then ready to incorporate in a fixed
base simulation of the control system.

(e) Simulation of the Attitude Control System

Simulation of the Gyro Relativity attitude control system
proceeded in two phases. Phase 1 was a closed loop analog sim-
ulation with the controller/estimator hardware electronics in
the loop. Phase 2 was a fixed base simulation with the vacuum
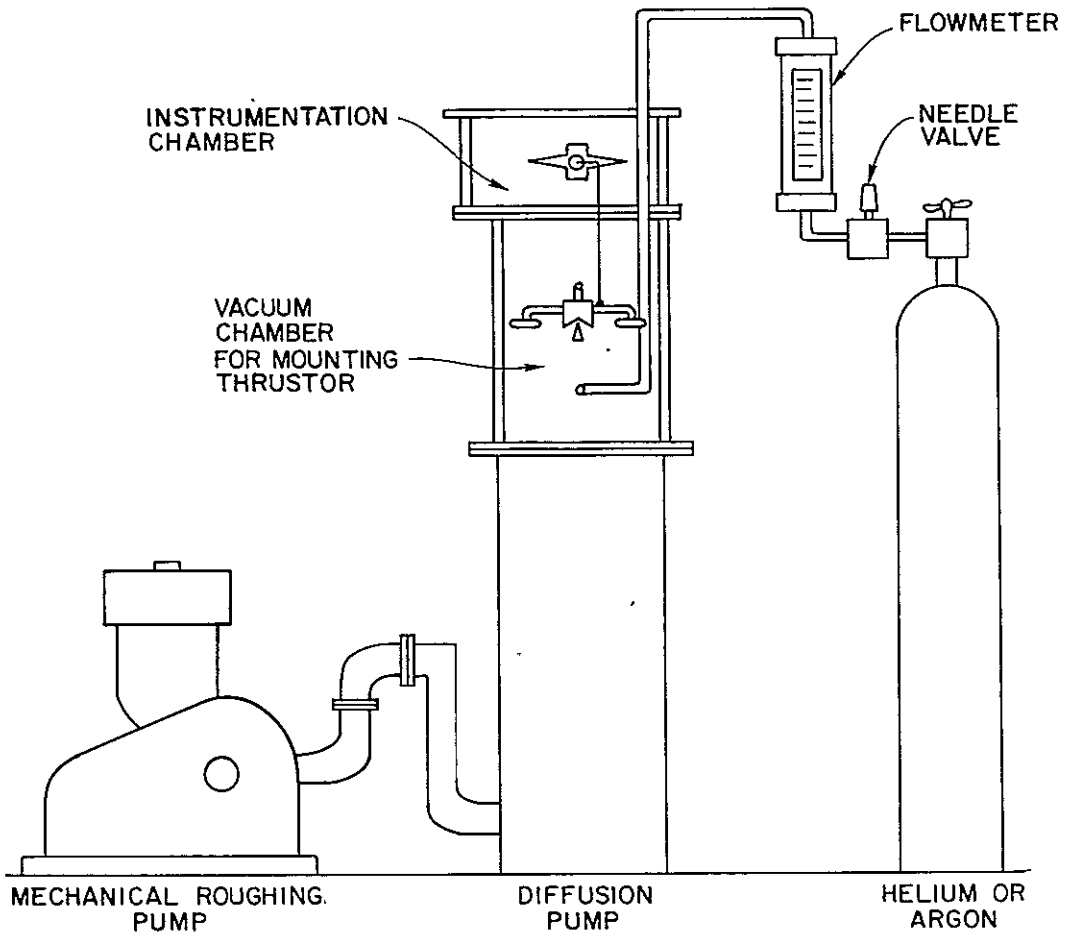
Figure 75:   Thrust Test Stand
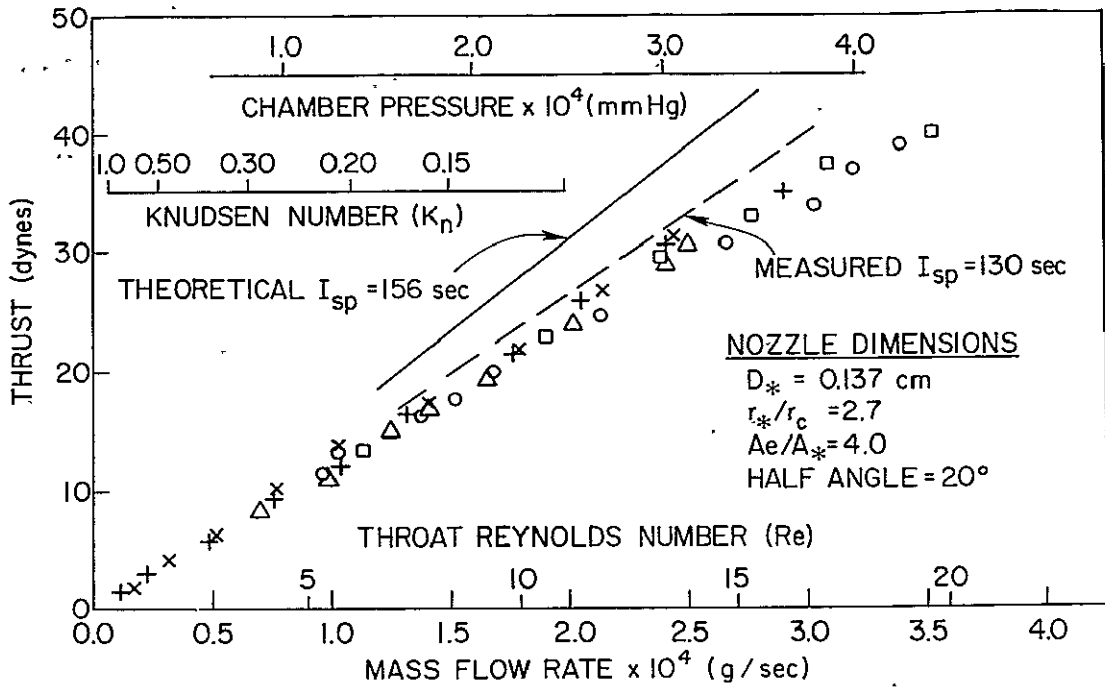
Figure 76:   Helium Specific Impulse as Function of Mass Flow Rate

chamber, thrust measurement instrumentation, thruster and electronics interfaces added in the path from the controller/ estimator to the satellite dynamics so that the natural dynamics of the satellite, as modelled on an analog computer, were driven by the measured rather than the desired thrust signals. Figure 71 illustrates the fixed base simulation. The satellite's natural dynamics were represented on the analog computer in a model that took into account disturbance sources as well as the mechanical parts of the satellite. The controller was bread-boarded using the mechanization proposed for flight including an analog estimator representing all the states of the system, from which the control laws generated the desired control signals for the helium thruster and cryogenic actuator. The inner actuator command was sent to the analog computer where that control was simulated while the helium thrust command was sent to the helium thruster. Thus all of the control hardware and the prototype thruster were evaluated together.

Phase 1 comprised a series of tests to investigate the following performance characteristics of the attitude control system:

- Transient response while acquiring the star
- Transient response to micrometeoroid impact
- Response to a step input torque on the outer body of the satellite
- Response to the dither signal used in matching gyro and telescope gains
- Response to process noise
- Parameter sensitivity.

Figure 78 illustrates a typical result from Phase 1: the transient response of the system while acquiring the star when the initial pointing error is great enough to saturate the helium thrusters. The initial offset angle α between the middle and outer bodies was taken as 1.0 arc-sec (twice the nominal value). The transient responses of all three bodies show good stability and satisfactory
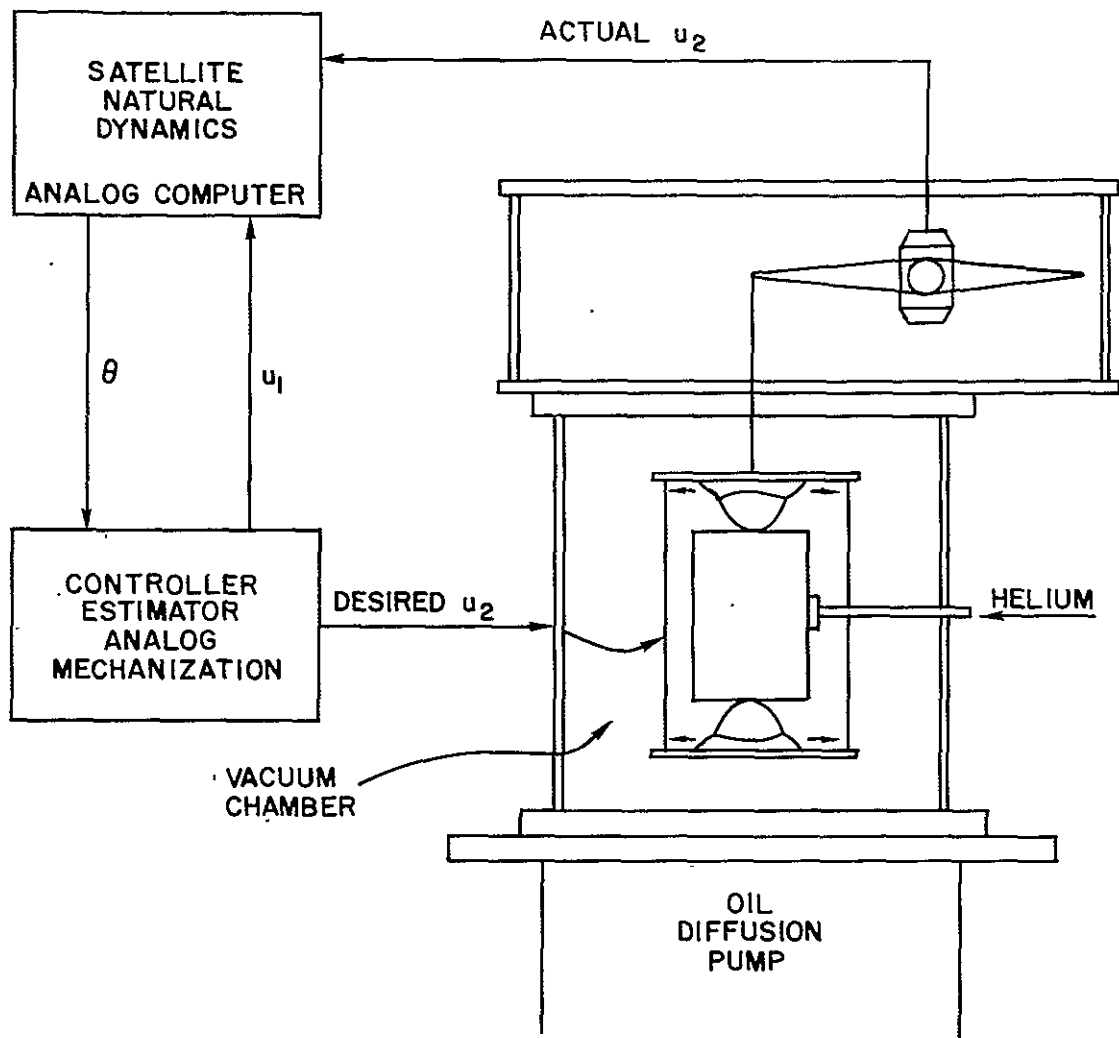
Figure 77: Closed Loop Simulation of Attitude Control
System
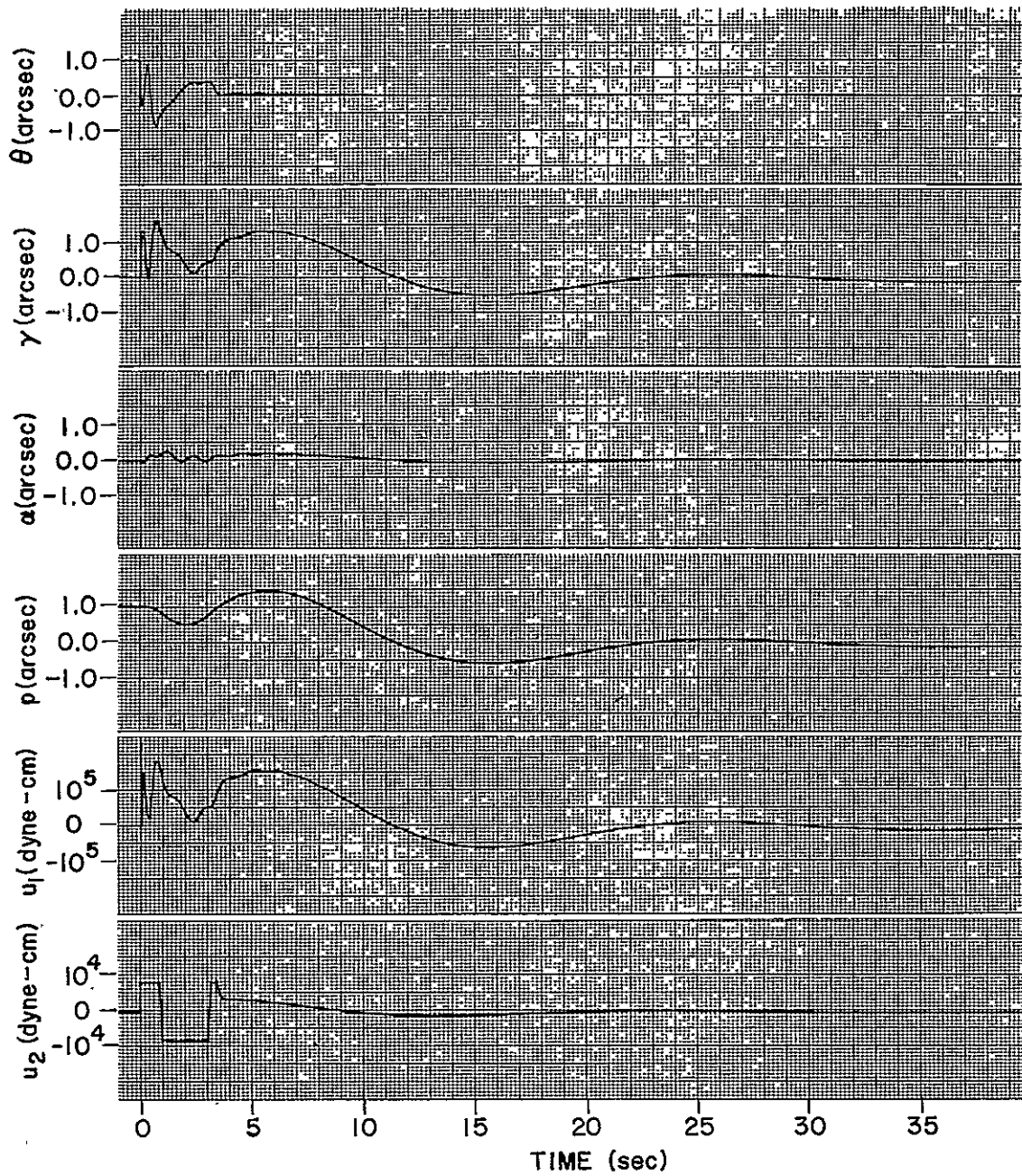
Figure 78: Transient Response of Attitude Control while Acquiring Star

settling times. The telescope angle decays to less than 0.05 arc-sec in 3.5 seconds, after which almost all telescope motion vanishes. The middle body makes an excursion out to 1.5 arc-sec at 6.0 seconds and then overshoots on its return to 0.6 arc-sec at 16.0 seconds, after which it decays to less than 0.1 arc-sec by 25.0 seconds. The inner actuator peaks instantly at 230,000 dyne-cm and then again at 180,000 dyne-cm after 0.8 seconds. The thrusters saturate at 8000 dyne-cm for the first second of acquisition and then saturate again at -8000 dyne-cm for the following 2.0 seconds. There is one more reversal of saturate to 8000 dyne-cm for 0.4 seconds, giving a total saturation time of 3.4 seconds after initial acquisition. Thruster torque then decays rapidly to less than 1000 dyne-cm after 8.0 seconds.

Curves similar to Figure 78 were generated to represent the time history of response to micrometeoroid impact and to the input of a step torque on the outer body. Other curves were generated to represent response to the dither signal, measurement noise and process noise.

The primary aim of the fixed base simulation (Phase 2) was to investigate effects of non-linearities and other performance characteristics of the thrusters departing from the nominal, for example:

●unusual helium flow characteristics at low Reynolds numbers

●null offset of pintle in open loop operation

●non-linearities in the springs supporting the pintle

●shortcomings in the electronics interfacing the thrust test stand to the controller/estimator

●abnormal mass flow rates

Figure 79 illustrates a typical result from the fixed base simulation: the response of the system to measurement noise and the calibrating dither signal. The rms amplitude of the measurement noise is 0.03 arc-sec. The telescope motion stays tightly locked on the dither signal (dither frequency 0.1 rad/sec)
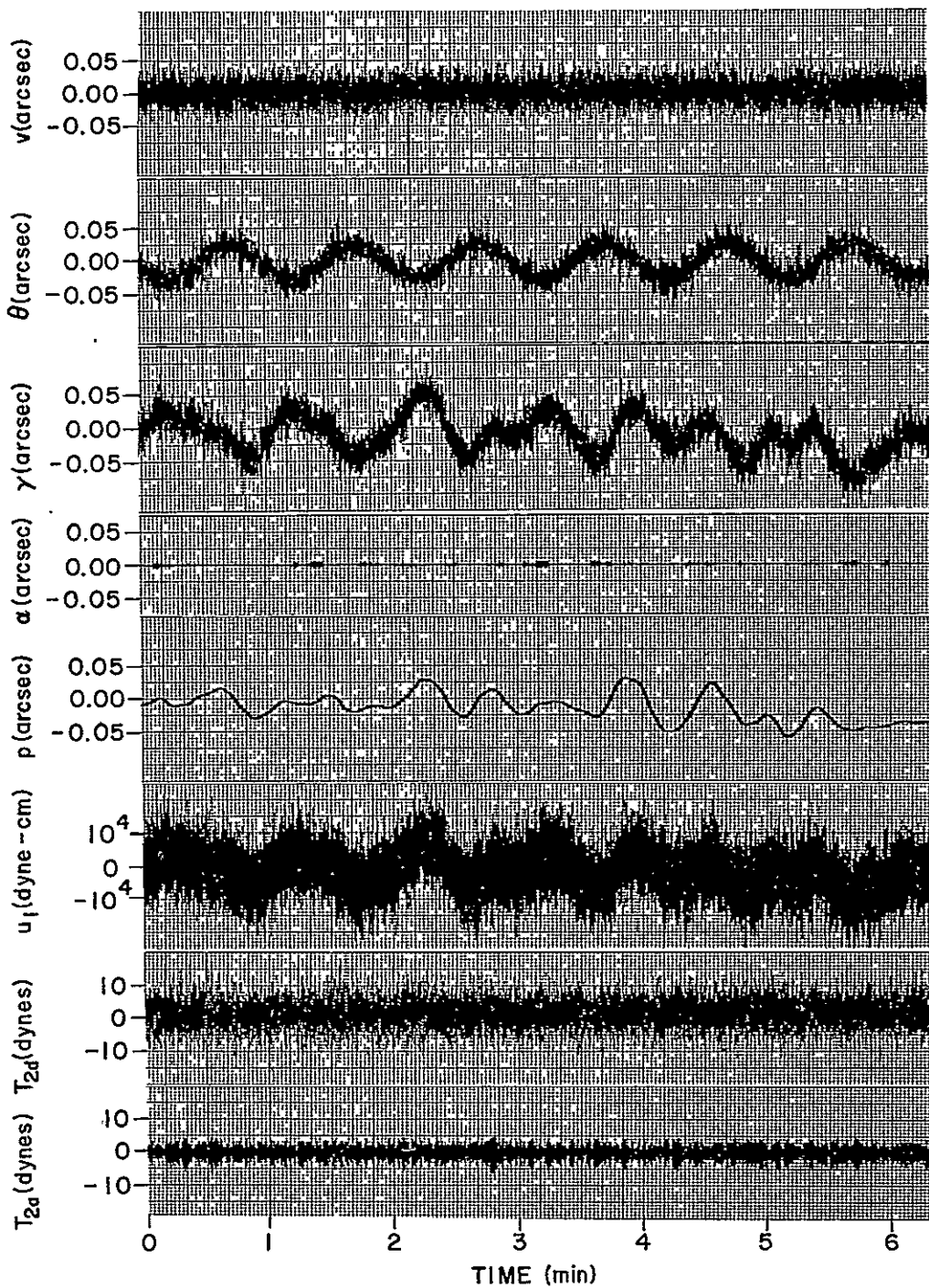
Figure 79:   Response of Attitude Control to Measurement
Noise and Calibrating Dither Signal

The telescope θ is effectively isolated from
thruster noise p by the fast inner loop while
precisely following the dither signal within
the limits of measurement noise attenuation.

329

and shows an attenuation of measurement noise by the full
state estimator down to about 0.075 arc-sec rms. There is a
low frequency random motion of the center of mass of the system
with exclusions as large as 0.06 arc-sec. Comparison with other
data suggests that this motion is attributable to large tran-
sients in the helium thrusters, caused by pressure fluctuations
in the test chamber due to intermittent operation of the
diffusion pump.

The most significant feature of Figure 79 is the effective-
ness of the inner loop in isolating the telescope from high
frequency disturbances and the effects of thruster non-
linearities. Pointing accuracy principally depends on how
much filtering of measurement noise is possible in the
estimator before disturbances and non-linearities start
degrading the control performance.

One important source of disturbance which we have modelled
mathematically and which continues to be an area of concern is
tidal sloshing of the liquid helium. A merit of the dual mode
control is that the cryogenic actuator can master slosh dis-
turbances owing to its high bandwidth. Since slosh is due to
internal momentum exchange the gas jet system does not have to
respond to it. On the other hand mismodelling of slosh behavior
and the change in mass from boil-off helium through the year
might limit stability and make it desirable to control the
position of the liquid helium by one of the methods described
in Section J (4). We do not think the issue is urgent from the
control point of view; it is one that should continue to receive
attention.

(f) Effects of Noise in the Pointing Controller on Gyroscope
Performance

An important question studied by J. S. Bull was the magni-
tude of the accelerations acting on the gyroscope from noise in
the pointing controller. Since some terms in the suspension

torque equations are quadratic in the acceleration, there is a
possibility of rectification and consequent gyro drift. The
rms acceleration from this source, calculated in Bull's assump-
tions, is in fact quite large: 3×10^{-6}g. However, since the
amplitude of motion is small -- only 0.4 µin or 0.25% of the
rotor-electrode gap -- any effect can be made negligible either
by appropriate modifications of the servo response of the gyro
suspension system or by damping in the pointing controller.
The source of the acceleration is the rms noise in the cryogenic
actuator; this can almost certainly be made far less than Bull
thought.

(3) Drag-Free Control Technology

(a) Background

The concept of the drag-free satellite occurred independently
to a number of people about 1961, including B. O. Lange, then
a graduate student in the Department of Aeronautics and Astro-
nautics, whose interest was sparked at the NASA Conference on
Relativity in Space held at Stanford in July 1961. The pos-
sibility of applying drag-free control to the gyroscope experi-
ment was discussed prior to that conference by G. E. Pugh.[64]

The principle has already been described. A proof mass
inside the satellite is shielded from external forces, so that
it follows a nearly ideal gravitational orbit, and a control
system activates gas jets (or other translational forces) to
make the satellite follow the mass. The problems are mechanizing
the control laws and minimizing extraneous effects, such as the
self-gravitational pull of the satellites. The extraneous forces
can be averaged in one plane by having a spinning vehicle.

The first thorough investigation of drag-free control
systems was given in Lange's 1963 Stanford University doctoral
dissertation.[66] Lange estimated the disturbances from self-
gravitation, the Earth's magnetic field, electric charge on the

proofmass, gas in the cavity, and similar phenomena. He developed control equations for spinning and non-spinning vehicles and suggested the concept of the unsupported gyroscope as discussed in K (3) (c).

Besides the application to the Gyro Relativity program, applications of drag-free control were conceived for aeronomy and geodesy. Aeronomy requires a more or less spherical satellite to make the drag coefficient independent of orientation. A design was studied by G. Chippendale as part of his Stanford doctoral program, and jointly proposed for flight by R. H. Cannon and B. O. Lange of Stanford, and Gordon MacDonald of the University of California, Los Angeles.[67] Studies of the satellite drag coefficient in free molecular flow were made by K. Moe, F. Sherman and F. Hurlburt.[67] A related study by W. R. Davis under B. O. Lange's supervision was for a single-axis controller to extend the lifetime of low altitude satellites.[68] A system was developed by Lockheed Missiles and Space Company but failed before it could be evaluated. The laboratory research for these programs was mainly supported under the Air Force supplement to NASA Grant NSG-582.

Following the studies the DISCOS disturbance compensation system was developed by the Guidance and Control Laboratory for the Navy's Transit Navigation Satellite, launched in 1972.

(b) Analysis and Laboratory Simulation

The analytic basis for drag-free control systems was started by B. O. Lange. In addition to work on non-rotating satellites Lange determined the proper compensation for a rotating satellite with linear error signal and bang-bang control system. He, and subsequently W. R. Davis, compared different thruster mechanizations, providing a variety of options for analytical study and simulation.

The choice of mechanization is often determined by the requirement to save fuel. For the Gyro Relativity experiment, as already explained in Section K (2) (a), fuel consumption is

not a principal limitation either in attitude control or translational control, and one can therefore use proportional thrusters, except possibly in an experiment at very low altitude. That is an unusual luxury, however; in general one must work hard to save fuel.

The principle of bang-bang control is to measure the position of the proofmass in its cavity, open a valve to fire gas in the proper direction and use the position signal to determine when to close the valve. There is a central dead band, which may be up to 40% of the gap, over which the proofmass is free to move without the control system responding.

The difficulty of bang-bang control is its need for a very quiet sensor: one is using a position measurement to control an acceleration. In unfavorable circumstances the sensor may be unable to resolve the signal and close the valve before the satellite has reached such a large velocity that it will reach the far side of the dead band, at which point the reverse valve fires. The mean thrust level will remain equal to the drag, but one will have the unhappy situation of the satellite bouncing from side to side, firing valves alternately in opposite directions and wasting large quantities of fuel.

Two mechanizations, both developments of research started elsewhere, were applied to overcome the limitations of bang-bang control. One was a "derived rate" method, studied initially by W. R. Davis and applied by D. B. DeBra to DISCOS; the other was "pulse-width pulse-frequency" control. With a pulse-width pulse-frequency mechanization, rather than close the valve in response to a position signal, one fires it in normal operation for a known length of time and uses the position measurement to vary the number of firings (the pulse frequency). In high drag condition the firing time (the pulse width) is sometimes also increased. Most of the laboratory simulator work described below utilized a pulse-width pulse-frequency controller.

In a spinning vehicle the center of rotation will not normally coincide with the center of the control deadband.

Another potential source of gas wastage, discovered by J. David Powell during work on the laboratory-simulator is "trapping." If the deadband is square, the proofmass may in effect become caught in the corner of the deadband, and the spacecraft will then rotate about the wrong location, spewing out gas at high rate to create the necessary centripetal acceleration. By combining a round deadband mechanization, due to R. A. Van Patten, with a center of mass estimator which adjusted the center of control to coincide with the center of mass, Powell eliminated trapping and unnecessary gas expenditure.

A limitation of different type on drag-free control is from effects of gradients in the force field acting on the proof-mass. Self-gravitation, residual magnetic fields, electric charge on the proofmass, all have body-fixed gradient terms such that if the mass is displaced in the cavity the acceleration acting on it will change. Since with an ordinary control system the mean position of the proofmass depends on the external acceler-ation the performance may depend quite strongly on the accelera-tion environment of the spacecraft. The solution is integral control. P. Jhin[69] and subsequently M. Tashker[70] undertook research that solved the problem of introducing integral control into a rotating spacecraft.

Mathematical simulation of a non-linear system is an approxi-mation at best; from the beginning we recognized the need for a laboratory simulation of the drag-free controller. The instru-ment used in a variety of investigations over the past ten years has been the two axis simulator illustrated in Figure 80, known as the Ground Effect Machine, or GEM. An air cushion vehicle floats on a granite surface plate; gas jets are fixed in the horizontal plane to keep the vehicle centered about a spherical proofmass suspended from a granite frame over the table. The design was started by R. Bourke, who built also the first capaci-tative pickoff, illustrated in Figure 81, with electronics assistance from Doyle Wilcox of Autonetics. Initial difficulties with the gas bearing support were resovled by F. Rehsteiner,

BALL
POSITIONER

ELECTRONICS
FILTER AND
DIFF. AMP.

ROTATION
JET

CONTROL
JET

CAPACITOR
PICK-OFF
HOUSING

MICROMETER
FOR FINE
BALANCING

SUPPORT
GAS REGULATOR

SUPPORT
GAS FLOWMETER

CONTROL
GAS REGULATOR

ELECTRONICS
P.W.P.F.

ROTATION
JET

CONTROL
JET

GYRO
SWITCH
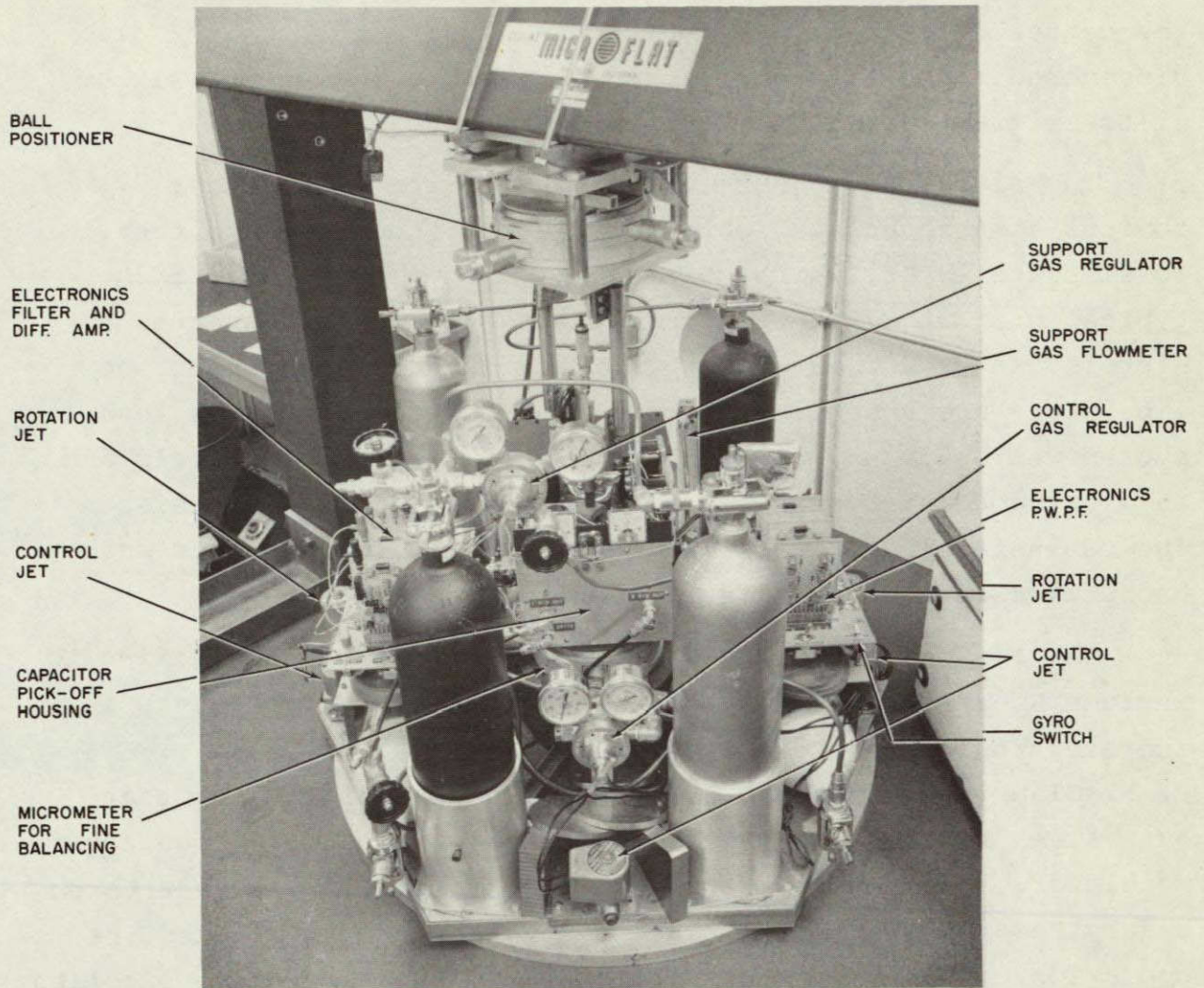
Figure 80:   The Ground Effect Machine (GEM):   Two Axis Air
Cushion Simulator of Drag Free Spacecraft

335

who explored requirements for bearing stability and determined
the geometry providing greatest stiffness against tipping when
the center of mass of the vehicle is offset. Rehsteiner also
discovered a translational force on the bearing due to slight
tilts originating in asymmetrical viscous gas flow.

The simulator is subject to wind currents and other
obvious disturbances. Table tilt is particularly important.
To simulate 10^{-6}g, which corresponds to a few percent of the
typical drag at 270 km altitude the table must be level to a
microradian or 0.2 arc-sec. Typical foundation tilts in the
laboratory are a few arc-seconds; so an automatic table levelling
system was built up, using Brunson automatic bubble levels and
an electromagnetic solenoid actuator designed by J. Mathiesen.
The table-leveller fulfilled the operating requirements and
has worked without failure for twelve years. [71]

The air cushion vehicle designed by Bourke was modified to
include Rehsteiner's findings on the bearing; improvements in
the electronics were progressively made by R. A. Van Patten and
R. R. Clappier. After the original bang-bang control of the
gas valves had been replaced by a pulse-width pulse-frequency
modulator, an extensive study of the performance was undertaken
by Ury Passy, [72] who calibrated the pickoff and evaluated the
operation of the thruster system. Passy was able to get excellent
correlation between theoretical table tilt and observed gas expend-
iture at levels down to 0.1 arc-sec. The data, which approximated
with reduced accuracy the performance at 400 km, covered nearly the
entire range of altitudes from 125 km to 470 km proposed for the
aeronomy experiment. Passy also optimized the design of the
pulse-width pulse-frequency modulator.

G. Chippendale pursued the development of thrusters which
could be used to measure very accurately the applied control,
following several ideas contributed by D. Wilcox. The thrust
stand developed for Chippendale's research was designed by J.R.
Mathiesen, with feedback control developed by Chippendale and

CAPACITOR PICKOFF +y EPOXY HOUSING

-x +x +z -y

337
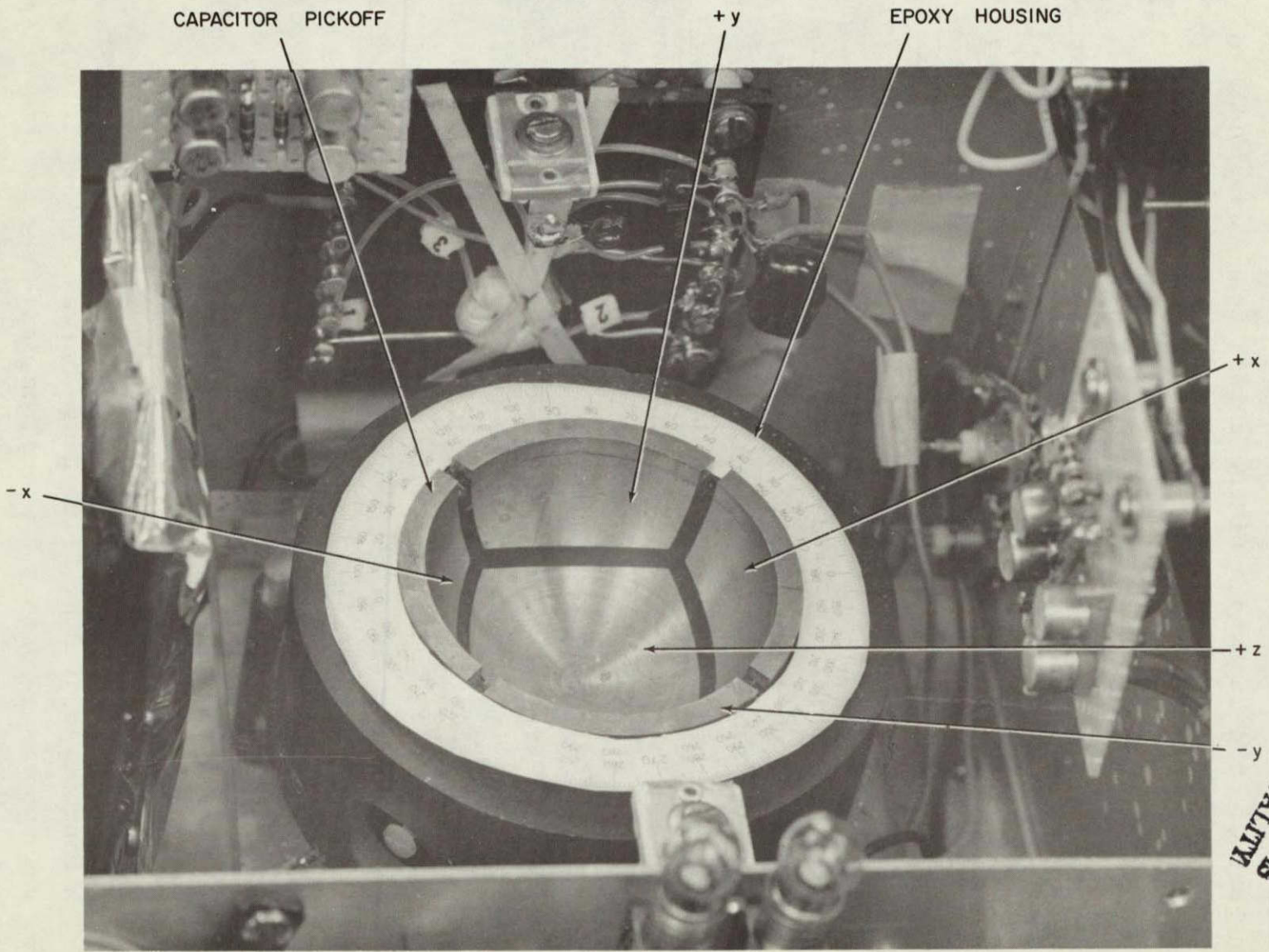
ORIGINAL PAGE IS
OF POOR QUALITY

Figure 81: Capacitance Pickoff for GEM Proofmass

Van Patten. The bandwidth of the thrust stand was 1500 Hz; measurement was accurate to a few micropounds, with resolution of a fraction of a percent during the build up and decay of the thrust. Quite good correlation was obtained between the measured thrust and high bandwidth measurement of the pressure just upstream of the throat. Hugo Schuck, formerly of Honeywell, Incorporated, made important contributions along with Chippendale to modelling these rapidly developing flows. The correlation of pressure and thrust was limited by inertia forces of the valve poppets.

All the studies so far described were with a capacitive pickoff and a spherical metal proofmass of 2 inch diameter. A limitation to capacitive pickoff is the relatively small gap between proofmass and cavity needed to have reasonable capacitive values. There is a tradeoff between capacitive requirements and the mass attraction between the proofmass and its surroundings. Mass attraction can be reduced by using a much larger cavity and some type of optical pickoff. Various optical schemes have been suggested. In 1975, under separate support, R. De Hoff built a fluorescent position detector for a 3 inch sphere inside an 8 inch diameter cylindrical cavity. A stroboscopic flash emits ultra-violet radiation, which is absorbed by the proofmass and re-emitted as infra-red to be measured on four horizontal Schottley barrier detectors in the cavity. The optical pickoff was coupled through a computer to a controller on the spinning simulator having a single gas jet only rather than the two pairs of opposed jets used with the capacitive pickoff.

(c) The Unsupported Gyroscope

A concept studied by B. O. Lange between 1963 and 1966 was the "unsupported gyroscope," where the drag-free proofmass it-self would be spun to make the gyroscope for a relativity mission. A gyro of this kind would be free of suspension and mass unbalance torques, to the level at least of the pickoff reaction force. Since there is only one drag-free mass only one gyro can be

operated unsupported, and it cannot be tested on Earth; nevertheless there is, as Lange emphasized, attraction in the simplicity of the concept. For a number of reasons Lange wanted to put the unsupported gyroscope in a rapidly spinning spacecraft.

Lange's proposal was for a room temperature gyroscope. Without superconducting shields the gyro would be exposed to the Earth's magnetic field or at least a field of 10^{-4} or 10^{-5} gauss obtained with conventional Mu-metal shields. If the spinning body were of metal it would be subject to the eddy current torques on a spinning conducting sphere first investigated by Maxwell[73] in 1855, and these would cause drifts much larger than the relativistic effect. If, on the other hand, the body were an insulator it would pick up stray electric charge and be subject to large electrostatic torques. Lange proposed the compromise of a semi-conductor. He calculated that eddy current torques on a silicon sphere might be reduced to an acceptable level in a Mu-metal shielded spacecraft.

With the room temperature unsupported gyroscope, as with the London moment gyroscope, the crucial problems are spin up and readout. For spin up Lange suggested an eddy current method similar to the one used by Honeywell in their room temperature electrically suspended gyros. This, of course, would be subject to problems like those discussed in Section C (2), of eddy current heating and the need to switch down the spin torque by some thirteen orders of magnitude. Room temperature operation makes the task of getting rid of heat easier than with the cryogenic gyroscope. Torque switching remains a severe problem, which was never explicitly faced by Lange; possibly the rolling of the spacecraft might help average the residual torque.

For readout Lange made the ingenious observation that since the support and mass unbalance torques on an unsupported gyroscope are negligible, the rotor does not have to be spherical. He therefore proposed putting a flat on the pole of one of the principal axes, from which the orientation could be read out by

means of an autocollimator attached to the reference telescope. An optical pick off of this kind could work to the resolution limit of the autocollimator, which might be in the range 0.1 to 0.01 arc-sec for conventional autocollimators, or much less for a Jones optical lever.[29] If the flat on the ball were considered objectionable one might try Everitt's suggestion (Section C (3) (a)) of a split quartz ball with a mirror at the equatorial plane and a semi-transparent metal surface coating, since this, like the semi-conductor, would be adequately free of eddy current torques.

The unsupported gyroscope, though free from mass unbalance torques, is subject to gravity gradient torques, and must have extremely small inertial differences if it is to be applied to a Gyro Relativity mission. A readout of the kind proposed by Lange must therefore overcome similar difficulties to those affecting conventional gyro readout, as discussed in Section C (3) (a). The flat has to be located at the pole of one of the principal axes of the ball, and the ball must be spun up about that axis. Two schemes were developed to achieve these requirements; they were tried out in the laboratory by Lange and his students on a spinning sphere mounted in an air bearing.

(i) Active damping: To make the ball spin about the right axis, B. Parkinson developed a method of applying eddy current torques during spin up in a way that would force the principal axis into the spin axis in a time short compared with the gyro's natural damping time.[74]

(ii) Laser mass rebalancing: To align the flat with the principal axis H. McKinely developed a mass rebalancer which fired a laser at the spinning ball to change the orientation of the inertial ellipsoid by removing small quantities of matter from the ball's surface.[75] The firings were timed by reference to the wobble in the mirror readout.

The combination of active damping and laser mass rebalance proved remarkably effective. However the resolution never

reached the level needed for a relativity experiment, and the directions of the principal axes tended to change with time and also to depend in a surprising degree on the temperature of the ball. This effect was investigated by W. Blanchard.[76] A change of a degree or so was enough to throw off the alignment of the flat.

Application of the room temperature unsupported gyroscope to the relativity experiment would mean solving the problems of instrumentation and telescope design reviewed in earlier sections of this report. Some but not all of the issues were discussed by Lange. He proposed a telescope with a wide angle readout based on a pyramidal image divider standing on a square quartz column. Mechanical actuators would keep the pyramid centered on the star image; an optical interferometer would be applied to measure lateral displacement of the column. Null shifts in the gyro and telescope readouts were to be averaged by rapid rotation of the spacecraft. The problems of matching and calibrating the readout gains and separating geodetic and motional relativity effects were not addressed by Lange.

The technical shortcomings of the room temperature unsupported gyroscope made us drop the idea, though particular difficulties might have been solved. However the notion of using a drag-free proofmass as a gyroscope, or conversely using one of the London moment gyroscopes for drag-free reference, remains intriguing and should be borne in mind in planning the final Gyro Relativity mission.

(d)   The DIsturbance COmpensation System (DISCOS) Program

Development of the DISCOS controller for the Navy's Transit Navigation Satellite TRIAD I was begun in 1968 under subcontract from Johns Hopkins Applied Physics Laboratory. The program was directed by D. B. DeBra. Simulation and studies of mass attraction disturbance on the proofmass were done mostly by A. Fleming and M. Tashker. Electronics design was by R. A. Van Patten and R. R. Clappier with support from M. Abelow on loan from Lockheed Missiles and Space Corporation.

Mechanical design was initiated by the late J. Mathiesen and carried on after his death by R. Hacker, also from Lockheed.

The design was for a satellite free from extraneous disturbances down to the level of 10^{-11}g. This goal was reached: in fact the measured in flight performance after correcting for initial errors was 5 x 10^{-12}g.

At 10^{-11}g mass attraction effects on the proofmass are of dominant importance. To separate the proofmass as far as possible from most of the satellite mass, the satellite was formed in three bodies (a TRIAD) joined by extendable booms, with the DISCOS a separate central package as illustrated in Figure 82. The top body contained the power supply; the bottom one the transmitter, receiver, telemetry and antenna. The satellite weighed 86.6 kg. It was launched in a collapsed form; roughly a cylinder 1.6 m high, 0.75 m diameter. In orbit both booms were extended 2.7 m. Besides minimizing the problems of controlling mass attraction asymmetries on the proof mass the TRIAD configuration provided simple passive gravity gradient stabilization. A small spinning wheel was included in the spacecraft to enforce 3-axis stabilization relative to a locally level system of coordinates.

The proofmass was 22 mm in diameter, placed in a 40 mm diameter cavity. It was made of a 70/30 gold-platinum alloy and weighed 110 gm, or 0.0013 of the satellite mass. The alloy was chosen for its high density and nearly zero magnetic susceptibility. The cavity contained three mutually perpendicular pairs of electrodes to sense the position of the proofmass by three capacitance bridges: the three signals were used in a control loop to fire three corresponding pairs of gas jets. In orbit the proofmass floated in the cavity with a 9 mm clearance. It was permitted to move over a deadband of ± 0.9 mm before the valves were fired, which meant establishing a specification of 10^{-11} g/mm for the gradient of the disturbing forces. A caging mechanism was provided to force the proof mass against one end of the housing during launch.

343

ORIGINAL PAGE IS
OF POOR QUALITY
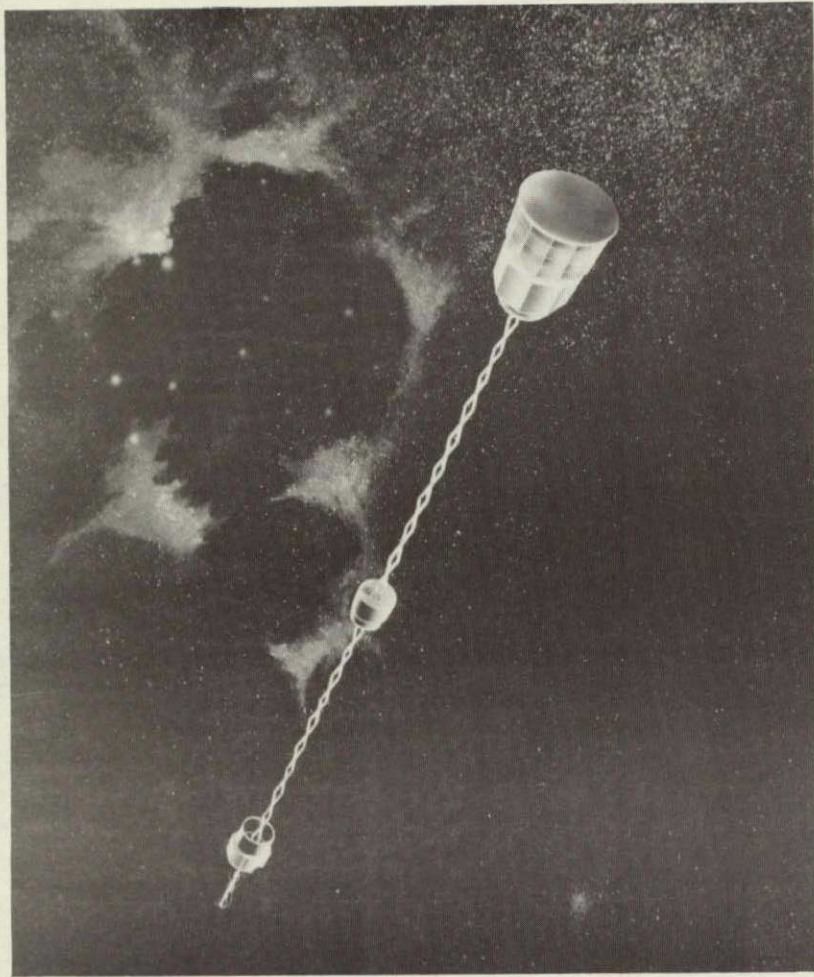
(a) Artist's Impression
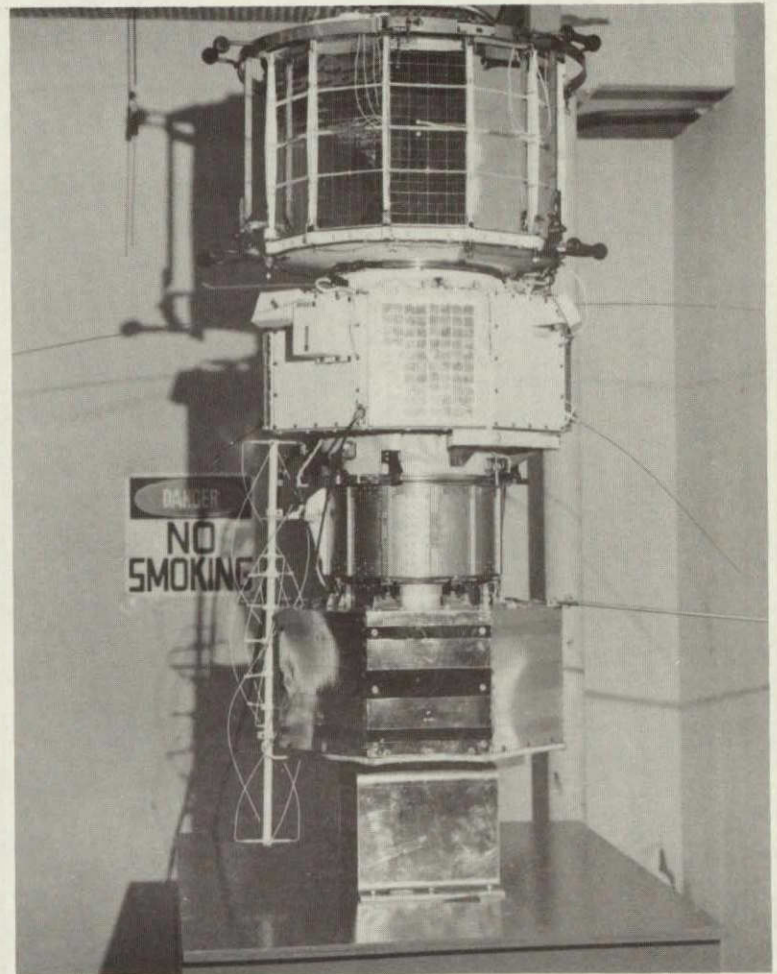
(b) Flight Hardware

Figure 82:   The TRIAD Satellite

Figure 83 (a) illustrates the DISCOS control system designed by Stanford including the pickoff, a complete propulsion system, and the electronics to control it and interface with the rest of the satellite. The functional diagram is shown in Figure 83 (b). All parts of the satellite not essential to the control system were located in the two bodies at the ends of the booms. In the final configuration the contribution to mass-attraction uncertainty from the two end bodies was restricted to a few percent without unusual fabrication tolerance or accuracy in determining mass properties.

Not surprisingly the mass distribution in parts closest to the proofmass required most attention. The beryllium oxide housing for the proofmass had to be allotted a share of the error budget five times larger than any other single component. Initially the housing represented 40% of the mass attraction error budget, but we were unable to obtain material of adequate density homogeneity to meet even this figure, and were forced to redistribute the error budget after the initial specifications had been written out.

Mass attractions of DISCOS components were calculated with great precision. With the regulator, for example, terms up to the third moment of mass were included in an expansion about the regulator mass center. The first and second moment terms were found experimentally by measuring the mass and the six elements of the moment of inertia. The third moment had to be calculated from drawings of the component parts and weights determined during assembly. The location of the regulator involved an accumulation of tolerances from the pickoff housing through the upper support tube, the top lid, and the propulsion subsystem. Fabrication tolerances in the structure as tight as 0.5 mil were required to model the mass attraction adequately. Similarly fabrication tolerances of measurements of 0.1 mil were required in the pickoff housing and thickness measurement of the propellant tanks. Finally a compensation mass was added immediately

PROPULSION
SUBSYSTEM

PROOF MASS
HOUSING

PROOF MASS

CAGING
MECHANISM
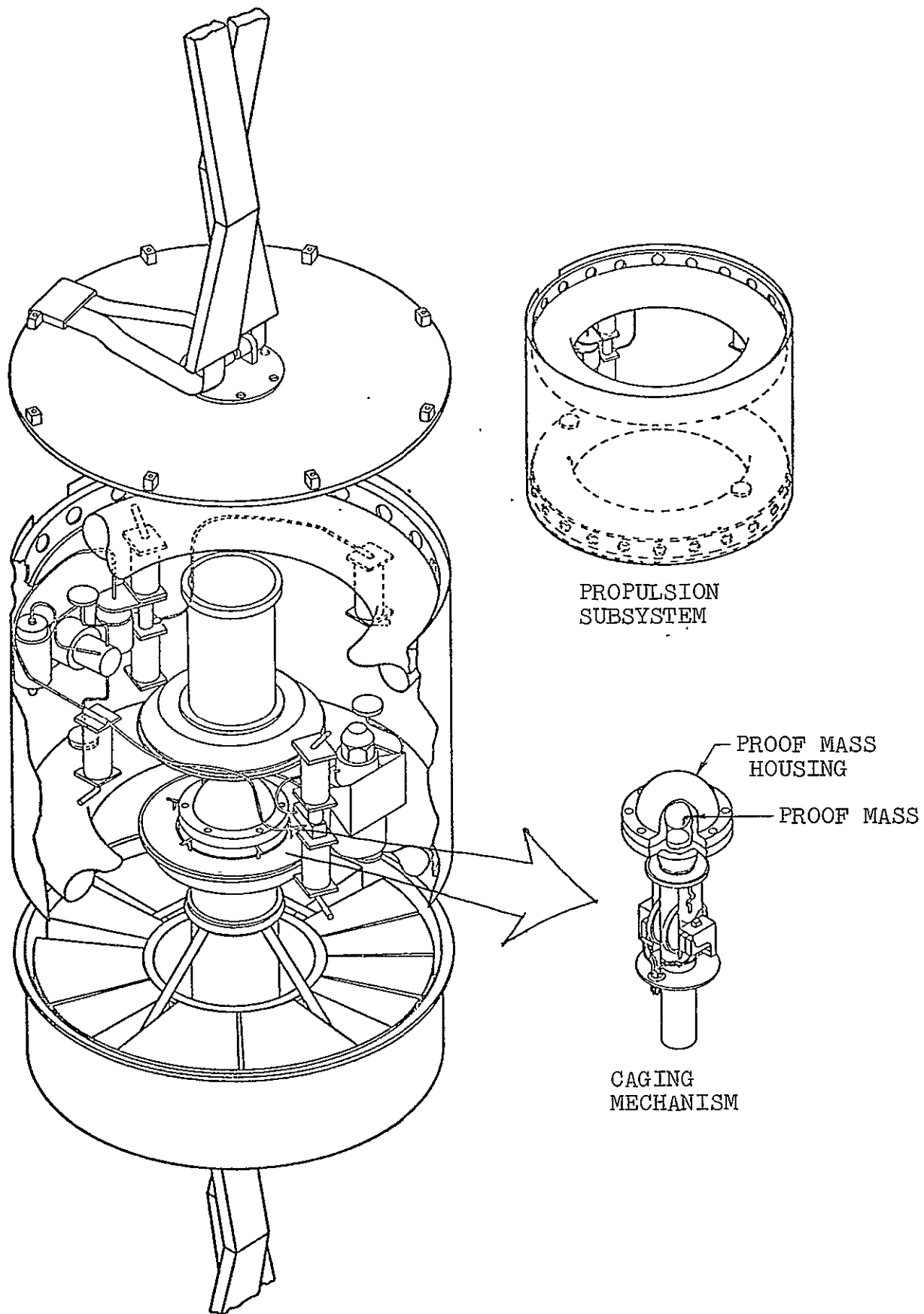
Figure 83:   the DISCOS Control System

above the pickoff housing. The residual attraction before compensation was calculated as 83.6×10^{-11}g in the vertical direction and only 0.8×10^{-11}g in the more sensitive "along-track" direction. With the compensating mass the maximum disturbances were calculated to be 2×10^{-11}g normal to the orbit plane and 0.7×10^{-11}g along track.

The propulsion subsystem was a conventional "cold-gas" propulsion system. However to satisfy the mass-attraction requirement it was necessary to have two toroidal propellant tanks, placed equidistant on opposite sides of the proofmass in a configuration making the gravitational analog of a pair of Helmholtz coils. Without some such arrangement there would have been changes in the mass center, center of attraction or mass attraction gradient of the propellant as the propellant mass decreased with time. Also the temperature differences across the propellant tanks had to be held below 2°C to prevent gas redistribution from compromising the mass attraction specification.

Electric and magnetic forces were kept to much lower values than the mass attraction forces. Radiation pressure due to temperature differences in the pickoff housing was kept small by the choice of beryllium oxide as the insulator. Beryllium oxide is unique among insulators in having excellent thermal conductivity.

The entire DISCOS including its electronics, some telemetry and common electronics also housed in the DISCOS package weighed 10.6 kg and consumed less than 3W power. It was expected to operate for over a year before the propellant was depleted, and that expectation was realized.

The satellite was launched on September 2, 1972. It was intended to be placed in a near circular orbit ($\varepsilon = 0.006$) at an average altitude of 874 km. Because of a malfunction of the launch vehicle guidance the actual orbit had an average altitude of 788 km but the correct eccentricity. The difference had no

significant effect on the DISCOS experiment. A failure in the satellite telemetry system two months after launch drastically reduced the aeronomy data because the signals giving the proof-mass position were lost; however telemetered DISCOS data included for each of the six thrusters the accumulated on-time in every four minute interval and from this in combination with tracking data much useful information was still to be had.

Figure 84 illustrates a sample of vector ball position data before the telemetry failure. The discontinuities in the parabolas correspond to thruster firings. From the velocity discontinuities, the thrusters could be calibrated in orbit. The thruster on-time data included one day when the sun was nearly normal to the orbit plane. In these conditions the radiation pressure and drag forces were nearly orthogonal. The data revealed three interesting features:

(i)   the drag force was on the average only 20% as large as the radiation pressure

(ii)   the drag force, consistent with the Jacchia model[77] and the polar orbit, had a strong orbital frequency component

(iii) surprisingly there was a large radial bias.

The last observation triggered an intensive search for the source of bias, the most likely cause being a displacement of the center of mass of the satellite from the center of the proofmass cavity. A 1 cm maladjustment in one of the boom lengths would have been enough to account for the bias. Had the telemetry not failed it would have been removed by adjusting the boom lengths in orbit.

TRIAD tracking experiments were carried out for both short arc predictions with time spans of two to three weeks and long arc predictions with time spans up to several months. The main effect of an unmodelled along track bias is a quadratic growth of the navigation error, amounting to about 110 meters in 10
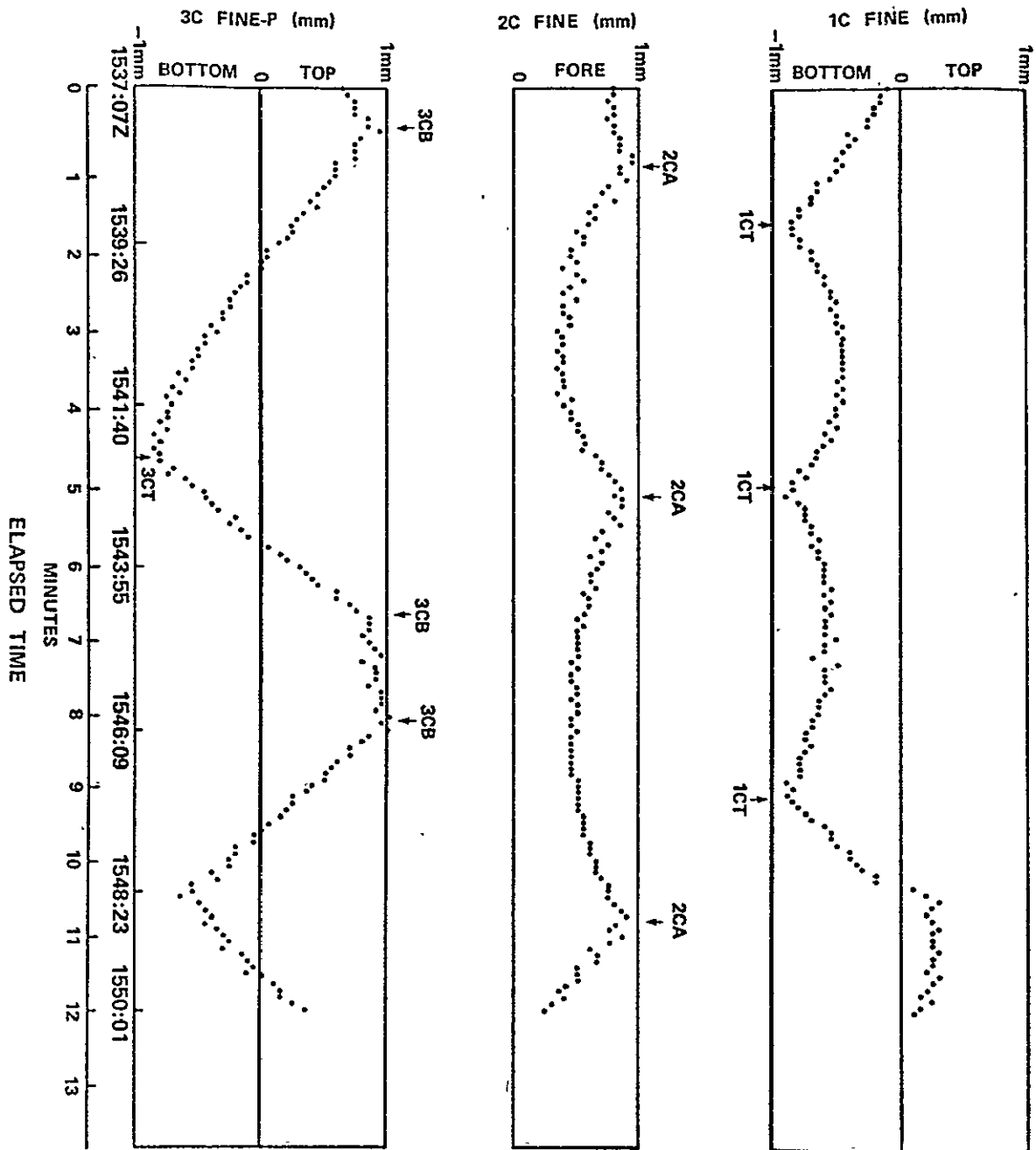
Figure 84: DISCOS Proofmass Position Data, Day 257

days for a self-bias force of $10^{-11}g$. Four different problems had to be solved to improve the results and reliably estimate the DISCOS self-bias force:

(i)   correct errors in the Earth-gravity zonal harmonics

(ii)   correct certain resonant non-zonal harmonics

(iii)   correct for differences in rate between the two universal times UT1 and UTC.

(iv)   correct errors in the numerical integration process used to generate the ephemeris

Data and details are given in Reference (78). The final results showed no evidence of an along track bias force greater than about $5 \times 10^{-12}g$.

L.   CONCLUSION AND MISSION DEFINITION STUDIES

The work described in this Final Report on NASA Grant 05-020-019 completes the conception and underlying technological development of the Gyro Relativity experiment. Important tasks remain to be done, but we can now say as we could not have done earlier that clear <u>paths</u> can be seen ahead in all of them.

The first Mission Definition Study was undertaken by Ball Brothers Research Corporation in cooperation with Stanford in the period August through December 1971. At that time the program was far less developed than it now is: the gyro had not even been levitated and spun, let alone read out, and there were many uncertainties about liquid helium in space. Accordingly BBRC recommended a three-phase program in which the final 1 milliarc-sec Relativity mission would be preceded by two test flights, the first to demonstrate dewar technology and the second to demonstrate and evaluate gyro performance in space. The overall cost of the three flight program including prototype hardware, launch costs and a complete backup experiment was estimated at 60 million 1971 dollars. The flight would last one year.

The second Study "Mission Feasibility for Stanford Experiment on Scout,"[61] completed in June 1973, was aimed at

developing a mission inexpensive enough to be considered for
flight under the Explorer program. Building on experience
and fresh thought since 1971 we suggested replacing the test
flights of the first study by a Relativity mission of lower
accuracy than finally desired, probably given about 0.1 arc-sec/
year, that is, a 1% measurement of the geodetic term. A mission
of this kind could be performed in an experiment lasting about
four months, launched on Scout in the 37° minimum energy orbit
from Wallops Island. The altitude would be 300 nautical miles.
The satellite would not have a drag-free controller, but advan-
tage would be taken of averaging effects in the aerodynamic
drag, which were by that time better understood.[25] The Study
confirmed the feasibility of a Scout Mission, although the
weight margin of 3% on a 170 kg spacecraft was thin. The cost
was estimated by Ball Brothers Research as $10.4 million 1973
dollars. The Scout Mission was to be followed at a later period
by a full-accuracy 1 milliarc-sec mission lasting one year.

Some dissatisfaction was felt with the concept of designing
large parts of the Gyro Relativity experiment twice over, once
for Scout and once for the final all-up mission. This, together
with the slender weight margin on Scout as well as doubts that
existed in some minds (not ours) concerning the realism of BBRC
price estimates led to the third study "Mission Definition for
a Relativity Explorer for the Stanford Relativity Experiment,"[79]
completed in November 1975. This compared a number of approaches
with either Shuttle and Delta launch to a two flight mission
in which the first flight would obtain relativity data of the
20 milliarc-sec/year level and the second at or below 1
milliarc-sec/year, with and without recovery of the first
spacecraft. The price estimate for the first flight was
estimated at $24.06 million 1975 dollars, with the relatively
small addition of about $8 million for a re-flight.

In November 1975 in response to NASA AO-6 we submitted a
proposal for a Phase B study of a first flight at the 20

milliarc-sec level assuming Shuttle or Delta launch and a price
of $25.5 million. The proposal was given a Category 3 rating
as being of high scientific importance but not yet ready for
a New Start.

We are continuing to study flight plans for the experiment
in cooperation with NASA Marshall Center and industry.

REFERENCES

(1) A. D. Fokker, Proc. Kon. Akad. Weten (Amsterdam) 23, 729 (1920).

(2) L. I. Schiff, Proc. Nat. Acad. Sci. 46, 871 (1960); Phys.
     Rev. Lett. 4, 216 (1960).

(3) G. E. Pugh, WSEG Research Memorandum No. 11, Weapons
     System Evaluation Group, The Pentagon, Washington 25 D.C.
     (November 12, 1959).

(4) W. M. Fairbank and L. I. Schiff, "Proposed Experimental
     Test of General Relativity," Letter to Dr. Abe Silverstein,
     NASA Office of Space Flight Programs dated January 27, 1961.

(5) A. F. Hildebrandt, Phys. Rev. Lett. 12, 190 (1964); M. Bol
     and W. M. Fairbank, Proceedings of the IX International
     Conference on Low Temperature Physics (New York 1965), 451;
     A. King, Jr., J. B. Hendricks and H. E. Rohrschach, Ibid, 466.

(6) M. Bol, B. S. Deaver, W. M. Fairbank, "Quantized Magnetic
     Flux in Superconducting Cylinders," Proceedings of the 8th
     International Conference on Low Temperature Physics LT8
     (R. O. Davis, ed. London 1962), 116.

(7) T. Dan Bracken and C. W. F. Everitt, Adv. Cryo. Eng. 13, 168
     (1968); Stanford University unpublished memorandum 1968,
     "Design of a Gas Spin Up System for an Electrically Sus-
     pended Cryogenic Gyroscope."

(8) C. W. F. Everitt in Experimental Gravitation (B. Bertotti,
     ed. New York Academic Press 1974), 331 - 358.

(9) B. M. Barker and R. F. O'Connell, Phys. Rev. Lett. 20, 69
     (1968); Phys. Rev. D2, 1428 (1970).

(10) D. C. Wilkins, Ann. Phys., 61, 277 (1968); Stanford University
     Ph.D. thesis "Topics in Spinning Bodies in General Relativity,"
     (August 1972).

(11) P. M. Selzer, W. M. Fairbank and C. W. F. Everitt, "A
     Superfluid Plug for Space," Adv. Cryo. Eng. 16, 277 (1970).

(12) Ball Brothers Research Corporation, "Mission Definition
     Study for the Stanford Relativity Satellite (BBRC Report
     F71-07 December 1971),

(13) J. T. Anderson and C. W. F. Everitt, "A High Accuracy All-
     Angle Gyroscope Readout Using Quantized Flux," IEEE Trans.
     on Magnetics MAG-13, 377 - 380 (1977).

(14) See "Ninth Semi-Annual Status Report on the Physics
      Portion of a Research Program to Develop a Zero-g
      Drag-Free Satellite and to Perform a Gyro Test of
      General Relativity in a Satellite," Stanford University
      Physics Department, May 1968.

(15) J. S. Bull, "Precise Attitude Control of the Stanford
      Relativity Satellite," Stanford University Center for
      Systems Research, Guidance and Control Laboratory Report
      SUDAAR No. 452, March 1973.

(16) See "Eighth Semi-Annual Status Report on the Physics Portion
      of a Research Program to Develop a Zero-g Drag-Free
      Satellite and to Perform a Gyro Test of General Relativity
      in a Satellite," Stanford University Physics Department,
      November 1967; also Reference (18).

(17) See Reference (14) Section F.

(18) Annual Report for the year 1971 to 1972 on a Program to
      Perform a Gyro Test of General Relativity in a Satellite
      and Develop Associated Control Technology (Stanford
      University, November 1972) Section K.

(19) See Appendix 1.

(20) B. M. Barker and R. F. O'Connell, Phys. Rev. D6, 956 (1972).

(21) C. W. F. Everitt, "Commentary on a Paper by B. M. Barker
      and R. F. O'Connell 'Effects of the Gyro's Quadrupole
      Moment on the Relativity Gyroscope Experiment' with a
      Review of the Significance of Gravity-Gradient Torques
      in Different Versions of the Experiment," Stanford Univer-
      sity Memorandum September, 1974. The Barker-O'Connell
      paper was published in Phys. Rev. D11, 711 - 715 (1975).

(22) C. W. F. Everitt, W. M. Fairbank and W. O. Hamilton, "From
      Quantized Magnetic Flux in Superconductors to Experiments
      on Gravitation and Time Reversal Invariance," in Magic
      without Magic (J. R. Klauder, ed., W. H. Freeman, San
      Francisco 1972), 217.

(23) J. R. Nikirk, "Fabrication of an Electronic Suspension
      Subsystem (ESS) for a Cryogenic Electrostatically Suspended
      Gyroscope for the Relativity Experiment," Final Report on
      NASA Contract NAS8-27333 Stanford University Center for
      Systems Research Guidance and Control Laboratory, January 1973.

(24) C. W. F. Everitt, "The Stanford Gyroscope Experiment,"
      Proceedings of the Conference on Experimental Tests of
      Gravitation Theory, (JPL Technical Memorandum 33 - 499,
      R. W. Davies, ed.), 68 - 81.

(25) Status Letter for March 1973 on the Stanford Gyro Relativity Experiment, W. W. Hansen Laboratories of Physics, dated April 3, 1973.

(26) Final Report on NASA Contract NAS12-542, "Research in Electrically Supported Vacuum Gyroscope," Vol. 2 - Electric Torque on an ESVG, November 1968.

(27) G. R. Karr, "Prediction of Initial Spin Up Torque Using the Theoretical Approach Developed by G. R. Karr," University of Alabama, Huntsville, Memorandum February 1977.

(28) J. C. Maxwell, Scientific Papers, Vol. 1, 257, 262, Treatise on Electricity and Magnetism, Vol. 2, Sec. 575. See a letter from C. W. F. Everitt to A. R. Berg of Honeywell Incorporated, dated February 27, 1964 and Mr. Berg's reply dated March 4, 1964.

(29) R. V. Jones and J. C. S. Richards, "Recording Optical Lever," J. Sci. Inst. 36, 90 (1959); See also R. V. Jones, Ibid 38, 37 - 45 (1961).

(30) J. E. Opfer, "Modulated Inductance Magnetometers," Rev. de Phys. Appliquée 5, 37 (1970).

(31) See Reference (8) Section 3.6.

(32) J. B. Hendricks, "A SQUID Readout System for a Superconducting Gyroscope," IEEE Transactions in Magnetics MAG11, 712 - 715 (1975). For futher comments on the direct-coupled readout see J. T. Anderson, "Preliminary Feasibility Study of the Direct SQUID," Stanford University Memorandum, dated November 20, 1976.

(33) Gail A. Massey and Anthony E. Siegman, "Fresnel Drag Technique for Determining the Spin-Axis Orientation of a Spherical Rotor," IEEE Journal of Quantum Electronics, Vol. QE-6, 500 - 506 (1970).

(34) J. C. Maxwell, Rep. Brit. Ass. 34, 192 (1864) correction E.

(35) See Reference (13).

(36) R. C. Spragg and D. J. Whitehouse, Proc. Inst. Mech. Engrs. 182, 397 - 405 (1968).

(37) G. J. Siddall and D. G. Chetwynd, "Improving the Accuracy of Roundness Measurement," J. Phys. E: Sci. Instrum. 9, 537 - 544 (1976).

(38) R. R. Donaldson and L. Bowen. See J. Bryan, R. Clouser and E. Holland, Am. Mach. Spec. Report No. 612, 149 - 164 (1967) and R. R. Donaldson, CIRP Annals 21, 125 - 126 (1973).

355

(39) See Reference (16) page 3.

(40) P. Peters, L. B. Holdeman and J. B. Hendricks, "Large
      Diameter SQUIDs," paper presented at the Applied Super-
      conductivity Conference, Stanford University August 1976.

(41) P. M. Selzer and W. M. Fairbank, "Thermally Generated
      Magnetic Fields in an Anisotropic Crystal at Low Tempera-
      tures," Phys. Lett. 48A, 279 (1974)

(42) J. A. Lipa, J. R. Nikirk, J. T. Anderson and R. R.
      Clappier, "A Superconducting Gyroscope for Testing
      General Relativity," Low Temperature Physics LT-14
      (Matti Krusius and Matti Vuorio, ed., North Holland/
      American Elsevier 1975), Vol. 4, 250 - 253.

(43) B. Cabrera, Stanford University Ph.D. Thesis, "The Use
      of Superconducting Shields for Generating Ultra-Low
      Magnetic Field Regions and Several Related Experiments,"
      77 - 83 (March 1975).

(44) Ibid, 26 - 32.

(45) Ibid, 180.

(46) Ibid, 115 - 116.

(47) R. A. Nidey, Memorandum to C. W. F. Everitt, dated
      October 21, 1968.

(48) NASA Contract No. NAS8-32605, "Cryogenic Experiments in
      Space."

(49) J. B. Murgatroyd and R. F. R. Sykes, J. Soc. Glass Tech.
      31, 17 (1947).

(50) G. O. Jones, "The Determination of the Elastic Properties
      of Glass at Temperatures below the Annealing Range,"
      J. Soc. Glass. Tech. 28, 432 - 462 (1944). See also
      the same author's Glass (Methuen, London 1963).

(51) See Reference (12) Section 5.1.

(52) NASA Contractor Report NASA CR-61385, "A Theoretical
      Study of Optical Contact of Fused Silica, T. D. Barber,
      April 21, 1972, NASA George C. Marshall Space Flight
      Center.

(53) J. A. Lipa, C. W. F. Everitt, W. M. Fairbank, "Research
      at Stanford on the Containment of Liquid Helium in Space
      by a Porous Plug and on a Long Hold-Time Dewar for the
      Gyro Relativity Experiment," paper presented at the
      NASA Cryogenic Workshop, NASA George C. Marshall Space
      Flight Center, March 29-30, 1972. Note the paper presented
      in the Workshop Proceedings, edited by C. C. Wood, 1972,
      is an abridgement of the original document.

(54) E. W. Urban, L. Katz, G. R. Karr, "Helium Flow Through and
      Vapor Separation by Porous Plugs," Low Temperature Physics
      LT-14 (Matti Krusius and Matti Vuorio, ed., North Holland/
      America Elsevier 1975) Vol. 4, 37 - 40.

(55) W. B. Davis, Ball Brothers Research Corporation Report
      F75-20 "Helium Dewar Technology Study," Final Report on
      NASA Contract NAS8-29848, October 1975.

(56) P. Mason, T. Collins, D. Petrac, T. Yang, F. Edeskuty and
      K. Williamson, "Experiments on Properties of Superfluid
      Helium in Zero Gravity," Proceedings of the Sixth Inter-
      national Cryogenic Engineering Conference, Grenoble, France,
      1976, 272 - 277.

(57) A. Elsner, Adv. Cryo. Eng. 18, 141 (1973).

(58) Ball Brothers Research Corporation "Dewar Test Flight
      for Stanford Relativity Experiment," Unsolicited Proposal
      to NASA Headquarters February 4, 1972. Section 3.2.2.

(59) M. Ledinegg, Die Warme 61, 891 (1938); See also B. A.
      Hands, "Pressure Drop Instabilities in Cryogenic Fluids,"
      Adv. Cryo. Eng. 20, 355 - 369 (1977).

(60) A. J. Witsmeer, "Preliminary Design Studies of Attitude
      Control Systems for the Stanford Relativity Satellite,"
      Stanford Center for Systems Research Guidance and Control
      Laboratory Report SUDAAR No. 337, January 1968.

(61) D. P. Chandler, Memo to C. W. F. Everitt, October 1967.

(62) Ball Brothers Research Corporation "Mission Definition
      Study for the Stanford Relativity Satellite on Scout,"
      Final Report on NASA Contract NAS8-29567, June 22, 1973.

(63) Reference (15) Section 3D.

(64) Zeev Hadass, "Design of State-Feedback Controllers Including
      Sensitivity Reduction, with Application to Precision
      Pointing," Stanford University Center for Systems Research,
      Guidance and Control Laboratory Report SUDAAR No. 482,
      August 1974.

(65) Conference on Experimental Tests of Theories of Relativity,
      Stanford University July 20 - 21, 1961 (R. T. Jones, ed.,
      NASA publication), page iv.

(66) B. Lange, "The Control and Use of Drag-Free Satellites,"
      Stanford Unviersity Center for Systems Research, Guidance
      and Control Laboratory Report SUDAER No. 194, June 1964.

(67) R. H. Cannon, B. O. Lange and J. F. MacDonald, "Proposal
      to Develop and Operate a Sustaining Earth Satellite in
      Two Orbital Flights," submitted to NASA Headquarters,
      February, 1966.

(68) W. R. Davis, "Control of the Relative Motion Between
      Satellites in Neighboring Elliptic Orbits," Stanford
      University Center for Systems Research, Guidance and
      Control Laboratory Report SUDAAR No. 274, May 1966.

(69) P. Jhin, "Control of a Spinning Drag-Free Satellite to
      Reduce Trajectory Errors Due to Mass Attraction," Stanford
      University Department of Aeronautics and Astronautics
      SUDAAR Report No. 408, August 1970.

(70) M. G. Tashker, "Integral Control of a Spinning Drag-
      Free Satellite," Stanford University Center for Systems
      Research, Guidance and Control Laboratory Report SUDAAR
      No. 472, April 1974.

(71) D. B. DeBra, J. Mathiesen and R. A. Van Patten, "A
      Precision, Active, Table Leveling System," J. of Space-
      craft and Rockets, September 1968, 1040 - 1045.

(72) U. Passy, "Simulation and Optimization Studies of Drag-
      Free Satellite, Ph.D. Dissertation, Stanford University
      Department of Chemical Engineering, SUDAAR No. 295,
      November 1966.

(73) J. C. Maxwell, Trans. Camb. Phil. Soc. 10, 1 (1856)
      Part II, Example XII; Scientific Papers, Vol. 1, 226 - 229.

(74) B. W. Parkinson and B. O. Lange, "The Active Damping of
      Free-Rotor Gyroscopes During Initial Spin-Up," Stanford
      University Center for Systems Research, Guidance and
      Control Laboratory Report SUDAAR-263, June 1966.

(75) H. L. McKinley, Jr., "The Stability and Control of the
      Principal Axes of Inertia of Almost Spherical Bodies,"
      Stanford University Center for Systems Research, Guidance
      and Control Laboratory Report SUDAAR No. 325, February 1968.

(76) W. N. Blanchard and B. Lange, "The Readout-Axis Stability
      of Elastic, Nearly Spherical Gyro Rotors," Stanford
      University Center for Systems Research, Guidance and
      Control Laboratory Report SUDAAR No. 431, September 1971.

(77) L. G. Jacchia, "Static Diffusion Models of the Upper
      Atmosphere with Empirical Temperature Profiles,"
      Smithsonian Contributions to Astrophysics, 8, No. 9 (1965).

(78) The Staff of the Space Department, Johns Hopkins Applied
      Physics Laboratory, and the Staff of the Guidance and
      Control Laboratory, Stanford University, "A Satellite
      Freed of All but Gravitational Forces: TRIAD I," AIAA
      12th Aerospace Sciences Meeting, January 1974. AIAA
      Paper No. 74-215, July 1974.

(79) Ball Brothers Research Corporation Report F75-12; "Mission Definition for a Relativity Explorer for the Stanford Relativity Experiment," October 1975.

APPENDIX I: Wilkins' Method for Evaluating the Precession of a Gyroscope
               in Orbit Around the Oblate Earth

(1) INTRODUCTORY

In 1969 R. F. O'Connell[1] and D. C. Wilkins[2] independently found

that the Earth's quadrupole mass moment the "equatorial bulge" would modify

the geodetic precession of the gyroscope predicted by Schiff by an amount

of about 10^{-2} arc-sec/year -- a factor of ten higher than the expected

measurement limit of the Gyro Relativity experiment.   The initial inves-

tigations gave the magnitude of the quadrupole precession angular velocity

at any point in space. For comparison with experiment, however, what is

needed is not just the angular velocity but its time integral. The angular

velocity depends on the field and the velocity as

$$v \times g$$

where v is the velocity with respect to the Earth's center of mass. Because

of the bulge the gyro does not follow an exact Keplerian ellipse, so we are

faced with the task of integrating a complicated vector function over time.

Wilkins' procedure applies a first order perturbation method due to

Geyling.[3]   This approach has substantial advantages over one using

Lagrange's planetary equations: a) it avoids the complication of converting

the orbital elements to rectangular coordinates, and b) it works for orbits

of small eccentricity -- the kind we are interested in.   To lowest order

the effects of eccentricity and Earth oblateness separate. An eccentricity

of 10^{-2} is several times more important than the bulge. The solution

developed below shows that even with the most accurate currently available

Earth-nodel, the approximations prevent us from calculating the orbit to

sufficient accuracy for more than a few days at best. Thus tracking

information on the position and velocity of the satellite is required in

evaluating the effects.

(2) WHAT EFFECTS ARE IMPORTANT?

The contribution of the Earth to the rate of precession of a gyroscope[4] is represented by the angular velocity

$$\underline{\Omega} = \underline{\Omega}_G + \underline{\Omega}_M$$

$$= \frac{3}{2c^2} (\underline{v} \times \underline{g}) + \frac{1}{r^3} \left[\frac{3(\underline{L} \cdot \underline{r}) \underline{r}}{r^2} - \underline{L} \right]$$

where $\underline{L}$ is $\frac{G}{c^2}$ times the Earth's spin angular momentum, and $\underline{r}$ is the satellite position relative to the Earth's center of mass. For a satellite in orbit for one year, the first term, "omega-geodetic," causes a drift of 7 arc sec, while the second, "omega mass-current," causes only 0.05 arc sec drift.

To ascertain the size of effects from higher multipole moments, we expand the potential in zonal harmonics[5]

$$V = \frac{GM}{r} \left\{ 1 - \sum_{n=2}^{\infty} J_n (R/r)^n P_n (\cos \theta) \right\}$$

where $GM = 3.98601 \times 10^{20}$ cm^3 sec^{-1},

$R = $ radius $ = 6.37816 \times 10^8$ cm.,

$J_2 = 1082.6 \times 10^{-6}$,

and the higher harmonics are at most of order 10^{-6}.

It is reasonable to suppose that if an acceleration of magnitude g_o produces some deviations in position in a given time, than a smaller force will produce a smaller deviation in proportion to its magnitude. This

being so we expect that the nth harmonic will produce an effect smaller
than the zeroth (of magnitude 7 arc-sec/year) by roughly

$$J_n \, (R/r)^n \quad .$$

Thus, over a single orbit, only the quadrupole moment should make a
measurable contribution, of magnitude ~ 0.01 arc-sec. If we considered
the mass-current term alone, then even the quadrupole moment becomes
unimportant. If the eccentricity is a few percent or less, we can "smooth
out" the time orbit to a Keplerian ellipse. Suppose the resulting ellipse
has semi-major axis a, normal $\hat{w}$, and an arbitrary inclination to the
equator. To first order in the eccentricity, the angle of drift after
one complete orbit can be found by a straightforward integration:

$$\oint \underline{\Omega}_M \, dt \; = \; \frac{\pi}{(GM \, a^3)^{1/2}} \; [\, \underline{L} - 3 \, \hat{w} \, (\underline{L} \cdot \hat{w})] \quad .$$

After a number of orbits the higher moments make their presence felt
through secular deviations in the orbit. We will discuss this problem
in the last section.

Non-gravitational perturbations such as radiation pressure or atmospheric
friction do not effect this "drag-free" satellite. The satellite senses
the position of the gyro ball and avoids bumping into it by means of gas
jets; thus permitting the ball to follow a true geodesic. Unfortunately,
the gyroscope responds also to the gravitational attractions of the satellite
itself. In the experiment planned this "self-gravitational" acceleration
will not pose a problem since it will amount to no more than 10^{-9} g.

(3) SOLUTION OF PROBLEM

Euler's theorem[6] tells us that a sequence of rotations is equivalent to a single rotation. Let us represent the exact angular drift of the gyroscope axis by $\underline{\varphi}$. The direction of $\underline{\varphi}$ is the axis of rotation and its magnitude gives the angle of rotation under the right-hand rule. In spite of the rotation, $\underline{\varphi}$ is not a true vector (in contrast to the axial vector $\underline{\Omega}$) since it doesn't obey vector addition. We can write

$$\underline{\varphi}(t) = \int_0^t \underline{\Omega}(t)\, dt + \underline{\epsilon}(t) \tag{1}$$

where $\underline{\epsilon}$ gives the error. An argument developed elsewhere

$$\epsilon \leq \left[\frac{\sin \alpha}{4} \left(\int_0^t |\underline{\dot{\Omega}}|\, dt \right)^2 \right] \tag{2}$$

where α denotes the largest angle (i.e. closest to 90°) that the direction of $\underline{\Omega}(t)$ shifts through. For example, when $\underline{\Omega}(t)$ does not change direction, $\alpha = 0$, and (2) says there is no error, which we know to be correct. For the gyroscope in orbit one year,

$$\int_0^{1\ yr.} |\underline{\Omega}(t)| = 3 \times 10^{-5} \ ,$$

so that the fractional error is still less than the experimental uncertainty of 10^{-4} .

We wish to evaluate $\underline{\varphi}$ for a single orbit. The method, due to Geyling, is as follows: set up an imaginary circular orbit ("nominal orbit")

which well approximates the actual trajectory. The position of
the satellite is then given by its rectangular coordinates (u,v,w) relative
to the position, O'(t), which the satellite would have had on the circular
orbit had no perturbation been acting. By the term "perturbation," we also
include initial conditions of position or velocity which would have led to
deviations from the nominal orbit.

The nominal orbit has radius r_c , is inclined to the equator at an
angle i , and θ is the angle from the node to O' . $\hat{u}$ points radially
outward, $\hat{w}$ is normal to the plane of the orbit, and $\hat{v}$, which points in
the direction of the unperturbed motion, complete the triad.

We are interested in determining

$$\int \Delta (\underline{v} \times \underline{g}) \, dt,$$

where, with subscript "o" denoting unperturbed motion,

$$\Delta (\underline{v} \times \underline{g}) = (\underline{v} \times \underline{g}) - (\underline{v} \times \underline{g})_o \quad ,$$

both terms on the right being evaluated at the same time.
To first order,

$$\Delta (\underline{v} \times \underline{g}) = \underline{\Delta v} \times \underline{g}_o + \underline{v}_o \times \underline{\Delta g}$$

$$= \underline{\Delta v} \times \underline{g}_o + \underline{v}_o \times \frac{d}{dt} \underline{\Delta v} \quad .$$

Define the quantity $\underline{I}$:

$$\underline{I} = \int \left[\underline{\Delta v} \times \underline{g}_o + \underline{v}_o \times \frac{d}{dt} (\underline{\Delta v}) \right] dt \quad .$$

We proceed to determine a general expression for I in terms of the deviation, (u, v, w). First we put

$$\underline{v}_o = V_o \; \hat{v}$$

$$\underline{g}_o = - g_o \; \hat{u} = - V_o \; \dot{\theta} \; \hat{u} \tag{3}$$

(The V_o is to be distinguished from v_o to be introduced later.)
Set

$$\underline{\Delta r} = u \cdot \hat{u} + v \cdot \hat{v} + w \cdot \hat{w}$$

in order to find $\underline{\Delta v}$ and $\underline{\Delta g}$, we may not simply differentiate u, v, w. The $(\hat{u}, \hat{v}, \hat{w})$ system is rotating relative to an inertial frame with angular velocity

$$\underline{\omega} = \dot{\theta} \; \hat{w} \quad . \; \left(\text{Thus } \frac{du}{dt} = \vec{w} \times \hat{u} \; , \text{ etc.}\right)$$

Thus, the time derivative of $\underline{\Delta r}$ as seen from an inertial frame is

$$\underline{\Delta v} = \frac{d}{dt} \left(\underline{\Delta r}\right) + \underline{\omega} \times \underline{\Delta r} \quad .$$

where $\hat{u}$, $\hat{v}$, $\hat{w}$ are treated as time-independent in the first term
$\underline{\Delta g}$ is then obtained from $\underline{\Delta v}$ by the same process. In this way, one finds

$$\underline{\Delta v} = (\dot{u} - v \dot{\theta}) \; \hat{u} + (\dot{v} + u \dot{\theta}) \; \hat{v} + \dot{w} \; \hat{w}$$

$$\underline{\Delta g} = (\ddot{u} - 2 \dot{\theta} \dot{v} - \dot{\theta}^2 u) \; \hat{u} \tag{4}$$

$$+ (\ddot{v} + 2 \dot{\theta} \dot{u} - \dot{\theta}^2 v) \; \hat{v} + \ddot{w} \; \hat{w} \quad .$$

In the expression for $\underline{\Delta g}$ one recognizes the Coriolis and centrifugal accelerations. A more laborious way of obtaining these same results is to differentiate the expressions given by Geyling for $(\Delta x,\ \Delta y,\ \Delta z)$ and then convert to the $(\hat{u},\ \hat{v},\ \hat{w})$ basis.

It is convenient to define two mutually perpendicular unit vectors $\hat{a},\ \hat{b}$ in the plane of the nominal orbit. $\hat{b}$ points toward the ascending node, N. $\hat{a}$ is at an angle of 90° to $\hat{b}$, going in the direction of the motion. If the x-axis is taken coincident with the line of the nodes,

$$\hat{a} = \cos i \cdot \hat{j} + \sin i \cdot \hat{k} \tag{5}$$
$$\hat{b} = \hat{i} \ .$$

We note moreover that

$$\hat{u} = \cos\theta\ \hat{i} + \sin\theta\ \cos i \cdot \hat{j} + \sin\theta\ \sin\ \hat{k}$$
$$\hat{v} = -\sin\theta\ \hat{i} + \cos\theta\ \cos i \cdot \hat{j} + \cos\theta\ \sin i \cdot \hat{k}$$
$$\hat{w} = -\sin i \cdot j + \cos i \cdot \hat{k} \tag{6}$$

From Eqs. (3) - (6),

$$\underline{\Delta v} \times \underline{g}_0 + \underline{v}_0 \times \underline{\Delta g} = V_0 \left[\dot{\ddot{w}}\ \hat{u} - \dot{w}\ \dot{\theta}\ \hat{v} \right.$$
$$\left. + (2\ u\ \dot{\theta}^2 - \ddot{u} + 3\ \dot{v}\ \dot{\theta})\ \hat{w} \right]$$

$$= V_0 \left\{ \left[2\ u\ \dot{\theta}^2 - \ddot{u} + 3\ \dot{v}\ \dot{\theta} \right]\ \hat{w} \right.$$
$$\left. + \left[\frac{d}{dt}\ (\dot{w}\ \sin\theta\ ) - 2\ \dot{w}\ \dot{\theta}\ \cos\theta \right]\ \hat{a} \right.$$

$$+ \left[\frac{d}{dt} \left(\dot{w} \cos \theta \right) + 2 \dot{w} \theta \sin \theta \right] \hat{b} \Bigg\} \ .$$

With $d\theta = \theta \, dt$, the time integral of this is immediate:

$$\underline{I} \ (t) \ = \ \int_o^t \Delta \left(\underline{v} \times \underline{g} \right) \ dt$$

$$= V_o \Bigg\{ \left[2 \dot{\theta} \int_{\theta_o}^{\theta} u \, d\theta \ - \ \dot{u} \Big/_{\theta_o}^{\theta} \right.$$

$$\left. + \ 3 \dot{\theta} \, v \Big/_{\theta_o}^{\theta} \right] \hat{w} \ + \ \left[\left(\dot{w} \sin \theta \right) \Big/_{\theta_o}^{\theta} \right. \qquad (7)$$

$$\left. - \ 2 \int_{\theta_o}^{\theta} \dot{w} \cos \theta \, d\theta \right] \hat{a}$$

$$+ \left[\left(\dot{w} \cos \theta \right) \Big/_{\theta_o}^{\theta} + 2 \int_{\theta_o}^{\theta} \dot{w} \sin \theta \, d\theta \right] \hat{b} \Bigg\} \ .$$

$\theta = \theta(t)$ is the angular position of O' at time t . $\dot{\theta}$ has the constant value

$$\dot{\theta} \ = \ \left(\frac{GM}{r_c^{\ 3}} \right)^{1/2}$$

Define the angle f by

$$f \ = \ \theta - \theta_o \ .$$

Then the general homogeneous solutions (10) of the coupled second-order

linear differential equations for u, v and w is

$$
u = \left(\frac{2}{\dot\theta}\, \dot{v}_o + 4\, u_o \right) - \left(\frac{2}{\dot\theta}\, \dot{v}_o + 3\, u_o \right) \cos\, f
$$

$$
+ \quad \frac{1}{\dot\theta}\, \dot{u}_o \, \sin\, f \; ,
$$

$$
v = \left(v_o - \frac{2}{\dot\theta}\, \dot{u}_o \right) - 3 \left(\frac{1}{\dot\theta}\, \dot{v}_o + 2\, u_o \right) \, f
$$

$$
+ \quad 2 \left(\frac{2}{\dot\theta}\, \dot{v}_o + 3\, u_o \right) \, \sin\, f + \frac{2\, \dot{u}_o}{\dot\theta}\, \cos\, f
$$

$$
w = \frac{1}{\dot\theta}\, \dot{w}_o \, \sin\, f + w_o \, \cos\, f \tag{8}
$$

These formulae describe ordinary Keplerian ellipses. The six

initial conditions of position ahd velocity are specified through choice

of the six parameters $(u_o , \; .. .., \; \dot{w}_o)$. It would be desirable

to express the parameters of the osculating ellipse in terms of these

others, since the former are more familiar.

We suppose that the satellite starts out at 0' or

$$
u_o = v_o = w_o = 0 \; .
$$

Further without loss of generality, we may choose the nominal orbit so

that

$$
\dot{w}_o = 0 \; .
$$

We seek the following parameters of the ellipse as a function of $\dot{u}_o$ and $\dot{v}_o$: eccentricity (e), semi-major axis (a), θ of the perigee (θ_p). And conversely, we express $\dot{u}_o$ and $\dot{v}_o$ as functions of the ellipse parameters.

Treat $\dot{u}_o$, $\dot{v}_o$ and e as small quantities of the first order and throw out higher order terms. Using Eq. (8),

$$r = r_c + u = (r_c + 2\,\dot{v}_o/\dot{\theta}) - \frac{2\,\dot{v}_o}{\dot{\theta}}\ \cos\ f$$

$$+ \frac{\dot{u}_o}{\dot{\theta}}\ \sin\ f \tag{9}$$

Let p = semi-latus rectum of the ellipse and θ' = exact θ of the satellite (which differs from θ by a term of the first order.) In terms of p , the equation for the ellipse is (11)

$$r = \frac{P}{1 + e\,\cos\,(\theta' - \theta_p)} = P\left[1 - e\,\cos\,(\theta - \theta_p)\right]$$

$$= p - \left[e\,p\,\cos\,(\theta_o - \theta_p)\right]\ \cos\ f$$

$$+ \left[e\,p\,\sin\,(\theta_o - \theta_p)\right]\ \sin\ f \quad . \tag{10}$$

Identifying coefficients in (9) and (10), and noting that $p = a$ to first order in e , we find

$$e = \frac{1}{r_c\,\dot{\theta}}\ \sqrt{\dot{u}_o^{\,2} + 4\,\dot{v}_o^{\,2}}$$

$$a = r_c + 2 \frac{\dot{v}_0}{\dot{\theta}}$$

$$\sin (\theta_p - \theta_0) = - \frac{\dot{u}_0}{\sqrt{\dot{u}_0^2 + 4 \dot{v}_0^2}} \tag{11}$$

$$\cos (\theta_p - \theta_0) = \frac{2 \dot{v}_0}{\sqrt{\dot{u}_0^2 + 4 \dot{v}_0^2}}$$

Inverting these equations,

$$\dot{u}_0 = - e a \dot{\theta} \sin (\theta_p - \theta_0)$$

$$\dot{v}_0 = \frac{1}{2} e a \dot{\theta} \cos (\theta_p - \theta_0) \tag{12}$$

If a perturbing force is acting, we require in addition the particular solutions for u, v and w . Geyling gives the particular solution for arbitrary perturbing potential. The correct orbit having desired initial conditions, is then the sum of the particular solution and the appropriate homogeneous solution.

The particular solution for the Earth's quadrupole potential (2) is

$$u = A' \left[- 1 + \sin^2 i \left(\frac{3}{2} + \frac{1}{6} \cos 2 \theta \right) \right]$$

$$v = A \left[(2 - 3 \sin^2 i) f + \frac{1}{12} \sin^2 i \sin 2 \theta \right] \tag{13}$$

$$w = A \sin 2i \left[\frac{f}{2} \cos \theta - \frac{1}{4} \sin \theta \right]$$

where

$$A \cdot = \frac{3}{2} \, J_2 \, \frac{R^2}{r_c}$$

For the sake of simplicity we decompose an arbitrary orbit into three parts: P, H 1 and H 2 . P is the particular solution (14). H 1 is that homogeneous solution which added to P yields zero initial conditions, i.e.

$$u/_0 = v/_0 = \ldots \ldots . = \dot{w}/_0 = 0 \ .$$

H 2 is another homogeneous solution for which $u_0 = v_0 = w_0 = \dot{w}_0 = 0$, while $\dot{u}_0$ and $\dot{v}_0$ may not vanish. H 2 has the effect that the initial osculating ellipse lies in the plane of the nominal orbit and can have a finite eccentricity. If we represent the total orbit by T , then we can write symbolically

$$T = P + H 1 + H 2 \ .$$

Since, by (7), $\underline{I}$ is linear in the deviation, it follows that

$$\underline{I}_T = \underline{I}_p + \underline{I}_{H1} + \underline{I}_{H2} \ .$$

Over how long a time interval should we evaluate $\underline{I}$? One of the two secular perturbations of a satellite orbit by the quadrupole moment is the regression of the nodes: "The orbital plane rotates about the Earth's axis. in the direction opposite to the satellite motion". [5] The angle of regression for small eccentricities is about

$$10^{-2} \left(\frac{R}{r} \right)^{3.5} \cos i \text{ radians per orbit,}$$

where i is the inclination. In deriving his linear equation for the deviation, Geyling threw out second order terms such as $O(v^2)$. In one orbit, the regression of the nodes may make v as large as $10^{-2}r$. The fractional error made in neglecting v^2 then amounts to perhaps 10^{-4}. This means that we may integrate for a time up to one orbital period before increasing deviations force us to choose a new, closer fitting nominal orbit.

We expect to obtain a particularly simple result if we choose one period, τ_o, of the nominal orbit, corresponding to the angular range $\theta = \theta_o$ to $\theta = \theta_o + 2\pi$. With this choice a good deal of cancellation will occur since most of the terms of the homogeneous and particular solutions are periodic with period 2π or π. For

$$t = \tau_o \text{ , eq. (7) yields}$$

$$\underline{I}_p (\tau_o) = g_o \pi A \left\{ [8 - 12 \sin^2 i] \ \hat{w} \right.$$

$$\left. - \sin 2 i \ [\hat{a} + \pi \hat{b}] \right\}.$$

And, for an arbitrary homogeneous orbit,

$$\underline{I}_H (\tau_o) = g_o \pi \left\{ [- 10 \frac{\dot{v}_o}{\dot{\theta}} - 20 u_o] \hat{w} \right.$$

$$\left. - \left[2 \frac{\dot{w}_o}{\dot{\theta}} \cos \theta_o + 2 w_o \sin \theta_o \right] \hat{a} \right.$$

$$+ \left[2 \frac{\dot{w}_o}{\dot{\theta}} \sin \theta_o - 2 w_o \cos \theta_o \right] \hat{b} \right\} .$$

Using this we obtain

$$\underline{I}_{H1} (\tau_o) = g_o \pi A \left\{ 5 \sin^2 i \cos 2 \theta_o \hat{w} \right.$$

$$\left. + \frac{1}{2} \sin 2 i \cos 2 \theta_o \hat{a} - \frac{1}{2} \sin 2 i \sin 2 \theta_o \hat{b} \right\}$$

$$\underline{I}_{H2} (\tau_o) = g_o \pi \left[- 10 \frac{\dot{v}_o}{\dot{\theta}} \right] \hat{w}$$

$$= g_o \pi \left[- 5 ea \cos (\theta_p - \theta_o) \right] \hat{w} \quad .$$

If we sum the three $\underline{I}$'s and include

$$2 g_o \pi r_c \hat{w}$$

for the nominal orbit, we find, after multiplication by $3/2c^2$,

$$\underline{\phi} (\tau_o) = \frac{3 \pi \left(\frac{GM}{c^2} \right)}{r_c} \left[\left(1 - \frac{5}{2} e \cos (\theta_p - \theta_o) \right) \hat{w} \right.$$

$$+ \frac{3}{4} J_2 \left(\frac{R}{r_c} \right)^2 \left\{ \left[8 - \sin^2 i (12 - 5 \cos 2 \theta_o) \right] \hat{w} \right.$$

$$\left. - \sin 2 i \left[\left(1 - \frac{\cos 2 \theta_o}{2} \right) \hat{a} + \left(\pi + \frac{\sin 2 \theta_o}{2} \right) \hat{b} \right] \right\} \right] \quad , \quad (14)$$

where

$$3\pi \left(\frac{GM}{c^2} \right) = 4.17992 \text{ cm} .$$

$$\frac{3}{4} J_2 = 8.12 \times 10^{-4} .$$

It should be kept in mind that r_c , e, θ_p , θ_o , i , $\hat{a}$, $\hat{b}$, $\hat{w}$, all refer to the instant when the satellite starts the orbit. We have chosen r_c as the initial radial distance.

Several checks on (14) are possible. First one verifies that for either a polar (i = $\pi/2$) or equatorial (i = o) orbit, $\underline{\phi}$ is strictly normal to the orbital plane, as is demanded by the symmetry of the situation.

When the quadrupole moment vanishes, an elementary calculation shows that for one complete elliptical orbit

$$-\frac{3}{2c^2} \oint \underline{v} \times \underline{g} \ dt = \frac{3\pi \left(\frac{GM}{c^2} \right) \hat{w}}{a (1 - e^2)}$$

By Kepler's third law, however, the time of one complete ellipse, τ_e ,

$$\frac{\tau_e}{\tau_o} = \left(\frac{a}{r_c} \right)^{3/2} \approx 1 + \frac{3}{2} \frac{\Delta a}{r_c}$$

where $\Delta a = a - r_c$. Thus, to first order

$$\underline{\phi}_e - \underline{\phi}_o = 3\pi \left(\frac{GM}{c^2} \right) \left(\frac{1 - \frac{3}{2} \frac{\Delta a}{r_c}}{a} - \frac{1}{r_c} \right)$$

$$= \frac{3\pi \ \frac{GM}{c^2}}{r_c} \quad \left(- \frac{5}{2} \ \frac{\Delta a}{r_c} \right) \quad ,$$

in agreement with the second term of equ. (14) by virtue of eqs. (11) and (12).

As a check on the quadrupole term, consider a circular equatorial orbit of radius r_c . The quadrupole potential of

$$\tilde{V} (\tilde{r}) = - \frac{r_c AGMm}{r^3} \quad (1/3 - z^2/r^2)$$

implies a force on the satellite of

$$\underline{F} = - \frac{GMm}{r_c^2} \quad (1 + A/r_c) \ \hat{r} \quad .$$

It follows that the tangential velocity exceeds that in the unperturbed orbit by

$$\dot{v}_o = V - V_o = \frac{A\dot{\theta}}{2}$$

A simple integration shows

$$\Delta \int_0^{T_o} \underline{v} \times \underline{g} \ dt = 3\pi \ A \ g_o \ \hat{w} \quad .$$

This is seen to agree with eq. (14) if one sets $i = 0$ and replaces $e \cos (\theta_p - \theta_o)$ by $2 \dot{v}_o (r_c \dot{\theta})^{-1}$

(4) LIMITATIONS OF THE ANALYSIS

As mentioned earlier, the approximations we have made render our results increasingly inaccurate as we extend them to longer times. In this section, we seek to examine the question of errors further.

First, let us determine the size of errors in position and velocity which can be tolerated in using eq. (14). The required theoretical accuracy is at least one part in 7000. Consider a polar orbit. We break $\not{\phi}$ up into an unperturbed part, a part due to eccentricity and another part due to the quadrupole moment:

$$\underline{\not{\phi}} = \underline{\not{\phi}}_o + \underline{\not{\phi}}_e + \underline{\not{\phi}}_q .$$

We take as independent variables the radial distance (r_c), speed (V_o) and, orientation of the orbital planes $(\hat{w})$. Apart from a uniform factor of $3\pi\,(GM/c^2)$, we then have

$$\underline{\not{\phi}}_o = \frac{\hat{w}}{r_c} ,$$

$$\underline{\not{\phi}}_c = \frac{-5\,\dot{v}_o}{(GMr_c)^{1/2}}\ \hat{w} , \tag{15}$$

$$\underline{\not{\phi}}_q = -3\,J_2\left(\frac{R^2}{r_c^{\,3}}\right)\ \hat{w} .$$

In the last expression, we have omitted a $\cos 2\,\theta_o$ since this term averages to zero over many orbits.

Define

$$\epsilon \equiv \left| \frac{\Delta\phi}{\phi_o} \right| = \left| \frac{\Delta\phi_o}{\phi_o} + \frac{\Delta\phi_e}{\phi_e} \frac{\phi_c}{\phi_o} \right. $$

$$\left. + \frac{\Delta\phi_q}{\phi_q} \frac{\phi_q}{\phi_o} \right| ,$$

where Δx denotes the signed error in the quantity x. Using (15) our accuracy requirement reduces to

$$\epsilon^2 = \left(\frac{\Delta r_c}{r_c} + \frac{5\,\Delta \dot{v}_o}{\dot{v}_o} \right) + (\Delta \Omega)^2 \lesssim (1.4 \times 10-4 . \quad (16)$$

We have replaced $\Delta \hat{w}$ by the equivalent $\Delta \Omega$, the error in the right ascension of the node.[8]   For a near orbit with

$$r_c \approx 4 \times 10^3 \text{ mi}$$

$$v_o \approx 1.8 \times 10^4 \text{ mi/hr.}$$

(16) implies the following limits on the permissible errors

$$\left| \Delta r_c \right| \lesssim 1/2 \text{ mi.}$$

$$\left| \Delta V \right| \lesssim 1/2 \text{ mi./hr.} \quad (V = \text{speed})$$

$$\left| \Delta \Omega \right| \lesssim 30 \text{ arc/sec.}$$

It is understood that in accordance with (16) all three uncertainties cannot approach their maximal values at the same time. If one is large the other two must be small. Although we have been treating a polar orbit, the limits in uncertainties of position and velocity should be typical of all orbits.

In the preceeding we have assumed that our formula for a single orbit is correct. We ask now under what circumstances formula (14) ceases to be accurate enough.

Let us list the two types of mathematical approximations implicit in the Geyling method:.

M.1)   neglect of $O(u \frac{2\tilde{V}}{2X})$ terms. ($\tilde{V}$ is the perturbing potential.)

M.2)   neglect of $O(u^2)$ terms.

a) e^2

b) $e \cdot J_2$

c) J_2^2

The first approximation occurs when Geyling evaluates the perturbing potential at the unperturbed position O' rather than the exact position. For this reason the equations do not constitute a true first-order theory.

Under M.2)   the quantities e^2 etc. give the expected fractional errors in position (and ϕ after a single orbit. The three terms represent the different types of second-order corrections.

We see that an $e \gtrsim 10^{-2}$ cannot be tolerated since it leads to the maximum allowable error 10^{-4}. If larger eccentricities are contemplated, we must either carry the theory to higher powers of $e^{(8)}$ or drop the attempt at analysis and use a computer.

The method also involves certain physical approximations in that we have neglected other perturbing forces. If g_m refers to the field of the nth multipole, then the accelerations neglected are

P.1) g_3 , g_4 , . . . $\qquad$ (each $\approx$ 10^{-6} g_0)

P.7) self-gravity, g_5 $\qquad$ ($\approx$ 10^{-8} - 10^{-9} g_0)

We mentioned earlier our assumption that if two perturbing forces f_1 , f_2 are small compared to g_0 then the ratio of the respective deviations they produce is $f_1 : f_2$. From the orbit formulae we can show that in one orbit the quadrupole moment yields

$$\Delta V = V(\tau_0) \sim 2\pi \; r \; J_2 \; (R/r)^2$$

$$\sim 2\pi \; r \; \frac{g_2}{g_0}$$

Accordingly for n orbits a perturbing acceleration f should yield

$$\underline{\Delta r} \sim (2\pi \; r \; n) \cdot \frac{f}{g_0}$$

This is in the nature of an upper limit since if $\underline{f}$ oscillates sufficiently the resulting deviation may be much smaller.

We are now in a position to answer the question "to how many orbits may we extend the analysis?" For e as large as 10^{-2} , the neglected e^2 terms are dominant and, as remarked earlier, we can perhaps follow the satellite through one or two orbits. At that point, we must obtain precise initial data from tracking. As e^2 falls to 10^{-6} , the neglected forces of the higher multipole now begin to dominate. The critical number of orbits for

$$\left| \underline{\Delta r} \right| = r/7000 \quad \text{is then}$$

$$n \sim \frac{1}{6 \times 10^{-6}} \cdot \frac{1}{7000} \approx 20 \quad , \quad (e^2 \lesssim 10^{-6})$$

An alternative procedure to our analytic approach is numerical integration on a computer .   Or one may supplement the analysis with accurate computer determined satellite positions. Since current knowledge (16) of the gravitational field is accurate to one part in 10^8 , the number of orbits to which we can track by computer may be 100 times as large as the above or 2000. This estimate however, is overly generous since it does not include the uncertaintly of the velocity. If we make the plausible assumption that our knowledge of velocity deteriorates at the same rate as that of position, and if we neglect $\Delta \Omega$, then (16) says that the critical number of orbits is reduced by a factor of 6 to

$$n \approx 300.$$

REFERENCES

(1) R. F. O'Connell, Astrophys. Space Sci., 4, 119 (1969).

(2) D. C. Wilkins, Stanford University Memorandum dated November 8, 1968.

(3) F. T. Geyling, Journal of the Franklin Institute, 269, 375 (1960).

(4) D. C. Wilkins, Annals of Physics, 61, 277 (1970).

(5) D. King-Hele, Theory of Satellite Orbits in an Atmosphere,
     (Butterworths, London, 1964). For present purposes one can ignore
     the effects of tesseral harmonics, which are averaged by the Earth's
     spin.

(6) H. Goldstein, Classical Mechanics, (Addison-Wesley Publishing Co.,
     Mass., 1950).

(7) D. C. Wilkins, "Precession of Gyroscope about Oblate Earth."

(8) F. T. Geyling, AIAA Journal 2, 1174 (1964).